SIMULATION AND PERFORMANCE CHARACTERIZATION OF AIR DENSE MEDIUM FLUIDIZED BED FOR COAL BENEFICIATION

By:

Ebrahim Azimi

A thesis submitted in partial fulfillment of the requirements for the degree of

Doctor of Philosophy

in

Mining Engineering

Department of Civil and Environmental Engineering

University of Alberta

ABSTRACT

The dry coal beneficiation method, Air Dense Medium Fluidized Bed (ADMFB) system, can offer an efficient solution for removal of ash forming minerals from run of mine (ROM) coal to improve coal quality and alleviate application issues and footprint. The investigation has been performed in several steps; ROM beneficiation studies, optimization of key operating parameters to reach optimum beneficiation levels, integrating coal beneficiation and drying, specifying effect of beneficiation on product quality, and finally, simulating particle segregation in ADMFB. For beneficiation studies, batch and continuous ADMFB apparatus were used to investigate segregation pattern of low and high ash ROM particles once added to a bed of fluidized Geldart type B particles.

Design of experiment methods were used to study the effect of main operating parameters (superficial air velocity, separation time and bed height) and their mutual interactions on the performance of batch or continuous ADMFBs. Product (clean coal) ash content, combustible material recovery and system separation efficiencies were considered as process evaluation criteria and desired levels of them were considered for process optimization. Based on the developed mathematical models, several significant mutual interactions were revealed for any of the evaluation responses, sometimes effective than the direct effect of main parameters. Considerably better separation results were obtained for high ash coal (more than 62% ash rejection) than low ash feed (at most 27% ash rejection). Beneficiation performance of ADMFB showed improvement once coarsest particles (5.6-13.2 mm) were fed to the bed instead of finer size fractions, regardless of feed ash content. Application of finer sand particles as fluidization media reduced number of bubbles in bed and its effective density, resulting further promotion in separation quality. Continuous beneficiation experiments on 2.8-5.6 mm high ash feed revealed that, almost the same level of separation (or even better) was achievable in continuous mode as the batch bed.

Optimization of mathematical model for minimum clean coal ash content suggested superficial air velocity, separation time and bed height of 19.5 cm/s, 76 cm (full bed length) and 15 cm, respectively for the 2.8-5.6 mm coal particles and the range of operating parameters used in experiments. Repeating experiments showed that, it was possible to produce a clean coal with ash content of 10% from a feed (5.6-13.2 mm) of 29.1% ash and ash rejection, combustible material recovery and system separation efficiency of 65.4, 89.11 and 67.42%, respectively. Staged coal separation and drying experiments presented promising results for combining two processes since acceptable particle separation could be reached in a short time interval. Moisture removal of 33.8 to 52.5% was obtained for 7.5 min fluidized bed (U=18 cm/s) coal drying.

Wide range of coal characterization techniques such as ultimate analysis, ICP-MS, Hg analysis, TGA, XRD, XRF and ash fusion temperature were applied. Characterization results indicated that due to beneficiation by ADMFB, HHV and reactivity (burn out rate) of clean coal products had increased (significantly for low ash coal) regardless of feed ash content. On the other hand, the amount of most hazardous elements and mercury content of clean coal products showed different (sometimes severe) levels of reduction. It was concluded that, Na, Fe and Ca are associated with coal phase. Pyritic type S content was not abundant in either of coal samples. Diagnostic experiments and available models predicted an increase in slagging propensity and decrease in molten slags viscosities.

CFD simulation of particles fluidization and segregation were investigated considering Euler-Euler approach and using commercial fluid dynamic software. Several stages considered before preparing final three phase model. After conducting several 2D simulations for grid sensitivity, drag function and solid-solid restitution coefficients studies, prediction of a 3D model was compared with the results of reference experiment. The predictability of 3D (3phase) model was found to be 89.33% which was 29.1% better than its equivalent 2D simulation model.

Preface

The conducted research was funded by grant from Carbon Management Canada (CMC) and Canadian Centre for Clean Coal/Carbon and Mineral Processing Technologies (C^5MPT) to Dr. Rajender Gupta and Dr. Jozef Szymanski. The results, analysis and discussions were performed by me under supervisory of Dr. Jozef Szymanski and Dr. Rajender Gupta.

Some of the technical apparatus referred in chapter 3, were initially built and used by Dr. Zhenge Xu, but for the purpose of this study, they are remodeled and upgraded by myself while, some apparatuses also were designed by me. The experimental work design and data analyses, in chapter 4, 5 and 6, are my original work as well as literature review in chapter 2. For the simulation models in chapter 7, commercial software (Fluent R14.0) was used. All models were established by me as well as any post processing step conducted after obtaining solution files from software. All of the experiments reported in the thesis, were conducted by me with some assistance from Dr. Shayan Karimipour and Dr. Moshfiqur Rahman for data collection. Also Dr. Shayan Karimipour and Dr. Petr Nikrityuk helped me with the numerical simulation part of the study.

Two journal papers in Energy & Fuel were published during this study using some of materials in chapters 2-4 and 6. In the first paper, some materials from chapter 2, 3 and 4 of this thesis have been published as: “Azimi, E., Karimipour, S., Rahman, M., Szymanski, J., Gupta, R, *Evaluation of the Performance of Air Dense Medium Fluidized Bed (ADMFB) for Low-Ash Coal Beneficiation. Part 1: effect of operating conditions.* Energy & Fuels, 2013. **27**(10): p. 5595-5606.”. And in the second paper, materials from chapter 6 of this thesis have been published as: “Azimi, E., Karimipour, S., Rahman, M., Szymanski, J., Gupta, R, *Evaluation of the Performance of Air Dense Medium Fluidized Bed (ADMFB) for Low-Ash Coal Beneficiation. Part 2: Characteristics of the Beneficiated Coal.* Energy & Fuels, 2013. **27**(10): p. 5607-5616.”. In both papers, I was responsible for the data collection and analysis as well as the manuscript composition. Karimipour, S. and Rahman, M. assisted with the experiments and data collection, and contributed to manuscript edits. Szymanski, J.,

Gupta, R. were the supervisory authors and were involved with concept formation and manuscript composition.

Also one editorial manuscript is recently accepted in the journal of Civil and Environmental Engineering. Some materials from chapter 4, 5 and 6 of this thesis have been published as: “Azimi, E., Gupta, R., Szymanski, J., *Dry Coal Beneficiation Method-Effective to Reduce Health, Environmental and Technical Coal Firing Issues*. J Civil & Environ Eng., 2014, **5**(4).”. I was responsible for the data collection and analysis as well as the manuscript composition. Szymanski, J., Gupta, R were the supervisory authors and were involved with concept formation and manuscript composition.

I lovingly dedicate this thesis to:

my parents, ***Ozra*** *and* ***Mohammad***

my brothers, ***Ali*** *and* ***Yousef***

for their endless love, support and encouragements.

ACKNOWLEDGMENT

I would like to thank both my research supervisors Dr. Jozef Szymanski and Dr. Rajender Gupta for their guidance and patience, and mention my gratefulness to Dr. Shayan Karimipour and Dr. Petr Nikrityuk for all support and wonderful discussions we had throughout the course of this thesis.

I should also appreciate all members of Dr. Gupta's research group, especially Dr. Moshfiqur Rahman and Dr. Mehdi Mohammad Ali Pour, for their kindness and understanding toward me.

My gratitude also expands to Carbone Management Canada (CMC) and Canadian Centre for Clean Coal/Carbon and Mineral Processing Technologies (C^5MPT) for their financial support.

Ebrahim Azimi
August, 2014

TABLE OF CONTENTS

LIST OF TABLES

LIST OF FIGURES

LIST OF SYMBOLS AND NOMECLATURES

A:	Bed cross section, representative of air superficial velocity (U)
B:	Representative of separation time (T)
C:	Representative of Bed height (H)
H:	Bed height
f:	Bed vibration frequency
d_p:	Particle diameter
U, u:	Superficial air velocity
Q:	Gas flow rate
e:	Porosity
e_{mf}:	Porosity (voidage) of a bed at minimum fluidization velocity
u_{mf}:	Minimum fluidization velocity (superficial)
g:	Gravitational acceleration (9.81 m/s^2)
X_1:	Independent input parameters
X_{norm}:	Normalized independent input parameters
y:	Random response variable
T:	Time
T°:	Temperature
IDT:	Initial deformation Temperature
ST:	Softening (spherical) Temperature
HT:	Hemispherical Temperature
FT:	Fluid Temperature
HHV:	Higher heating value
X_k:	Mole fraction of k
p:	Pressure
ΔP:	Pressure drop

ρ:	Density
$\emptyset_s$:	Solid particles sphericity
μ:	Viscosity
β_k:	Coefficient
L_i:	Sampling intervals
CV:	Coefficient of variation
$CC^{\%}_{Ash}$:	Clean coal (product) ash content
$R^{\%}_{C\ to\ l_1}$:	Combustible material recovery to L_1 layer
$SE^{\%}_{sys}$:	System separation efficiency
α:	Volume fraction
$\overline{\overline{\tau}}_s$:	Stress tensor, (Pa)
λ:	Bulk viscosity, kg/s.m
$\overline{\overline{I}}$:	Stress tensor, dimensionless
K_{gs}:	Exchange coefficient (gs: gas-solid, ks: solid-solid)
C_D:	Drag coefficient
Re:	Reynolds number
ω_i:	Coefficient
e_{ks}:	Restitution coefficient (solid-solid)
$C_{fr,ks}$:	Coefficient of friction (soild-solid)
$g_{0,ks}$:	Radial distribution coefficient
Θi:	Granular temperature m^2/s^2
$\gamma_{\Theta s}$:	Collisional dissipation of energy
ϕ_{gs}:	Solid-fluid energy exchange coefficient
$k_{\Theta s}$:	Diffusion coefficient of granular energy
I_{2D}:	Second invariant of the deviatoric stress tensor

CHAPTER 1

INTRODUCTION

Coal is a brown to black non-renewable combustible solid, formed by decomposition of plants without free access to air under influence of increasing pressure and temperature in a humid environment as a result of long term trapping between sedimentary rock strata, called overlaying and bottom rocks. Such environment produces coal as heterogeneous mixture of organic and inorganic materials with infinite variations in consistency of the components. The type of dominant plant in peat, level of decomposition as well as peat pressure, moisture and temperature affect the type of coal, categorized as brown, lignite, bituminous, and anthracite coals (the mentioned order does not necessarily mean as formation or coalification stages) [1].

Coal is the second largest energy source of today's world after oil [2]. Also it is the first available resort for energy acquisition (except solar energy) when all other energy sources including oil, gas, nuclear power are converted into equivalent tone of coal [2, 3]. According to International Energy Agency, world energy demand will grow approximately 60% over the next 30 years which necessitates the utilization of low rank coals to support the production of low cost energy [2].

About 66% of the total fossil fuel resources of Canada is coal and Canada produces between 65 and 75 Mt of thermal or coking coals annually where most of the coal mines are located in Western Canada (around 70% in Alberta) [4]. Almost all of mined thermal coal is domestically consumed for power generation (more than 60% of energy supply in some provinces) [4]. Direct run-of-mine (ROM) ore feeding into furnaces for energy production in the ever increasing demand world for energy has accelerated the air pollution by human over the last

century. ROM coal contains substantial amounts of ash forming minerals and moisture which lowers the efficiency of the power generating plants, generates additional particulate materials, Oxides of sulfur (SOx) and emission of trace elements such as mercury and arsenic. The release of toxic metals as well as GHGs during coal combustion has been targeted for emission control due to their detrimental effects on human health, environmental and climate.

The clean coal technology campaign has started in most of countries that are using coal as main source of energy and is intended to increase coal utilization efficiency, decrease the carbon footprint and environmental/health related pollutions. The clean coal technology is a collective term, covering all steps related to the energy produced from coal, i.e. coal mining and preparation, conversion processes, and flue gas treatment. The ROM coal preparation is an essential component of the clean coal technology. Most of the environmental issues encountered today could be solved or mitigated by employing efficient coal beneficiation methods (which are not widely practiced by power industry yet) that results in smaller carbon footprint and also expanding exploitation horizons of coal deposits, previously marked as uneconomical due to commercial or environmental limitations.

Clean coals (coal beneficiation products) are not only more efficient in terms of combustion, but also more uniform in size, composition, calorific value and moisture content. The outstanding benefits of an efficient beneficiation processes to the downstream industry and environment includes: more reliable and uniform operation, lower particulate matter or SOx emissions (and consequently less flue gas desulfurization requirement and cost), less maintenance and lower overall operating costs of coal to energy conversion units as well as reduction in coal transportation costs ($/t) [1, 5-9].

The ROM coal characteristics, accompanying mineral type, coal-mineral interlocking, selected cleaning method and its efficiency determines the extent of the ash minerals removal and process economy. Generally two wet and dry coal beneficiation or coal cleaning methods, in terms of water involvement, have been applied to achieve clean coal goal. Acceptable results are obtained for wet coal

beneficiation methods such as froth flotation, jigging, spiral separators, or heavy media separators for years. But, higher process costs, fresh water resources scarcity and subsequent water recycling expenses, sliming of wastes, high clay content of the low rank coals, high operating costs of coal and waste slurry treatment and lower thermal efficiency due to higher moisture content of the product are some issues motivating implementation of the dry coal cleaning methods [7, 8, 10, 11].

Considering the mentioned issues of accompanying ash minerals and wet beneficiation processes beside recent progresses of dry coal beneficiation methods such as Air Dense Medium Fluidized Beds (ADMFB), air jigs, magnetic separators, electrostatic separators, and pneumatic oscillating tables; application of dry beneficiation methods for cleaning ROM coal seems to be inevitable for industry. Although Canada has excessive amount of water resources but its cold weather along with process water treatment issues have made wet methods less desirable. Recent developments, lower upward air flow rates and pressure requirements and consequently less and smaller dust collecting equipment with minimum possible moving parts and the possibility of utilizing waste heat (low quality heat) as a process advantage for simultaneous coal drying and cleaning, as well as lower capital and operational costs makes ADMFB separator to be one of the best choices to deal with ash forming minerals in ROM coals.

Air dense medium fluidized bed (ADMFB) coal beneficiation has been recently examined widely by several researchers, but scanty comprehensive information is available on the effect of the various operating parameters and their effective ranges or their mutual interactions on the performance of the apparatus even though industrial application of it is reported. Available literature (will be discussed extensively in next chapter) indicates that the separation efficiency of an air dense medium fluidized bed coal separator could be affected by several factors such as fluidizing medium type and size, feed size, superficial air velocity, bed pressure drop, bed stability, air distributer, separation time and coal to medium ratio.

The objective of this thesis is to investigate the effect of operating parameters on ADMFB coal separator performance and clean coal characteristics, dealing with different ROM coals in terms of type and ash content. Since some particles are rejected selectively and not homogeneously, therefore head and product samples are characterized and compered. The numerical simulation of particle segregation in a gas-solid fluidized bed environment is also studied. A literature review on principals of gas-solid fluidization and utilization of fluidized beds for coal beneficiation is presented in CHAPTER 2. The materials properties and characterization methods, experimental set up configuration and utilization, applied design of experiments methods and considered responses for evaluating separation process quality are provided in more details in CHAPTER 3. Comprehensive batch and continuous beneficiation experiment results and discussions and such separation processes optimizations are discussed in CHAPTER 4 and CHAPTER 5. The ROM coal and clean product characteristics and quality changes are covered in CHAPTER 6. Results of computational fluid dynamic simulation model for particle segregation in fluidized beds, using Eulerian multiphase model scheme of Ansys-Fluent, are discussed in CHAPTER 7. Finally, conclusions and recommendations are given in CHAPTER 8, respectively.

CHAPTER 2

COAL CLEANING METHODS OVERVIEW

Coal upgrading can generally be classified into three main categories, physical, chemical and biological upgrading methods (Figure 2-1). Both chemical (solvent treatment) and biological methods (bioleaching/desulfurization of organically bounded sulfur), which are generally developed to deal with unwanted elements, are widely under examination (even in pilot scale) but currently too expensive to expand them to commercial production scales for conventional coal usage purposes (burning, coking). Some of the physical coal upgrading or in specific terms coal beneficiation, coal cleaning or coal washing methods are developed well enough in terms of capacity, effective range of operating parameters, satisfactory yield and separation efficiency to fulfill needs of low ash coal production. As mentioned physical coal preparation methods can be categorized to wet and dry methods from the process view point. In all methods several processes might be considered to liberate and separate the inherent or extraneous (added during peat formation or coal seam mining) mineral matters from carbon-rich phase in as-mined coal where separation yield and process costs balance economically in an acceptable point.

Physical methods regardless of wet or dry, usually take advantage of the difference between components hardness, luster, density, surface characteristics (such as conductivity, hydrophobicity or hydrophilicity), magnetic susceptibility, particle size, shape and their coefficient of friction when free falling in fluids. Regardless of which method to use, there are some cones and pros for each. Coal washing practiced for a lone time mostly for steel production purposes. Wet separation methods (such as froth flotation, dense medium separators and jigs) got more chance to progress as they generally have higher separation efficiency (low

ash, high yield) and operating capacities since they provide more stable separating environment and more control on affecting variables. On the other hand they are usually involved with higher capital and operational costs, water consumption and recycling issues (thickening, tailing pounds …), ground water pollutions (acidic water, employed reagents) and waste material sliming when dealing with low rank high clay content coals. Lower product (clean coal) thermal efficiency and possibility of product freezing while storing or transporting at cold areas due to high moisture content are some other intrinsic disadvantages of wet processing methods when are compared to dry method [1, 7-9, 12, 14, 15].

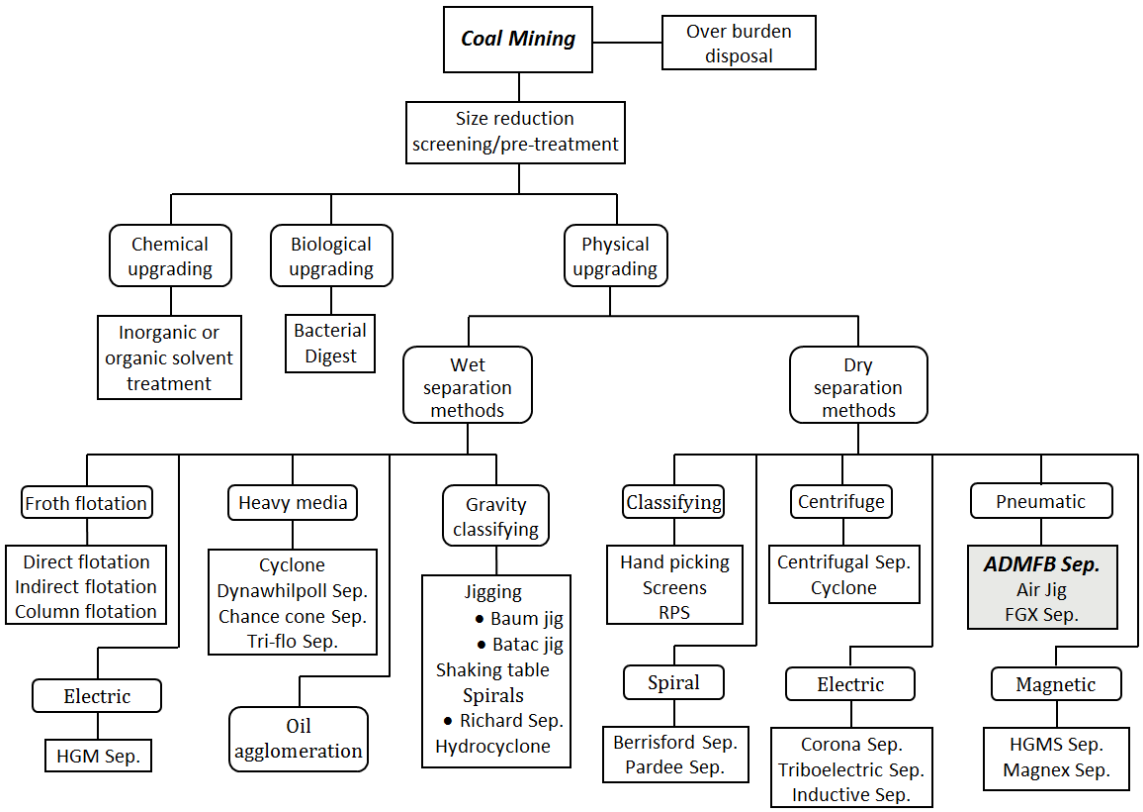

Figure 2-1: Coal upgrading chart

In case of dry methods, other than elimination of hazardous process chemicals and water issues, a low ash and moisture content clean coal with higher heat efficiency (calorific value per kg) can be produced. Even though the separation efficiency and product quality are lower than wet methods but their capital and operational costs are considerably low in comparison. Lower capital

and process costs facilitate establishment of small cleaning units in coalfields at mine gates increasing coal processing benefits in terms of lower transport costs and limited waste dumps. The lack of adjustability, high sensitivity to feed change and necessity for narrower feed size distribution to obtain suitable results are main concerns related generally to all dry separation methods which most of them nowadays are easy to deal with. High moisture content of the feed is generally a problem when coal is meant to be beneficiated via dry methods. Feed particles agglomeration and material flow clogging can occur due to high moisture content of ROM. Dust formation can be the most serious safety challenge of the dry coal beneficiation methods as fine coal particles need a slight stimulus to start a disaster, but still dealing with that is much easier than dealing with aqueous slurries produced in wet processing methods [1, 5-17].

Intrinsic and operational advantages of dry preparation methods with support of current improvements on instrumentation and system controlling can outweigh its disadvantages and if the involved factors are recognized and their effects on the performance of the apparatus are studied carefully, appropriate separation could be achieved here as well. One of the newly expanded methods for coal cleaning is the application of fluidized beds for selective particle segregation. The idea is to set and use a stable pseudo fluid to classify crushed ROM coal particles according to their (different) densities. Therefore in the next sections, a brief explanation on the concept of gas-solid fluidization is given and then a review of conducted research on coal separation employing ADMFBs is followed after that.

2.1 Principals of gas-solid fluidization

Transferring solid particles from packed bed state in to a fluid-like state by an upward stream of gas or liquid is called fluidization where the total pressure loss of the fluid throughout the bed increases as the frictional resistance increases with increasing fluid flow. With increasing fluid velocity, particles start separating one from another (compressive forces between adjacent particles disappear) when the frictional drag force on the particles due to upward flow of

fluid counterbalance with their apparent weight, i.e. weight of particles when buoyancy force is considered. At this point the expanded bed is described as incipiently fluidized bed or a bed at minimum fluidization state where the stationary particles are supported freely in the fluid and the bed offers lowest resistance to the flow of fluid and maximum void fraction compared to fixed or packed bed. At minimum fluidization velocity and above, the pressure drop through any section of the bed is about equal to the weight per unit area of the bed [18, 19].

When full fluidization state is reached the dense phase reacts like a pseudo fluid (fluid-like), exhibiting the same characteristics of a stationary or boiling liquid as illustrated in Figure 2-2. For instance the pressure difference between two points in bed can be estimated fairly by the static head, considering the average bed density. Solids will flow out like a liquid jet from the hole in the side of the container. The levels of two connected beds equalize as well as being horizontal if the containers are tipped. Objects with a density lighter than the bulk density of the bed will float on the surface (also known as float Sam [20]) even if pushed into the bed intentionally while the heavier ones will sink into it (also known as jet Sam [20]). Other fluid like properties of the fluidized beds and their advantages when applied in industry are described and studied in more details in references [18-24] and just some basic ones are pointed out here.

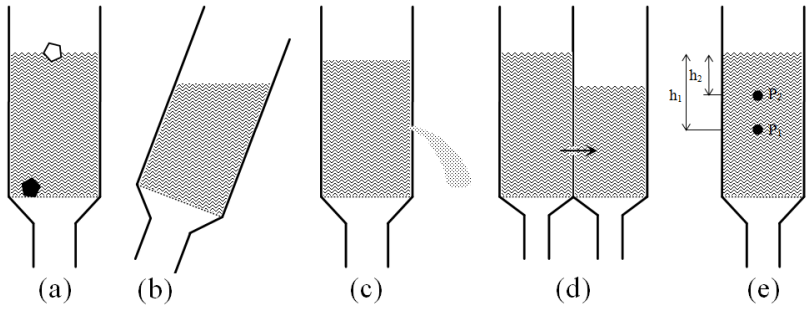

Figure 2-2: Liquid like behavior of gas fluidized beds, (a) light object floats and heavier one sinks, (b) surface stays horizontal even if bed is tilted, (c) solids gush from hole, (d) connected vessels solid levels equalize (e) static head determines the pressure difference between two points [adopted from 25]

2.2 Fluidization regimes

In general, progressive bed expansion, damped flow instabilities, more homogeneous and less bubbling are characteristics of liquid fluidized beds. With increasing fluid velocity several regimes may be experienced depending on the type of fluid and properties or arrangement of the bed forming solid particles. A brief description of some of these regimes is followed below.

Fixed bed: upward low flow rate fluid percolates through the void space between particles until the velocity reaches a point where the pressure drop across the bed equals to the weight per unit area of the particles, i.e. minimum fluidization velocity, u_{mf}. Particles remain in contact with each at $u<u_{mf}$ [18, 19, 21, 22, 26].

Particulate fluidization: by increasing fluid velocity above u_{mf}, bed may continue expanding while retaining its uniformity with some local particle agitations. This type of fluidization is easy to achieve by liquids while is restricted in gas fluidized beds to a very narrow range of gas velocities or even sometimes not achievable. Particulate fluidization is also known as homogeneously, smoothly or liquid fluidization in references [18, 19, 22, 26].

Aggressive fluidization: this regime is also known as aggregative, heterogeneous or bubbling fluidization. Forming two separate phases as dense or discontinuous phase made up of mainly solid particles and bubble phase (due to channeling) is the main characteristics of this regime. More chaotic structure, violent bed agitation and vigorous movement of the solid particles happen at higher flow rates. It can be sub-categories into three Bubbling, slugging flow and turbulent regimes as the fluid velocity increases [18, 19, 21, 22, 26].

Fast fluidization and pneumatic conveying regimes: such regimes are also expected as the air velocity keeps increasing after reaching turbulent fluidization regime. At this stage particles are transported vertically where such condition is very beyond the intended operating regime for ADMFB separator [18, 19, 21, 22, 26].

2.3 Minimum fluidization velocity determination

2.3.1 Experimental/Empirical method

Recognizing transition status from fixed bed to particulate regime (or bubbling regime) is an essential step in understanding fluidization phenomena and is extensively discussed in literature both empirically (experimental justification) and theoretically. The empirical minimum fluidization velocity could be predicted via conducting experiments and monitoring the total bed pressure drop (ΔP) versus fluid superficial fluid velocity (u).

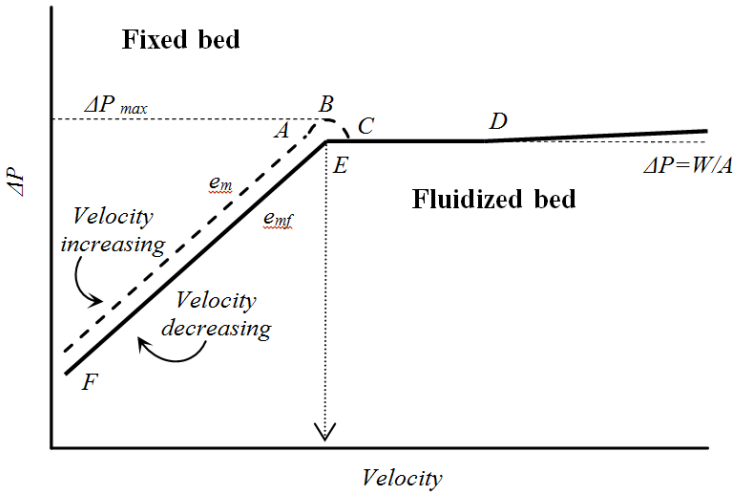

Figure 2-3: Bed pressure drop versus fluid velocity [adopted from 18 and 19]

As Figure 2-3 describes, the pressure drop of the packed bed increases proportional to fluid velocity, from bed static pressure up to A, where the bed starts expanding due to rearrangement of the particles. At this point the drag force acting on particles equalizes the gravitational force on them. At maximum pressure drop point, B, suddenly bed "unlocks" and simultaneously pressure drop falls slightly. The frictional forces between particles cause this peak. The CD presents the static steady state fluidized bed pressure drop, and is independent of fluid velocity. By increasing gas velocity, bed expands and bubbles rise in gas fluidization but the pressure drop remains practically unchanged. A slight increase in pressure drop may be experienced because of increasing wall-fluid friction force at high velocities as it is negligible at lower fluid velocities [18, 19].

If the fluid velocity is reduced, pressure drop obeys DCE where particles rest on each other at E. At this point the bed has maximum void fraction of its packed state which may decrease some if any vibration is introduced to the bed. Reformed fix bed with higher void fraction as result of freely settlement of particles is retainable as velocity decreases. The obtained EF trend falls below AB due to lower pressure drop of the reformed bed compared to the initial closely packed bed [18, 19, 23].

The minimum fluidization velocity may be determined experimentally by obtaining relevant velocity of point B, or by intercepting best fitting two EF and CD straight lines on measurement data for decreasing and increasing fluid velocities, respectively.

2.3.2 Theoretical method

The onset of fluidization occurs when all of the particles are essentially supported by flow, which means the drag force acting on particles due to flow is equal to the apparent weight of them. Thus the additional pressure drop across the bed attributes to the apparent weight of the particles per unit area of the bed as Equation 2-1.

Equation 2-1:

$$\begin{pmatrix}\text{Pressure drop}\\ \text{accross the bed}\end{pmatrix}\begin{pmatrix}\text{cross sectional}\\ \text{area of bed}\end{pmatrix} = \begin{pmatrix}\text{Volume}\\ \text{of bed}\end{pmatrix}\begin{pmatrix}\text{fraction}\\ \text{of solids}\end{pmatrix}\begin{pmatrix}\text{Specific}\\ \text{gravity}\end{pmatrix} \quad [18]$$

Therefore for void fraction of e in the bed, the excess pressure drop could be presented as Equation 2-2 which applies from initial expansion status until transportation of solids out of bed take place.

Equation 2-2: $\Delta P = \frac{HA(1-e)(\rho_s-\rho_f)g}{A} = H(1-e)(\rho_s-\rho_f)g$

Where $\Delta P, A, H, e, \rho_s$ and ρ_f are bed pressure drop, bed cross section, bed height, bed porosity, solid particles density and fluid density, respectively.

Considering Equation 2-2 and widely used Ergun equation (Equation 2-3) for fixed bed pressure drop (uniformly sized particles), theoretical value of minimum fluidization velocity may be calculated for a wide range of flow regimes (applicable to wider range of Reynolds number). According to Kunii and

Levenspiel [18] if e_{mf} (void fraction at minimum fluidization velocity) is substituted with e then the u_{mf} is obtainable through:

Equation 2-3: $\frac{\Delta P}{H} = \frac{150(1-e)^2}{e^3}\frac{\mu u}{(\emptyset_s d_p)^2} + 1.75\frac{1-e}{e^3}\frac{\rho u^2}{\emptyset_s d_p}$

Equation 2-4: $\frac{1.75}{\emptyset_s e_{mf}^3}Re_{mf}^2 + \frac{150(1-e_{mf})}{\emptyset_s^2 e_{mf}^3}Re_{mf} = \frac{d_p^3 \rho_f(\rho_s-\rho_f)g}{\mu^2}$,

$$Re_{mf} = \left(\frac{d_p u_{mf}\rho_f}{\mu}\right) \qquad [21,24]$$

Where $\emptyset_s$and μ are the solid particles sphericity (the ratio of surface of sphere with same volume of the particle to the surface of particle) and fluid viscosity. It should be mentioned that voidage of a bed at incipient fluidization (e_{mf}) is equal or greater than the loosest status of a packed bed.

The calculated minimum fluidization velocity could be different than the experimentally determined one, as result of solid particles channeling, agglomeration or being supported by bed wall, electrostatic forces due to particles friction or wall-fluid friction at higher fluid velocities [18, 19, 22].

A wide range of study has been carried out on predicting or modeling fixed bed pressure drop for general or specific flow conditions. For instance, the Carman-Kozeny equation is established based on predicting pressure drop in laminar flow through randomly packed particles. Most of reference books in fluidized bed area have discussed and used Carman-Konzey equation to predict the u_{mf} under laminar flow condition. Also many alternate models and procedures such as Wen and Yu (simplified version of Ergun equation), Lava, Rowe etc. have been proposed and investigated (extensively discussed and summarized in reference number 23). Ergun model will be used in the calculations, predictions and comparisons as it is widely accepted and applicable as both laminar and turbulent conditions are considered in it [18-23].

2.4 Solid particles classification

Several factors and parameters affect fluidization behavior and quality (Equation 2-4) but physical properties of solid particles (size, density, shape and

solid volume fraction) are the most dominant and influencing factors on fluidization behavior of a bed.

Generally spherical particles fluidize better and more uniform than needle like particles. Also mass of particles with mixed size distribution may fluidize more smoothly than uniform size bed due to coating of coarse particles with finer ones and acting as lubricant between them [19, 22, 26-28].

Geldart [29-31] classified solids (fluidized by gas) into four distinguishable groups considering mean particle size and solid-gas density difference $(\rho_s - \rho_g)$ at ambient pressure and temperature as illustrated in Figure 2-4. Group A powders are recognizable from group B where u_{mb}/u_{mf} ratio is greater than one for group A particles. Also for group D particles bubbling velocity is less than u_{mf}/e_{mf} which could be used as demarcation criteria to recognize between group B and D [22].

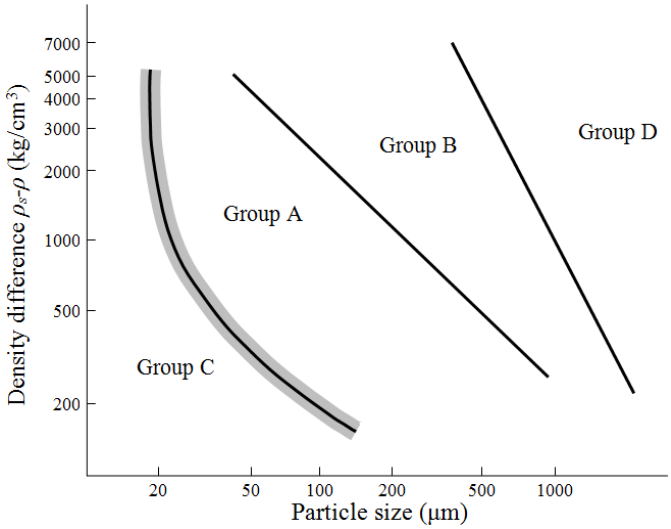

Figure 2-4: Geldart powder classification diagram [adopted from 29]

Generally speaking, group C particles are difficult to fluidize due to high inter-particle forces, while group A particles present smooth fluidization or bubbling corresponding to superficial air velocity. Vigorous bubbling occurs for group B at velocities $>u_{mf}$ while group D particles form stable spouted beds. These characteristics may not be identical since the temperature and pressure changes from the reference values.

To date no single method has been widely accepted and used, but Geldart's classification which is the simplest and more comprehensive one. Others as Molerus [32] modified Geldart's classification by tacking account the inter particle cohesion force. Different demarcation criteria were introduced for particles group transition. Grace [33] suggested new boundaries for particles of group A, B, C and D which could be expanded to beds operating with gases other than air with temperature and pressure other than ambient condition. Goossen [34] classified particles based on Archimedes number into four groups. This classification is acceptably applicable for liquid or gas fluidization regimes where group determining boundaries are well compatible with Geldart and Molerus classifications (except A/B boundary) when air is used as fluidizing fluid.

2.5 Utilization of Fluidized beds for dry coal cleaning

As mentioned a stable and uniformly fluidized bed, a pseudo-fluid of suspending solid particles (medium), is obtainable via passing a controlled upward flow of air through solid particles forming a packed bed. Such environment with the average density residing between air and solid particles has been utilized for density base particle separation. Due to the direct relationship between coal particle density and its ash content, once coal particles are introduced to the created pseudo-fluid all particles would stratify along the bed depth based on their densities and their interactions with the pseudo-fluid forming particles (i.e. lightest on top to heaviest at the bottom).

Air dense medium fluidized bed (ADMFB) coal beneficiation has been examined widely but, with not much comprehensive information available on the effect of various operating parameters on the performance of the apparatus even though industrial application of it is reported. Available literature conforms that the separation efficiency of an air dense medium fluidized bed coal separator, a gravity separation operation, is affected by several factors such as fluidizing medium type and size, feed size range, superficial air velocity, bed pressure drop, air distributer, separation time, coal to medium ratio …. A significant amount of research and development is conducted and going on trying to investigate and

determine how mentioned parameters affect ADMFB coal separation process and its product quality. A summary of conducted research works and obtained results are presented in the following paragraphs.

Major steps toward developing an ADMFB coal separator and its commercialization have been taken at mineral processing research center of China University of Mining and Technology (CUMT), where the first 50 t/hr coal preparation unit for beneficiating 6-50 mm was reported installed and operated in 1994 [25, 35-38]. Proper separation quality (Ep of 0.05-0.07) for 6-50 mm feed with magnetite powder or mixture of magnetite and fine coal (<1 mm) as medium solids, lower construction and operational costs compared to the wet methods and almost no environmental pollution regarding waste management and slimming are reported as process advantages [25, 35, 36, 38].

Luo et al. [39] from mineral processing engineering research center of CUMT studied the mechanism and separation efficiency of 6-50 mm coal in a bed of 210 μm magnetite. A product of 11.8% ash (85.75% ash rejection) with separation Ep of 0.03 was obtained from feed of 21.84% ash. Chen and colleagues [36, 38] suggested dipper fluidized beds (~1.2 m) to deal with >50 mm ROM to achieve acceptable separation efficiency while triboelectrostatic separators are suggested and examined for fine coals (<1 mm).

Misplacing and back mixing are addressed as sources of separation errors (unexpected positioning of heavy or light particles in bed) which could be avoided by determining and operating at optimal gas velocity. Misplacing effect of viscosity could be dominant at lower gas velocities. Such misplacement is caused by coal particles (not able to move freely in bed) due to lower medium activity or in another word un-proper dispersion of medium particles. Misplacement effect of motion and back mixing phenomena is the dominant source of error at high gas velocities. In motion misplacement, coal particles are trapped in the circular flow of medium particles and transported in bed involuntarily. In back mixing phenomena particles (medium or fine coal particles) are transferred to the upper levels due to entrainment in bubbles' wake area [25, 35, 37-40]. It has been demonstrated that the back mixing of solids is minimum at lower velocities (near

minimum fluidization velocity) where bubble formation is at minimum rate. Utilizing finer medium particles for beneficiating finer coal, increases bed viscosity and consequently particle back mixing therefore continuous efforts have been made to reduce the lower limit of separable particle size in ADMFB separator. Use of vibration energy to improve the fluidization status of the medium solids and breaking down the bubble size; magnetic field to stabilized suspended medium particles and consequently the bed density and dual density beds are some of the strategies applied to reduce the back mixing and instability of ADMFB separator to improve separation efficiency or ability to deal with finer coal particles (<6 mm).

Chikerema et al. [13] verified the effect of particle size and shape on the performance of a magnetite-silica bed. The bed height of 32 cm and separation times of 5 s to 60 s were considered for the four particle size fractions within the range of 9.5 mm to 53 mm. Lower Ep (Ecart probable error) values of 0.05 was obtained for the coarse particles (22 to 53 mm), while for the smaller particles the Ep values of 0.07 and 0.11 were considered to be high and as an indication of lower effectiveness of the separation process for finer particles. Also large (blockish) particles with smaller surface area to volume ratio showed lower Ep values (0.08) compared to the other two classes of flat and sharp-pointed particles. Increasing of separation time was found adversely affecting the Ep.

In another study, Mohanta and colleagues [41, 42] used a 15 cm diameter column with 20 cm active bed height and 4.7 t/m^3 magnetite particles (d_{50} of 212 μm) as fluidization medium to investigate the effect of feed size (4.75-13 mm, 13-25 mm and 25-50 mm) on the performance of the ADMFB separator in Indian Institute of Technology, Kharagpur, India. The separation tests performed under both constant air velocity of 3.5 l/s and separation time of 30 s, respectively. The obtained Ep values showed decreasing trend with increasing the coal size until leveling off for particles larger than 25 mm (with Ep of 0.04). They used organic efficiency (ratio of actual yield of clean coal to theoretical yield of product of the same ash content), combustible recovery (ratio of combustible in clean coal to the combustible in a unit mass of feed), ash rejection and separation efficiency as

judgment criteria for separation experiments besides conventional Ep values. They used four high ash Indian coals and for all samples the organic efficiency, separation efficiency and combustible recovery decreased when coarse feed was introduced to the separator. Generally ash rejection increased when coarse coal particles were fed into bed. The non-stability of the process (back mixing) was reported by Mohanta and others [43] as a reason of lower separation efficiency of 4.75-13 mm coal. Highest combustible recovery, ash rejection and separation efficiency of, respectively, 78.97%, 63.22% and 42.20% were obtained for Hingula coal sample with original ash content of 44.7%. Recently, in 2013, Mohanta et al. [44] used response surface methodology to investigate the effect of gas velocity, bed height and coal to magnetite ratio on product ash and combustible recovery. The resultant quadratic model for both responses, product ash and combustible recovery, determined gas velocity as main effecting parameter and gas velocity and coal to magnetite ratio interaction with maximum interaction level. Repeating tests for determined optimum operating conditions reduced coal ash content from 39% to 32% with 77.4% combustible recovery and Ep of 0.115.

Sahu and colleagues [45] studied magnetite medium stability in a 10 cm cylindrical bed and then scaled that up to a 600 kg/hr (solid flow rate) continuous fluidized bed separator at Institute of Minerals and Materials Technology, Bhubaneswar, India. Several bed stability characterization criteria were discussed and measured for the scope of obtaining a non-bubbling fluidized bed. With fluidized medium average density of 1.6 g/cc, they removed around 6% ash of the 6-25 mm coal, where the yield of separation determined to be 60%-72%. High amount of near separation gravity materials reported as a reason for poor ADMFB separation efficiency (experiment Ep of 0.12).

Sahan and Kozanoglu [46] of Lehigh university of Pennsylvania, USA, studied the effect of main operational parameters, namely bed height, coal to magnetite ratio, superficial air velocity and time on separation performance of a 15.2 cm cylindrical bed using one factor at-a-time method. Four different size fractions (in range of 44 to 300 μm) of coal were added to the fluidized magnetite

medium. Various optimum operating conditions for parameters were found for different feed size ranges. They found that, in general, higher separation time (necessarily more than 30 s), lower bed height (around 3 cm) and coarser feed particles improve separation performance. High inter-particle cohesive forces were observed for 44 to 106 m particles. Best sulfur removal between 65-72% was obtained for +180 to -300 μm particles when coal to magnetite ratio of 1.6 and air velocity of 2-2.75 times of minimum fluidization velocity was used. Sahan [47] suggested that for uniform and stable fluidization status the air velocity should be kept around two times of the minimum fluidization velocity (1.75 to 2.75 times). Higher coal-to-magnetite ratios (one to two) were suggested while for deep beds lower ratios (0.1 to 0.7) improved separation efficiency. Bed slugging and channeling was observed for finer (-140 mesh) coal samples.

Sarunac and others [17], from energy center of Lehigh University, USA, in conjunction with Great River Energy performed experiments in a moving two stage fluidized bed, to achieve coal beneficiation and drying simultaneously. The bed was designed in a way that the segregated high density mineral matters (rich in sulfur and mercury) were discarded at first stage while lighter particles were then passed to the four connected drying zones; forming second stage to form dry product. The rejected proportion of feed at first stage was carrying 2.9 to 3.4 times more sulfur. 22% and 34% reduction in sulfur and mercury was obtained, respectively, due to density base separation phenomena in first stage where the segregated stream had in average 15% more mineral matter.

Choung et al. [48] used a 4 cm column to investigate the effect of medium size, feed size air velocity with one factor at-a-time method. Magnetite particles with different size ranges (between 0-0.3 mm) were used to deal with coal of <6 mm. It is found that, better separation (Ep of 0.03) is achievable for coarser coal particles (3.35-5.6 mm) while separation efficiency deteriorates (Ep of 0.1) by decreasing coal size (0.42-1 mm). Application of finer magnetite improved separation efficiency for finer coal by providing stable fluidized environment where increasing air velocity for fluidizing bigger size medium imposes circular motion to the bed. Ideal size of magnetite was identified to be 45-75 μm, while

finer magnetite powders (<45 μm) increased bed viscosity and deteriorate separation efficiency. It is reported that lower bed heights could improve separation efficiency.

Mak et al. [49] performed a series of experiments in a 20 cm cylindrical bed to investigate the potential of air dense medium fluidized bed separator on removal of ash or other unwanted components of coal such as sulfur and mercury. Here also magnetite particles were selected as fluidization medium for coal samples in different classes of 1 to 22.6 mm. It is reported that, the optimum air velocity (6 cm/s) is insensitive to coal size [49]. The Ep value decreased once coarser coal particles are introduced to the separator (0.1 to 0.03). 58% ash rejection (9% absolute decrease) with separation yield of 80% and combustible recovery of 89% was reported as the best separation results for coal of 5.6-22.6 mm particle size. It is also found that due to strong association of mercury and ash forming minerals, ADMFB separator could be used as pre-treatment choice for mercury removal prior to burning in power stations. An acceptable accurate linear correlation between mercury and ash rejection of the ADMFB products established based on the test results and measurements. 60% rejection of mineral matter resulted in 58% mercury rejection.

Prashant et al. [50] performed separation tests on a cylindrical and rectangular batch beds to obtain the effect of separation time on apparatus performance. They used magnetite and silica sand as fluidization medium and reported not significant change in separation performance when either of mediums was used. Optimum separation air velocity for sand and magnetite was determined to be 5.5 and 4.5 cm/s, respectively, resulting in ash reduction from 25% down to 10 with 80% yield. Also for a certain yield, 1 min separation time resulted the lowest product ash content when compared with 30 s and 5 min separation times.

Some ideas rather than employing a simple fluidized bed (single solid type used as media) were put in practice to affect segregation of high ash and low ash particles in coal by improving viscosity, uniformity and stability of the bed. Employing a mixture of two solids (with different size and density) as fluidization

medium, utilizing vibrating and magnetic field energy and multi-density beds for obtaining three classified products in single step separation, are some of the referable ideas which have been put in practice to enhance fluidized zone; where some promising results were also obtained. For instance using mixture of fine coal and magnetite powder as fluidization medium is investigated by some researchers at CUMT to improve the stability of the fluidized bed [27, 28, 51]. Lower average density of bed, some improvements in separation efficiency and increase in capability of the apparatus when dealing with finer coal particles are reported as result of mixed medium application. It has been explained that that fine particles can enhance fluidization of coarser medium by acting as lubricant between them. Luo and colleagues [51] added 0.45-0.9 mm coal particles to the magnetite and studied bed density stability (uniformity of bed density) in a pilot scale bed. They found that the fine coal is distributed almost uniformly (mass and particle size distribution) in depth and along the bed. He et al. [28] studied the effect of mixing fine coal particles with magnetite in bed density stability at 15*20 cm box column and a 5 t/hr continuous fluidized bed. The bed density was measured at different horizontal and vertical locations in bed, operating at a range of air velocities (8.2-8.45 cm/s) and fine coal (0.15-0.3 mm) to magnetite ratios. They found that adding up to 14.2% fine coal (by weight) is not affecting bed density uniformity in terms of distinguishable density stratification zones. Using mixed medium in a 5 t/hr continuous pilot separator, 6-50 mm coal sample was treated with separation Ep of 0.045. Tang et al. [27] suggested adding of <4.5% of 1-3 mm coal particles to magnetite medium can be helpful for increasing separation quality. In their study they showed that adding more than 4.5% 1-3 mm coal could reduce or eliminate density stability, by coal zone stratification in bed, and consequently deteriorating separation performance of the bed.

Fan et al. [52-54] and Luo and colleagues [55, 56], applied magnetic field to a cylindrical bed to improve bed uniformity and avoid back mixing of magnetite powder to beneficiate fine coal particles (1-6 mm). Ep of 0.06 obtained for 40 s separation time at 12.3 mm/s gas velocity. Based on the experiment

results they determined 50 mm as the lower limit beneficiation under magnetically stabilized bed status.

In another study, Jin et al. [57, 58] studied the effect of vertical vibration in a 148 mm cylindrical bed on fluidization and segregation characteristics of a wide range of particles (0.1 to 6 mm) with density ranging between 1.3 and 2.66 t/m^3. They found that vibration can aid fluidization of medium by increasing gas-solid contact and prevent coalescence and growth of bubbles resulting uniform and stable bed. Gas superficial velocities of 1 to 1.5 times of minimum fluidization velocity were determined to result in the optimum particle separation. In the range of studied Geldart A, B and D particles, lower fluidization velocity and larger vibration parameters (vibration angle frequency and amplitude) are suggested for larger Archimedes numbers while opposite of that is suggested for smaller values.

Van Houwelingen et al. [15] investigated the effects of air velocity, composition and moisture content of the coal on the performance of a 160*20 cm vibrating fluidized bed in Delft University of Technology considering one factor at-a-time method. Along the separation tests mixture of 20-30 mm coal particles and shale were separated in a bed of 220 μm (d_{50}) Sand. Increasing air velocity resulted in coal particles lost (to sink zone) where the lost intensified by excess moisture of the feed coal. Higher unwanted species in the feed resulted in better separation. The existence of coal particles versus shale particles in the sink or float zone were used to evaluate the separation performance in conjunction with Ep values.

Luo et al. [11, 40] studied the effect of horizontal and vertical vibration on the contaminant elimination performance of a 2 m long fluidized bed. The performed experiments revealed lower size limit of 0.5 mm for ADMFB separation with magnetite medium. They also determined the critical vibration frequency to restrain bubble formation in the bed. They suggested operation of the bed at frequencies higher than f (Equation 2-5) to break the bubbles where Q and g are the gas flow rate (m^3/s) and gravitational acceleration (m/s^2).

Equation 2-5: $f > \left({}^{6Q}/_{\pi}\right)^{1/5} g^{-3/5}$ [11]

In 2009, Fan and others [59] studied the effect of vibration on separation of coal in the size range of 0.5-6 mm and found that the Ep significantly reduces from 0.15 to 0.06-0.08 in presence of vibration.

In 1977, Beeckmans and colleagues [60] at University of Western Ontario, Canada, started several separation tests on coal and other granular mixtures using a 27.9 cm diameter batch cylindrical fluidized bed [61, 62] and probably the first counter-current cascade semi-continuous fluidized bed separator [60, 61, 63] with a rectangular chamber of 2.44*0.203 m. Beeckmans et al. [60] started counter-current coal-sand separation in the semi-continuous rectangular bed which a baffle chain dipped 50 mm into the bed surface with total depth of 300 mm material to collect the flotsam. 0.91 mm sand particles mixed with maximum 20% of 1.33 mm carbon particles were used as bed body. The jetsam particles moved at the bottom due to gravity force. Better separation of sand from coal at the sand end is obtained compared to the separation of coal from sand at the carbon end of cascade. Beeckmans and colleagues [61] also used the cylindrical bed with several materials such as coal, limestone, magnetite and sand to conduct separation tests. Lighter and substantially larger particles separated rapidly at the surface of the bed. Later Chan et al. [62] and Dong et al. [63] modified the semi-continuous apparatus by relocating the baffle chain from top to bottom or even by replacing the baffle chain with air jet to obtain consistent movement of materials in the bed. Dong and Beeckmans [63] had separated magnetite (444 μm) from coal (1.6 mm) in a salt matrix (346 μm) in the air driven cascade bed at almost the same satisfaction level of the chain baffle bed. Chan and Beeckmans [62] found acceptable separation of coal (153-233 μm) from synthetic or natural pyrite (0.3% of non-liberated pyrite was left in clean coal) in the bottom baffle chain set up.

Double density bed concept is also examined by Wei and others [64] via specially designed bed structure for obtaining three different products (clean coal, middling and tailing). Bed structure consisted of two rectangular prisms connected via a pyramidal piece with the bigger prism on top. Magnetite powder and magnetic pearls were used, respectively, as the heavy and light dense

mediums for the lower (high air superficial velocity) and upper (low air superficial velocity) parts of the bed. A wide range of Ep value between 0.06 and 0.11 was obtained for lighter or heavier separation zones when model materials are used in separation tests. The average densities of lighter and heavier zones were 1.52 and 1.87 g/cm^3, respectively. They showed that by increasing gas flow rate, the bed zone density and Ep values are increasing in the upper zone of the bed while vice versa occurs at the lower (high density) section of the bed. A summary of some of the conducted research works is presented in Table 2-1 with some more details of used apparatus, materials and settings as well as outstanding points of each study.

Table 2-1: Summary of coal separation research work performed by ADMFB

Investigator	Bed geometry (cm)	Fluidization medium	Medium size (μm)	ρ_{medium} (g/cm^3)	H_{bed} (cm)	Gas velocity (cm/s)	d_{coal} (mm)	Separation time (s)	C/M ratio	Evaluation criteria	Outstanding specification	Parameters investigated
Zhenfu et al.[25]	200*500*35	Magnetite / Magnetite-coal	150-300	B=1.95	35	11.1	6-50	Continuous	--	Ep;0.05-0.055	Continuous (50 t/h)	Bed effective density adjusted by adding fine coal (<1mm) to system
Zhenfu et al.[37]	Rectangular (200*500*35)	Pearls (magnetic)	47-74	B=1.57	~40	--	6-50	Continuous	--	Ep;0.05	Continuous (5 t/h)	Studying just separation feasibility
Zhenfu et al.[39]	15*20	Magnetite	K_{50}=210	--	25	6.2	6-50	20	--	Ep;0.03		Studying just separation feasibility
Luo et al.[40]	Rectangular 20*200*8	Magnetite	74-300	--	7.5	1.65	0.5-6	--	--	Ep;0.07	Vibration assisted	Fine particle separation improvement by applying vibration
Luo et al.[11]	Rectangular 10*10*22	Magnetite	43-74	B=1.95	7.5	1.0	0.5-6	20	--	Ep;0.07	Vibration assisted	Fine particle separation, minimum frequency restraining bubble formation
Fan et al.[52, 53]	Column d@10	Magnetite	K_{80}=90	B=1.78	30	1.23	1-6	40	--	Ep;0.066	Magnetic field assisted	Fine particle separation improvement by applying magnetic field to bed
Wei et al.[64]	Two prism, rectangular	Magnate pearl-magnate powder	K_{50}=63.8 K_{50}=176	B=1.6 B=2.15	--	Q:4-4.6m^3/h	6 & 13	--	Model materials	Ep1;0.06 Ep2;0.07	Double density bed	Three product feasibility study
He et al. [28]	--	Magnate powder & fine coal	150-300 &150-300	--	33	8.2	6-50	--	--	Ep;0.045	Continuous (5 t/h)	Bed density distribution stability when 14.2% fine coal is added to magnetite
Tang et al. [27]	30*30	Magnate powder & coal	74-300 &1-3mm	B=2.3	35	--	6-50 (TB)	--	Tracker balls (TB)	Ep;0.08		Effect of adding coarse coal to magnetite in bed density and separation
Beeckmans et al. [60]	Rectangular (20.3*244*71)	Sand	91	2.65	30	>1.13	1.33	Semi-continuous	--	Accumulation of phases at expected zone	Continuous cascade	Gaining control on particle movement considering horizontal paddle speed
Chan et al.[62]	Rectangular (19*366)	Separation of pyrite from coal	Coal size: 122-360		18	1.8-8.5	0.12-0.36	Continuous	--	Pyrite/ash removal	Baffle chain enhanced	Pyrite/ash separation at continuous counter-current fluidized cascade bed
Mak et al. [49]	Column d@20	Magnetite	75-425	5.1	--	5.8-6.3	1-22.6	480	1/15	Ep, Ash removal		Co-rejection of mercury and minerals, optimum fluidization velocity
Choung et al. [48]	Column d@4	Magnetite	45-300	5.1	2.6-5	2.9-23.4	0.42-5.6	120	20-40%	Ep;0.03-0.1		Studying effect of u and medium particle size
Prashant et al. [50]	Column d@20	Magnetite Silica sand	-- --	B=3.45 2.6	-- --	4-7	1-5.35	30-420	--	Ash removal		Studying effect of separation time and medium type
Mohanta et al. [41]	Column d@15	Magnetite	75-600	4.7	20	19.82	4.75-50	30	--	OE, CR		Studying effect of feed size
Mohanta et al. [43]	Column d@15	Magnetite	75-600	4.7	20	19.82	4.75-50	30	--	OE, CR		Suitability of fluidized bed for coal beneficiation
Mohanta et al. [44]	Column d@15		K_{50}=212	4.7	10-40	17.92-25.46	13-25	30	0.016-0.066	Product ash, Ep, CR		DOE study for the effects of u, H_{bed} and C/M ratio
Chikerema et al. [13]	40*40	Mixture of sand and magnetite	--	--	32	--	9.5-53	5-600	--	Ep; 0.07-0.11		Studying effect of particle size, shape and density
Sahan et al.[45]	Column d@15.2	Magnetite	44-300	5.2	3-12	u_{mf}×(1.4-3.8)	0.44-0.3	30-120	0.1-5.7	Ash, Sulfur removal, Ep	Bubbling bed	Studying effect of u, H_{bed}, C/M ratio and separation time
Van Houwelingen et al.[15]	15*160*20	Sand	K_{50}=220	--	--	5.8-7.16	20-30	--	--	Ep, Coal/shale separation	Vibrating continuous	Studying effect of u, feed composition, feed moisture

H_{bed}: effective bed height, d_{coal}: coal particles diameter, C/M ratio: coal to medium ratio, B=Bulk, OE: Organic efficiency, CR: Combustible recovery

2.6 Statement of the problem

Considering worldwide increasing need for low cost energy which pushes industry to acquire it from low rank coals, environmental issues related to wet coal washing methods as well as their higher moisture content product beside specific concerns of western Canadian coals, such as high sliming tendency of ash forming clay minerals (APPENDIX A) and very cold weather in most coal occurring areas which seriously restricts wet washing methods, the necessity for development of an efficient and reliable coal cleaning method is getting more and more recognition. Application of an efficient low cost beneficiation method in addition to a solution to the mentioned issues and concerns can increase the usable amount of ore by pushing mining cut-off grade to consider higher ash content material as ore in mines and expand coal mine horizons by number or volume through affecting mine design economic scene.

Based on the available dry coal beneficiation methods and also considering results obtained in different research centers (as discussed in 2.5 section), ADMFB coal cleaning seems to be one of the viable alternatives for dry processing of Western Canadian coals. Advantages of the existing dry beneficiation methods as well as ADMFB separators simplicity, lower capital and operational costs due to using lower air flow rates (less dust issues), minimum moving parts, possibility of establishment of small mobile units for on-site beneficiation and simultaneous ability to improve coal calorific value by utilizing waste heat in conjunction with process air to excessively remove moisture, are some additional motivations supporting further study of application of ADMFB separator for coal cleaning.

Although, application of ADMFB in industrial scale is reported in china, there is very little information available on the behavior of this method, hydrodynamics of separation and how various operating parameters interact or affect the performance of these separators. The available results of such studies would cause a definite improvement in the control and optimization of the separation process. The conducted literature review shows that over the years newer concepts are realized and investigated using one factor at-a-time approach

to determine the effect of operating parameters or optimum range of them; usually on high ash coals. One factor at-a-time analysis method may be misleading if the response of the system to the change of one factor depends to the level of second or third parameter (response is correlated). In such case the interrelationship or mutual interactions of the factors will not be recognized, resulting in inappropriate estimation of the overall system performance. This indicates why the parameters mutual interaction should be carefully examined to get more realistic understanding of their effect on the system performance.

As discussed, in most experiments a wide range of feed particle size is used e.g. 6-50 mm. It is vital in a physical separation method to distinguish between size and density effects independently. Small heavy particles in most processes, especially in gravity separation apparatus, act like lighter but bigger particles. Therefore using very wide feed size distribution which is considered as an advantage in some studies, should be reconsidered as it could be one of the reasons of unsatisfactory separation efficiencies of dry methods when are compared with equivalent wet apparatus. Classifying the ROM feed size distribution into a well-adjusted size fractions and investigating each size range behavior and response to the variation of operating parameters have been seen rare in existing studies.

Ecart probable error (Ep) of separation is an old and useful parameter to evaluate or compare separators efficiencies; but there are some concerns regarding the applicability and accuracy of sink float test results and also subjective separation quality determination ranges. In summary, to determine partition coefficient curve and consequently Ep of a separation test, minimum two full series of sink float tests should be performed while several weighting and ash analysis should be performed to finally have enough information to do the calculations and plot the necessary graphs. On the other hand the estimated final Ep number could be different from person to another as slope of a curve (Tromp curve) at its central part (between 25% and 75%) need to be determined. This determination might need some interpolations. Also in case of low rank high clay content coals when aqueous heavy solutions are used (due to safety and health

considerations), some of clay minerals might dissolved in solution which will result in solid-liquid separation issues and also weight losses. Therefore when ash forming minerals tend to slim fast, heavy liquids should be chosen properly to minimalize error level of the final Ep value. Any of these factors could impose error in final process Ep.

One other problem when using experimental or model Ep values for operation comparison is that, there is no clear limit defined for Ep to evaluate individual separation process. The lower Ep (close to zero) is much preferred as describes a separation close to ideal separation case. But for other numbers every author defines or interprets the resultant Ep, e.g. some consider 0.09 as very good separation while others might consider it not very good or poor (as seen in Table 2-1). In order to make the results of analysis comparable (even universally) there is a need to define a parameter more meaningful, comparable and realistic to interpret the obtained results. As postulated, the use of clean coal ash content and a translation of metallurgical wanted species recovery to product in coal beneficiation processes can provide more realistic and clear economic sight and evaluation of the separation process where they are meaningful by themselves and also are comparable from test to test.

2.7 Scope and objectives of the study

Considering the conducted literature survey, some attempts have been made to verify applicability of ADMFB for Canadian coal beneficiation at University of Ontario [60-63] or University of Alberta [48-50] where experiment results showed levels of satisfactory separation. These studies are not comprehensive enough to consider accurately the effect of important operating parameters and their mutual interactions as well as effective range of the parameters on the separation performance of the apparatus. In addition, the possibility of simultaneous coal beneficiation and drying or effect of scale up on separation process when switching ADMFB from batch to continuous mode is not recognized adequately yet in the studies. Therefore in present study an effort has

been made to address some of these issues in more details. The detailed scope and objective of this research work could be categorized as:

As shown, the performance of ADMFB separator is significantly affected by operating parameters and their magnitudes is of great importance from operating and controlling standpoint.

Based on these findings the main objective of this research work is to investigate the effect of critical operating parameters such as, bed height, separation (residence) time, fluidizing medium size and superficial air velocity as well as the effect of ROM particle's characteristics such as size and ash content on a batch ADMFB separator performance considering possible interactions between parameters by taking advantage of Design of Experiments methods when necessary.

Another aspect in fluidized bed coal beneficiation will be performing continuous separation of high and low ash particles in a small pilot scale continuous ADMFB. Applying the achieved optimum condition (through batch or independently acquired from continuous separation experiments) to a continuous apparatus will provide the opportunity to evaluate the effect of process scale up on separation quality and product characteristics.

Effects of different chemical compounds on the behavior of organic phase or the resultant ash or slag after combustion have been studied extensively in the literature. Therefore the effect of beneficiation on clean coal product or the combustion residual materials characteristics will be assessed and addressed in terms of widely accepted indices. This characterization will cover original ROM coal, clean coal products and their resultant ash XRF, XRD, ultimate analysis, hazardous elements, determination of slagging and fouling indices and fusion temperatures. As the product is intended to be used for power generation, the influence of beneficiation and rejection of ash forming minerals on products reactivity and heat value will also be considered in characterization.

The moisture content of feed decreases the heating value (specific energy) of the product and consequently, the efficiency of the coal fired power plant. It can also affect the performance and accuracy of the separation process by causing

agglomeration of solid particles (ROM-ROM or ROM-fluidization media) as agglomeration of magnetite particles is reported as an issue in ADMFB coal beneficiation. Therefore the opportunity of application of waste heat (from hypothetical power plants) for moisture removal and consequently increasing product useful heating value will be considered by conducting packed bed and fluidized bed coal drying experiments. Some important parameters involving the packed bed or ADMFB coal drying are: time, bed temperature and air velocity (flow rate). Simultaneous or even sequential coal beneficiation and drying could be a strong advantage for application of this method over the all wet coal cleaning methods.

A proper process simulating model will help predicting system response to new inputs (different sample) or change of settings without conducting further experiment, once the effect of operating parameters are established. Such model could be helpful for scaling up of process and industrialization. Therefore efforts have been made to establish, evaluate and validate a computational fluid dynamics model for particle segregation in a gas-solid fluidized bed.

CHAPTER 3

MATERIALS, EXPERIMENTAL SETUP AND METHODS

3.1 Materials

3.1.1 Coal samples

Two different types of coal samples in terms of rank and ash content were used to evaluate the performance of the ADMFB separator i.e. Boundary Dam (BD) lignite coal as the low ash coal sample and Genesee (GE) sub-bituminous as medium to high ash coal sample. Both samples were first crushed down to smaller than 13.2 mm, and then divided into several 1-2 kg index samples by a riffle after homogenizing. Particles of each index sample were divided into four size fractions, namely very fine (0-1 mm), fine (1-2.8 mm), middle (2.8-5.6 mm), and coarse (5.6-13.2 mm) and three size fractions (fine, middle and coarse) were used in beneficiation experiments. Similar size fractions of index samples were mixed together, for homogenization purposes, to obtain necessary amount of each size fraction to perform the separation tests. The results of proximate analysis of the samples are presented in Table 3-1.

Table 3-1: Proximate analysis of BD and GE samples (average of multiple measurements)

	GE				BD			
	Very Fine	**Fine**	**Middle**	**Coarse**	**Very Fine**	**Fine**	**Middle**	**Coarse**
Mass weight (%)	17.5	18.4	20.7	43.4	20.6	20.4	31.5	23.5
Moisture (%)	12.3	10.3	14.4	13.6	22.1	21.5	20	17
Volatile matter (%)	25.1	27.4	28.3	31.4	39.5	40.5	40	39.5
Ash (%)	45.4	35.5	31.5	26.5	18.2	14.4	12.5	11.7

3.1.1.1 Petrographic images of coal samples

Ash minerals distribution in coal phase determines the maximum possible separation extent obtainable by physical separation methods. Therefore some polished sections, using epoxy resin, were prepared to study coal-mineral liberation of the two coal samples.

Index samples of both coals (~200 g) were prepared and after drying in vacuum drying oven (Yamato scientific America, Inc. DP43), were crushed stepwise to finer than 1 mm. Different size fractions (0-180, 180-325, 325-500, 500-850 and 850-1000 μm) were generated through sieving. Epoxy resin and solid particles were mixed, and viscosity of the mixture was reduced by heating up to 70˚C to further release the entrapped bubbles in the epoxy or the attached ones to the particles. The mixture temperature reduced before adding hardener to that. LECO Spectrum system^{TM} 1000, automatic polisher was used to polish samples once, epoxy resin was cured. 2-Propanol (99.9%) was used as lubricating media while polishing the samples as, ash minerals were highly dissolvable in water. Use of water while polishing the samples created some holes due to washing away of mineral particles reaching the surface.

Keyence Digital microscope VHX-2000 with a VH-z250R lens (RZ x250-c2500) was used to prepare images. Using automatic stitching option of the microscope, sample surface was scanned (up to 19*25 images at lens magnification of X300). Two sample images of BD and GE coals, taken under polarized light, are presented in Figure 3-1 and Figure 3-2, respectively. It should be mentioned that, under polarized light, mineral particles appear in bright color while, amorphous phase (coal particles) appear black. Some of the completely liberated (free) coal and ash minerals were marked in figures (as C and M) for more clarification.

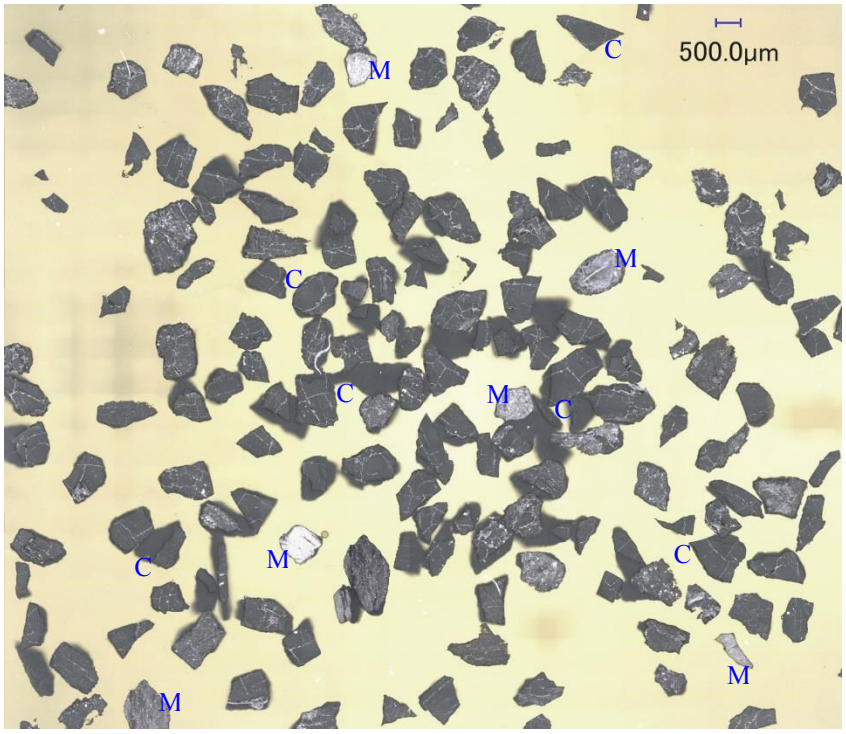

Figure 3-1: Polished section image of BD 500-850 µm particles (polarized light),
C: coal, M: mineral

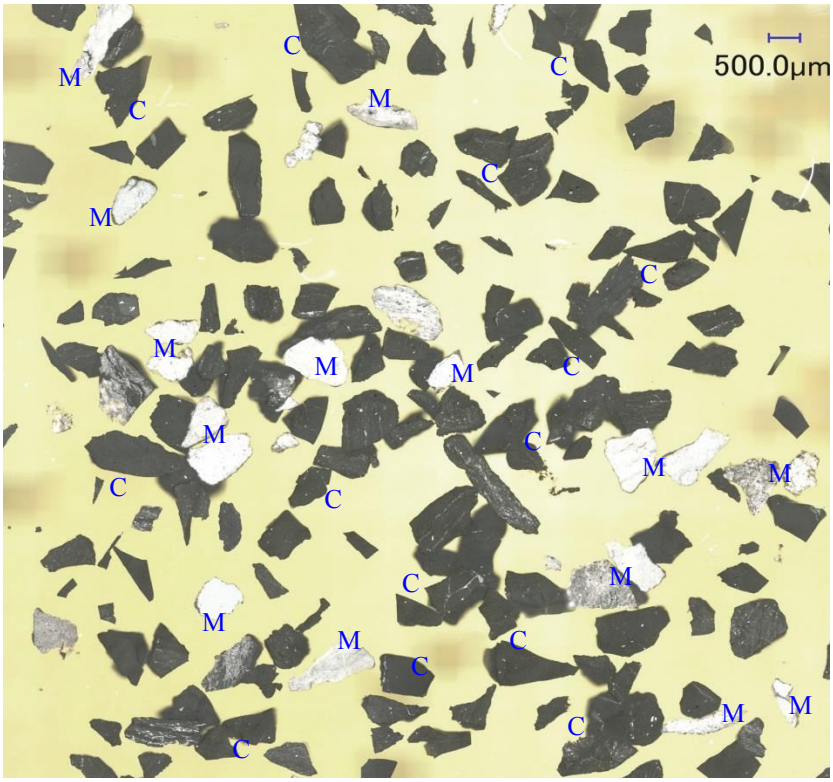

Figure 3-2: Polished section image of BD 500-850 µm particles (polarized light)
C: coal, M: mineral

Study of the prepared images revealed that large number of completely liberated coal and mineral particles are detectable for GE samples. The amount of interlocked particles were low for bigger GE samples where, even reduced more once images of finer size fractions were studied. The higher fully liberated coal and ash particles could be deduced initially if high the ash content of GE coal was taken into consideration. Considering low amount of interlocked particles it is possible to conclude that, majority of ash minerals were either intrinsic mineral matters occurring in the form of segregations and lumps or bands in the coal seam or were extraneous materials mixed from top and bottom surrounding layers while mining it. Of course the level of extraneous material mixing depends on the method of mining and level of mechanization.

Observations were completely different for BD samples as very little number of free ash particles was observed for BD samples even for finer size fractions. Most of particles with majority of coal phase in them, presented lighter colors under polarized light or some degrees of darkness once white light was used. That was due to distribution of ash phase (intrinsic or inherent mineral matter) in coal phase. Intrinsic mineral matter could originate from the source plants or very fine layers of mud lying between plants in the formation stage. Considering such severe interlock of coal and ash phase, utilization of physical separation methods for obtaining high reduction in ash content seemed to be highly challenging.

A brief discussion on ratio of free heavy particles (ash minerals) and lighter particles (organic or combustible phase) is addressed in APPENDIX A.

3.1.2 Fluidization medium

According to Table 2-1, magnetite power or pearls are the most popular fluidization medium but due to high bed viscosity when operated at near minimum fluidization velocity (which may cause misplacing of particles and consequently lower separation efficiency) and also high sensitivity of magnetite powder to the bed moisture content (which causes particles agglomeration and consequently loss of bed stability) silica sand is selected as fluidization media. Silica sand is easily obtainable almost everywhere. It is cheap and has almost no

preparation cost (compared to magnetite or process costs) if used in such processes as consumable but highly recoverable medium.

Therefore silica sand with the density of 2.6 g/cm^3 from SIL Industrial Minerals is used as fluidization medium. As discussed, the physical properties of the medium particles (i.e. size, density and sphericity) are the dominant parameters affecting the bed stability, minimum fluidization velocity and then the fluidization regime of the bed. All sand stack was screened to a narrow particle size ranges and then two types of fluidization medium, coarse and medium, was prepared by mixing segregated size fractions of silica sand. The mean particle sizes of coarse and fine media were determined to be 390 and 275 μm, respectively, where both could be classified as Geldart group B [29] particles.

3.2 Experimental set-up

For the purpose of this study, three different set ups were used; two batch ADMFB and a continuous ADMFB apparatus. The basic structures of both batch apparatuses are the same except the bed diameter. They consist of a plenum chamber, air distributor and the bed body. The coal beneficiation experiments are conducted using bigger batch bed and the small bed is used to perform coal drying experiments. Images of both big and small batch ADMFB are presented in Figure 3-3 a-b.

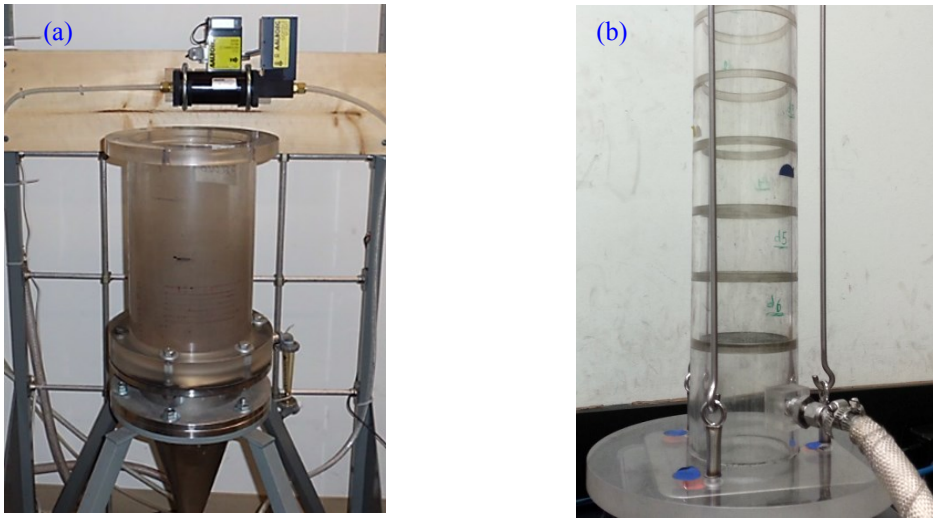

Figure 3-3: Batch ADMFB set up, (a): big bed, (b): small bed

The big batch ADMFB unit (Figure 3-3 a) is made of a 40 cm height Plexiglas cylinder with 20 cm inner diameter fitted on a 0.3 cm metallic porous plate as air distributer with an average pore size of 40 µm (Matt Corporation in Farmington, Illinois). The same materials are used in the small bed, except the 7.5 cm Plexiglas cylinder which is designed to be detached as 5 cm pieces for easy sample discharging.

An Aalborg GFC67A thermal mass flow controller with an accuracy of ±1% is used for air flow adjustments. The filtered exhaust air by Nederman filter box (Helsingborg, Sweden) was discharged into the atmosphere. A schematic diagram of the experimental setup is presented in Figure 3-4. The air heater was switched off along separation experiments.

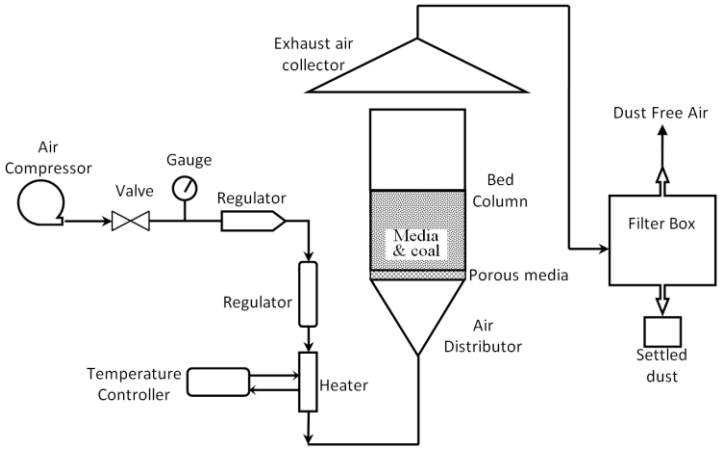

Figure 3-4: Schematic diagram of the experimental setup

The continuous ADMFB apparatus consisted of four fully connected cells called A, B, C and D as illustrated in Figure 3-5. Walls of each unit are made up of 1 cm Plexiglas and the same metallic porous media is used as air distributor. Air flow rate to each unit is adjusted by an Aalborg GFC67A thermal mass flow controller individually. Sand hopper is connected to the lower side of the cell A using a metallic pipe. The product discharging channel is positioned prior to tailing gate position, to collect the floating particles before entering the turbulent zone created by discharging of materials from the bottom tailing gate.

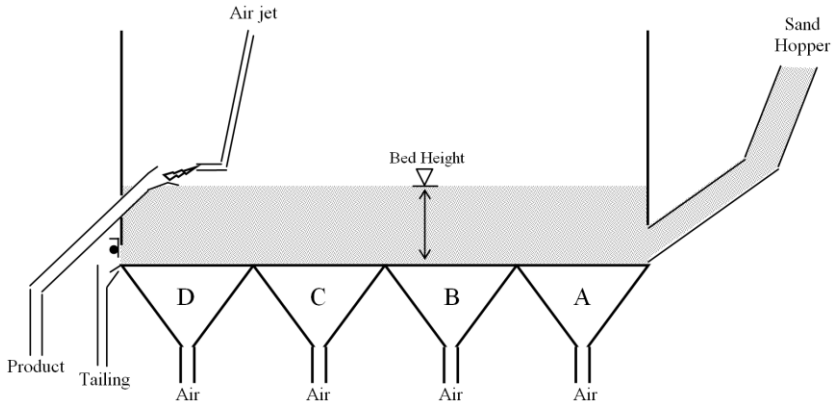

Figure 3-5: Continuous ADMFB apparatus.

3.3 Separation experiments procedure

Using three size fractions of two types of coals, several separation and drying experiments were performed according to the following general experiment trends.

3.3.1 Batch experiments

For batch beneficiation tests, the designed bed height was achieved by filling the bed chamber with a pre-determined weight of sand particles. A stream of air was allowed into the bed column (for less than one minute) to unlock particles from each other and retain stable status. Test feed particles were poured uniformly on surface of the bed and the bed was frozen by a sudden stop of the fluidizing air once the designed experiment time is reached. Total bed height was divided into 5 cm intervals (cut levels) and the sand and segregated coal particles were discharged carefully from each interval by means of a scoop. The sampling intervals were called L_1 to L_{end}, numbering from top layer to the bottom one. A schematic view of bed with five layers is presented in Figure 3-6.

Coal particles of each layer were separated from accompanying sand by an 800 μm sieve, weighted, sealed and processed later to generate representative samples for proximate, ultimate and other characterization experiments as will be discussed in the following sections. The coal particles collected from top layer (L_1) are described as clean coal.

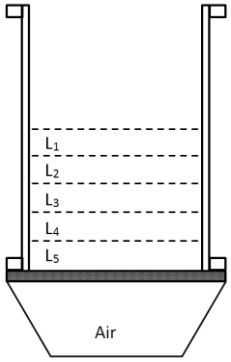

Figure 3-6: Schematic view of batch ADMFB column with five layers

3.3.2 Continuous experiments

The general procedure for continuous set-up operation is almost the same as batch with some exceptions due to apparatus configuration differences. At the beginning, mass flow controllers of cell B, C and D were switched on to gain and retain the designed air flow rate. Then sand was allowed into bed chamber by opening the sand hopper gate. Bed height was adjusted through controlling the cell A air flow rate and level (position) of the product channel. Once bed steady state flow of sand was obtained after opening bottom tailing gate, coal particles were fed continuously to the surface of the moving sand. Two solid streams were collected at the end of machine separately one from product channel and the other from tailing gate. At the end of experiments when air stream was stopped, particles staying higher or lower than product channel (along with the remaining sand in the bed) were added to the product or tailing streams, respectively. Collected coal particles of each stream were treated the same as batch products after separation from sand. An air jet was used to assist particles movement in the inclined product channel, fabricated from steel sheet.

3.3.2.1 Packed bed drying experiments

For the packed bed coal drying experiments, hot air was passed through the bed until internal space of bed reaches a stable temperature. Two thermocouples (one close to bed bottom and one 5cm above expected surface of solids in bed) were used to check steady state temperature in bed. For a short

period of time, heated bed was detached from hot air and weighted on a balance (accuracy of 0.1 g). The inlet air flow rate was adjusted by the Aalborg GFC67A thermal mass flow controller and an inline heater (controlled by Fluke 54IIB dual input digital thermometer) was used to increase and retain its temperature at the determined level. Attaching hot air to bed, prepared coal sample with known initial weight was added to empty the bed. Bed body and drying coal mass were measured in determined time intervals (1, 2.5, 5, 7.5, 10, 15, 20, 25 … minutes) by detaching bed from air using quick connection. At the end of experiment, all coal particles were discharged from bed, weighted and sealed for further characterizations.

3.3.2.2 Fluidized bed drying experiments

Almost the same set-up configuration and procedure as packed bed drying was used for fluidized bed coal drying. Initially bed was filled with determined volume of sand and then hot air was allowed through that. Once stable thermal condition was reached (checking through two thermocouples close to sand surface and 5 cm above that), the weight of bed and sand was measured and after connecting air, known amount of coal was added to the fluidized sand bed. Bed and solids mass was measured in the determined time intervals (1, 2.5, 5, 7.5, 10, 15, 20, 25 … minutes) by disconnecting air from bed and reconnecting it after. Finally all solids were discharged from bed and coal particles were separated from sand through sieving. The separated dried coal particles were weighted and sealed for further characterizations.

3.4 Sample characterization

Selective removal of some particles from head sample is the main purpose of beneficiation experiments. On the other hand, such selective removal can affect or change physical and chemical properties of the particles in clean coal or tailings compared to initial head sample. Therefore several characterization tests performed on selected samples to gain extensive information about head samples and separated particle's properties and characteristics. It should be mentioned that

Canadian center for clean coal and mineral processing technology instruments are used for characterization tests unless otherwise mentioned.

Prior to characterization experiments; index sub-samples were prepared by grinding the whole sample to finer than 200 μm, mixing and then sub-sampling. The proximate analysis of the samples were performed by either of Barnstead Thermolyne furnace (Muffle furnace model: 6000) or LECO TGA701 after drying samples in vacuum oven for 8 hrs. The amount of moisture removed in vacuum oven (according to weight of sample before and after drying) was taken into consideration once reporting the moisture content of the samples. For proximate analysis in Thermolyne furnace, ASTM methods of D-3173, D-3174, and D-3175 were followed for determination of moisture, ash and volatile matter of the samples, respectively. Also ASTM D-7582 was followed in operation of LECO TGA701 for samples proximate analysis. Also Emiteck K1050X low temperature asher (K1050X Plasma Etcher/Asher/Cleaner, Quorum Technologies Ltd.) is used to produce ash samples for XRD analyses.

For ultimate analysis of the samples Vario Micro CHNS analyzer (USA) is used. Elemental, oxide and mercury analysis were performed by ICP-MS (Perkin Elmer's Elan 6000 ICP-MS), EDAX Energy dispersive XRF microprobe system (Rhodium X-Ray source) and Direct Mercury Analyzer (DMA-80), respectively. Rigaku Co-Kα XRD analyzer (Department of Earth & Atmospheric Sciences, University of Alberta) is used for crystallographic studies of low temperature ashes.

Combustion rate of the head samples and clean coal products were measured through burning samples in Q600 thermogravimetric analyzer (TGA-DSC, TA Instruments, USA). Preiser automated ash fusion furnace (test performed by Birtley Coal & Minerals Testing Division, Calgary) was used for samples ash fusion temperature determination.

3.5 Optimization of process operating parameters

3.5.1 Design of experiments and response surface methodology

AS discussed previously; the performance of ADMFB separator is significantly affected by operating parameters, and their magnitude is of the great importance from operational and controlling standpoint. In most of the studies one factor at-a-time method is used to study the effect of parameters on the performance of ADMFB for coal cleaning, discounting the possibility of mutual interaction of the operating parameters (in case of interaction, more than one factor should be considered to explain the output) due to complex hydrodynamics associated with the fluidized beds. Such interactions could mislead the effectiveness of certain parameters as well as their effective and functional range. Therefore in this study, the effect of critical operating parameters on the separation performance of the batch and continuous ADMFB was studied by taking advantage of response surface methodology (RSM) and design of experiments (DOE) methods to recognize possible interactions.

RSM supported by DOE combines both mathematical and statistical techniques useful for modeling and analyzing engineering problems, in which a dependent response of interest is influenced by series of independent process parameters [70, 74, 75]. The main objective of this method is to analyze the effect of independent input variables on the interested output (response), and obtain levels of operating parameters optimizing the response function.

In order to practice RSM following steps should be followed:

i- Conducting a series of experiments to collect a range of reliable measurements of the interested response.

ii- Establishing a functional relationship between response variable and the independent input parameters with the best fit to generate the response surface.

iii- Representing the direct and interacting effects of the input parameters on the responses via two dimensional or three dimensional plots.

iv- Determining a set of input parameters based on the response surface to fulfill the optimum response condition. The optimum condition may not fall in the range of variables examined.

v: Verifying the model by repeating the obtained optimal input set, to check for the prediction validity of the model as well as reproducibility of the output response [70-72].

Full factorial, partial factorial and central composite rotatable design are the most common DOE methods used for process analyses. Full factorial design methods are used when two or more independent input variables are involved. In full factorial design all possible combinations of the input variables (possible conditions) are taken into consideration leading to larger number of experiment trials if the number of input variables is big. The total number of experiments for a k input variables at m levels will be $m^k + n_c$, where n_c is the number of replicating experiments, used for evaluating repeatability and independent estimation of the experiments error. An example full factorial matrix of variable levels for studying three variables (A, B and C) at two, high (+1) and low (-1), levels are presented in Table 3-2. The raw number 9 presents the repeating test condition (could obtain any other levels).

Table 3-2: Full factorial design experiment settings for three input variables at two levels (+1, -1)

Run	A	B	C
1	+1	+1	+1
2	+1	+1	-1
3	+1	-1	+1
4	+1	-1	-1
5	-1	+1	+1
6	-1	+1	-1
7	-1	-1	+1
8	-1	-1	-1
9	0	0	0

Central composite design is other alternative for this study as it gives almost same information as three-level factorial design, while requires many

fewer tests than the full factorial design. Also central composite design is one of the most common designs fitting second-order polynomials which can reveal non-linear interactions between parameters as well as linear interactions that are important in this study [70, 73]. Total number of tests in central composite design is a function of the standard factorial runs, 2^k, axial runs, $2k$, and replicate tests at center point, n_c. It is important to assume the replicating tests at center point of design. Total number of experiment for a central composite design consisting k variables at m level will be $2^k + 2k + n_c$ [70, 71, 73]. Example central composite design matrixes for studying three variables (A, B and C) is presented in Table 3-3. The number 15 presents the repeating test condition.

Table 3-3: Central composite design experiment settings for three input variables with one central point run

Run	A	B	C
1	0	1	0
2	0	-1	0
3	-1	-1	1
4	1	1	1
5	0	0	-1
6	1	0	0
7	-1	-1	-1
8	-1	1	1
9	1	-1	-1
10	1	1	-1
11	1	-1	1
12	-1	1	-1
13	-1	0	0
14	0	0	1
15	0	0	0

3.5.2 Response surface function development

In the RSM, if the independent input parameters (x_1, x_2, …,x_k) are assumed to be continuous with a negligible measurement error, then the random response variable (y) could be presented functionally as in Equation 3-1 [71, 72, 74-76].

Equation 3-1:

$$y = f(X_1, X_2, ..., X_k) + \varepsilon = \beta_0 + \sum_{i=1}^{k} \beta_i X_i + \sum_{i=1}^{k} \beta_{ii} X_{ii}^2 + \sum_{i<j}^{k} \sum_{i=1}^{k} \beta_{ij} X_i X_j + \varepsilon$$

where, ε is the error component of the response.

The response surface could be established based on $f(y-\varepsilon) = \hat{y}$ values. Usually first- or second-order polynomials are used to present the response functions, where the residual error least square method is used to determine the coefficients. The final fitted equation for response surface is presented in Equation 3-2, where $\beta_k s$ are presenting the fitted coefficients [74].

Equation 3-2: $$\hat{y} = f(y-\varepsilon) = \beta_0 + \sum_{i=1}^{k} \beta_i X_i + \sum_{i=1}^{k} \beta_{ii} X_{ii}^2 + \sum_{i<j}^{k} \sum_{i=1}^{k} \beta_{ij} X_i X_j$$

It should be reminded that, this correlation is valid in the range of tested operating conditions and is very useful for studying the relative influence of the effective variables, their interactions or to get a rough estimation of the system performance.

As various inputs and responses have different scales, and usually non-comparable, normalization concept should be applied before performing the regression and calculating the coefficients. Values are usually normalized in to the [-1 , 1] intervals through using Equation 3-3 where X_{norm} presents the normalized version of X_i. Under such normalization, all parameters are equally scaled [71, 74, 77].

Equation 3-3: $$X_{norm} = \frac{2X_i - \left(X_{\max} + X_{\min}\right)}{\left(X_{\max} - X_{\min}\right)}$$

3.5.3 Response function evaluation

To evaluate the reliability (quality) of the suggested model for a response variable, several statistical justifications should be satisfied. The model and its

component should be verified through analysis of variance (ANOVA), R^2, adjusted R^2, lack of fit and coefficient of variation (CV) tests.

Results of ANOVA test are used to verify the significance of the effect of each parameter (X_1, X_2, …,X_k) or their interactions on the response function. ANOVA test uses all collected data at once which makes it more reliable in interpreting the results than the one factor at-a-time methods. Usually, a significance level of 95% or a p-value less than 0.05 is considered satisfactory in engineering analyses. Also terms with 0.1 p-vales are considered marginally significant.

R^2 evaluates the proximity of the model predictions to the experimental results. R^2 is a relative value ranging between 0 and 1 where high values (very close to 1) imply accurate prediction of the experimental data by the model [77-79]. For instance a 0.9 R-squared value indicates that 10% of the total variations are not explained by the model [77, 78]. Besides obtaining model R^2; the magnitude of adjusted R^2 and its difference from R^2 should also be considered. The adjusted R^2 compensates the inherent increasing tendency of R^2 when new term is added to the model. Maximum adjusted R^2 could be equal to R^2 value.

The lack of fit test determines systematic or randomness origin of discrepancies between measured and expected values of the fitted model by comparison of residual error to the pure error based on the results of the replicated runs in a defined (usually 95% or p-values of 0.05) threshold confidence level. Significant lack of fit means the suggested model is not fitting all the design points well and may occur due to noise [71, 72, 77, 80].

CV is the standard deviation as a percentage of the mean and describes the dispersion degree of the data. The lower CV values imply better reproducibility of the results [72].

3.5.4 ADMFB coal beneficiation process evaluation responses

In this study the application of Ep is avoided since the accuracy of the final value depends largely on precision of the performed sink float tests, reading from graph and correlations, type of heavy liquids used as separating medium and

in general expertise of the researcher in developing partition (Tromp) curve. Also recently strong safety limitations imposed on application of heavy liquids due to toxicity and carcinogenic nature of organic heavy liquids, leads researchers toward usage of water base heavy liquids (such as zinc chloride, Cesium Chloride,...) where makes development of accurate washability cures (in acceptable error level) almost impossible for samples used in this study due to high solubility of ash forming minerals in aqueous liquids.

Also as discussed, there is no clear limit defined for Ep to evaluate the individual separation tests. The lower Ep (close to zero) is much preferred as it describes a separation close to ideal case. However, for other Ep values every researcher defines or interprets the resultant Ep. For instance, some researchers consider 0.09 as an indication of a very good separation while others might consider it as not very good or poor separation. To compare or interpret the separation results, there is a need for more meaningful, comparable and realistic measures to be used rather than Ep, which includes more economical concepts in it, besides describing the separation quality.

Therefore considering coal particles collected from L_1 (form batch ADMFB) or product channel (from continuous ADMFB) as clean coal product; three responses namely clean coal ash content ($CC^{\%}_{Ash}$), combustible material recovery to clean coal (considering two species in coal; combustible and incombustible materials) and separation efficiency of the system were defined as responses and used in comparisons and analysis toward determining optimum operating condition. Combustible material recovery and system separation efficiency are defined in Equation 3-4 and Equation 3-5.

Equation 3-4:

$$R^{\%}_{C\,to\,l_1} = \left({Weight\ of\ comb.material\ in\ L_1}/{Weight\ of\ comb.material\ in\ feed}\right) * 100$$

Equation 3-5: $SE^{\%}_{sys} = R^{\%}_{C\,tol_1} \times R^{\%}_{Ash\,to\sum(Total-L_1)}$

The defined combustible materials recovery can vary between 0 and 100%. The lower boundary means there is no combustible material in the product while minerals can still occur in product portion. The upper limit could occur under two conditions: i) zero separation where the whole feed including minerals are delivered as product ii) completely liberated mineral particles are separated as rejects, so that the product's weight would be less than the feed weight with some ash particles still there.

The system separation efficiency (product of combustible material recovery to clean coal and recovery of ash minerals to rejects) determines the general performance of the separator by tracking both coal and mineral materials destinations along the separation process. In an ideal separation process, it is expected that the high combustible (organic) material content particles to appear in the clean coal product while the high mineral content particles to appear in the high ash product or reject proportion. The separation efficiency can vary between 0% and 100% as both recoveries could obtain any values between them.

Obviously including L_2 (in batch system) into clean coal product can increase both the ash content and combustible material recovery of the separation process. For any industrial decision; the market demands and economy of the separation should also be considered along the theoretical criteria discussing in this study for making final decision.

CHAPTER 4

ADMFB COAL BENEFICIATION AND OPTIMIZATION

4.1 Introduction

Two different coal samples were used in this study, Boundary Dam coal representing a low ash (lignite) coal with lower liberation of mineral species from organic phase and Genesee coal as intermediate to high ash coal (sub-bituminous) with higher liberated mineral phase. In this chapter, the effect of operating variables on beneficiation of each sample as well as optimization of the operating parameters were studied by conducting batch ADMFB separation experiments in the pre-determined range of main operating variables for each sample individually. Experiment pattern determined by DOE methods were applied for each sample, and the results was used for determining optimum separation condition. Beneficiation under optimum variable settings was re-examined to check for reliability of experiments as well as reproducibility of the results. Next, using small batch bed, a series of packed and fluidized bed coal drying experiments were conducted to compare drying behavior of coal in packed bed with fluidized bed under various air superficial velocities and temperature. Later stage ROM beneficiation and clean coal product fluidized bed drying were practiced to find out how effective combination of coal beneficiation and drying could be.

4.2 Boundary Dam coal batch ADMFB beneficiation and optimization

Central composite design method was used to study the effect of superficial air velocity (U), separation time (T) and bed height (H) on ADMFB beneficiation of middle size fraction (2.8-5.6 mm) BD coal using coarse sand (390

μm) as fluidization medium. Three levels were considered for main variables and considering six central point repetitions, 20 experiments were carried out in total. The lowest U was considered to be equal to u_{mf}, (Levenspiel [18]), and air velocity was increased by 10% intervals to generate higher air velocity levels. The H design points were based on the aspect ratio of the bed (h_{Bed}/d_{Bed}) and set to 0.75, 1, and 1.25. Preliminary tests revealed that for separation durations less than one minute, a sufficient segregation of the particles along the bed depth was not obtainable. Therefore, the separation time was considered to vary between 90 s (1.5 min) and 300 s (5 min) during the experiments. More details on operating parameters values, levels and their coding are provided in Table 4-1.

Table 4-1: Variables, symbols, actual and coded levels of parameters used in central composite design

Variable	Unit	Symbol	Low level	Central level	High level
			-1	0	+1
Superficial air velocity	(cm/s)	U	15	16.5	18
Separation time	(s)	T	90	195	300
Bed height	(cm)	H	15	20	25

Beneficiation experiments were conducted according to explained procedure (3.3.1) and necessary information were collected by measurements or analysis based on the discussed methods. The individual experiment settings of the designed experimental points as well as calculated responses are presented in Table 4-2. The runs order was put in random order to minimize the systematic error. The runs 1, 2, 5, 10, 17 and 19 pertain to the repeating experiments. The samples feed ash content, ash rejection of each experiment as well as ash content of the particles in last zone are reported in Table 4-2.

The combined results of all experiments were analyzed separately for each of the response functions by Design Expert 8.0.7.1 [81] to find the best fitting quadratic polynomial models representing the effect of investigated factors on the selected response functions.

ANOVA test revealed that the experiments were not sensitive enough to distinguish between different experiment results in terms of ash content. Thus, no

significant model at 95% confidence level was obtained for the clean coal ash content. The average ash contents of the middle size BD feeds and their standard deviation were found to be 12.46% and 0.8% where, were decreased to 10.09% and 0.58% due to ADMFB cleaning. This shows how narrow the distribution of the clean coal ash content was.

Table 4-2: Central composite design experiment settings and resultant responses

Run	U	T	H	Feed ash (%)	$CC_{Ash}^{\%}$	$R_{C\ to\ L_1}^{\%}$	$S.E._{sys}^{\%}$	Ash rejection (%)	L_{end} Ash (%)
1	0	0	0	11.93	9.11	77.24	33.08	23.61	52.62
2	0	0	0	12.39	10.14	73.95	30.30	18.13	55.11
3	0	1	0	14.19	11.04	71.48	33.12	22.18	49.06
4	0	-1	0	13.36	11.02	76.96	29.38	17.50	46.00
5	0	0	0	12.75	10.45	74.12	30.26	18.06	32.69
6	-1	-1	1	11.45	9.41	87.79	25.88	17.82	70.32
7	1	1	1	13.36	9.86	57.97	34.13	26.18	39.13
8	0	0	-1	12.05	10.22	88.22	23.59	15.22	46.93
9	1	0	0	11.24	9.31	72.66	29.88	17.20	41.49
10	0	0	0	12.45	10.10	70.73	31.21	18.88	41.16
11	-1	-1	-1	12.13	10.39	97.36	17.77	14.36	49.53
12	-1	1	1	13.55	9.81	68.07	35.91	27.59	64.70
13	1	-1	-1	11.78	9.90	83.19	26.25	15.97	30.41
14	1	1	-1	11.96	9.72	77.73	29.84	18.73	28.61
15	1	-1	1	11.58	9.99	58.09	29.49	13.73	19.04
16	-1	1	-1	12.36	9.86	89.83	27.25	20.24	58.27
17	0	0	0	11.56	9.33	77.77	30.16	19.30	50.94
18	-1	0	0	13.14	10.30	84.39	30.35	21.63	71.50
19	0	0	0	12.81	10.81	72.43	29.17	15.64	45.22
20	0	0	1	13.06	11.00	65.43	30.22	15.80	45.10

Figure 4-1 compares the BD feed and clean coal ash contents for each individual test. The maximum, minimum and average ash removals relevant to the samples original feed ash contents were 27.6%, 13.8% and 19%, respectively.

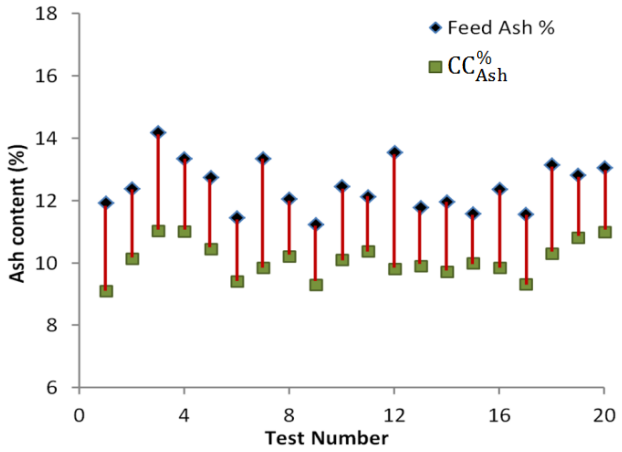

Figure 4-1: The BD middle size feed and clean coal ash contents of the 20 runs

A summary of statistical analysis for combustible material recovery and system separation efficiency are presented in Table 4-3. It is important to note that no 95% statistically significance implies that there is no effect or interaction of the eliminated parameter, but rather than that the effect could be significant at a lower confidence levels. The correlated coded quadratic polynomial models describing the product combustible material recovery and system separation efficiency as a function of significant variables and their interactions are presented in Equation 4-1 and Equation 4-2, respectively. In both models the insignificant terms were eliminated.

Equation 4-1: $R^{\%}_{c\ to\ L_1} = 74.83 - 7.78A - 3.83B - 9.9C + 2.71(AB) + 2.88A^2$

Equation 4-2: $S.E.^{\%}_{sys} = 30.96 + 1.24A + 3.15B + 3.09C - 1.41(AB) - 1.15(AC) + 2.66B^2$

Table 4-3: Results of statistical analysis for combustible material recovery and system separation efficiency

Source	Combustible materials recovery			System separation efficiency		
	Mean square	F-value	p-value Prob.> F	Mean square	F-value	p-value Prob.> F
Model	366.34	38.37	< 0.0001	45.36	25.21	< 0.0001
A-U	605.16	63.39	< 0.0001	15.47	8.60	0.0117
B-T	146.73	15.37	0.0015	99.15	55.11	< 0.0001
C-H	979.8	102.63	< 0.0001	95.65	53.17	< 0.0001
(A B)	58.67	6.15	0.0265	15.91	8.848	0.0108
(A C)				10.67	5.93	0.0301
A^2	41.33	4.33	0.0563			
C^2				35.29	19.61	0.0007
Residual	9.55			1.80		
Lack of Fit	10.73	1.45	0.3573	1.81	1.02	0.5174
Pure Error	7.42			1.78		
R^2	0.932			0.921		
Adj. R^2	0.908			0.885		
C.V.%	4.05			4.57		

Very low values of the Fisher's F tests (P-value<0.0001) indicated that both models were significant. There was only 0.01% chance that recovery or separation efficiency models were originated from noise. Lack of fit was also found to be not-significant for both correlated response functions. Based on ANOVA test (Fisher's F tests) and considering lack of fit test, it could be concluded that both obtained response models (Equation 4-1 and Equation 4-2) were suitable for predicting the target responses within the range of variables tested here.

Larger R^2 and smaller gap between R^2 and adjusted R^2, as well as lower CV values for response models, confirmed the significance of the model and reproducibility of the data points. As reported in Table 4-3, R^2 and CV value for both, combustible material recovery and separation efficiency were more than 0.9 and less than 5%, respectively. Combustible material recovery model presented better R^2 and CV than system separation efficiency model. The actual and model predictions for the recovery and separation efficiency are shown in Figure 4-2a-b.

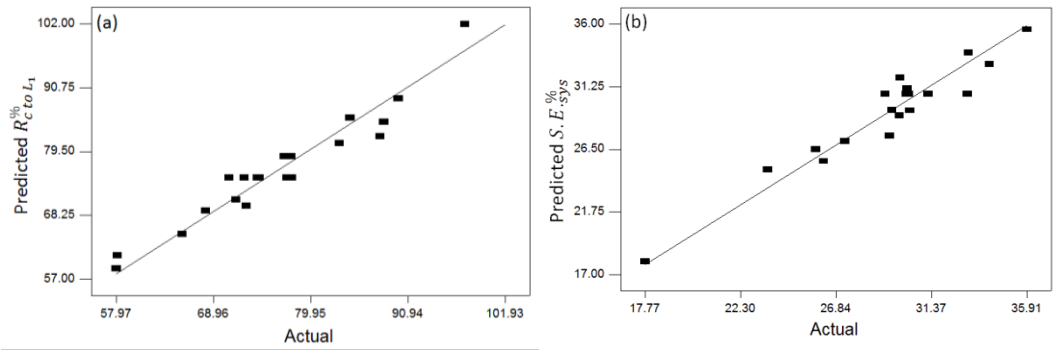

Figure 4-2: Experimental values vs. model prediction, a) combustible material recovery, b) system separation efficiency

4.2.1 Main parameters effect on responses

Based on proposed coded recovery model (Equation 4-1), and their significance levels (Prob. > F in Table 4-3) all three variables had negative effect on the response function (i.e. an increase in U leads to a decrease in $R^{\%}_{c\ to\ L_1}$). The order of influence or effectiveness (imposing more variation on the response when changes were made on one parameter) of operating variables on recovery (according to their coefficients in Equation 3-4) was H>U>T.

The perturbation plot for recovery is presented in Figure 4-3. The effect of all factors could be assessed simultaneously through perturbation plot which shows how the response behaves as one factor varied within the defined range while all other factors were held constant at a reference point. A steep slope or curvature in a factor shows that the response was sensitive to that factor while a relatively horizontal flat line shows insensitivity to that particular factor [71, 81, 82]. It should be mentioned that coded values were used for this plot and middle levels of all variables were chosen as reference point while plotting. As seen in Figure 4-3a (and also confirmed via ANOVA test), all three factors inversely affect the combustible material recovery to L_1. This means that better recovery of coal to clean product can be obtained at lower levels of the operating conditions. The bed height affects response function more intensively as the range of variations imposed by changes of bed height throughout the tested parameter range was the greatest compared to other parameters. The recovery increased

from 64.6% to 84.6% when 15 cm H was replaced with 25 cm H while T and U were kept at their central levels.

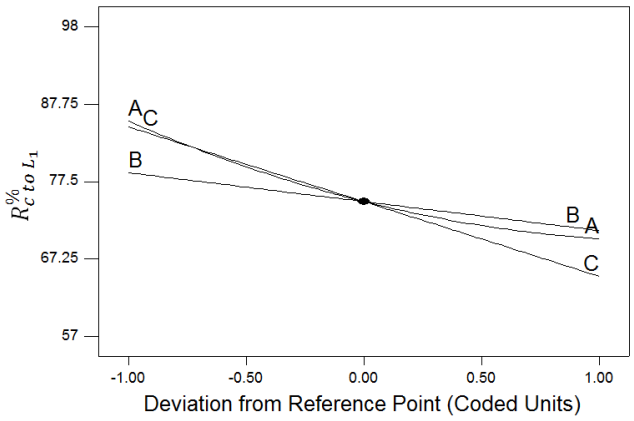

Figure 4-3: Combustible material recovery perturbation plot (for BD sample)

The mathematical presentation of system separation efficiency for BD coal (Equation 4-2) indicated, all three variables had positive effect on the separation efficiency. The order of influence for operating variables was T>H>U.

The perturbation plot of operating variables for system separation efficiency is presented in Figure 4-4. The middle levels of variables were used as reference point while plotting Figure 4-4. It was seen that, all three factors were positively affecting the $S.E^{\%}_{sys}$ and in contrary to the recovery, the separation efficiency increased by increasing the three tested operating variables. The higher limits of U and T maximized the recovery while the quadratic shape of H curve, maximized the separation efficiency somewhere between levels of 0 and 1. The separation efficiency varied from 27.6% to 33.8% when time was increased from 90 s to 300 s. Neglecting the quadratic shape of H, it caused 6% increase of separation efficiency (25% to 31%) when 15 and 25 cm H bed heights were considered. More variation in separation efficiency was achieved when the minimum and maximum points of the quadratic trend were considered instead of start and end points of the curve. The highest separation efficiencies achievable for T and H in their tested operating ranges were 33.8% and 31.6%, respectively.

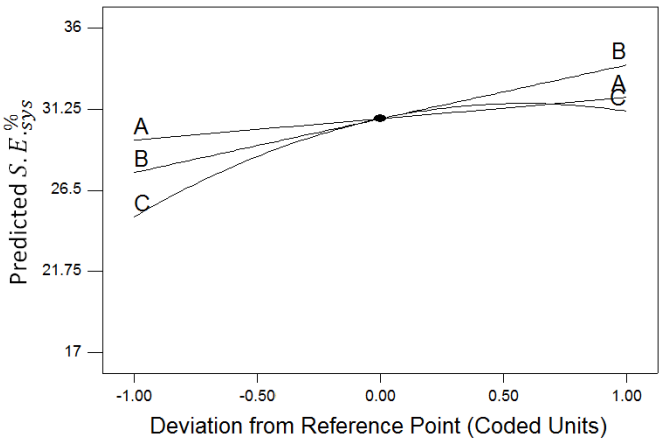

Figure 4-4: System separation efficiency perturbation plot (for BD sample)

4.2.2 Mutual interaction of operating parameters

ANOVA test on the collected data revealed existence of mutual parameter interactions on the assumed responses (combustible material recovery and system separation efficiency). Such interactions occur when the effect of one factor depends on the level of the other factors [73, 81].

There was a significant interaction between superficial air velocity and separation time at a 95% confidence level with positive effect on recovery as indicated in Equation 4-1. This interaction is further illustrated in Figure 4-5. The non-parallel or crossed lines in such plots confirm the presence of an interaction between two variables. Since the general shape of the interaction graph was not changing with H level, therefore the middle level of H was assumed when generating both interaction plots.

The recovery was higher for low separation times across the U range than the high separation time due to the dependency between parameters. The difference between high and low separation time recoveries decreased with increasing U. According to the Figure 4-5 when both U and T were set at lower limit, the recovery of 92% was achievable while got lower to 68% at higher levels of U and T considering central level of H.

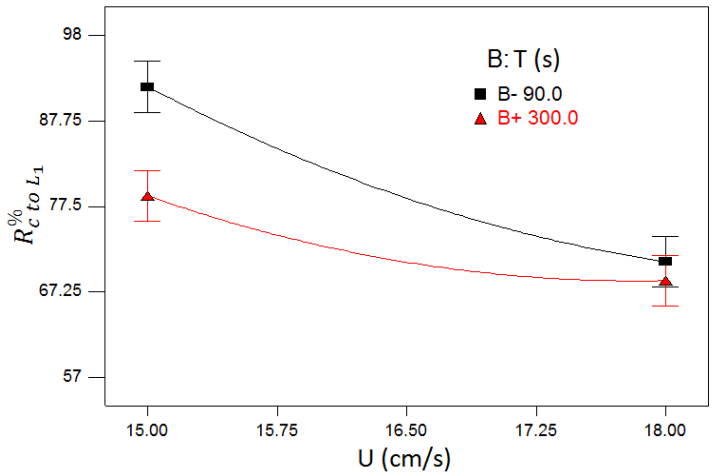

Figure 4-5: 2D plot of mutual interaction of U and T on combustible material recovery at H=0

Considering the positive effect of interaction on the recovery and negative effect of parameters themselves, there seemed to be an opposing effect involved with U and T. This opposing effect also might cause the optimum condition to not to occur at exact lower levels of the U and T. Thus, employing the optimization methods was necessary to make sure that the optimum condition was achieved.

Figure 4-6 presents the effect of U and T and their mutual interaction on the recovery in a contour plot for a bed height of 20 cm. The recovery values for different sets of air velocities and separation times can be extracted from this figure. Figure 4-6 indicates that the recovery was more sensitive to a step size change of U and T at their lower levels, where small changes in the U and T could influence the recovery more effectively compared to their higher levels. Based on this plot, recovery was not affected much by changes in U and T levels when they both are set to level of 0 or higher.

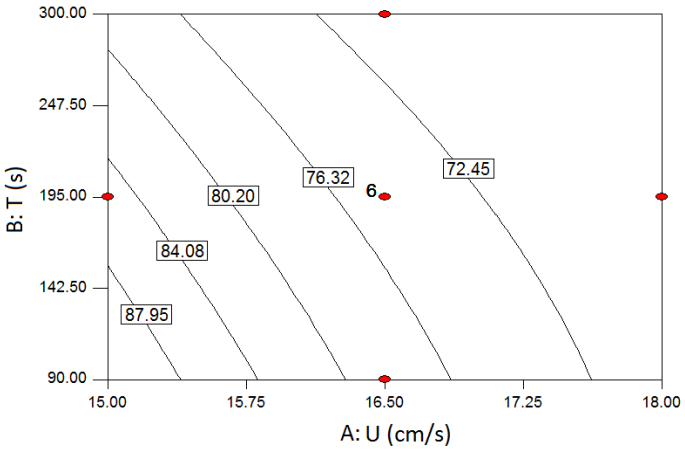

Figure 4-6: Contour plot of combustible material recovery: U, T and their mutual interaction at H=0

Figure 4-7 depicts the 3D response surface plot (graphical representation of the model) of U and T at H of 20 cm.

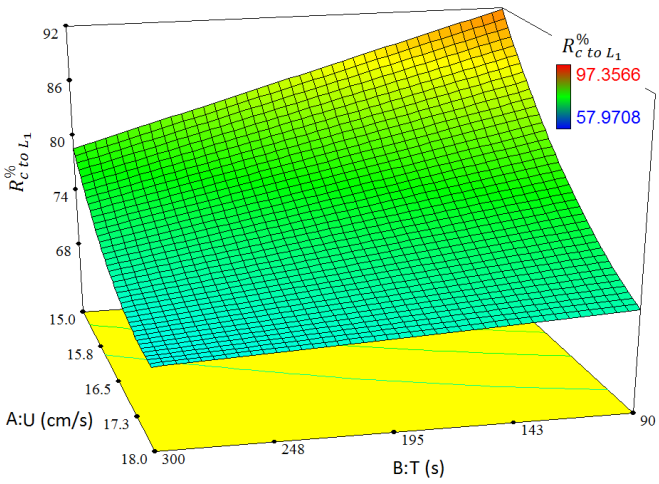

Figure 4-7: 3D interaction plot of U and T at H=0

The combustible material recovery decreased from (almost) 90% down to 70% when U and T levels were increased from -1 to +1 when H=0. Also as seen here, U affected recovery more than T, as the edges of the response surface showed more variation toward U than T.

Two negative mutual interactions between U and T or H revealed (ANOVA test results and Equation 4-2) when separation efficiency of ADMFB was considered as response function for the separation process.

Figure 4-8a-b exhibit the interaction plots of U and T at two different levels of H (0 and 1). As discussed, crossing lines are indication of the presence of parameter interaction. The interaction was much more obvious for 25 cm bed as in Figure 4-8b.

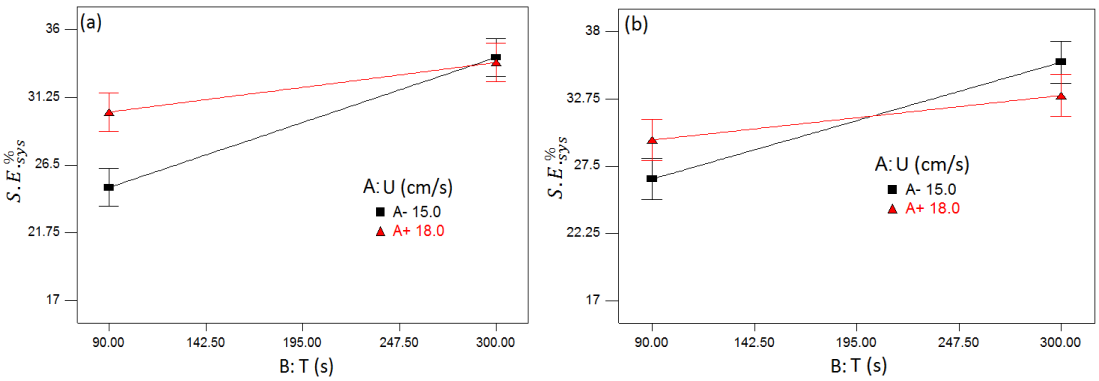

Figure 4-8: Mutual interaction between U and T affecting separation efficiency, a) at H=0, b) at H=1

Figure 4-8a-b shows that, the achieved separation efficiency at each level of U depended on the level of respective T, and vice versa. For low separation times, the separation efficiency was higher for higher air velocities, while opposite happened for high separation times. In both Figure 4-8a and b, the changes imposed on separation efficiency in the range of T, for low level of U was greater than its high level regardless of the H level.

The mutual interaction of U and H is presented in Figure 4-9a-b. Here also the interaction was dependent to the third parameter and was more obvious for the higher separation time. For low bed heights, the separation efficiency was higher for higher air velocities while, opposite happens for high bed heights (particularly see Figure 4-9b). In both Figure 4-9a and b, the changes imposed on separation efficiency, for low level of U was greater than its high level regardless of the T level.

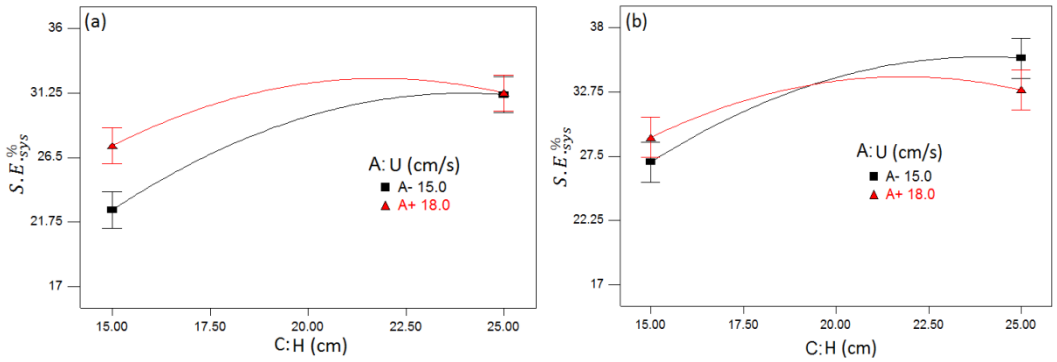

Figure 4-9: Mutual interaction between U and H affecting separation efficiency, a) at T=0, b) at T=1

Figure 4-10a-c present the mutual interaction of the air velocity and time in a contour plot. As H also interacts with U; therefore three plots were generated for three levels of the H (-1, 0 and +1).

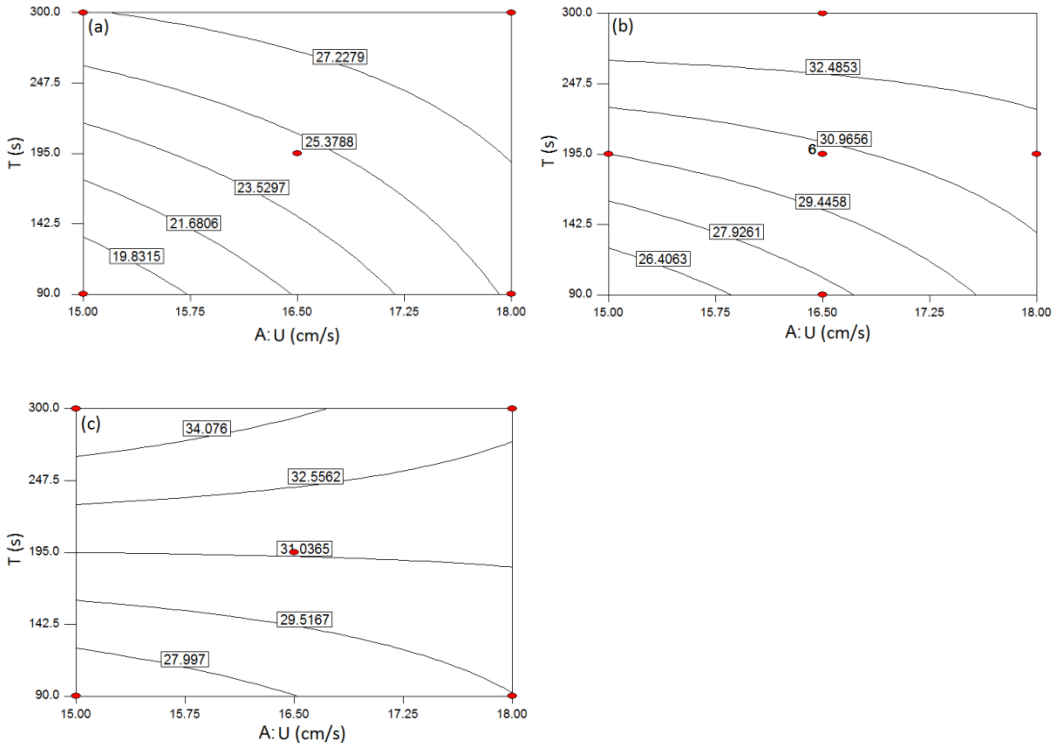

Figure 4-10: Contour plots of the system separation efficiency: the effect of U, T and their mutual interaction, a) at H=-1, b) at H=0, c) at H=+1

The arrangement of contour lines changed by changing the level of H and as a result, three different behaviors were obtained. In Figure 4-10a with H=15 cm, U and T seemed to have similar effect on the separation efficiency and a

change in U and T in the tested range, resulted equal change in the separation efficiency. However, as Figure 4-10b illustrates, separation efficiency was more sensitive to T rather than U at middle H level; any step size change in T affected separation efficiency more than U. This became more severe at high H, Figure 4-10c, where separation efficiency showed insensitivity (almost) to U.

Similar contour plots for the mutual interaction of U and H on the separation efficiency of the system are presented in Figure 4-11a-c. Since T also interacts with U, three plots were provided for three separation time levels (-1, 0 and +1).

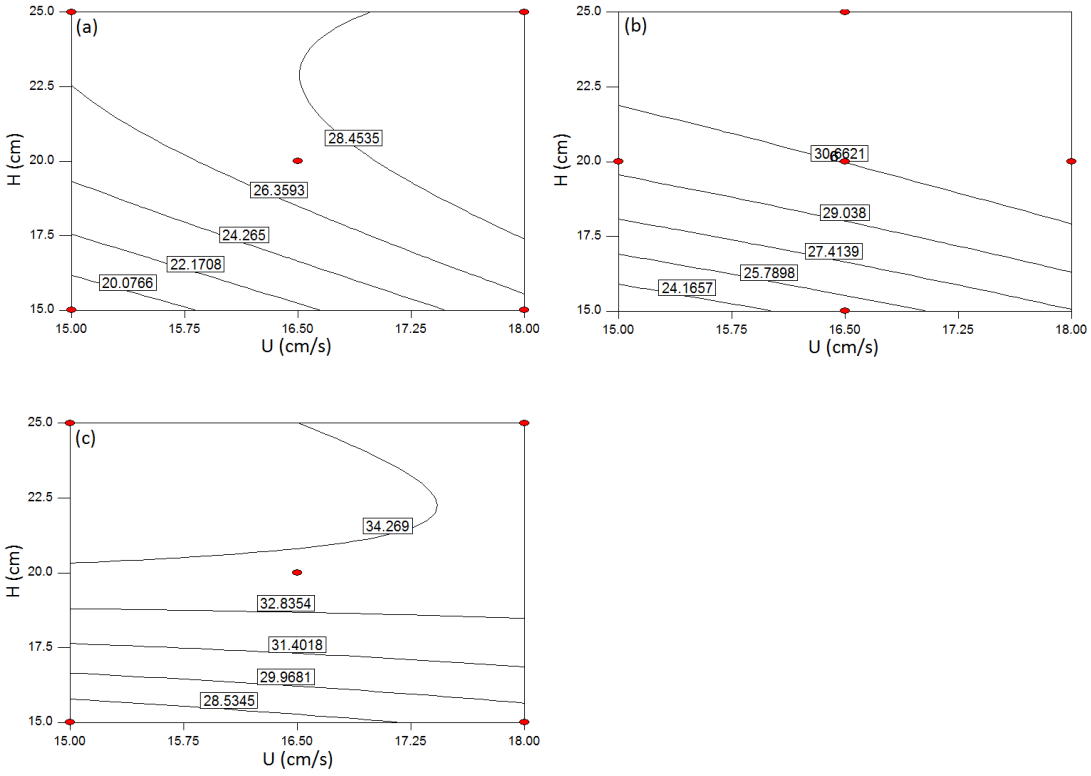

Figure 4-11: Contour plots of system separation efficiency: the effect of U, H and their mutual interaction, a) at T=-1, b) at T=0, c) at T=+1

Considering Figure 4-11a and b, low values of H and U affected the separation efficiency at the same extent, but had almost no serious effect at their higher levels. But Figure 4-11c shows a different behavior at T=+1. In this case, the separation efficiency did not show sensitivity toward changes of U while it was severely affected by any changes made to H. An increase of more than 6%

was achieved when H increased from its lower to higher level at highest separation time.

Figure 4-12 and Figure 4-13 show the 3D response surface plots of U vs. T and U vs. H, respectively. The value of the third parameter at any of these plots was kept at the central level when generating the plots. As the general shape of the graphs did not change when manipulating the third parameter, therefore only one graph is presented and discussed for each interaction.

Considering inclined flat surface in Figure 4-12, although both U and T seemed to be effective at H=0; T may considered more influencing if the edges of the created surface was taken into consideration. The separation efficiency varied between 25 and 34% in the range of T by variation of U.

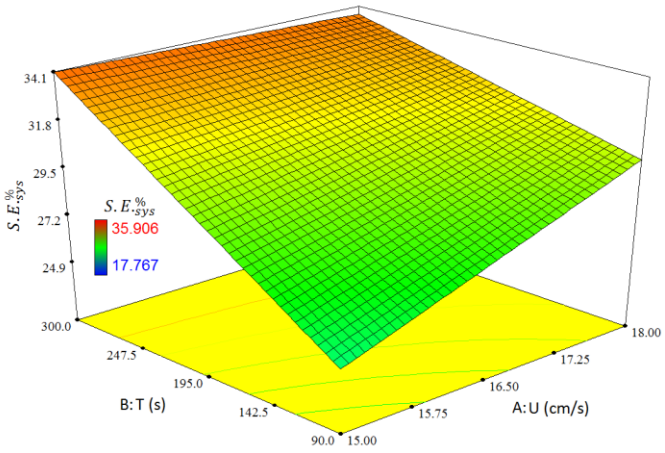

Figure 4-12: 3D interaction plots of U and T at H=0

The U and H interaction surface seems more like a conical surface as presented in Figure 4-13. H was more determinative on separation efficiency maximization than U and imposed more variation to that when was manipulated from 15 to 25 cm. Based on Figure 4-13 operating ADMFB with deeper bed heights could assure high separation efficiencies for the process.

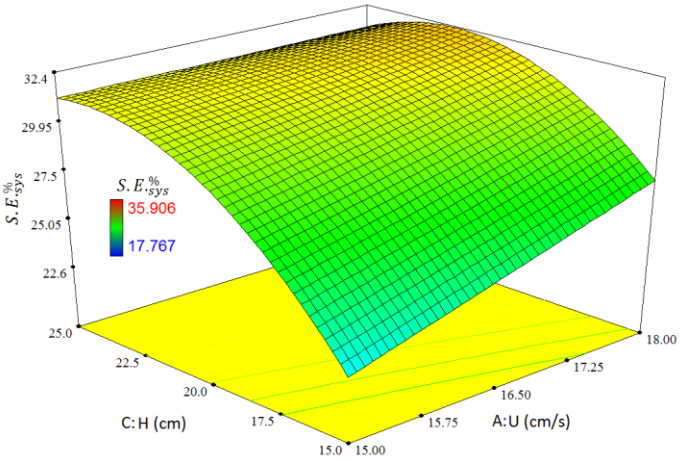

Figure 4-13: 3D interaction plots U and H at T=0

4.2.3 Optimization of parameters for ADMFB BD coal beneficiation

The three selected responses are the most used and well-known criteria employed for industrial process evaluation in mineral processing plants where the final product passes through multiple separation stages. For the apparatuses locating at the beginning of the processing circuit dealing with fresh ROM (primary/rougher cleaners), the recovery of the targeted species (combustible materials) is more important where, severe reduction of the ash content is not desired or expected. Usually the rejects of the primary separators are considered as a part of final waste and therefore the lost valuables in those streams are not recoverable any more.

On the contrary, minimum ash content of the final product is the goal of the final separating machines (re-cleaner separators), where recovery becomes less important at this stage as the rejected materials will be re-circulated in the system for further re-treatment.

The defined separation efficiency could be applied for single apparatus, independent from the whole circuit, to study the destiny of individual particles entering that separator or could be assumed for whole separation plant considering ROM feed, final clean coal product and final tailings. In general, the obtained separation efficiencies for the two mentioned concepts are often different from each other. Based on the foregoing arguments, for the purpose of

optimization several strategies could be selected and followed. The desired conditions for the considered responses are to minimize clean coal ash content or maximize combustible materials recovery or system separation efficiency.

As discussed, a significant model was not obtained for the product ash content and thus, the operating conditions to reach optimum value of the ash content could not be predicted. The proposed levels of the main operating parameters (by Design Expert software 8.0.7.1) to reach the discussed level of the responses are presented in Table 4-4.

Table 4-4: Optimum parameters for various response strategies (for BD coal)

Response	Optimization goal	U (cm/s)	T (s)	H (cm)	Model prediction
$CC_{Ash}^{\%}$	Minimum	--	--	--	--
$R_{C\ to\ L_1}^{\%}$	Maximum	15	90	15	95.6%
$S.E._{sys}^{\%}$	Maximum	15	300	25	>35%

Using middle size BD coal, three separation tests were carried out at the mentioned optimum conditions of recovery model to verify models reproducibility and reliability. The recoveries to the clean coal product were calculated based on the weights and ash analyses for the tests. The difference of the average experimental results ($R_{C\ to\ L_1}^{\%}$=93.9%) with model prediction was found to be ~3%.

4.2.4 Effect of BD coal particle size on the ADMFB separator performance

The results of six tests performed to investigate the effect of particle size on the ADMFB performance are presented in Table 4-5. U, T and H variables were set at their central levels (16.5 cm/s, 195 s and 20 cm, respectively) when performing these tests. The results of six middle particle size tests (runs 1, 2, 5, 10, 17 and 19) from Table 4-2 were averaged and compared with these testes when interpreting the particle size effect.

Table 4-5: Separation results to study the effect of BD coal particle size

Feed size (mm)	Feed ash content (%)	$CC_{Ash}^{\%}$	$R_{C\ to\ L_3}^{\%}$	$S.E._{sys}^{\%}$
1-2.8	14.63	13.25	68.36	26.72
1-2.8	15.01	13.10	75.83	26.77
1-2.8	14.00	12.27	65.59	28.62
+5.6	12.03	9.21	84.73	31.56
+5.6	11.25	8.77	87.72	29.49
+5.6	11.45	8.8	86.12	29.78

The fine size fraction results are chosen as the base, for the purpose of comparison. The average feed and clean coal ash contents as well as the ash rejection (ash reduction relative to average ash content of test feed) for three size fractions are presented in Figure 4-14.

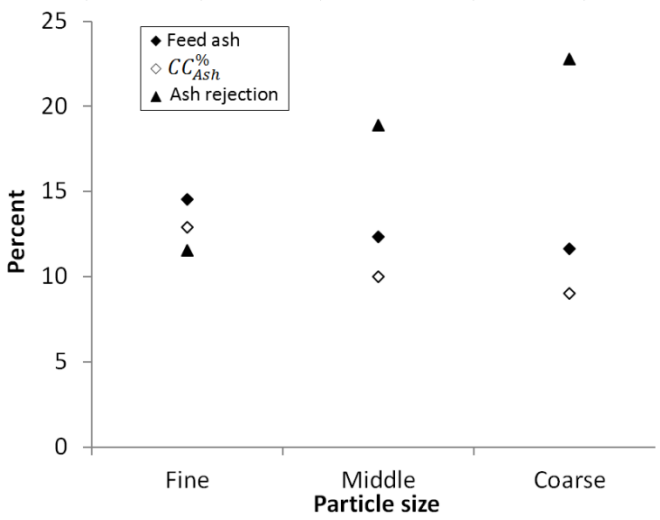

Figure 4-14: Different BD particle size feed, product ash contents and ash rejection tested by ADMFB

As Figure 4-14 shows, the ash contents of both feed and clean coal samples decreased by increasing the feed particle size. The lowest ash content of the products achieved for coarse particles equals to 8.9%. As seen, although the coarse size fraction had the lowest ash content, but it offered the maximum absolute ash reduction (2.65%) as well as highest ash rejection among three size fractions tested here. It can be concluded that the performance of ADMFB separator was much better with coarser samples where the relative ash removal for the coarse samples were found to be twice of the finer samples.

The average recovery of the combustible material to clean coal (L_1), middlings (L_2+L_3) and high ash tailings (L_4) for three size fractions are presented in Figure 4-15. The summation of the three combustible material recoveries (clean coal product, middlings and tailings) for each size fraction should be equal to 100%.

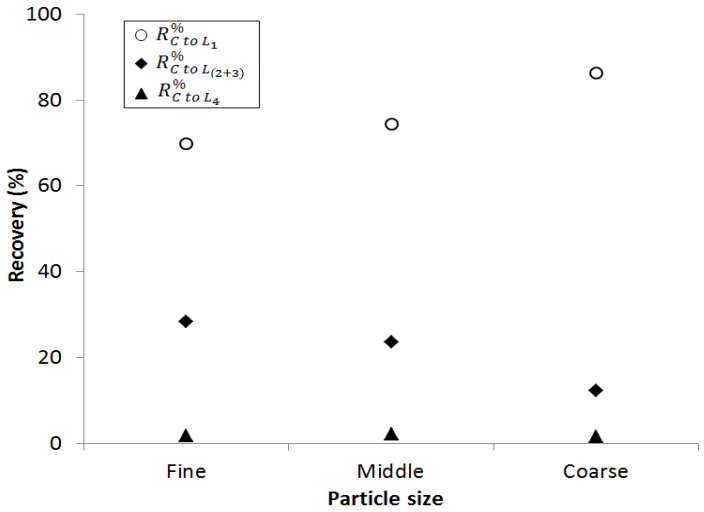

Figure 4-15: Recovery of the combustible material to different zones for three size fractions of BD coal

As illustrated in Figure 4-15, the clean coal recovery increases from 70% to 86% when coarser particles were used as feed. Considering all three recoveries depicted in Figure 4-15, it could be concluded that particles migration from L_1 to L_2 or L_3 increased once finer particles were fed instead of coarse ones but the amount of particles received in L_4 was retained almost constant and did not affected by the particle size of the samples. In fact, for the coarser size fraction more particles were kept or pushed in the upper layer than the finer ones as a result of higher resistance from other particles against settlement of coal particles and also higher drag force acting on them due to bigger cross section area of these particles.

The separation efficiencies for fine middle and coarse size fractions calculated to be 27.4%, 30.4% and 30.7%, respectively. It was seen that, by increasing the feed particle size from fine to middle, the separation efficiency improved while it almost leveled off at 30% once middle particles were replaced by coarse sizes.

4.3 Genesee coal batch ADMFB beneficiation and optimization

Full factorial DOE method with three repeating tests was used to investigate the effect U, T and H on beneficiation performance of the ADMFB separator when dealing with high ash coals (GE). Different levels of U, T and H with their actual and coded values are presented in Table 4-6. Coarse sand and GE middle coal particle size was used to perform the factorial experiments.

Table 4-6: Actual and coded values of U, T and H

Variable	Unit	Symbol	Low level	High level	Repeating tests
			-1	+1	0
Superficial air velocity	(cm/s)	U	15	16.5	15.75
Separation time	(s)	T	90	195	143
Bed height	(cm)	H	15	20	17.5

The individual experiment settings for 11 experimental points as well as calculated responses for each run are presented in Table 4-7. The repeated tests were performed at mid-point of the parameters. The samples feed ash content, ash rejection achieved in each experiment (considering its feed ash content) as well as ash content of the particles in last zone are reported in Table 4-7. The runs order was put in random order to minimize the systematic error. The runs 1, 2 and 5 pertain to the repeating experiments.

Table 4-7: Full factorial design experiment settings and resultant responses

Run	U (cm/s)	T (s)	H (cm)	Feed ash (%)	$CC_{Ash}^{\%}$	$R_{C\ to\ L_1}^{\%}$	$S.E._{sys}^{\%}$	Ash rejection (%)	L_{end} Ash (%)
1	0	0	0	30.34	20.21	92.00	42.48	33.07	88.84
2	0	0	0	32.15	20.65	93.43	45.67	35.96	92.42
3	+1	+1	-1	32.12	15.36	39.10	33.24	52.18	61.58
4	-1	+1	+1	33.26	25.68	96.87	31.79	22.78	87.95
5	0	0	0	32.32	20.38	91.54	46.35	36.64	92.6
6	+1	-1	+1	29.74	15.10	77.36	52.22	49.24	88.67
7	+1	-1	-1	31.89	12.00	71.22	56.45	62.38	87.12
8	+1	+1	+1	29.94	12.33	59.44	47.81	58.82	80.26
9	-1	-1	-1	31.55	25.36	95.68	28.21	19.63	89.97
10	-1	+1	-1	34.34	19.90	50.27	38.27	42.06	55.48
11	-1	-1	+1	28.92	17.14	92.16	48.98	40.74	92.13

The results of conducted experiments as presented in Table 4-7, were analyzed separately for each of the response functions by Design Expert 8.0.7.1 [81] to find the best fitting model representing the effect of investigated factors on the selected response function. Table 4-8 provides the statistical details of the quadratic response functions for different operating parameters where A, B and C represent U, T and H, respectively.

The correlated coded quadratic polynomial models describing the product ash content, combustible materials recovery and separation efficiency as a function of significant variables and their interactions are presented in Equation 4-3 to Equation 4-5, respectively.

Table 4-8: Results of statistical analysis for clean coal ash content, combustible material recovery and system separation efficiency

Source	Clean coal ash content			Combustible materials recovery			System separation efficiency		
	Mean square	F-value	p-value Prob.> F	Mean square	F-value	p-value Prob.> F	Mean square	F-value	p-value Prob.> F
Model	49.67	105.38	< 0.0001	551.91	128.66	0.0010	154.00	31.74	0.0026
A-U	138.61	294.06	< 0.0001	964.97	224.95	0.0006	225.44	46.46	0.0024
B-T	1.69	3.59	0.1166	1028.89	239.85	0.0006	150.96	31.11	0.0051
C-H				604.96	141.02	0.0013	75.95	15.65	0.0167
(A B)							52.51	10.82	0.0302
(B C)	7.74	16.42	0.0098	517.04	120.53	0.0016			
(A C)				34.44	8.03	0.0660			
(A B C)	50.65	107.46	0.0001	161.17	37.57	0.0087	265.12	54.64	0.0018
Curvature	14.25	30.24	0.0027	834.79	194.60	0.0008	16.04	3.31	0.1431
Residual	0.47			4.29			4.85		
Lack of Fit	0.75	15.29	0.0620	10.92	11.19	0.0789	5.44	1.27	0.4400
Pure Error	0.05			0.98			4.27		
R^2	0.9883			0.9961			0.9754		
Adj. R^2	0.9789			0.9884			0.9447		
C.V.%	3.7			2.65			5.14		

Equation 4-3: $\mathrm{CC}^{\%}_{\mathrm{Ash}} = 17.86 - 4.16\mathrm{A} + 0.46\mathrm{B} + 0.98(\mathrm{BC}) - 2.52(\mathrm{ABC})$

Equation 4-4: $R^{\%}_{C\ to\ L_1} = 72.76 - 10.98A - 11.34B + 8.7C - 2.07(AC) + 8.04(BC) - 4.49(ABC)$

Equation 4-5: $S.E.^{\%}_{sys} = 42.12 + 5.31A - 4.34B + 3.08C - 2.56(AB) + 5.76(ABC)$

Very low values of the Fisher's F tests indicated that all three mentioned models were significant. There was <0.26% chance that clean coal ash content, recovery and separation efficiency models were originating from noise. Lack of fit was also found to be not-significant for three correlated response functions. Based on ANOVA test (Fisher's F tests) and considering lack of fit test, it could be concluded that three suggested response models (Equation 4-3 to Equation 4-5) were suitable for predicting the target responses within the range of variables tested here.

The model curvature was measured by the difference between the average of the center points (repeating tests) and the average of the factorial points. For significant curvature in the design space, any prediction or estimation around the middle of the design space should be made carefully. Considering the F-values shown in Table 4-8, the curvature was significant for $CC^{\%}_{Ash}$ and $R^{\%}_{C\ to\ L_1}$ but insignificant for $S.E.^{\%}_{sys}$. As discussed, larger R^2 and adjusted R^2 and lower CV values confirmed the significance of the model and reproducibility of the data points. A careful look at Table 4-8 shows that R^2 and adjusted R^2 for three models were above 0.97 and 0.94, respectively, and all models CV were lower than 5.2%. Among the three responses, the lower R^2 (0.975) and higher CV (5.14%) belong to $S.E.^{\%}_{sys}$ which still was very satisfactory. The actual and model predictions for the response models are shown in Figure 4-16a-c.

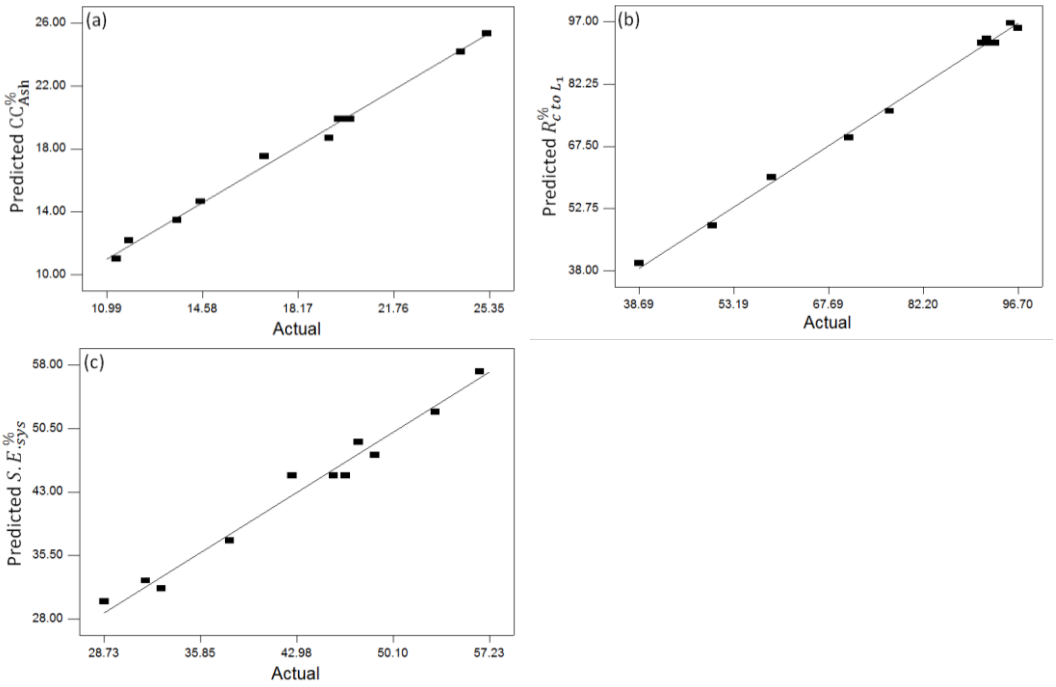

Figure 4-16: Experimental values vs. model prediction, a) clean coal ash content, b) combustible material recovery, c) system separation efficiency

4.3.1 Main parameters effect on responses

On the basis of parameters coded coefficients for the clean coal ash content (Equation 4-3), and their significance levels (Prob. > F in Table 4-8) superficial air velocity was inversely affecting $CC^{\%}_{Ash}$ (i.e. an increase in U leads to a decrease in $CC^{\%}_{Ash}$) while time had a marginally positive effect on $CC^{\%}_{Ash}$.The perturbation plot of the main operating parameters for the $CC^{\%}_{Ash}$ is shown in Figure 4-17. The middle levels of all variables were used as reference points while plotting Figure 4-17. The ANOVA test results as well as perturbation plot (Figure 4-17) revealed that changes in H had no significant effect on $CC^{\%}_{Ash}$. Based on the coefficients in the Equation 4-3 and also the perturbation plot, the order of influence of the operating parameters on the $CC^{\%}_{Ash}$ was U>T. The ash content of the product was totally insensitive to H (at 95% confidence level) while, T affected that positively though negligible when compared to U which was intensively and negatively influencing the selected response function suggesting lower $CC^{\%}_{Ash}$ obtainable at high levels of U and low levels of T.

Product ash content decreased from 22.2 to 13.9% when U was changed from -1 to +1 while T was set to 0 and regardless of H level.

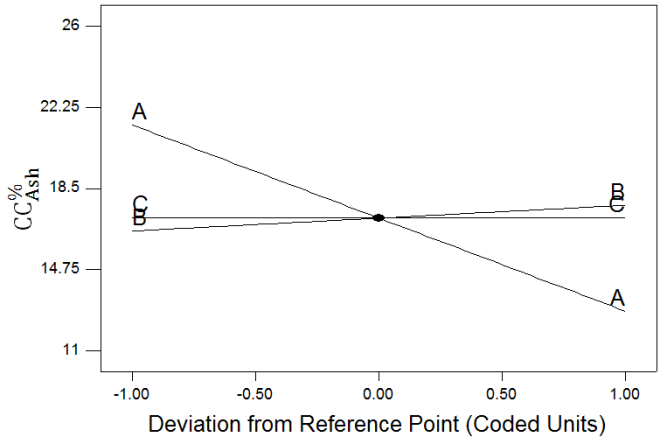

Figure 4-17: Perturbation plot of clean coal ash content (for GE sample)

The coded coefficient of the main operating parameters (see Equation 4-4 and Table 4-8) as well as perturbation plot for $R^{\%}_{C\ to\ L_1}$(Figure 4-18), confirmed the positive effect of H and negative effect of U and T on $R^{\%}_{C\ to\ L_1}$. The effectiveness order of the operating parameters on $R^{\%}_{C\ to\ L_1}$was T>U>H. In the $R^{\%}_{C\ to\ L_1}$perturbation plot the U and T lines were coinciding with each other because they had almost same magnitude of effectiveness on recovery. If the interactions of the parameters were neglected, improvements of $R^{\%}_{C\ to\ L_1}$could be deduced from Figure 4-18 when lower levels of U and T were used in conjunction with the higher levels of H (i.e. when deeper beds were used). The individual effect of either U or T ($\Delta\ R^{\%}_{C\ to\ L_1}$= 22.8%) was more than H ($\Delta\ R^{\%}_{C\ to\ L_1}$= 23.3%) within the examined range of each parameter when the other two variables were set to their 0 levels. For instance when T=143 s and H=17.5 cm, decreasing U from 16.5 to 15 cm/s increased the combustible materials recovery from 61 to 83.8%.

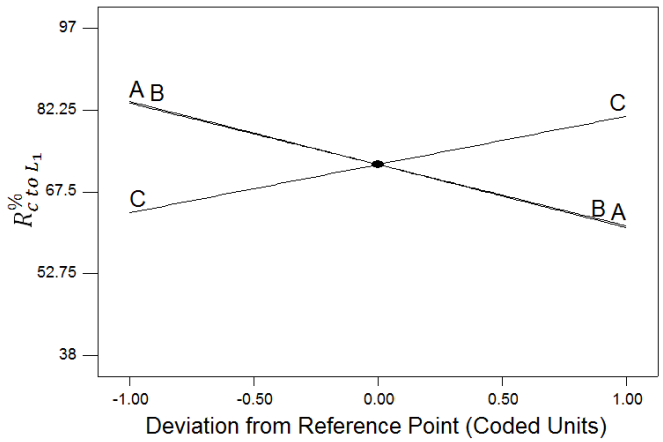

Figure 4-18: Perturbation plot of combustible materials recovery (for GE sample)

Positive effect of U and H and negative effect of T on $S.E._{sys}^{\%}$ could be deduced from statistical analyses of the collected data obtained from full factorial design. Considering the sign of the coefficient of the main operating parameters (Equation 4-5), their significance level (Prob. > F in Table 4-8) as well as perturbation plot for $S.E._{sys}^{\%}$ (Figure 4-19) the effectiveness order of the parameters on $S.E._{sys}^{\%}$ was U>T>H. According to Figure 4-19 and ignoring the mutual parameters interaction, the best option to obtain better $S.E._{sys}^{\%}$ was to set the parameters around the lower levels of T and higher levels of U and H.

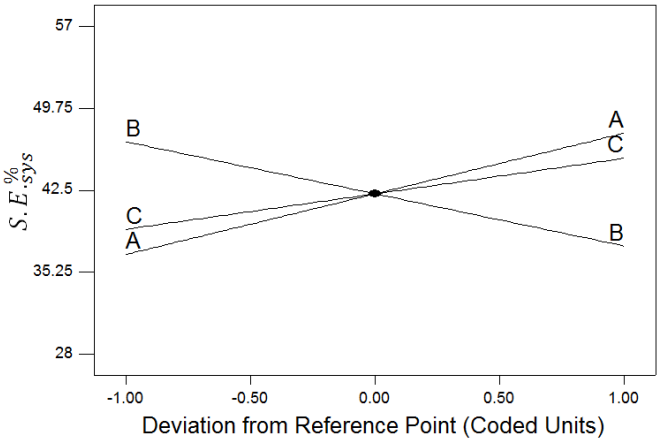

Figure 4-19: Perturbation plot of system separation efficiency (for GE sample)

4.3.2 Mutual interaction of operating parameters

The results of ANOVA test on collected data revealed several mutual interactions of the parameters for the assumed responses when dealing with GE

sample. 2D interaction or 3D response surface plots of the effective interactions of the operating parameters on different responses are presented through Figure 4-20 to Figure 4-28.

As Equation 4-3 indicated, there was a 95% significant interaction between T and H with positive effect on $CC^{\%}_{Ash}$, which is further graphically illustrated in Figure 4-20a-b as 2D plots at two different levels of U. As shown in Figure 4-20a-b the effect of T on $CC^{\%}_{Ash}$ depended upon H and vice versa. It is important to note that H by itself showed no significant effect on the $CC^{\%}_{Ash}$, but when the test results were analyzed, for the parameters interactions, a stronger and more effective interaction between T and H than the direct effect of the individual parameters (T or H) was revealed. It is impossible to recognize such effect when the one factor at-a-time method has been used, as one might eliminate H from results of analysis due to its low influence on the response.

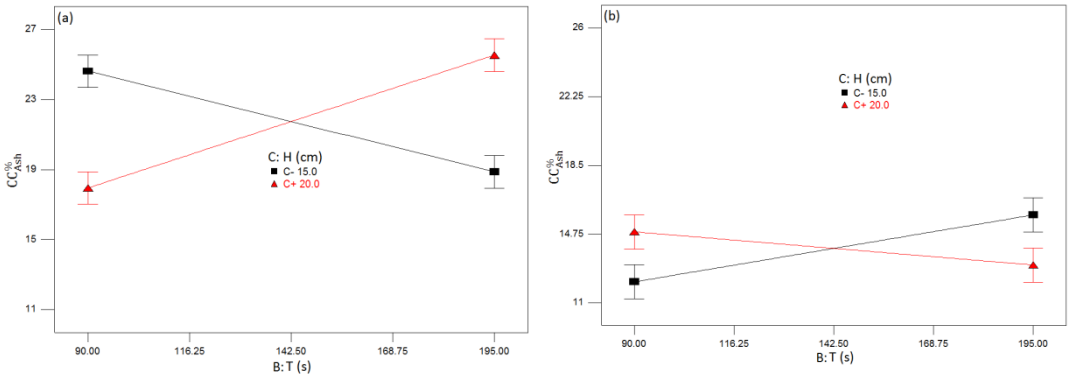

Figure 4-20: 2D plots of mutual interaction of T and H on clean coal ash content, a) at U=-1, b) at U=1

The presented 2D plots show that the range of variations imposed by T and H interaction was wider ($\Delta CC^{\%}_{Ash} = 8\%$) at low U values, whereas lower $CC^{\%}_{Ash}$ values (ranging between 12 to 15.5% ash content) were obtainable at higher levels of U. Obviously the behavior of this interaction depended on the level of U (third parameter), since the order of the increasing or decreasing H lines by increasing T, changed when different levels of U were considered. For minimum and maximum $CC^{\%}_{Ash}$ values when U was set to -1, H needed to be set to +1 in the considered range of T (18.1 and 26%, respectively). In the range of T the

minimum and maximum $CC_{Ash}^{\%}$ values of 11.7 and 15.6%, respectively, occurred at H=-1 when U was set to +1 (Figure 4-20b).

There is a direct relationship between the density of the coal particles and their ash content. So to obtain a product with minimum ash content it is necessary to selectively separate particles with lower densities. Therefore from Figure 4-20a-b and considering the fact that only U, T and H were investigated, it could be said that a lower effective bed density occurred at short separation time when U=15 cm/s and H=20 cm or U=16.5 cm/s and H=15 cm. For higher separation times low bed density formed when U=15 cm/s and H=15 cm or U=16.5 cm/s and H=20 cm (regardless of effect of other parameters).

Figure 4-21a-b present the effect of T and H and their mutual interaction on the $CC_{Ash}^{\%}$ as contour plots. The product ash content for different sets of variables could be deduced from these figures. As shown in Figure 4-21a, the contour lines were almost symmetrical to the center of the graph (T=0 and H=0) and the range of variations imposed by step size change of one of the parameters was the same for both T and H ($CC_{Ash}^{\%}$ varies between 19.4 and 24.7%). But for high H as Figure 4-21b shows, $CC_{Ash}^{\%}$ was more sensitive to a step size change of T than H (especially at low H level).

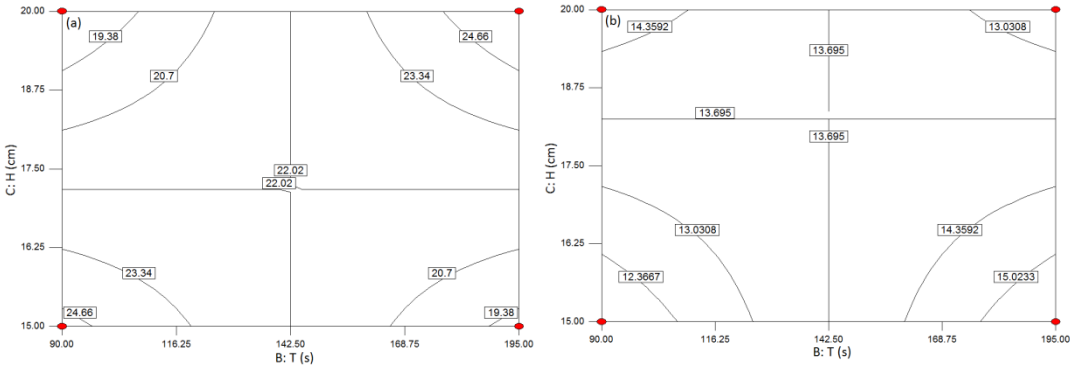

Figure 4-21: Contour plots of mutual interaction of T and H on clean coal ash content, a) at U=-1, b) at U=1

The 3D response surface plots of T vs. H are depicted in Figure 4-22a-b at low and high U levels, respectively. Generally speaking high U, resulted in lower feed product ash content in the selected domain of variables when both graphs were compared. Also it should be noted that the minimizing or maximizing

corners of the response surfaces in the domain of T and H changed their positions when Figure 4-22a is replaced by Figure 4-22b. Minimum product ash coordinates for low U as seen in Figure 4-22a (low [T, H] or high [T, H]) produced maximum product ash at high U setting which is depicted in Figure 4-22b. This emphasizes the necessity of employing an optimization method for achieving the optimum or desired response function value in the domain of the tested variables.

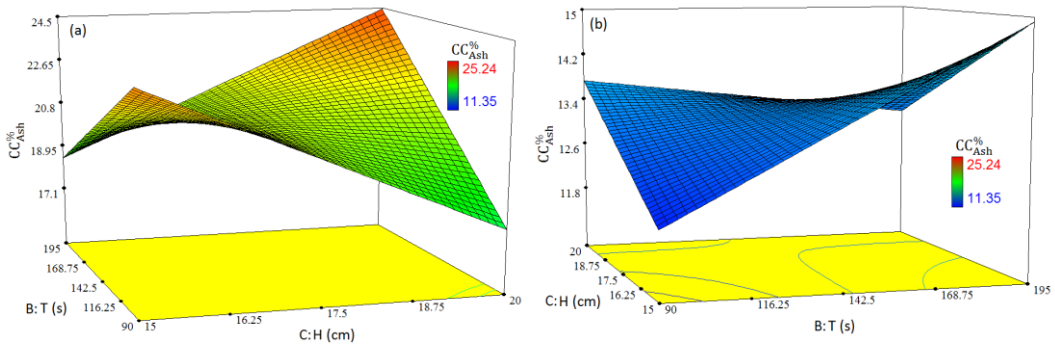

Figure 4-22: 3D interaction plot of T and H on clean coal ash content, a) at U=-1, b) at U=1

From the ANOVA test results (Table 4-8 and Equation 4-4), two mutual interactions of the operating parameters were found to be significant (T and H) or marginally significant (U and H) when combustible material recovery was considered as the response function for evaluating the separation process in ADMFB. Since the interaction of U and H was marginally significant and its effect on recovery was less than T and H interaction, only T and H interaction discussed here but its effect had considered in parameter optimization section.

The 2D mutual interaction plots of the T and H at two different levels of U (+1 and -1) are presented in Figure 4-23a-b. Except a small zone in the Figure 4-23a, $R^{\%}_{C\ to\ L_1}$ was higher for high H regardless of the level of U or T. As Figure 4-23a shows, there was no need to increase the separation time when H=20 cm and U=15 cm/s as $R^{\%}_{C\ to\ L_1}$ just increased by 1.4% over an extra 105 s separation time. On the other hand, the $R^{\%}_{C\ to\ L_1}$ dropped dramatically from 96.8 to 49.1% (i.e. a 47.7% decrease) for lower bed height when U=15 cm/s and T was increased from 90 s to 195 s. Improvement in $R^{\%}_{C\ to\ L_1}$ by increasing H at U=+1

was clearly deducible through Figure 4-23b since in the full range of domain H=+1 resulted in higher $R^{\%}_{C\ to\ L_1}$ and the difference intensified by increasing T.

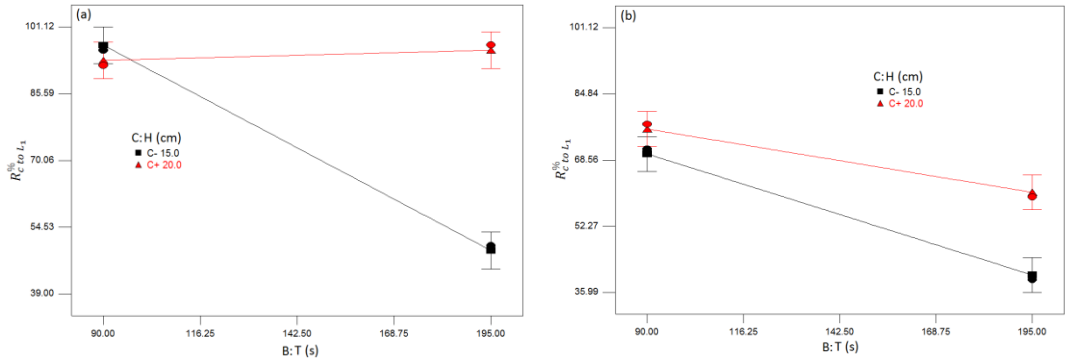

Figure 4-23: 2D mutual interaction plot of T and H on combustible material recovery, a) at U=-1, b) at U=1

Figure 4-24a-b show the effect of T and H and their mutual interactions on $R^{\%}_{C\ to\ L_1}$ at two levels of U. As shown in Figure 4-24a, higher values of $R^{\%}_{C\ to\ L_1}$ were obtainable at lower U values when T=-1, in the full range of H. According to Figure 4-24a-b, higher $R^{\%}_{C\ to\ L_1}$ is obtainable at lower level of T and higher level of H regardless of U setting. In both graphs $R^{\%}_{C\ to\ L_1}$ increases form lower right corners of the plots toward upper left corners.

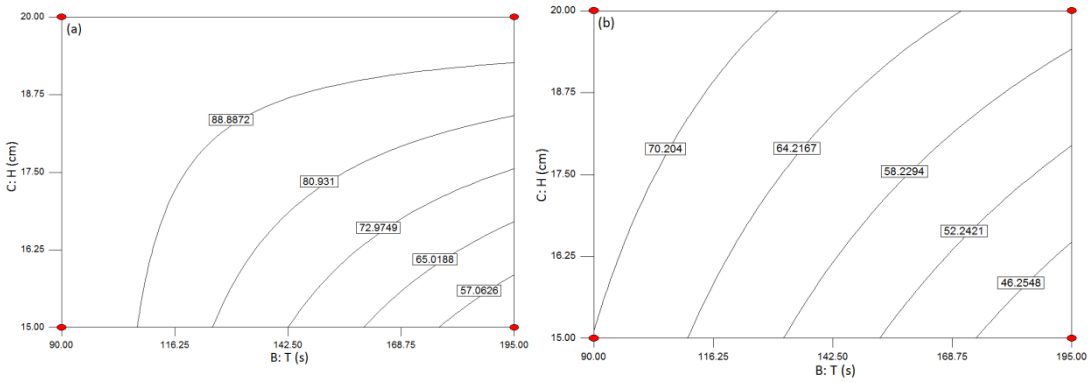

Figure 4-24: Contour plots of mutual interaction of T and H on combustible material recovery, a) at U=-1, b) U=1

The 3D response surface of the mutual interaction of H and T is presented in Figure 4-25. Since the general shape of 3D surfaces for U=-1 and U=+1 were almost the same only the response surface for U=-1 is presented here. As seen $R^{\%}_{C\ to\ L_1}$ was so sensitive to step size change when T was around 195 s and H was

close to its low level (15 cm). In fact increase of H from 15 cm to higher bed heights and decrease of T from 195 s to lower values could cause more than 47% increase in $R^{\%}_{C\ to\ L_1}$, while setting operating conditions around H=20 cm and T=90 s could assure a safe and high separation $R^{\%}_{C\ to\ L_1}$.

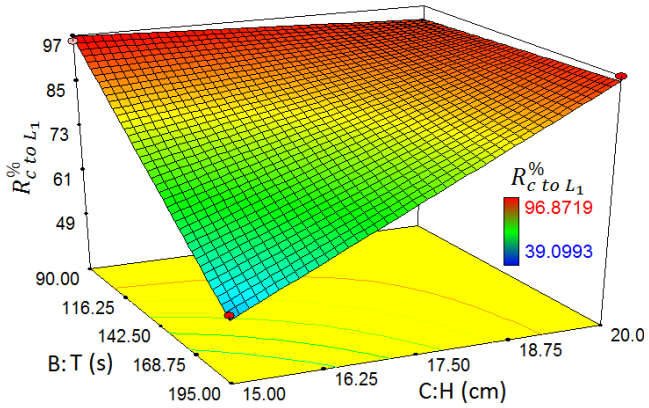

Figure 4-25: 3D interaction plot of H and T on combustible material recovery at U=-1

According to the ANOVA test results (Table 4-8 and Equation 4-5) there is a 95% significant interaction between U and T once system separation efficiency was considered as evaluation response. The mutual interaction of U and T on $S.E.^{\%}_{sys}$ is further illustrated in Figure 4-26a-b and Figure 4-27a-b as 2D and contour plots for both low and high levels of H. This interaction was more obvious when low levels of H are used for separation (Figure 4-26a) as the two lines cross each other within the range of the selected separation time. For low levels of H (Figure 4-26a) low level of T cause more changes in the separation efficiency ($\Delta S.E.^{\%}_{sys} > 27\%$) while for high H values, high level of T impose more variation on the separation efficiency ($\Delta S.E.^{\%}_{sys} > 17\%$) when U varies between 15 cm/s and 16.5 cm/s. But regardless of the range of variation of H, low levels of T and high levels of U resulted in maximum $S.E.^{\%}_{sys}$ (Figure 4-26a-b). This means more combustible materials to L_1 and more ash forming minerals to other layers.

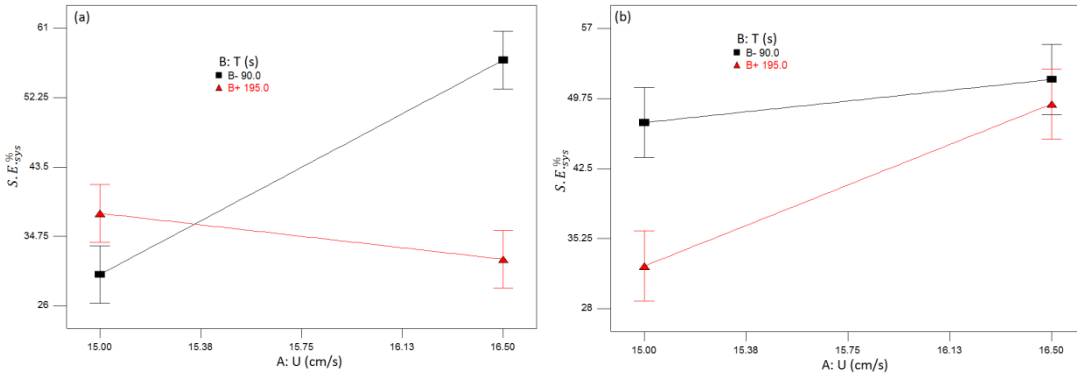

Figure 4-26: 2D plots of mutual interaction of U and T on system separation efficiency, a) at H=-1, b) at H=1

The contour plot of this interaction is shown in Figure 4-27a-b at both levels of H. From Figure 4-27a, $S.E._{sys}^{\%}$ was almost constant (around 34%) for low U and high T values, but not sensitive to both U and T. At high levels of U, $S.E._{sys}^{\%}$ was increased with decreasing T and increasing U. This was due to shorter separation time which limits back mixing phenomena (transferring high ash middlings to L_1). For H=-1, U=+1 and T=-1, $S.E._{sys}^{\%}$ values higher than 52% were achieved.

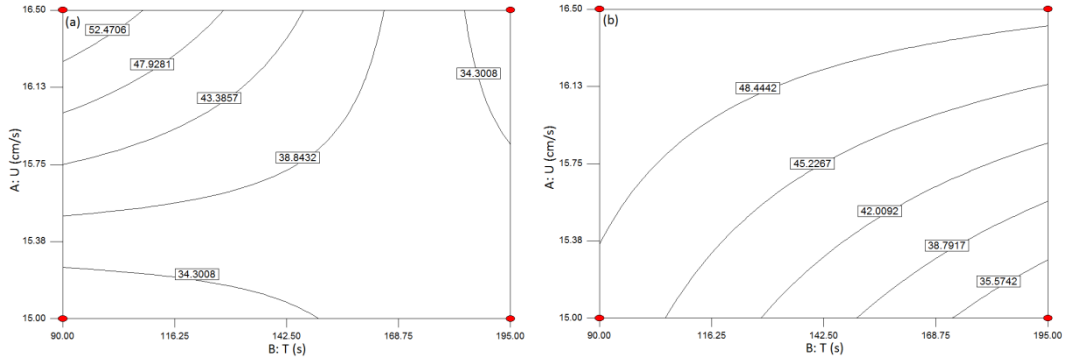

Figure 4-27: Contour plots of mutual interaction of U and T on system separation efficiency, a) at H=-1, b) at H=1

The position of the insensitive region changed at high level of H (Figure 4-27b), whereas $S.E._{sys}^{\%}$ remained almost constant at low T and high U levels ($S.E._{sys}^{\%}$~49%). As Figure 4-27b illustrates, $S.E._{sys}^{\%}$ was more sensitive to a step size change of T at low air velocities or to step size change of U at higher separation times. Here also the maximum system separation efficiency was obtainable when back mixing was limited i.e. U=+1 and T=-1.

Both response surface plots created for low and high levels of H, conform to the maximization of system separation efficiency at high fluidization air velocities and low separation times (Figure 4-28a-b). As shown in Figure 4-28a, the variation was more intense at lower levels of H, whereas the separation efficiency increased from almost 32%, at three corners of the plot, rapidly to 56% at the far corner of the plot. In fact in most areas the separation efficiency was low. On the other hand, from Figure 4-28b, the separation efficiency increased almost uniformly from the lower corner of plot (U=15 cm/s and T=195 s) to 52% at the opposite corner. One of the main reasons for higher system separation efficiency at lower separation times could be limitation of high ash middling particles back mixing to the product zone.

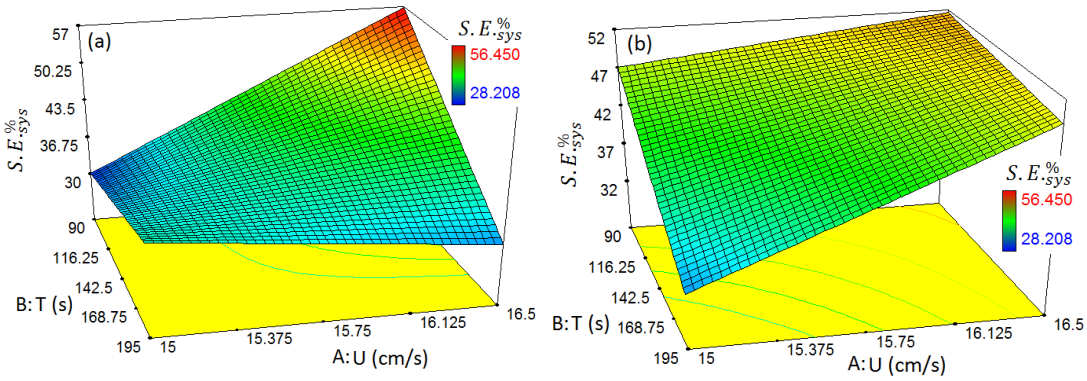

Figure 4-28: 3D interaction plot of U and T on system separation efficiency, a) at H=-1, b) at H=1

4.3.3 Optimization of parameters for ADMFB GE coal beneficiation

As discussed in section 4.2.3, the desired conditions for the considered responses are to minimize clean coal ash content or maximize combustible materials recovery or maximize system separation efficiency.

The proposed levels of the main operating parameters (by Design Expert) for three mentioned strategies are presented in Table 4-9.

Table 4-9: Optimum parameters for various response strategies (for GE coal)

Response	Optimization goal	U (cm/s)	T (s)	H (cm)	Model prediction
$CC^{\%}_{Ash}$	Minimum	16.5	90	15	11.7%
$R^{\%}_{C\ to\ L_1}$	Maximum	15	90	15	70%
$S.E.^{\%}_{sys}$	Maximum	16.5	90	15	48.1%

Three tests were performed under the optimum product ash content and system separation efficiency conditions using middle size GE coal (with average feed ash of 31.6%) to verify the reproducibility and reliability of the analysis. The average test results for $\mathrm{CC^{\%}_{Ash}}$, $\mathrm{R^{\%}_{C\ to\ L_1}}$, and $\mathrm{S.E.^{\%}_{sys}}$ were found to be 13.2%, 67.7% and 48.1%, respectively. Except $\mathrm{S.E.^{\%}_{sys}}$, the experimental and theoretical values for two other responses were matching model predictions (Equation 4-3 to Equation 4-5) close enough; whereas, the difference between prediction and repeating tests for $\mathrm{CC^{\%}_{Ash}}$ and $\mathrm{R^{\%}_{C\ to\ L_1}}$ were 1.5% and 2.3%, respectively.

As shown in Equation 3-5, a decrease in $R^{\%}_{C\ to\ L_1}$ and $R^{\%}_{Ash\ to \sum L_{2-5}}$ lead to a decrease in $S.E.^{\%}_{sys}$. For a certain test feed, increase of $\mathrm{CC^{\%}_{Ash}}$ results in lower mass of ash forming minerals in the lower levels of the bed or in another words lower $\mathrm{R^{\%}_{Ash\ to \sum L_{2-5}}}$. The results of the repeating tests were in such direction (both higher $\mathrm{CC^{\%}_{Ash}}$ and lower $\mathrm{R^{\%}_{C\ to\ L_1}}$) causing decrease of experimental $S.E.^{\%}_{sys}$ (9.2% lower).

Generally speaking, by comparing the three sets of numbers (repeating optimum tests, model calculations and Test No. 7 in Table 4-7), as well as considering the heterogeneous nature of coal; performed experiments and proposed model seemed to reasonably explain the behavior of GE coal particles when they were introduced into the batch ADMFB separator.

The ash content and recovery of different zones for test No. 7 (from Table 4-7) are presented in Figure 4-29. Compared to 31.9% ash content of the feed sample, both L_1 and L_2 ash contents were reduced. On the other hand the ash content of L_3 zone increased to 87.1% with the dry solid yield of 21.2% and just 4% combustible material recovery.

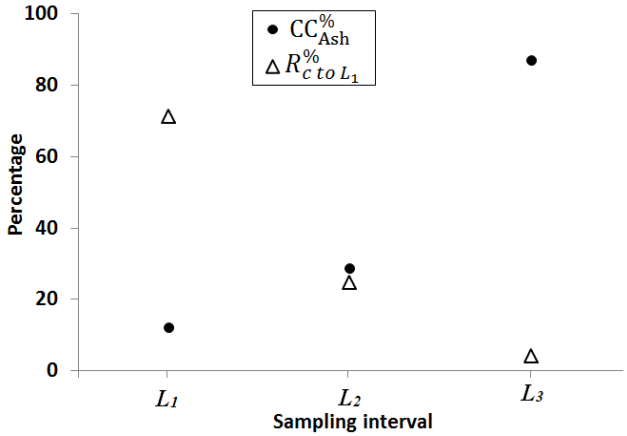

Figure 4-29: Ash content and combustible material recovery for the different layers of test No. 7 from Table 4-7

4.3.4 Effect of GE coal particle size on the ADMFB separator performance

To study the effect of GE coal particle size on the separation performance of ADMFB, three repeating separation tests were carried out on each size fraction at U=16.5 cm/s, T=90 s, and H=15 cm (minimum product ash content). Table 4-10 presents the results of nine experiments performed.

Table 4-10: Separation results to study the effect of GE coal particle size

Feed size (mm)	Feed ash content (%)	$CC^{\%}_{Ash}$	$R^{\%}_{C\ to\ L_1}$	$S.E.^{\%}_{sys}$
1-2.8	38.93	28.78	79.31	39.45
1-2.8	34.89	27.36	80.09	35.00
1-2.8	34.11	27.06	80.60	34.06
2.8-5.6	31.44	12.84	68.91	44.66
2.8-5.6	31.59	13.96	65.66	46.18
2.8-5.6	31.68	12.84	68.44	50.60
+5.6	25.14	8.95	61.49	50.42
+5.6	27.51	11.08	75.89	56.97
+5.6	26.60	10.35	64.98	51.53

The average feed and clean coal ash contents as well as the ash rejection for three size fractions are presented in Figure 4-30. Considering fine particle size fraction as the base, feed ash content decreased with increase in the particle size.

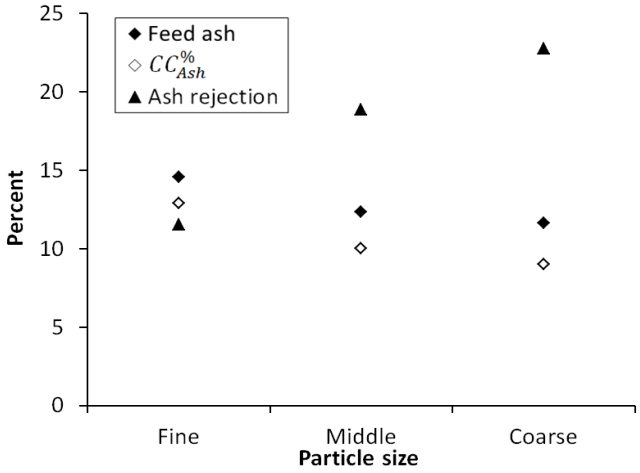

Figure 4-30: Different GE particle size feed, product ash contents and ash rejection tested by ADMFB

It was seen that, the performance of the ADMFB in terms of ash rejection and the quality of product (lower ash content) was improved by increasing feed particle size. As Figure 4-30 implies, the observed reduction in ash content was severe for GE coal compared to BD coal. In spite of lower feed ash content of the coarse particles lower product ash contents and higher ash rejection rates are obtained for coarse particles. The ash content of the coarse product was determined to be 10.1% with ash rejection of 61.7%.

Recovery decreased by 12% (in contrary to BD coal) when GE middle or coarse particles were fed into ADMFB separator, as illustrated in Figure 4-31. Of course regardless of ash content of the ADMFB feed, acceptable recoveries (≥68%) were always obtained for the single stage ADMFB coal beneficiation. As discussed in section 4.2.4, the combustible materials recovery to L_3 showed little variations (3-5%) for all particle size fractions. Therefore, a decrease in recovery due to increase in particle size could be attributed to the positioning of more low ash middlings to L_2 instead of L_1 (travelling down) which was a dipper zone (7.5 cm).

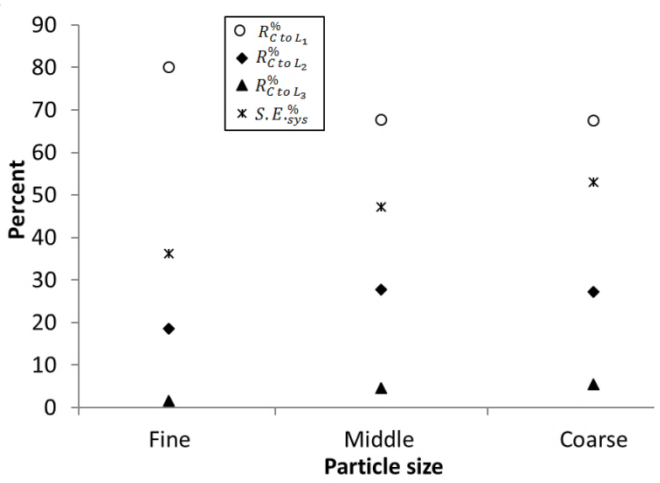

Figure 4-31: Separation efficiency and recovery of the combustible material to different zones for three size fractions of BD coal

As shown in Figure 4-31, the separation efficiency improved when larger particles were fed into ADMFB. Improvement in separation efficiency of the system was more obvious for GE coal than BD coal. The separation efficiency increased from 36 to 53%. This was due to the fact that separation efficiency is proportional to combustible material recovery to L_1 and ash rejection from L_1 which both significantly increased for both middle and coarse GE samples in beneficiation tests.

4.3.5 Effect of fluidization medium particle size on separation performance

In order to study the effect of fluidization medium particle size on ADMFB coal beneficiation; nine experiments were carried out with fine sand (270 μm) at U=16.5 cm/s, T=90 s and H=15 cm. GE coal was used as feed, and beneficiation experiments were repeated three times for each coal size fraction. The average results were obtained and compared to the average results of 390 μm bed (Table 4-10). The averages of 18 experiments are presented in Table 4-11.

As seen in Table 4-11, by increasing feed particle size from fine to coarse the separation evaluation responses were moving toward preferred direction as the $CC^{\%}_{Ash}$ decreased while the $R^{\%}_{C\ to\ L_1}$, $S.E.^{\%}_{sys}$ and ash rejection were increasing. In fact, separation quality improved regardless of sand size when feeding bigger coal particles. Although, improvements were bolder for finer sand than, coarse sand.

The ash rejection percentage increased more than 100% for coarse coal compared to fine feed even though its feed ash content was considerably lower.

Table 4-11: Average results of beneficiation experiments conducted in 270 and 390 µm sand fluidized bed

Feed size (mm)	Sand size	Feed ash (%)	$CC_{Ash}^{\%}$	$R_{C\ to\ L_1}^{\%}$	$S.E._{sys}^{\%}$	Ash rejection (%)
1-2.8	270 µm	36.08	24.26	59.52	39.56	32.76
2.8-5.6		34.18	12.27	55.97	47.57	64.17
+5.6		24.40	7.63	61.93	51.97	68.65
1-2.8	390 µm	35.98	27.73	80.00	36.17	22.79
2.8-5.6		31.57	13.21	67.67	48.1	58.14
+5.6		26.41	10.13	67.45	52.97	61.74

Lower products ash content, higher ash rejections and slightly higher system separation efficiencies were obtained, for any respective coal size fraction, once fine sand was used as fluidization medium rather than coarse sand (Table 4-11). Combustible material recovery showed levels of decrease in fine sand bed. This could be explained through improved stability and lower effective bed density as result of fine sand application. Slight decrease in bed effective density facilitated elimination of low ash middlings from L_1 toward lower zones. Therefore product ash content decreased (improves) and, due to transporting of some extra combustible materials out of L_1, combustible material recovery decreased. In general, it could be concluded that, application of fine sand had improved bed stability and decreased bed density which consequently resulted in improvement in ADMFB coal beneficiation.

4.4 Coal drying experiments

The moisture content of coal in addition to decreasing its heat value, and consequently the efficiency of the coal fired power plants, increases its handling and hauling costs significantly. As discussed in section 2.5, it can also affect the performance and accuracy of the ADMFB separation processes by facilitating particles agglomeration. Simultaneous coal beneficiation and drying by utilizing

waste heat of power plants could be considered as a strong advantage for ADMFB coal beneficiation method over the others. Therefore two different sets of drying experiments performed in small batch bed to acquire some understanding on behavior and kinetics of fluidized bed coal drying. Next, beneficiation and clean coal drying were examined.

4.4.1 ROM coal packed/fluidized bed drying

For both packed bed and fluidized bed drying experiments, the settings of operating parameters were selected identical or closest to the batch separation experiments. Middle size BD coal was used as coal sample and three air superficial velocities of 15, 16.5 and 18 cm/s were adjusted using mass flow controller. Considering the adjusted air flows, packed bed of coal developed when only coal particles were used in bed. Fluidized bed status was achieved through adding coarse sand particles (390 μm) to the bed. The air temperature at the end of heater (Figure 3-4) was used for determining experiment temperature since the readings were consistent and more reliable than thermocouples readings from bed depth or its surface. Enough time was given to the whole system to reach stable temperature prior to adding coal particles. Both batch and fluidized bed drying experiment procedures were discussed in more details in 3.3.2.1 and 3.3.2.2, respectively. Three selected nominal hot air temperatures were 100, 130 and 160 ˚C.

As expected, by increasing superficial air velocity (not enough to fluidize coal particles) and its temperature, the rate of moisture loss increased. The effect of air temperature is presented in Figure 4-32. Since similar curves obtained for two other tested air velocities, just one graph at U=15 cm/s is presented here. Figure 4-34 is also presenting the effect of air velocity on moisture content of coal particles at 130 ˚C for instance.

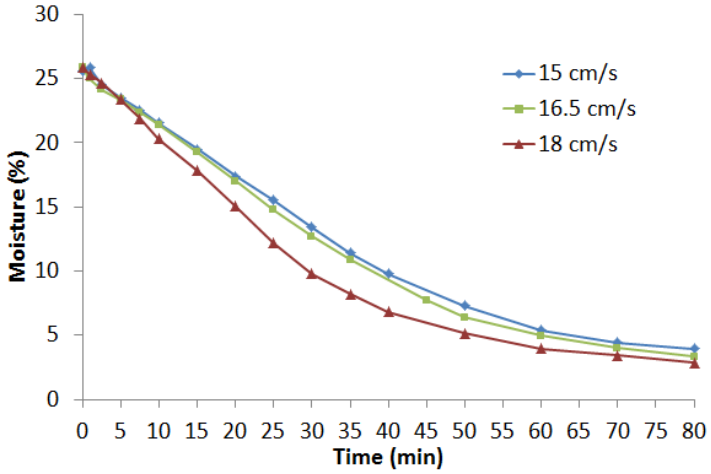

Figure 4-32: Effect of air velocity on packed bed coal drying (temperature: 130 ˚C)

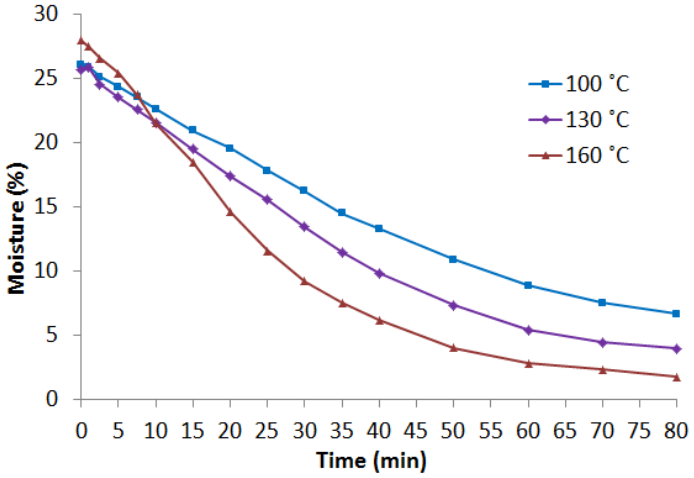

Figure 4-33: Effect of air temperature on packed bed coal drying (U=15 cm/s)

As seen (Figure 4-32 and Figure 4-34), increasing air temperature was more effectively influencing the particles drying than increase of air velocity. In fact, available energy for vaporization was more limiting than available transferring (away) force of vapor.

The effect of air velocity (e.g. 15 cm/s) and temperature (130˚C) on fluidized bed coal drying is presented in Figure 4-34 and Figure 4-35, respectively.

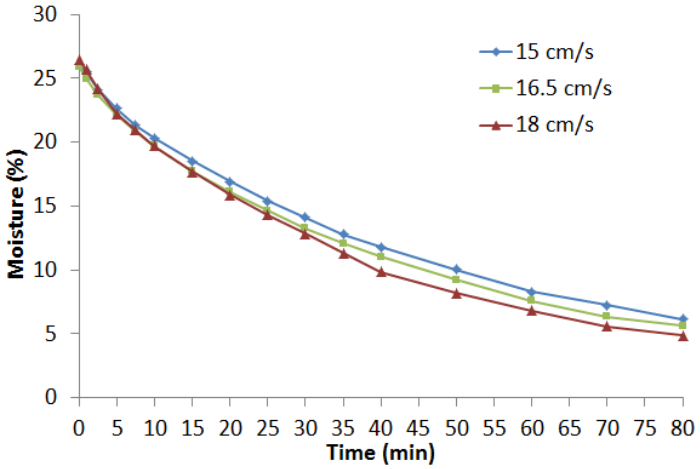

Figure 4-34: Effect of air velocity on Fluidized bed coal drying (temperature:130 ˚C)

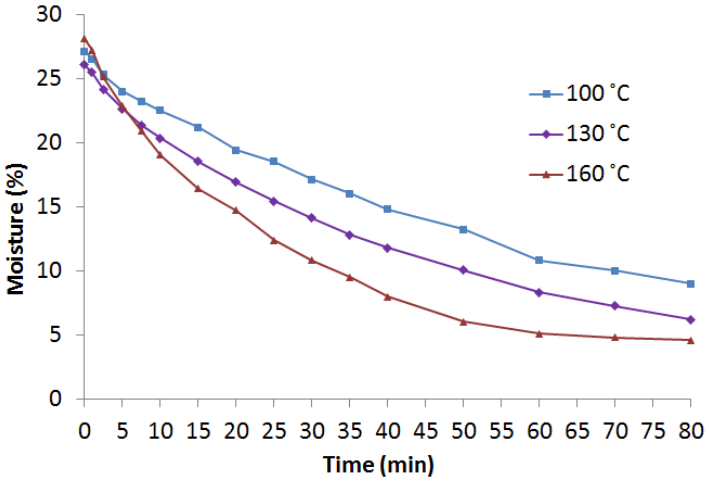

Figure 4-35: Effect of air temperature on fluidized bed coal drying (U=15 cm/s)

Similar conclusions as packed bed drying could be made for fluidized bed coal drying system also. By increasing air velocity and temperature, particle drying process improves. The increase of air temperature influences moisture removal more significantly than air velocity.

Packed bed drying experiments showed that drying under any temperature and air velocity (the range studied here), always, followed two different kinetic behaviors. At first (up to 30 min), mass reduction showed zero order kinetic where, shifted to first order after that. On the other hand, mass loss in fluidized bed coal drying showed first order kinetic. A simple mathematical relationship

between mass of coal moisture and time was considered for determining kinetic order of the drying processes. Therefore zero and first order kinetic rates (k) could be retained through $M=M_0-kt$ and $M=M_0\exp-kt$, respectively. M, M_0 and t were moisture mass (g), initial moisture in coal (g) and time (min). The kinetic rates of drying experiments under various air velocities and temperatures are presented in Table 4-12. As seen, drying rate increased by increasing temperature or air velocity for both scenarios.

Table 4-12: Packed bed vs. fluidized bed coal drying rates (k)

	Packed bed zero order (g/min)			Packed bed first order (1/min)			Fluidized bed first order (1/min)		
˚C / U (cm/s)	100	130	160	100	130	160	100	130	160
15	0.3278	0.4123	0.6501	0.018	0.025	0.034	0.016	0.018	0.029
16.5	0.3901	0.4274	0.6374	0.022	0.027	0.029	0.017	0.019	0.025
18	0.4073	0.5425	0.678	0.021	0.025	0.027	0.017	0.02	0.025

Zero order kinetic occurs once available surface moisture (free moisture) is abundant compared to drying force or, drying force is strongly limited compared to available moisture therefore, drying becomes independent of moisture content or drying force. Vice versa, if the drying force predominates or available moisture is limited, first order (or higher) kinetics take place. Therefore as a preliminary conclusion, by considering combination of T and U as drying force and sample identically, it could be concluded that, drying force was stronger in fluidized bed (due to pre-heated media in bed) as it presented first order kinetic from the beginning. The first order kinetics was obtained after 30 min in packed bed once available moisture was reduced and consequently, drying force (assuming identical during experiment) become able to switch drying process to a first order phenomena. Thus particle drying could be improved in fluidized bed by further amplifying drying force.

It should be mentioned that, performed experiments and determined rates are in preliminary stages and obviously, more parameters (e.g. coal mass and particle size, humidity of inlet and outlet air …) and wider ranges of parameters

(i.e. temperature, air velocity) should be taken into consideration to obtain extensive knowledge over the fluidized bed coal particle drying. Also effective parameters, such as air temperature and velocity and coal particle size, should be included in the mathematical model describing drying phenomena and drying rates. Consequently the activation energy of coal drying should be determined considering obtained kinetic rates.

Figure 4-36 compares results of coal drying in packed bed and fluidized bed, both under 16.5 cm/s and 130 ˚C. The discussed two kinetic behaviors for packed bed drying are indicated on the graph. As seen, for the first 25 min fluidized bed performed effective drying than packed bed and after that packed bed took the privilege. In fact moisture of coal adsorbed more energy as hot air residence time was higher in fluidized bed (due to excessive pressure drop created by sand volume) and also coal particles were in contact with warm sand particles other than just passing hot air. After a while, once bed lost its pre-reserved heat energy (in sand) drying became slower than packed bed. The same behavior as shown in Figure 4-36 was observed for similar drying experiments. Considering the advantages of shorter process time and also possibility of preparing circulating hot sand before adding coal to bed (used for separation and drying, simultaneously or sequentially), first part of Figure 4-36 graph seems to be more attractive to industry than considering longer packed bed drying process.

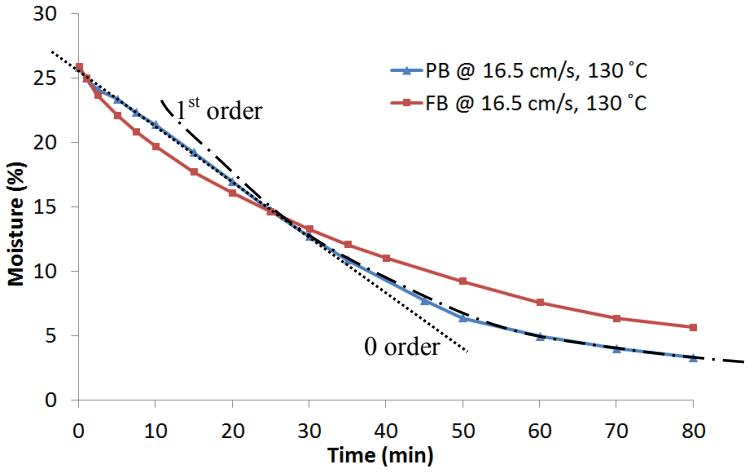

Figure 4-36: Packed bed vs. fluidized bed coal drying

4.4.2 Integrating ADMFB cleaning and fluidized bed drying

In order to follow the concept of stage beneficiation and drying, three clean coal products were prepared using big batch ADMFB separator. The clean coal products were introduced to the pre-heated fluidized bed (160 ˚C, 18 cm/s). The 0, 0 and 0 levels of air velocity, separation time and bed height (Table 4-1) were used in beneficiating products. The average feed and product ashes and combustible material recovery of three experiments were measured to be 13.37, 10.5 and 64.9%, respectively. The drying curves of three clean coals as well as drying curve of relevant ROM under the same settings are presented in Figure 4-37.

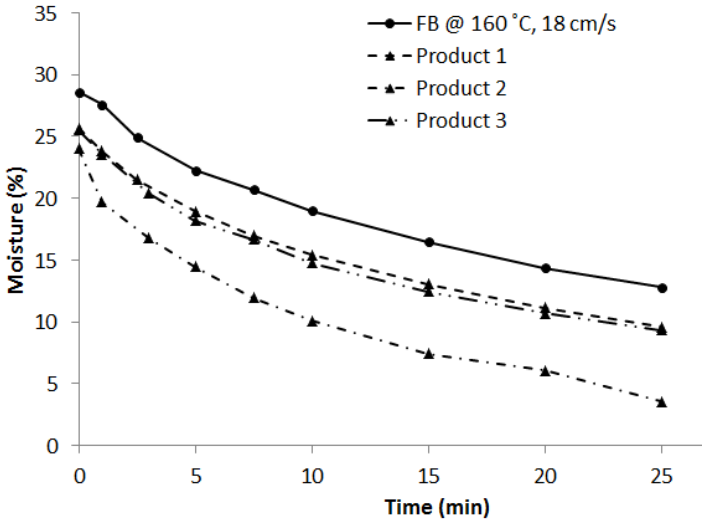

Figure 4-37: Drying curve of ROM and ADMFB clean coal products

As seen, drying curve of clean coal products were parallel to ROM but positioning lower than that since, they had lower initial moisture content. Further investigations showed that, the rejected material in beneficiation stage had also lower moisture contents and dry solid yields than products. The moisture reduction (difference between instantaneous moisture and feed moisture) was between 8.5 and 13.2% for 7.5 min and 15 to 10.2% for 10 min drying. This means 33.8 to 52.5% reduction in moisture content in 7.5 min or 39.8 to 59.8% in 10 min drying.

CHAPTER 5

CONTINUOUS ADMFB BENEFICIATION

One of the obvious differences between batch and continuous separator is that, in continuous separator a major horizontal movement of particles (sand and coal) is introduced to the system which directly or indirectly affects particles residence time and effective bed height and consequently segregation of particles. Also unlike batch separator, influx and discharge of sand (as dominant phase) could introduce turbulence and as a result cause mixing of segregated coal particles (mainly around discharge zone). In general, continuous operation could impose extra in-stability to system by nature. Therefore, in this chapter, continuous ADMFB beneficiation of coal was tested through a set of experiments designed to evaluate the main operating parameters effect (U, T, H and coal particle size) once ADMFB is up-scaled from batch to pilot scale continuous mode.

Full factorial experiment design method was used to investigate the effect U, T and H on beneficiation performance of continuous ADMFB separator when coarse GE coal was fed to the separator. Enough amount of coarse sand (390 μm) was produced in lab to run the continuous apparatus. The 19.5 and 17.7 cm/s were considered as high and low levels of superficial air velocity as based on preliminary runs, full bed fluidization in continuous set up was developed around 17 cm/s. Bed heights of 15 and 20 were considered as low and high levels in the experiments, while full and half segregation zone length (Figure 5-1) were assumed as representatives of high and low separation times. Mean of high and low levels of each parameter was considered for three repeating tests.

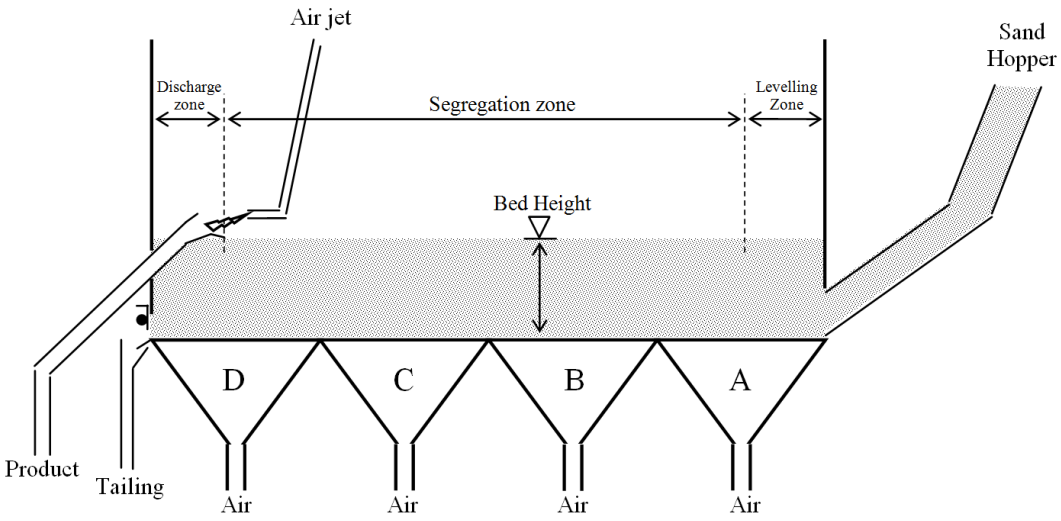

Figure 5-1: continuous ADMFB illustration

As shown schematically in Figure 5-1, the total length of bed had been divided into three sections; namely leveling, segregation and discharging zones. Due to influx of sand from hopper, as result of gravity force as well as pressure drop because of motion of sand particles in bed, some disturbances occur (local turbulence) at the beginning section of the bed. Therefore half of cell A is considered as leveling zone and coal feeding port is considered after that. In the preliminary design of bed, low ash and high ash particles discharge gates were considered as gates on the end wall of bed. Preliminary experiments revealed that when both gates were open the lower gate was discharging sand and accompanying coal particles with very high flow rate (compared to product gate) causing entrainment of low ash coal particles from top layers to the tailings stream; even though the bed surface was horizontal and flow of solid particles was retained at product gate. In order to avoid remixing of low and high ash particles while discharging from bed, a product channel was designed and positioned before end wall to collect the floating particles before entering the suction affected zone. Practically no significant phenomenon was occurring after the edge of product channel, named as discharge zone, except providing enough medium height to avoid extra medium surface level gradient in bed. Considering total bed length and levelling and discharge zones length, 76 cm of bed length were considered as active segregation zone. Movement of media and sunken high

ash particles at the bottom of bed (on the porous media) were confirmed visually and practically through conducting preliminary experiments.

The real bed height in continuous set up was found to be function of product discharge channel position and air flow rate at cell A. It was possible to create any gradient of height starting from leveling zone and decreasing toward the edge of product channel. Creating some gradient on the bed surface facilitated the movement of low ash particles toward the end of bed where in combination with the segregation zone length could also affect material residence time in bed.

Beneficiation experiments were conducted after obtaining stable bed height and continuous media flow, by adding ROM particles continuously to the top of moving bed. Coal particles were separated from both product and tailings streams via screening, and necessary information were obtained by measurements or analysis proceeded based on the discussed methods in chapter 3. The obtained responses for main design and repeating experiments (6, 9 and 11) as well as some useful information for each run are presented in Table 5-1.

Table 5-1: Full factorial design experiment settings and resultant responses (continuous ADMFB separator)

Run	U (cm/s)	T (s)	H (cm)	Feed ash (%)	$CC^{\%}_{Ash}$	$R^{\%}_{C\ to\ L_1}$	$S.E.^{\%}_{sys}$	Ash rejection (%)	L_{end} Ash %
1	-1	-1	1	25.63	24	98	30	6.34	91.3
2	-1	1	1	25.63	9.63	83.30	61.85	62.44	60.51
3	1	-1	1	30.62	14.05	94.07	61.29	54.12	82.9
4	-1	1	-1	25.08	11.11	97.61	62.06	55.72	89.89
5	-1	-1	-1	27.93	21.57	99	29.44	22.77	91.98
6	0	0	0	29.04	9.23	82.48	65.58	68.21	65
7	1	-1	-1	26.76	16.7	95.6	45.48	37.62	79.82
8	1	1	-1	28.62	10.76	89.58	65.45	62.4	73.76
9	0	0	0	30.1	10.39	92.78	69.61	65.5	81.74
10	1	1	1	26.32	9.46	77.66	60.02	64.06	55.27
11	0	0	0	26.56	9.43	91.82	67.55	64.5	76.5

The results of continuous experiments were analyzed in the same manner, similar to that of batch experiments. Table 5-2 provides the statistical details of the quadratic response functions for different operating parameters. Here also A, B and C represent U, T (bed length) and H, respectively.

Table 5-2: Results of statistical analysis for clean coal ash content, combustible material recovery and system separation efficiency (continuous ADMFB separator)

Source	Clean coal ash content			Combustible materials recovery			System separation efficiency		
	Mean square	F-value	p-value Prob.> F	Mean square	F-value	p-value Prob.> F	Mean square	F-value	p-value Prob.> F
Model	70.46	46.17	0.0002	103.49	7.26	0.0259	475.01	19.25	0.0018
A-U	29.4	19.27	0.0046	55.08	3.86	0.1065	298.75	12.1	0.0132
B-T	156.36	102.46	< 0.0001	185.41	13.01	0.0154	864.37	35.02	0.001
C-H				103.32	7.25	0.0432			
(A B)	25.61	16.78	0.0064				261.92	10.61	0.0173
(B C)				70.14	4.92	0.0773			
Curvature	54.03	35.4	0.001	17.38	1.22	0.3197	533.18	21.6	0.0035
Residual	1.53			14.25			24.68		
Lack of Fit	2.1	5.51	0.1595	2.18	0.067	0.9723	34.98	8.58	0.1071
Pure Error	0.38			32.37			4.08		
R^2	0.958			0.853			0.906		
Adj. R^2	0.938			0.736			0.859		
C.V.%	9.29			4.15			8.84		

The correlated coded quadratic polynomial models describing the product ash content, combustible materials recovery and separation efficiency as a function of significant variables and their interactions are presented in Equation 5-1 to Equation 5-3, respectively.

Equation 5-1: $\mathrm{CC}^{\%}_{\mathrm{Ash}} = 14.66 - 1.92\mathrm{A} - 4.42\mathrm{B} + 1.79(\mathrm{AB})$

Equation 5-2: $R^{\%}_{C\ to\ L_1} = 91.85 - 2.62A - 4.81B - 3.51C - 2.96(BC)$

Equation 5-3: $S.E._{sys}^{\%} = 51.95 + 6.11A + 10.39B - 5.72(AB)$

Very low values of the Fisher's F tests indicated that all three mentioned models were significant. There was <2.56% chance that clean coal ash content, recovery and separation efficiency models were originating from noise. Lack of fit was also found to be not-significant for three correlated response functions. Based on ANOVA test (Fisher's F tests) and considering lack of fit test, it could be concluded that three suggested response models were suitable for predicting the target responses within the range of variables tested here.

The F-values of response models indicate that, the curvature was significant for $CC^{\%}_{Ash}$ and $S.E.^{\%}_{sys}$ but insignificant for $R^{\%}_{C\ to\ L_1}$. Comparing R^2, adjusted R^2 and CV values of the batch experiments (Table 4-8) with continuous one (Table 5-2), reveals a little bit lower quality for the continuous models, but still good enough to be used for studying parameters effect or their interactions. Highest model R^2 and adjusted R^2 belongs to $CC^{\%}_{Ash}$ and lowest CV belongs to $R^{\%}_{C\ to\ L_1}$. The actual and model predictions for the response models are shown in Figure 5-2a-c.

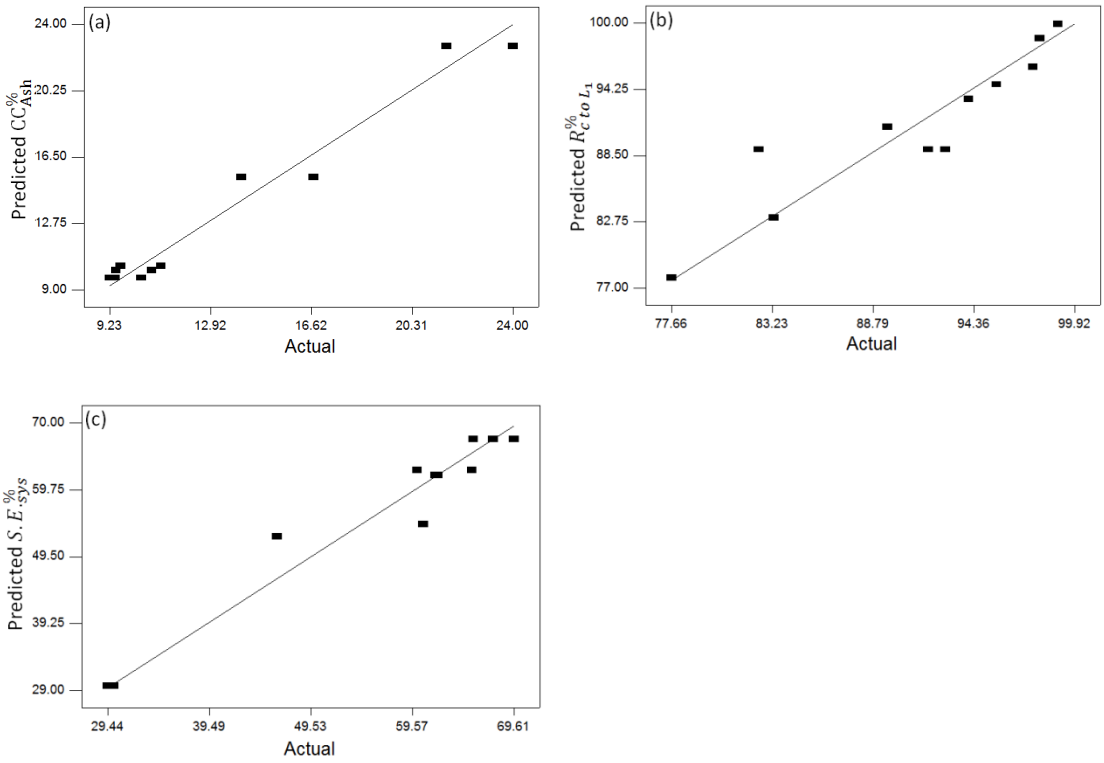

Figure 5-2: Experimental values vs. model prediction a) clean coal ash content, b) combustible material recovery, c) system separation efficiency

5.1.1 Main parameters effect on responses

On the basis of parameters coded coefficients for the clean coal ash content (Equation 5-1), and their significance levels (Prob. > F in Table 5-2) both superficial air velocity and separation time were inversely (negatively) affecting $CC^{\%}_{Ash}$ while, bed height had no significant effect on $CC^{\%}_{Ash}$ at 95% confidence level. The perturbation plot of the main operating parameters for the $CC^{\%}_{Ash}$ is

shown in Figure 5-3. As discussed, the parameters coded values were used for development of perturbation plots and the midpoint of all variables were chosen as reference points while plotting. Based on the coefficients in the Equation 5-1 and also the perturbation plot, the order of influence of the operating parameters on the $CC^{\%}_{Ash}$ was T>U. Product ash content decreased from 19% to 10.2% when T was changed from -1 to +1 while U was set to 0 regardless of H level.

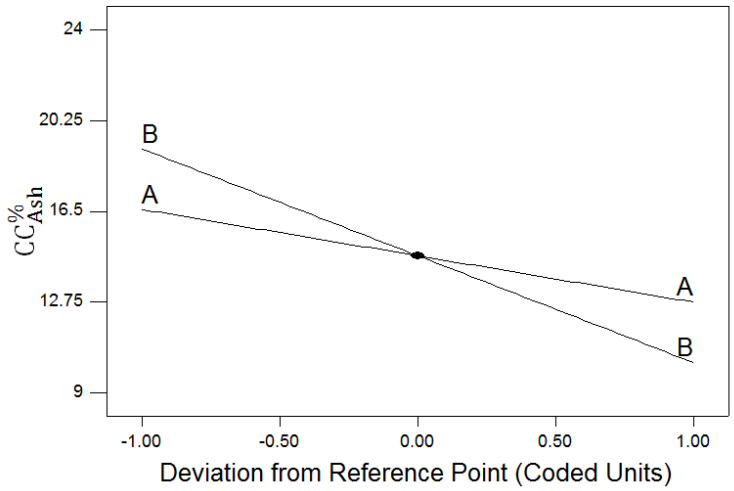

Figure 5-3: Perturbation plot of clean coal ash content (continuous ADMFB)

The coded coefficient of the main operating parameters (see Equation 5-2), their significance level (Prob. > F in Table 5-2) as well as perturbation plot for $R^{\%}_{C\ to\ L_1}$(Figure 5-4), confirmed the negative effect of T, H and U (marginally significant) on $R^{\%}_{C\ to\ L_1}$. The effectiveness order of the operating parameters on $R^{\%}_{C\ to\ L_1}$was T>H>U. If the interactions of the parameters are neglected, improvements of $R^{\%}_{C\ to\ L_1}$could be deduced from Figure 5-4 when lower levels of all parameters are used. Interestingly, $R^{\%}_{C\ to\ L_1}$ was found to be always higher than 88% if any individual parameter was manipulated between -1 and +1 while two others were fixed to their 0 levels.

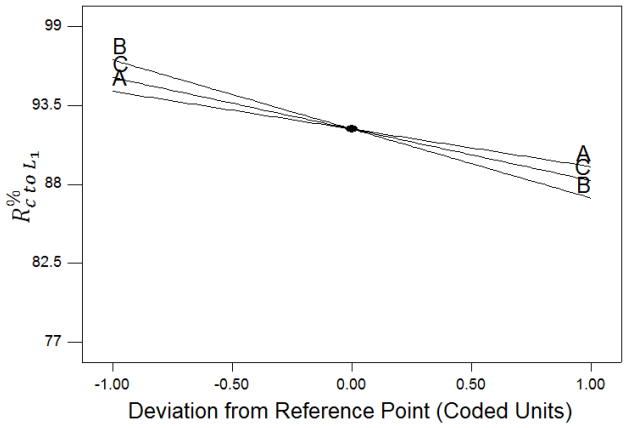

Figure 5-4: Perturbation plot of combustible materials recovery (continuous ADMFB)

Positive effect of U and T on $S.E._{sys}^{\%}$ could be deduced from statistical analyses of the collected data obtained from full factorial design. Here also bed height showed no significant effect on $S.E._{sys}^{\%}$ at 95% confidence level (the same as $CC_{Ash}^{\%}$). Considering the sign of the coefficients of the main operating parameters (Equation 5-3), their significance level (Prob. > F in Table 5-2) as well as perturbation plot for $S.E._{sys}^{\%}$ (see Figure 5-5), the effectiveness order of the parameters on $S.E._{sys}^{\%}$ was T>U. The range of variations imposed on $S.E._{sys}^{\%}$ was significant. The $S.E._{sys}^{\%}$ increased from 41.25% to 62.75% when full length of the segregation zone was used instead of its half. Figure 5-5 suggested obtaining of higher $S.E._{sys}^{\%}$ when high levels of U and T were used; of course the mutual interaction of parameters should be ignored for such decision.

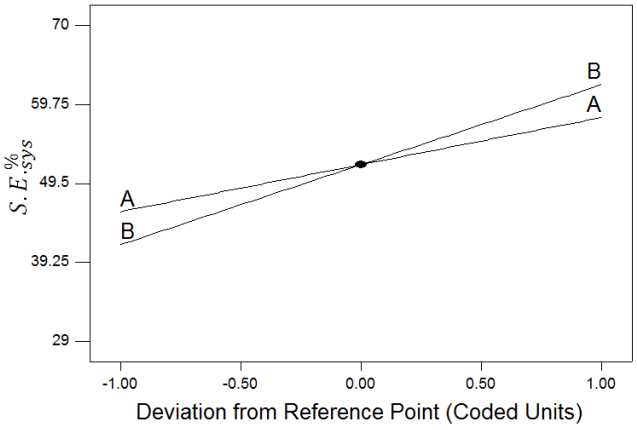

Figure 5-5: Perturbation plot of separation efficiency (continuous ADMFB)

5.1.2 Mutual interaction of operating parameters

The results ANOVA test on collected data, revealed mutual interactions of the parameters for the assumed responses when continuous apparatus is employed for coal beneficiation. 2D interaction or 3D response surface plots of the effective interactions of the operating parameters on different responses are illustrated in Figure 5-6 to Figure 5-14.

According to Equation 5-2, there was a 95% significant positive interaction between U and T, where presented as 2D and contour plots in Figure 5-6 and Figure 5-7, respectively. The H was set to -1 while producing both plots. Since the $CC^{\%}_{Ash}$ was not sensitive to H, the shape of 2D or contour plots remained identical when level of H is changed from -1 to +1. According to Figure 5-6, lower ash product could be produced in the full range of T when U was at its higher level. By increasing T from its -1 level to +1 when U was at -1, a 12.1% cleaner coal could be produced. Figure 5-7 shows that a step size change in U and T at their lower levels affects $CC^{\%}_{Ash}$ more than their higher levels.

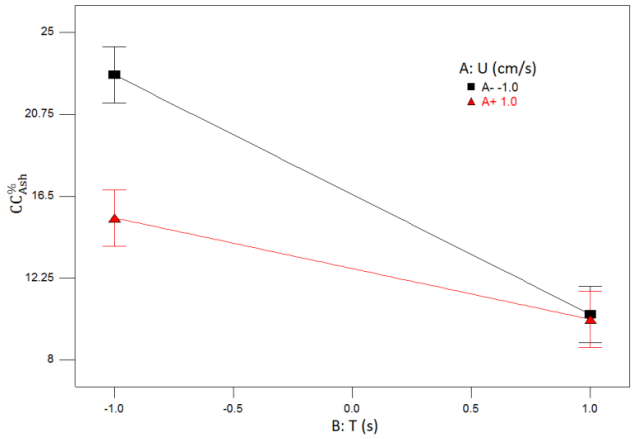

Figure 5-6: 2D plot of mutual interaction of U and T on clean coal ash content at H=-1

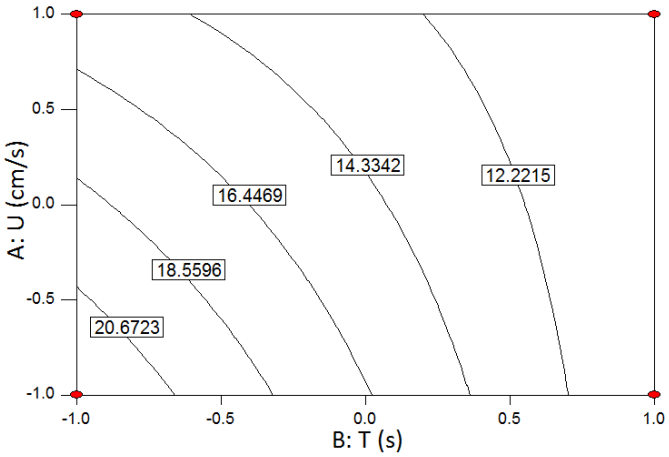

Figure 5-7: Contour plot of mutual interaction of U and T on clean coal ash content at H=-1

The 3D response surface plot of U and T interaction at H=-1 is presented in Figure 5-8. Generally speaking, the presented response surface resembles a sloped plate which maximized $CC^{\%}_{Ash}$ at U and T of (-1,-1) and minimized that at (+1,+1) in the domain of parameters studied here. In fact the combination of lower air velocity and shorter bed length caused a denser pseudo fluid which consequently pushed heavier particles to the top while higher air velocity and longer bed length facilitated segregation of semi-liberated particles and accordingly just lighter particles (low ash) remained on the top layer of bed.

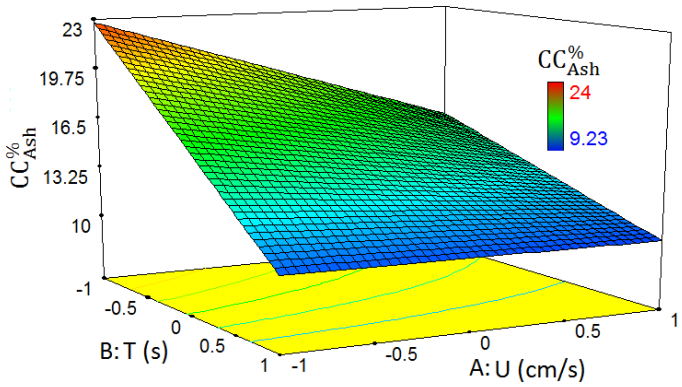

Figure 5-8: 3D interaction plot of U and T on clean coal ash content at H =-1

The ANOVA results (Table 5-2 and Equation 5-2) revealed a significant mutual interaction between T and H when $R^{\%}_{C\ to\ L_1}$ was considered as an evaluation response for the process. Based on the analysis results (Table 5-2 and Equation 5-2) the effect of this interaction on response was stronger than U,

chosen as main operating parameter. This interaction affects $R^{\%}_{C\ to\ L_1}$ negatively. The 2D and contour plots of T and H interaction are illustrated in Figure 5-9 and Figure 5-10, respectively. U was set to +1 while producing the graphs since the general shape of both graphs were the same except the numerical values of the parameters or the response.

Higher recoveries were obtained for lower bed heights in the full range of T regardless of U settings (Figure 5-9). The difference between higher and lower recovery increased when higher bed heights were used. Also the difference between higher and lower recoveries for longer bed length was much bigger compared to the cases which shorter bed lengths were utilized for separation.

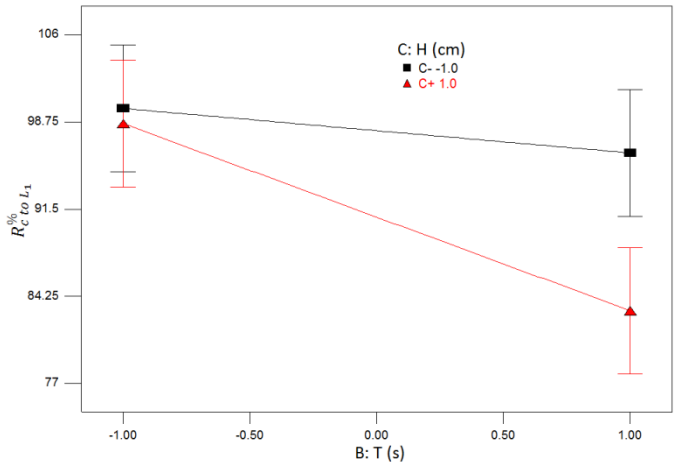

Figure 5-9: 2D plot of mutual interaction of T and H on combustible material recovery at U=+1

Figure 5-10 shows that the recovery was more sensitive to a step size change of T and H at their higher levels, where small changes in the T and H could influence the recovery more effectively compared to their lower levels. Higher recoveries with more stability in results were obtained for lower levels of T and H (in any level of U).

Figure 5-11 depicts the 3D response surface plot of T and H at U=+1. A similar and parallel surface, positioned higher than the one presented in this figure, obtained when U=-1 was used therefore just one of them is illustrated here.

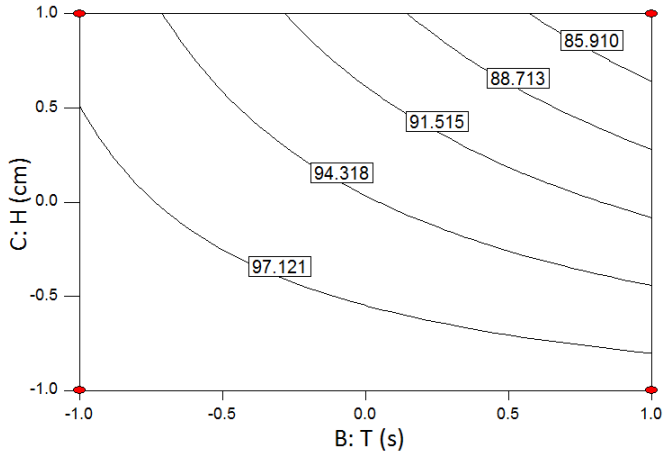

Figure 5-10: Contour plot of mutual interaction of T and H on combustible material recovery at U=+1

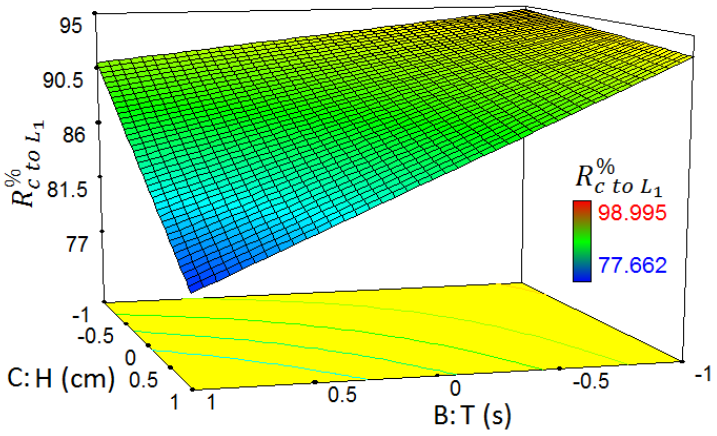

Figure 5-11: 3D interaction plot of T and U on combustible material recovery at U=+1

As Figure 5-11 indicates using lower T and H levels (shorter bed length and shallow beds) could result in higher recoveries where using full bed length and deeper beds could deteriorate beneficiation performance of a continuous ADMFB coal separator. The difference between maximum and minimum recoveries in the studied domain of variables exceeds 20%.

According to Equation 5-3, there was a 95% significant negative interaction between U and T where presented as 2D and contour plots in Figure 5-12 and Figure 5-13, respectively. The H was set to +1 while producing both plots. Since the $S.E._{sys}^{\%}$ was not sensitive to H, the shape of both plots remain identical when level of H is changed from +1 to -1.

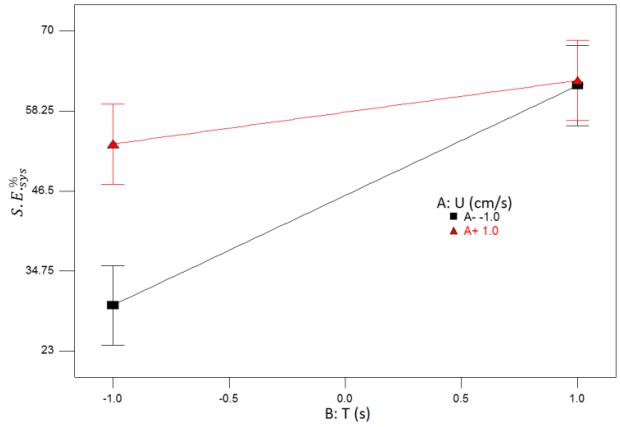

Figure 5-12: 2D plot of mutual interaction of U and T on system separation efficiency at H=+1

According to Figure 5-12, higher system separation efficiency could be achieved in the full range of T when U was at its higher level. The magnitude of variations on $S.E._{sys}^{\%}$ when U was at its higher level, was a lot bigger than that when lower air velocities were used in continuous bed to fluidize sand particles (in the domain of investigated bed length and at both levels of bed depth).

Figure 5-13 shows that the $S.E._{sys}^{\%}$ was more sensitive to a step size change of T than U. This sensitivity was higher at lower levels of both U and T. Higher separation efficiencies with more constancy in results were obtained for higher levels of U and T (in any level of H).

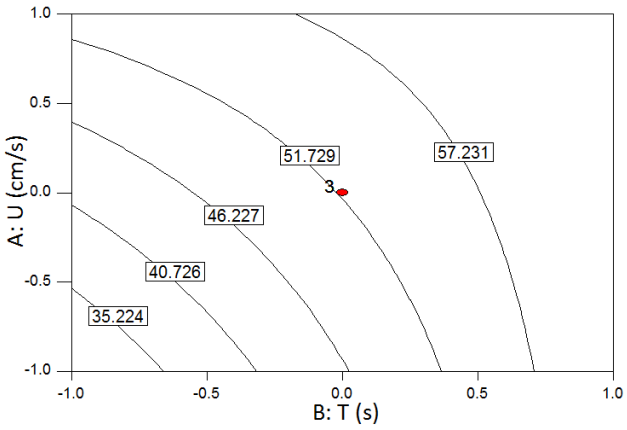

Figure 5-13: Contour plot of mutual interaction of U and T on system separation efficiency at H=+1

The 3D plot of response surface of U and T at H=+1 is presented in Figure 5-14. Similar to the previous responses; a parallel surface obtained when H=-1 was used therefore just one of them is presented here.

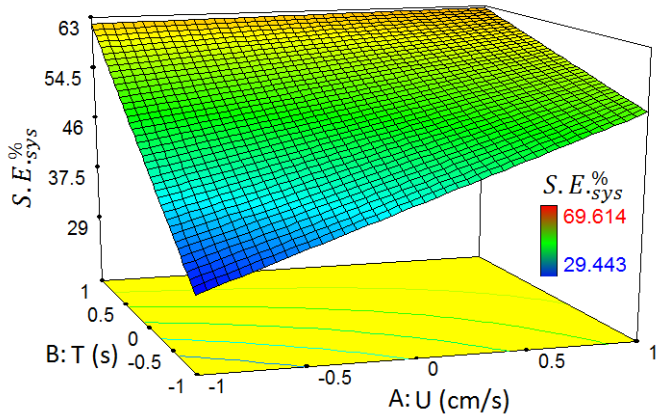

Figure 5-14: 3D interaction plot of U and T on system separation efficiency at H=+1

As Figure 5-14 indicated, using higher U and T levels (longer bed length) could result in higher separation efficiency where using lower air velocity and shorter bed length could deteriorate separation efficiency of the continuous ADMFB coal separator. The difference between maximum and minimum system efficiencies in the studied domain of variables exceeded 31%.

5.1.3 Optimization of operating parameters for continuous ADMFB coal beneficiation

As discussed in section 4.2.3, the desired conditions for the considered responses are to minimize clean coal ash content or maximize combustible materials recovery or maximize system separation efficiency. The proposed levels of the main operating parameters (by Design Expert) for three mentioned strategies are summarized in Table 5-3.

Table 5-3: Optimum parameters for various response strategies

Response	Optimization goal	U	T	H
$CC^{\%}_{Ash}$	Minimum	+1	+1	-1
$R^{\%}_{C\ to\ L_1}$	Maximum	-1	-1	-1
$S.E.^{\%}_{sys}$	Maximum	+1	+1	-1

Using coarse size GE ROM, three experiments were performed under U, T and H of +1, +1 and -1, respectively, to verify the reproducibility and reliability of the analysis. The addressed settings match with experiment No. 8 in Table 5-1. The average ash content of feed for three samples was determined to be, 29.1%. The averages of the obtained results for three experiments are presented in Table 5-4.

Table 5-4: Results of continuous ADMFB coal beneficiation optimization

	Feed ash (%)	$CC^{\%}_{Ash}$	$R^{\%}_{C\ to\ L_1}$	$S.E.^{\%}_{sys}$	Tailings ash (%)	Ash rejection (%)
Repeat # 1	30.14	10.06	86.88	67.33	71.83	66.64
Repeat # 2	28.68	10.27	88.35	66.15	72.11	64.21
Repeat # 3	28.46	9.86	92.08	68.79	78.97	65.38
Average	29.1	10.06	89.11	67.42	74.3	65.41
Model prediction	--	10.11	90.89	62.73	--	--

The average repeating experiments results are similar to the results of experiment No. 8 in Table 5-1. Of course there are some variations which could be attributed to the heterogeneous nature of coal and also the difference between feed samples initial ash content. The difference between models predictions (Table 5-4) and average repeating experiments results were calculated to be 0.5, 2 and 7% for $CC^{\%}_{Ash}$, $R^{\%}_{C\ to\ L_1}$ and $S.E.^{\%}_{sys}$, respectively, which indicated models high accuracy and reproducibility.

5.1.4 Effect of coal size on the performance of continuous ADMFB separator

Beneficiation results of GE middle and coarse size fractions were used to study the effect of particle size on separation performance of the continuous ADMFB coal separator. The experiments conducted under U, T and H of +1, +1 and -1, respectively, (the same as optimization-section 5.1.3). The average results for both size fractions are presented in Table 5-5 (some are adopted from Table 5-4). As pointed out previously, in batch experiment section, the coarse size fraction has lower feed ash content compared to middle size fraction.

Table 5-5: Test results to study the effect of particle size on the continuous ADMFB performance

Feed size	Feed ash (%)	$CC_{Ash}^{\%}$	$R_{C\ to\ L_1}^{\%}$	$S.E._{sys}^{\%}$	Tailings ash (%)	Ash rejection (%)
Middle	31.7	21.37	93.23	42.23	75.57	32.5
Coarse	29.1	10.06	89.11	67.42	74.3	65.41

Particle size change presented similar behavior for continuous separator the same as the batch one. Feeding bigger particles to the bed improved separation efficiency in terms of lower product ash content and higher system separation efficiency. Ash rejection had increased significantly (almost twice) once coarse particles were fed to separator. Also high ash tailing materials were collected from bed just at a single separation step regardless of feed size. The combustible material recoveries higher than 89% were obtained for either of size fractions where showed some decrease by increase in feed size.

CHAPTER 6

CHEMICAL CHARACTERIZATION OF CLEAN COAL PRODUCTS

As discussed, burning coal in coal-fired power plants is under huge pressure due to health and environmental issues, mostly associated with the inorganic phase (minerals) accompanying the organic phase (carbon). Therefore this section investigates the effect of selective removal of some (high ash) particles from ROM coal, through ADMFB coal cleaning on the quality of product and shrinking coal electricity footprint. Pre-combustion unwanted elements and compounds removal is attractive in a sense that it is likely less expensive and more effective than post-combustion clean up.

Two clean coal products with lowest ash contents from each of low ash (BD) and high ash (GE) coals as long as index head samples of them were used to perform characterization analysis and comparison. The properties of four clean coal products of middle size feed are presented in Table 6-1. Sample preparation steps for all of the analysis were the same as discussed in section 3.4.

Table 6-1: Characterization samples specifications

Sample name	Refer to:	Original ash (%)	$CC_{Ash}^{\%}$	$R_{C\ to\ L_1}^{\%}$	Ash rejection (%)
BD head	--	12.5	--	--	--
BD.-1	Table 4-2-No. 9	11.24	9.31	72.7	17.2
BD.-2	Table 4-2-No. 10	12.45	10.10	70.7	18.9
GE head	--	31.5	--	--	--
GE.-1	Table 4-7-No. 7	31.89	12.00	71.22	62.38
GE.-2	Table 4-7-No. 8	29.94	12.33	59.44	58.82

6.1.1 Ultimate (CHNS) analysis

The ash free ultimate analysis and Higher Heating Value (HHV) of six coals are presented in Table 6-2. Each measurement was repeated at least three times to ascertain the accuracy and consistency of the measurements. Also the oxygen content of the samples was calculated based on CHNS data and considering dry ash content of samples.

Table 6-2: The ultimate analysis (DAF) and HHV of the coal samples

Sample name	N (%)	C (%)	H (%)	S (%)	O (%)	HHV MJ/Kg
BD head	1.12	64.79	4.80	0.69	28.85	21.87
BD.-1	1.18	64.73	4.68	0.72	28.72	22.64
BD.-2	1.18	65.29	4.69	0.69	28.06	22.71
GE head	1.03	70.54	5.10	0.45	22.81	17.77
GE.-1	1.01	70.08	4.77	0.42	23.91	24.1
GE.-2	1.02	69.49	4.66	0.47	24.15	23.99

A review of Table 6-2 revealed some minor changes for all measured components but not significant for any of the elements. The clean coal products were used for measurements and afterword the elemental analysis were converted to ash free basis. Considering the fact that particle separation in ADMFB occurred by balancing physical forces (in mega scale compared to molecular scale); the more or less identical composition of coal phase in product and reject solids seemed to be acceptable. Some minor changes could be attributed to very slight selective maceral type rejection.

One of the main advantages of coal beneficiation, besides reduction of hazardous environmental pollutant concentrations, is to increase the HHV of clean coal products. Obviously due to beneficiation the weight of product material would be less than input feed into the processing plant. On the other hand, firing the same amount of clean coal would result in more energy generation and also severe reduction in furnace fly ash weight (and consequently less fly ash handling problems) per unit weight of furnace feed.

For HHV calculations the correlation presented in Equation 6-1 [83] was used. The correlation was developed based on dry base mass percentage of components in the fuels.

Equation 6-1: $HHV = 0.3491 * C + 1.1783 * \mathrm{H} - 0.1034 * \mathrm{O} - 0.0151 * \mathrm{N} + 0.1005 * \mathrm{S} - 0.0211 * \mathrm{Ash}$

In general HHV of all products increased but this increase was significant for GE samples. The HHV of BD.-1 and BD.-2 products increased 3.5 and 3.8%, respectively, when compared to BD head sample while, HHV of GE.-1 and GE.-2 had experienced 35.6 and 35% increase, respectively, relevant to GE head sample.

As discussed a coal with higher HHV could decrease the weight of the solid fuel into furnace and also produce less amount of fly ash. Using data collected from e.g. experiment No. 7 of Table 4-7 (GE.-1) could be helpful for energy and fly ash re-arrangement demonstrations. Solid yield of feed into L_1, L_2 and L_3 were 55.1, 23.7 and 21%, respectively, and HHV of material in L_1, L_2 and L_3 were determined to be 24.14, 19.37 and 1.1 MJ/Kg, respectively. It is worth to mention that the ash content and HHV of L_2 particles were lower (28.7%) and higher than head sample, respectively. Different components mass percentages as well as HHV of GE.-1 sample in different zones (collected from ADMFB) are presented in Figure 6-1a-b as an example.

As seen, by moving from the top layer, L_1, to the bottom layer, L_3, all components show different levels of decrease except ash content which severely increased for the deepest layer. Such ash reduction profile along the bed depth could also be used for determination of the best removal location for main clean coal product and side streams of the separation process with desirable qualities.

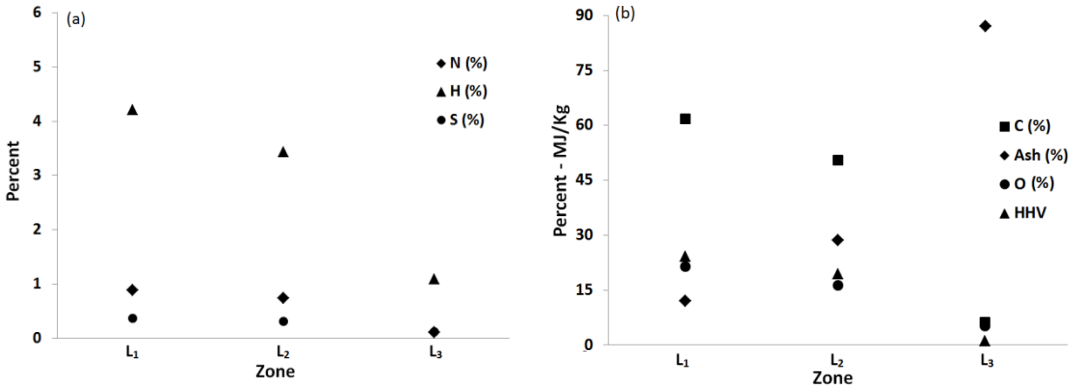

Figure 6-1: Component and parameter distribution along the bed depth a) N, H, and S, b) C, O, ash, and HHV

With a simple calculation considering gross energy of head sample (17.8 MJ/Kg) and its clean coal product (just particles in L_1), it is possible to acquire the same amount of energy by firing 73.7 Kg of clean coal product instead of firing 100 Kg (for instance) of ROM coal. Both cases would produce roughly 1800 MJ gross energy. By firing 73.7 Kg clean coal and 100 Kg of ROM coal, roughly 31.5 and 8.85 Kg of fly ash would be produced at furnace which means 72% reduction in resultant fly ash.

Under such circumstances, the power generation plant could be compared between two scenarios; first, lower furnace feeding rate while recovering the same amount of energy from it (73.7 instead of 100 kg) and producing 72% less fly ash. Second, to continue with previous nominal plant feeding rate (as designed for non-beneficiated ROM) using clean coal product, and produce 36% more energy due to burning 44.9% extra solid (consider 55.1% solid yield to L_1) using the same facilities, but still, with lower fly ash generation (62% less compared to direct ROM feeding). Of course it should be pointed out that, in order to operate furnace with clean coal at its nominal feeding rate, more coal should be produced from mine and processed. Also the solid materials recovered from L_2 was not considered in the above mentioned discussions even though theirs HHV is higher and their ash content is less than head sample.

6.1.2 Trace elements

Most trace elements in coal are associated with the mineral portion of the coal and considered to have an inorganic association. Others may be intimately associated physically or chemically with the organic matter in the coal, thus having an organic association. Often, the mode of occurrence is much more important than the actual concentrations because it is the former that dictates the mobilization of these elements during processes such as pyrolysis, combustion, and gasification and also the type of elements that could be removed from coal by various separation techniques. The elements whose concentration increase with increasing ash content are considered to be associated with the mineral matter and are termed inorganically bound. Al, K, Si, Ti, Sb, As, Be, Cs, Li, Ni, Pb, V, Zn, Rb, Mn, Fe and most rare earth elements usually follow the ash trend while some elements such as Na, Sr, S, Br and B are mostly organically bound and their concentration decreases with increasing the ash content. Some elements such as As and Mn exhibit a mixed association [84].

Pyrite and other iron-sulfide minerals have been found to attract trace elements introduced to the coal from anthropogenic and natural sources [85]. Studies based on data collated from USA, Australia, and Great Britain coals show that As, Cd, Co, Cu, Fe, Hg, Mo, Ni, Pb, S, Sb, Se, Ti, W, and Zn occur in iron-sulfides in particular pyrite form, while Ba, Ca, Fe, and S tend to the sulfates [86]. It has been shown that Cu, Mn, Ni, Pb, and Zn can also be associated with silicates/carbonates as well as pyrite [87, 88]. A positive correlation between Hg and organic sulfur is reported by some researchers [89, 90] and an affinity of Cr and V for clays by others [86].

Trace elements with major concern for human health are considered to be As, Cd, Hg, Pb, and Se [91, 92]. The European Pollutant Emission Register (EPER) [93] requires the reporting of As, Cd, Cu, Cr, Hg, Ni, Pb, and Zn, and the USA Clean Air Act Amendments Bill of 1990 [94] lists 11 elements to be of potential concern, namely As, Cd, Cr, Hg, Ni, Pb, Sb, Be, Mn, Se, and Co. Therefore ICP-MS analysis was performed on the selected clean coal products to study the change in the trace elements distribution due to the beneficiation. The

analyses results of the most hazardous trace elements of the products are presented in Figure 6-2. To avoid reporting too many un-similar numbers (which makes judgment and comparison confusing), results were reported relevant to corresponding head samples in terms of percentage of increase (positive sign, above dashed line) or decrease (negative sign, below dashed line).

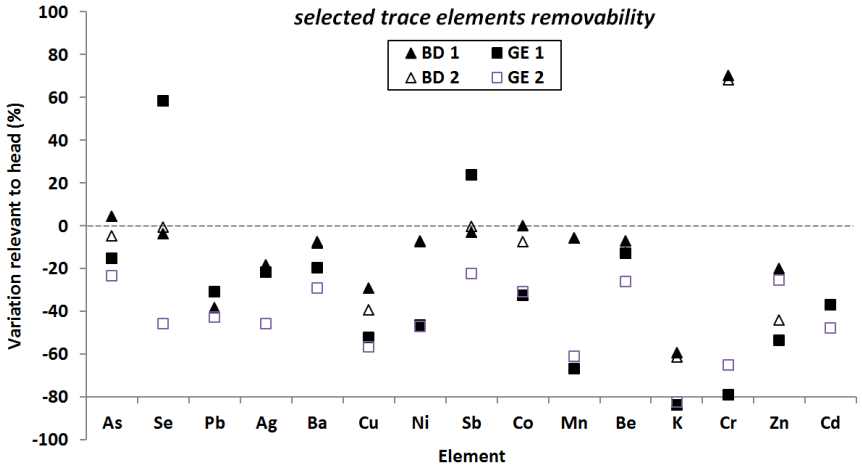

Figure 6-2: Trace elements removability due to beneficiation of coal by ADMFB

As seen, amount of most of the selected hazardous elements decreased after treating with ADMFB separator where negative percentages in graph indicated rejection of that specific trace element. Magnitude of changes is usually bigger for GE than BD products as higher ash rejections were obtained for GE samples at the beneficiation stage. Of course trace elements rejection was also significant for BD samples in most cases even though lower ash rejections were obtained in coal beneficiation experiments compared to GE sample. In general, the higher ash rejection, the more elimination of unwanted elements was.

Decrease in hazardous elements of the clean coal products was an indication of a strong positive affinity of these elements with ash forming minerals in the coal regardless of the type of coal used in beneficiation experiments. This trend has also been reported in literature [95] for coals with ash contents of greater than about 5%. Generally Cu, K and Pb exhibit the highest degree of removal which is an indication of their strong bonding with coal mineral matter. Low rank coals, usually contain more organically-bound elements due to being enriched with oxygen-bearing functional groups such as carboxylic

acid (-COOH) and phenolic hydroxyl (-OH) groups, which are lost with increasing the coal rank [84, 96]. The -COOH group readily participates in ion-exchange reactions and the formation of organo-metallic complexes, (commonly reported in lignite coals) [96-98].

The different behavior of Se, Sb and Cr with decreasing ash contents of the coals revealed the presence of some organically-bound fraction of these elements or in another term association of these elements with organic phase. Cr showed strong association with mineral phase in BD coal where the opposite behaviors, strong organic phase association, was detectable for GE coal. It should be mentioned that more than 60 elements were traced down in six selected samples but the elements of most concern were discussed here.

6.1.3 Mercury content

Mercury content was measured by DMA-80 analyzer. Changes in mercury content of coal due to ash minerals removal was discussed discretely as the mercury content of samples.

Studies have shown that the mercury in the coal is mostly associated with the mineral impurities, in most cases with pyritic sulfur [99, 100]. Although pyrite is not a significant component of the Canadian coals, a direct relation between the rejection of ROM mineral matters and hazardous elements as a result of cleaning processes has been revealed [49, 100-102]. The independency of Hg content to the coal particle size is also reported in some studies [49, 102].

The mercury content of the selected samples as well as mercury rejection of each product relative to its feed sample is provided in Table 6-3.

Table 6-3: Mercury content analysis results

Sample name	Hg content (ppb)	Hg Rejection (%)
BD head	94.3	--
BD.-1	51.8	45.1
BD.-2	62.5	33.7
GE head	59.8	--
GE.-1	32.7	45.3
GE.-2	36	39.8

Table 6-3 shows that, initially GE coal (head sample) had lower mercury content compared to BD coal regardless of its higher ash content. In fact Hg of GE head was lower than both BD products. On the other hand Hg rejections of GE samples were the same or even more than BD samples which was due to higher ash rejections obtained for GE during ADMFB beneficiation experiments. This emphasizes on mineral association of the Hg in ROMs which seems to be stronger for BD coal as with lower ash rejections higher Hg rejections obtained.

6.1.4 Coal reactivity (Thermogravimetric Analysis)

The effect of demineralization (mostly chemical treatment) and addition of specific inorganic compounds on the reactivity of coal in combustion or pyrolysis had been investigated extensively [103-108]. Several criteria have been suggested for characterization of the reactivity. The maximum rate of weight loss (R_{max}) and peak temperature (T_{max}), defined as the temperature corresponding to the R_{max}, are two parameters that have been used by many researchers [103-108].

Hanzade et al. [103] investigated the effect of chemical demineralization of 25 different lignite coals and observed that reactivity in terms of T_{max} increased in 17 samples and decreased in the remaining. Increase in the porosity of coal particles due to chemical demineralization and loss of the catalytic effect of the ash minerals are two competing effects that determine the final outcome of the demineralization on coal reactivity [103, 108]. Quanrun and colleagues [105] used Al_2O_3, CaO and K_2CO_3 as catalyst to the demineralized coal which resulted in improvement of coal reactivity (R_{max}) and lowering activation energy necessary for coal pyrolysis. Katherine et al. [106] found CuCl, AgCl and $Cu(NO_3)_2$ as the most effective catalysts increasing coal chars TGA burnout rate among several tested compounds. Therefore it can be concluded that ash reduction, demineralization or added compounds could increase or decrease the coal reactivity; depending on the properties of the studied coals due to severe heterogeneous nature of the coal. Since ADMFB separator selectively eliminates heavy particles that are mostly formed of non-organic phase (rich in chemical

compounds rather than carbon); it was necessary to check for any changes in reactivity of products due to changes in overall chemistry of coal.

The non-isothermal TGA study was carried out to investigate the reactivity of the beneficiated coal samples towards combustion. For TGA experiments, <20 mg sample were heated up to 800 ˚C on an aluminum pan at a constant heat rate of 15 C˚/min and dry air flow rate of 100 ml/min. Initially, 10 minute drying time at 105 ˚C was allowed for a complete removal of moisture. The combustion (burn out) profiles of two selected clean coal products of BD and GE samples are compared with relevant feed samples in Figure 6-3 and Figure 6-4, respectively. It should be mentioned that due to small amount of solid used for every TGA experiment, several repetition for each sample were performed to obtain average behavior of samples.

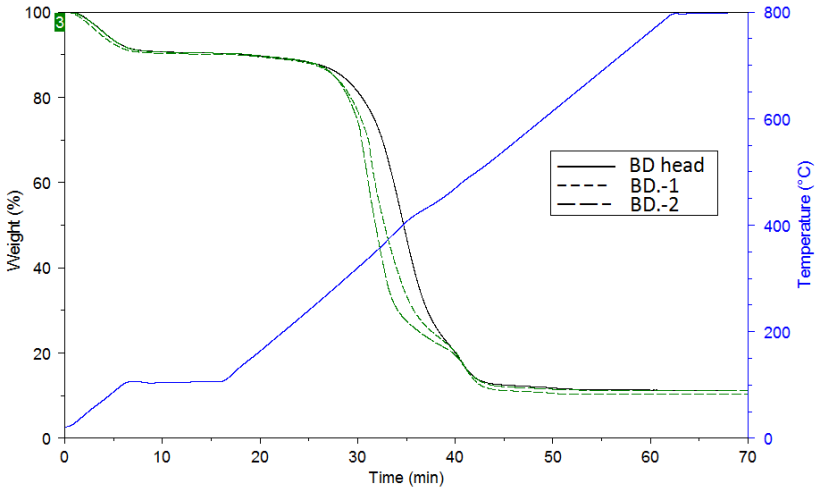

Figure 6-3: Combustion (TGA) profiles of BD head sample and two selected products

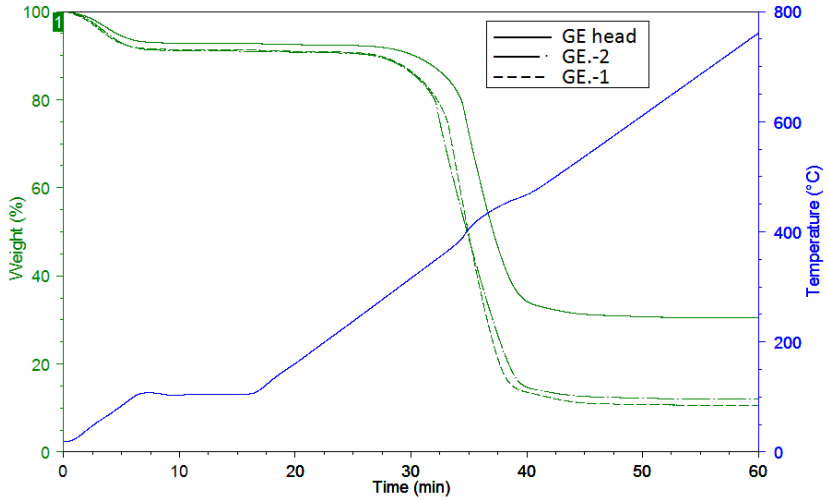

Figure 6-4: Combustion (TGA) profiles of GE head sample and two selected products

DTG (first derivative of TGA curve) graphs were obtained for each TGA experiment and using DTG graphs, R_{max} (%/min) and T_{max} (°C), were determined as measurements of coal reactivity. DTG graphs represented the rate of mass conversion at each moment and were generated based on the TGA data for each sample. A sample DTG graph (BD.-1) is presented in Figure 6-5. Whenever more than one peak with different magnitude is observed (e.g. Figure 6-5) the major peaks were used for evaluations.

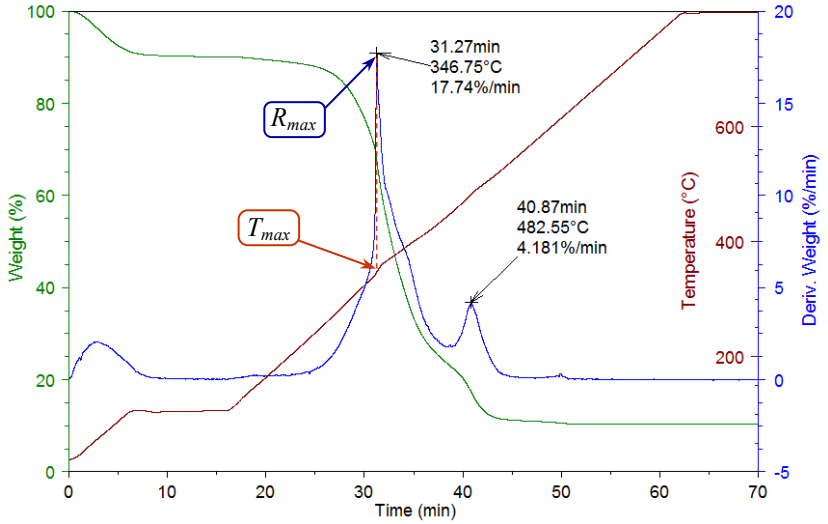

Figure 6-5: The BD.-1 DTG graph

The average values, C.V. (the standard deviation as a percentage of the mean) and changes in the R_{max} and T_{max} respect to their feed samples for all feed and selected products are presented in Table 6-4.

Table 6-4: Information obtained from DTG graphs

Sample Name	R_{max} (%/min)	T_{max} (˚C)	R_{max} C.V.	T_{max} C.V.	R_{max} Change (%)	T_{max} Change (%)
BD head	8.03	383.9	7.79	0.52	- -	- -
BD.-1	18.33	316.6	9.57	8.77	128.27	-17.54
BD.-2	19.92	288.3	6.15	6.22	148.07	-24.89
GE head	10.49	389.6-5	4.72	0.33	- -	- -
GE.-1	13.75	367.13	6.17	0.72	31.12	-5.78
GE.-2	14.96	378.13	8.02	1.94	42.69	-2.96

As reported values in Table 6-4 indicated, initially burning rate of GE head sample was higher than BD (expected due to higher coal ranking). Regardless of sample type R_{max} were increased and T_{max} decreased for all clean coal products; of course to a different extends for GE or BD samples.

The increase in R_{max} for BD products was significantly higher (>130% increase) than GE products even with lower ash rejections (~17-18%) in ADMFB separation stage for BD products compared to higher ash rejections obtained for GE samples (~60%). The same trend in increase of reactivity was obtainable once T_{max} values were used for judgment. As reported in Table 6-4, T_{max} drops more than 17% for BD coals where it was in the order of 3-5% for GE products.

In summary, beneficiation affected reactivity of BD products (in terms of R_{max} and T_{max}) significantly and the reactivity of BD product had passed reactivity of GE head or clean coal products regardless of higher elimination of ash minerals obtained for GE products. In general two major factors could manipulate the reactivity of coal samples namely the dominant maceral type in coal [109-112] and catalytic effect of ash minerals (chemical compounds forming minerals) [105, 106].

It has been reported that the vitrinite macerals of the coal which are more reactive, have lower densities compared to the inertinites which are less reactive [109-112]. Since the separation in the current work was density base, increase in

the vitrinite content of the products (low density particles were collected from top layer) was expected while the rejection of the heavier inertinites to the lower zones happens. The increase in the reactivity of the products observed here could be attributed to the accumulation of the low density and reactive vitrinites and rejection of inertinites form product cut. Also changes in the concentration of trace elements (acting as catalyst) could change the reactivity of coal samples (can cause both positive and negative effect on reactivity) as most elements faced with severe increase or decrease in concentration due to elimination of high density particles from coal samples (will be discussed in more details in section 6.1.5).

6.1.5 Characterization of clean coal ash

6.1.5.1 Ash XRD

Low temperature ash (LTA) was prepared for each of the selected samples as XRD analysis of the coal samples presented no significant distinguishable peaks of crystalline phases due to intense back ground, caused by higher proportion of amorphous carbon phase. The LTA XRD patterns of BD and GE head and their products are presented in arbitrary scale in Figure 6-6 and Figure 6-7, respectively. The diffraction patterns were prepared by Rigaku Co-Kα analyzer at 38 kV and 38 mA by scanning between 5˚ and 90˚ with 1.6˚ degree per minute.

Considering analytical peaks presented in Figure 6-6, four major crystalline phases; quartz, anhydrite, kaolinite and calcium silicate hydrate were detectable for BD head and its clean coal products. As Figure 6-6 showed two highest peaks of BD head belong to quartz (2θ~31˚) and calcium silicate hydrate (2θ~34˚). It could be concluded that almost all crystalline phases were preserved in products after ADMFB coal beneficiation. Of course the intensity of peaks was decreased for beneficiation products which could be considered as decrease of such phases in product.

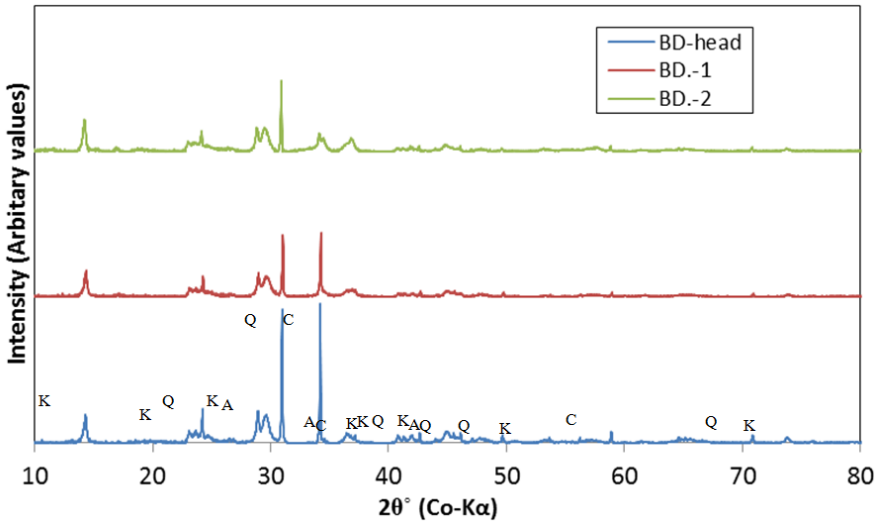

Figure 6-6: XRD pattern of BD head and product LTA
Q: quartz (SiO_2), A: anhydrite (Ca_SO_4), K: kaolinite ($Al_2Si_2O_5(OH)_4$), C: calcium silicate hydrate ($Ca_{1.5}SiO_{3.5}xH_2O$)

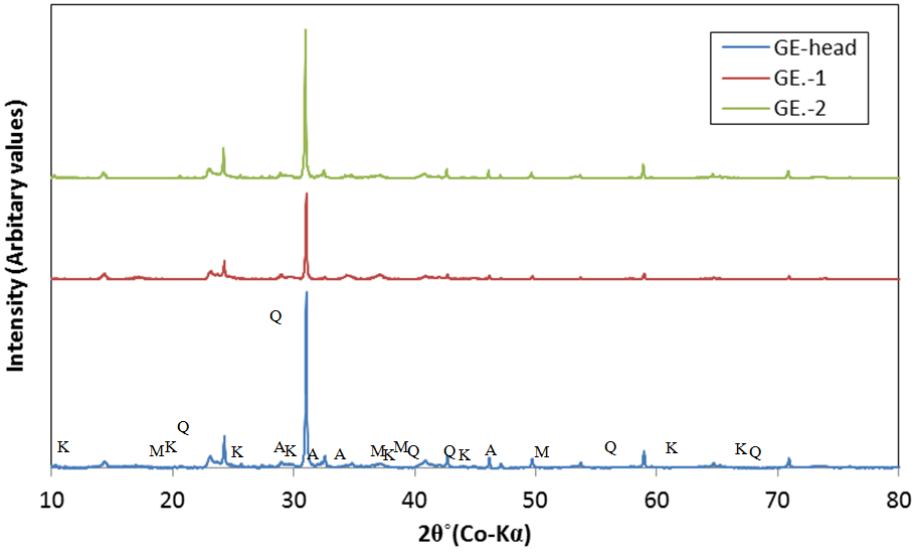

Figure 6-7: XRD pattern of GE head and product LTA
Q: quartz (SiO_2), A: anorthite ($CaAl_2Si_SO_8$), K: kaolinite ($Al_2Si_2O_5(OH)_4$), M: Muscovite ($(K,Na)(Al,Fe,Mg)_2(Si_{3.1}Al_{0.9})O_{10}(OH)_2$)

The same behavior is obvious for GE head and relevant products as in Figure 6-7. The quartz, kaolinite, anorthite, and Muscovite were major crystalline phases in GE head and relevant clean coal products. The same as BD coal, all peaks were detectable in the products, of course with some reduction in intensity except for quartz peak at 2θ~31˚.

XRD studies of LTA implies that, ADMFB coal beneficiation was not able to significantly and selectively eliminate or reduce specific mineral type from ROM coals regardless of the reduction in ash contents of the samples.

6.1.5.2 Ash composition (Ash XRF)

Ash composition of selected samples was determined through XRF analysis. The major oxides assay (grade) for six samples are presented in Table 6-5. Generally ash analysis results are more reliable than the analysis of whole coal, as for the most of compounds (non-volatile) higher enrichment in the mass of solid is obtained when dominant organic part is burnt out, making it detectable with more accuracy [113]. When comparing the ICP-MS and XRF results, this point should be considered that XRF directly measures the total amount presenting in the sample, while ICP-MS only detects the elements that are totally or partially leached into the acid [114]. Therefore, the results for the elements which may organically or covalently be bound to the coal phase (e.g. organic S or Al, Cl, Fe, trace elements etc.) should be interpreted with caution [96, 114].

Table 6-5: Chemical composition of ash samples

Sample Name	Na_2O (%)	MgO (%)	Al_2O_3 (%)	SiO_2 (%)	SO_3 (%)	CaO (%)	Fe_2O_3 (%)	P_2O_5 (%)
BD head	9.06	4.06	17.65	26.18	17.92	17.14	3.77	2.25
BD.-1	11.11	4.16	17.11	23.06	17.00	19.13	4.03	2.46
BD.-2	10.65	3.99	17.04	23.16	17.95	19.00	3.92	2.36
GE head	3.07	2.24	16.62	60.27	5.58	4.20	4.39	0.33
GE.-1	4.19	2.00	15.75	46.52	13.93	10.31	4.62	0.41
GE.-2	4.40	2.20	15.84	45.58	14.50	10.44	4.42	0.36

The characterization results in Table 6-5 indicated that the Na_2O, CaO, Fe_2O_3 and P_2O_3 content of all products had increased to different extents regardless of coal type. This increasing trend was much stronger for GE products where higher ash rejections (Table 4-7) were obtained compared to BD products (Table 4-2). Considering the fact that all products had lower amounts of ash minerals than their corresponding feed and also the increasing trend (negative

affinity) of the three mentioned elements, it could be concluded that Na, Ca and Fe were generally associated (bounded) with organic phase than the ash forming minerals [96, 114]. As addressed in several references, such inorganic elements can bound to the organic phase directly, ion-exchange or as salts of carboxylic acids (-COOH groups) particularly for low rank coals [84, 96, 98, 114].

Decrease in ash content resulted in reduction of Al_2O_3 and SiO_2 contents of product ashes for both GE and BD samples. The MgO has also showed reduction for GE products but not a clear trend was deduced for BD products as the MgO assay fluctuates above and under the head sample for the two selected products. The three mentioned elements (Si, Al and Mg) are the basic components of mainly clay minerals (Kaolinite, Illite and Smectite) which were expected to be abundantly distributed in the coal seams (either syngenetic or epigenetic) or were introduced from roof or floor rocks during the mining operations (extraneous material). Generally Si, Al and Mg could be associated with mineral matter of the coal samples rather than the possibility of organic bounding between them and the organic phase. Such conclusion was made considering the positive affinity of the elements with the ash content of the coal samples.

Sulfur content measurements on BD ash samples were not providing any clear guide to the source of sulfur. Based on the XRF measurements, it seems that any of two most common S types in coal had no privilege to the other one where as if organic or Pyritic (Fe_2S) sulfur were dominant in sample, its content should has presented some degrees of increase in analysis, considering ash reduction and Fe increase identified. The organic origin of S (i.e. organic S) for GE sample could be strongly concluded [114] since SO_3 content of products show more than 140% increase for both selected samples.

6.1.6 Slagging and fouling properties of clean coal ashes

Coal ash minerals contain many components posing different behaviors when heating up to their melting point [115, 116]. The removal of some ash forming minerals can affect the slagging and fluxing properties of the beneficiated coal ash and consequently the operation of coal conversion units. The slagging

and fouling decreases the efficiency of heat exchange surfaces in conventional coal firing furnaces while in slagging gasifiers where, ash is intentionally converted into liquid slag (better operation, control particulate matter emission and trap trace elements and heavy metals in a un-leachable glass phase) to achieve free flux toward the bottom of the gasifier, the higher slagging propensity as well as lower viscosity at operating temperature is required [115, 117, 118]. Several indices and factors such as base to acid ratio, silica percentage, slagging factor and Fe to Ca ratio are suggested in literature to predict and evaluate slagging propensity of ashes [119-121].

Obviously beneficiation can change the composition of the clean coal ash by removal of various mineral components in the ash, partially or completely, depending how bounded they are to the coal phase. The slagging and fouling tendency of selected samples are presented in Table 6-6 in term of base to acid ratio (B/A), slagging factor, silica percent and Fe to Ca ratio (Fe/Ca), as are described in Equation 6-2 to Equation 6-5, respectively. Ash XRF results are used to calculate these indices.

Equation 6-2: $\frac{B}{A} = \frac{Fe_2O_3+Na_2O+K_2O+MgO+CaO}{SiO_2+Al_2O_3+TiO_2}$

Equation 6-3: Slagging factor $= \frac{B}{A} * S_{(\%)}$

Equation 6-4: Silica percent $= \frac{SiO_2*100}{Fe_2O_3+SiO_2+MgO+CaO}$

Equation 6-5: $\frac{Fe}{Ca} = \frac{Fe_2O_3}{CaO}$

Table 6-6. Calculated slagging indices

Sample Name	B/A ratio	Slagging factor (%)	Silica percent	Fe/Ca ratio
BD head	0.61	7.23	58.63	0.21
BD.-1	0.94	11.37	45.76	0.21
BD.-2	0.92	11.80	46.25	0.21
GE head	0.21	0.89	84.7	1.04
GE.-1	0.35	3.72	73.32	0.45
GE.-2	0.36	3.97	72.76	0.42

Changes imposed on slagging and fouling criteria imposed on both BD and GE clean coal products are graphically presented in Figure 6-8 in percentage relevant to corresponding head samples absolute values. As seen, general increase or decrease trend was in the same direction for all for beneficiation products. GE products usually presented biggest variations due to higher ash rejections in beneficiation stage.

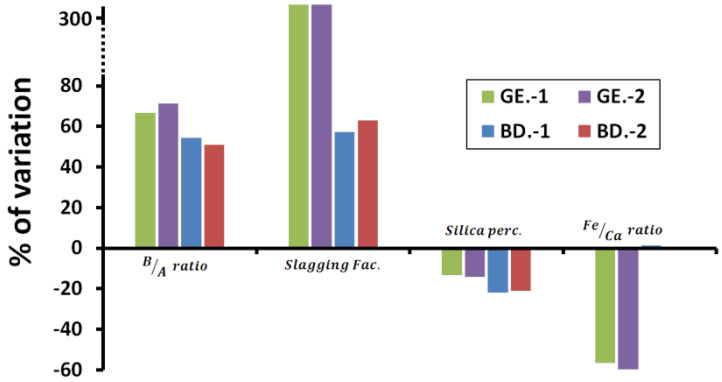

Figure 6-8: Variation of products slagging factors corresponding to their head samples

As seen in Figure 6-8, the B/A ratio had increased almost 52% for BD and 67% for GE products. Usually, the B/A ratios lower than 0.7 results in higher slagging propensity while compared to that, for the ratios higher than 0.7 lower slagging tendencies are expected [119, 120]. The B/A ratio of both BD and GE head samples were calculated to be less than 0.7 initially (Table 6-6). But considering 0.7 limit, BD products were expected to present higher slagging propensity (good for slagging gasifiers) while the GE products seemed to be better feed for conventional coal firing furnaces in spite of experiencing bigger changes in B/A ratio due to ADMFB beneficiation.

The slagging factor had increased for all selected products but significantly for GE samples (> 300%) as reported in Table 6-6. Ashes with slagging factors higher than 2.6 are expected to exhibited increasing (good) slagging behavior [120]. Initial slagging factor value of BD head revealed its high tendency for slagging in spite of GE head which was very far from determining criteria. Considering the slagging factors calculated for both BD and GE products (Table 6-6), increase in slagging tendency of both clean coal products was

predictable due to ADMFB coal separation. This increase in slagging propensity was a lot more promising for BD products.

The silica percent is a good indication of the slagging and fusion properties of the coal ashes in burners and gasifiers. Lower silica percent (less than 65%) is usually considered as lower fusion temperature and viscosity for the molten slag from the ashes. As seen in Figure 6-8 this index had decreased for all products (more for BD products). In spite of decrease in silica percent of GE products, lower slagging could be expected for GE products as both values in Table 6-6 are above 65%. Of course the effect of beneficiation was toward increasing slagging as mentioned. For BD samples all analyzed head or product samples had silica percent less than 65% meaning high tendency to produce earlier melting low viscosity slags where for products silica percent decreased even more intensifying slagging phenomena.

Medium to high slagging tendency is expected when Fe/Ca ratio falls between 0.3 and 3. The Fe/Ca ratio calculation for BD head or products resulted in 0.21, showing no detectable changes. This ratio decreased significantly (around 60%) for GE products compared to their head samples but still falling in the same medium to high slagging zone.

The calculated indices presented in Table 6-6 indicated that, in general, the physical beneficiation of both BD and GE coal samples increased the slagging propensity of the clean coal ashes. For GE coal, ROM sample had very low slagging tendency where beneficiation increased that. The slagging propensity was high for BD coal initially but rejection of high ash particles intensified that severely which is an advantage when these products are fed into the slagging gasifiers.

6.1.6.1 Ash fusibility

As mentioned high slagging and fouling propensity of ash decreases the efficiency and increases maintenance on the conventional coal firing furnaces while it is considered as an advantage for slagging gasifiers operation. In such gasifiers ash is preferred to melt into a free flux (low viscosity) liquid slag for

better operation; flue gas control and minimize gasifier maintenance [115, 117, 118]. For such purpose the temperature of the gasifier should be maintained above the fusion temperature of the ash to enable continuous slag tapping [117, 122].

It is well demonstrated in literature that increase of some basic oxides such as Fe, Ca and Na oxides reduce slag viscosity and fusion temperature while increase of acidic oxides such as Si and Al oxides increase viscosity and coal ash melting temperature [115, 117, 123]. Of course this should be considered carefully as molten ash creates an environment of several compositions which can react or destroy other components network structure and develop un-expected results. For instance Kim et al. [115] reported low fusion temperature for high quantity of SiO_2 and low CaO where everyone expected high fusion temperature. Fayalite (Fe_2SiO_4) formation as result of high amount of Fe_2O_3, with low fusion temperature is reported as the main reason for that. In contrast, Kim et al. [117] and Song et al. [122, 124] reported an increase in the fusion temperature when the amount of inherent or externally added reducing agents (Fe, Ca, Na and Mg oxides) exceeded a certain amount. The minimizing level (of fusion temperature) varies from coal to coal.

Several indices and factors such as ash fusion temperature (AFT), slagging index as well as viscosity prediction models are suggested in literature and extensively used to predict the behavior of solo ash slags or mixture of ash and some additives [115, 116, 121, 122, 125]. The widely accepted viscosity model, Urbain model, was discussed and used to predict molten ash viscosity of the selected samples in this section.

Severe slagging is expected when the reducing ash fusion temperature is below 1350 ˚C [119, 120] where the closer flow and initial deformation temperatures (obtained from ash fusion test), results in thinner and adhesive ash deposit on reactor surface [115, 117]. Generally, fusion temperature in a reducing atmosphere is equal or less than that in the oxidation atmosphere where the decrease in Fe content of the ash reduces the difference [117].

AFT experiment results for selected samples are presented in Table 6-7 at both under reducing and oxidizing environments. Oxidizing environment occurs

when coal is burnt with abundant amount of oxygen at lower temperatures (around 800 ˚C) such as in conventional burners while, the reducing atmosphere develops in gasifiers where the operating temperature is high and oxygen is not abundantly available.

Table 6-7: Ash fusion temperature experiment results (all numbers are in ˚C)

Sample Name	Reducing atmosphere				Oxidizing atmosphere				Slagging index
	IDT [a]	ST [b]	HT [c]	FT [d]	IDT	ST	HT	FT	
BD head	1091	1141	1155	1213	1150	1281	1331	1400	1104
BD.-1	1131	1161	1166	1196	1197	1413	1418	1431	1138
BD.-2	1144	1167	1174	1200	1191	1422	1424	1432	1150
GE head	1197	1271	1334	1486	1249	1347	1407	1502	1224
GE.-1	1133	1244	1302	1355	1165	1270	1313	1381	1167
GE.-2	1139	1251	1305	1361	1174	1278	1322	1390	1172

[a]: Initial deformation Temperature [b]: Softening (spherical) Temperature

[c]: Hemispherical Temperature [d]: Fluid Temperature

As seen, AFT in reducing environment had decreased for both beneficiated samples especially for GE products dropping down 130 ˚C. All BD samples (head or products) showed lower AFT than 1220 ˚C. This reduction in AFT for beneficiated products (especially as for BD products) was favorable for slagging and fluxing needs in slagging gasifiers. As discussed lower AFT for beneficiated products results in faster slagging as well as lower molten slag viscosity at a certain operating temperature in the gasifier.

Also AFT under oxidizing environment was higher than its equivalent AFT under reducing environment for any individual sample as reported in references [117]. AFT of the BD products increased compared to the corresponding head sample where vice versa occurred for GE product. Increase in oxidizing AFT for the beneficiated products leads to reduced slagging.

Slagging indices (Equation 6-6), calculated based on the reducing AFT for each sample, are presented in Table 6-7.

Equation 6-6: Slagging Index$= \frac{4\mathrm{IDT}+\mathrm{HT}}{5}$ [119, 120].

As seen, slagging factor for all selected BD samples were less than 1170˚C. ADMFB beneficiation caused an increase in BD products slagging factor, but the produced clean coal products slagging factors were still below 1170˚C. For such slagging factors, sever or high slagging as well as low flux viscosities were expected [119, 120]. Even though, slagging factor of GE samples were almost higher than 1170˚C, but one can say, beneficiation lowered that down to 1167˚C, changing slagging propensity of GE coal (head sample) from high to sever slagging ash type.

6.1.6.2 Ash viscosity

As mentioned, the increase of some basic oxides such as Fe, Ca and Na oxides, reduce slag viscosity while increase of acidic oxides such as Si and Al oxides increase slag viscosity in furnaces [115, 117, 123]. The main concept of ADMFB coal cleaning is to eliminate ash forming minerals which consequently changes the original ratio of reducing or increasing oxides in the product. Slag viscosity might be measured directly or calculated through developed models.

Urbain correlation is one of the most widely used slag viscosity models [126-130]. The model is developed based on Al-Si-Ca oxides system in ashes. Three categories of glass formers (X_G), modifiers (X_M) and amphoterics (X_A) are considered in slag composition. The absolute and normalized form of X_G, X_M and X_A are presented in Equation 6-7 and Equation 6-8 where X presents the mole fraction of corresponding oxides.

Equation 6-7:

$$\begin{cases} X_G = X_{SiO_2} + X_{P_2O_5} \\ X_M = X_{CaO} + X_{MgO} + X_{FeO} + X_{MnO} + X_{CrO} + X_{NiO} + X_{Na_2O} \\ \qquad +X_{K_2O} + X_{Li_2O} + 2X_{TiO_2} + 2X_{ZrO_2} + 3X_{CaF_2} \\ X_A = X_{Al_2O_3} + X_{Fe_2O_3} + X_{B_2O_3} \end{cases}$$

Equation 6-8:

$$\begin{cases} X_G^* = X_G/(1 + X_{CaF_2} + X_{TiO_2} + X_{ZrO_2}) \\ X_M^* = X_M/(1 + X_{CaF_2} + X_{TiO_2} + X_{ZrO_2}) \\ X_A^* = X_A/(1 + X_{CaF_2} + X_{TiO_2} + X_{ZrO_2}) \end{cases}$$

The Urbain viscosity model assumes Weymann-Frenkel correlation (Equation 6-9) to predict the slag viscosity ($\mu(P)$) at temperature of T˚ (˚K).

Equation 6-9: $\mu(P) = AT^{\circ}exp\left[\frac{1000B}{T^{\circ}}\right]\ ;\ -LnA = 0.29B + 11.57$

Equation 6-10: $B = B_0 + B_1X_G^* + B_2(X_G^*)^2 + B_3(X_G^*)^3$

Equation 6-11: $\begin{cases} \alpha = X_M^*/(X_M^* + X_A^*) \\ B_0 = 13.8 + 39.9355\alpha - 44.049\alpha^2 \\ B_1 = 30.481 - 117.1505\alpha + 129.9978\alpha^2 \\ B_2 = -409429 + 234.0486\alpha - 300.04\alpha^2 \\ B_4 = 60.7619 - 153.9267\alpha + 211.1616\alpha^2 \end{cases}$

The components of Urbain model have been modified by him or other researchers to consider various possible changes or conditions might rise in industry. Since the main purpose of this section is to compare variation in viscosity of the head and ADMFB beneficiated products, the above addressed equations were used in calculations. Equation 6-7 to Equation 6-11 are adopted from references No. 126-130.

The predicted viscosities of all selected products and their relevant feed samples calculated using Urbain viscosity model at 1250 ˚C under both oxidizing and reducing environment are presented in Table 6-8. It should be mentioned that slag viscosity less than 250 poise is suggested to avoid problems of slag tapping from the slagging gasifiers [115, 117, 125].

Table 6-8: Molten ash slag viscosities at 1250 ˚C (all numbers are in Poise)

Sample name	Reducing Environment	Oxidizing Environment
BD head	66. 6	71.5
BD.-1	31	33
BD.-2	31.8	33.9
GE head	6556.3	9164.3
GE.-1	360.9	457
GE.-2	309.7	384.1

For the six selected samples, reducing environment viscosity was less than oxidizing environment viscosity. Such difference could be addressed by conversion of FeO to Fe_2O_3 under oxidizing environment. The effect of oxidizing or reducing agents was obviously recognizable when very low calculated BD viscosities were compared with GE ones (in either environment). Referring to Table 6-5, the CaO and Na_2O of GE samples were almost 50% lower than BD while SiO_2 content of GE samples were more than twice of BD samples.

As reported in Table 6-8, viscosity of BD head sample was primarily very low where; ADMFB beneficiation reduced that even more than 50% at both environments. Considering changes in oxide contents of BD head sample and both selected products in Table 6-5, the amount of Fe, Ca and Na oxides in products were increased along with decrease of Al and Si oxides which both were in favor of viscosity reduction. Of course these changes were not as significant as changes experienced for GE products. The same viscosity decreasing trend was detected for GE products but changes of Si and Ca oxides, as important compounds effecting slag viscosity, were very significant. The SiO_2 content of products were decreased from 60% to 46% in average while the CaO had increased from 4.2% to 10.4%. Such changes in oxide contents of GE products resulted in severe reduction of GE products viscosity from very high values (6500-9100 poise) to almost 350 poise meaning 96% reduction.

Based on Table 6-8, BD head was suitable for slagging gasifiers where beneficiation resulted in even more fluxing ash slag. Burning BD in conventional furnaces, operating at higher temperatures, might increase operation and maintenance issues of power generation plant. The viscosity of GE head was too high for slagging gasifiers but by ADMFB ash removal it decreased significantly providing suitable slag viscosity range for gasifiers. If just the slag viscosity was the determining criteria to choose between conventional furnaces and slagging gasifiers, ADMFB coal cleaning could change conventional furnace option to gasifier for GE coal.

CHAPTER 7

CFD SIMULATION OF PARTICLE SEGREGATION IN FLUIDIZED BED

7.1 Introduction

Fluidized bed has been extensively used in different industries for several decades, but modelling of such systems is still a challenging task due to the complexity of the underlying physics. Complex hydrodynamic behavior of gas–solid flows, phase interactions and transient behavior of the systems are some of these challenges. Currently no systematic guideline is defined for the appropriate selection of the model parameters [131, 132]. As any other simulation study, the results need to be validated against experimental data before being used as design guidelines. Grace and Taghipour [133] discussed some of the challenges involved in gas–solid CFD models validation in their paper.

Extensive computational time and expense is another challenge in dealing with 2D or 3D CFD models. 2D models are smaller in cell number compared to actual 3D models, so it is easier and faster to work with 2D models, but sometimes they do not accurately represent the reality. Comparison of 2D columns (one dimension much smaller compared to two others) with its simulation results are helpful for studying fluidization phenomena and bubble properties, but wall effect on motion of bubbles and particles should not be ignored here. Using 3D geometries (1:1 scale) will definitely increase the cell number and computational time, but their superior performance is proven [134-136]. 3D simulation of the problem after preliminary 2D model runs is getting more recognition these days due to increase in computational performance of processors and introduction of parallel computing systems.

In this study, several simulation models were developed and run using commercial CFD simulation software, ANSYS-Fluent R14.0 to simulate particle segregation in a gas-solid fluidized bed. The Eulerian multiphase model was used in these simulations. The actual data of sand fluidized bed as well as reference experiments performed using batch ADMFB separator were used to establish and evaluate CFD models. Bed expansion and solid volume fraction (VF) of different identified coal classes (zone base, average density of coal particles) after analyzing reference experiment results were used as model performance evaluation.

7.2 Multiphase modelling approaches

Two approaches are available for numerical multiphase flows modelling; the two-fluid model or Euler-Euler approach, treating phases as interpenetrating continua (continuum mechanics) and the discrete particle model or Euler-Lagrange approach. It should be mentioned that, definition of phase in numerical studies is broader than distinctive physical phases (gas, liquid solid). Here any identifiable class or category of materials could be defined as distinct phases even though the difference is just density, size, shape, and etc. with other categories of the same material [137, 138].

7.2.1 Euler-Lagrange approach

In Euler-Lagrange approach, the dispersed phase is tracked individually or as parcels of particles in the fluid field in specified time intervals during the continuous fluid phase calculations. Momentum, mass and energy exchange between particles and continuum phase is permitted in Euler-Lagrange method. The time averaged Navier-Stocks equations are employed to model fluid phase [137-139]. The dispersed phase could obtain high mass loading compared to fluid phase but its VF should be low. Particle collisions are described considering the energy dissipation due to non-ideal solid-solid interactions by means of restitution coefficient and friction or dissipation constants (spring stiffness) [137, 140, 141].

7.2.2 Euler-Euler approach

In Euler-Euler approach which is the most commonly used approach for fluidized bed simulations, different phases are considered as interpenetrating continua [142, 143]. This model is suitable when particle loading is high [144]. It is computationally cost effective compared to Euler-Lagrange method and also more useful when VFs of phases are comparable or particles are separating due to body forces such as gravity [137, 145, 146]. The conservation equations for each continuum are derived individually, considering each phase VF. The phase VFs are assumed to be continuous function of time and space and since the volume occupied by one phase cannot be taken by other phases, partial VFs are considered for phases with sum of unity once all phases are considered in a time and space frame [137, 144, 147]. As a result, a set of similar conservation equations (one equation for any involved phase) are closed by providing constitutive relations obtained empirically or in case of granular flows through application of kinetic theory of granular flows [148, 149].

Three different Euler-Euler multiphase models are available in Fluent software, namely; volume of fluid model, the mixture model and Eulerian model. The interface of immiscible fluids could be described properly using the volume of fluid model where VF of fluids is tracked in each mesh cell through solving a set of momentum equations, shared for all fluids involved. Homogeneous or dilute dispersed multiphase systems could be simulated by mixture model through solving mixture momentum equations as phases (including solids) are considered as interpenetrating fluids [137].

7.3 Eulerian model

In the Eulerian scheme, the n set of momentum and continuity equations are solved for each phase while pressure and interphase exchange coefficients are used to couple the equations [142, 148, 150]. Kinetic theory is employed to obtain the necessary properties of granular flows (solid-fluid mixture with VF_{solid}>10%) which are treated different than non-granular flows (fluid-fluid). Momentum exchange between particles is possible here.

The kinetic theory of granular flow, extension of classic dense gas kinetic theory, is the key approach in simulation of dense collection of nearly elastic spherical particles motion as a continuum. This theory defines pressure and viscosity of the solid phase through empirical relations considering the energy dissipation due to particle-particle (or particle-wall) collisions by means of restitution and specularity coefficients. According to this theory particles dissipate energy as result of inelastic collisions or because of drag force acting between particles and fluid. The granular temperature is defined to measure random oscillation of the particles (specific kinetic energy of velocity fluctuations), which is the average of the three variances of the particle's instantaneous velocities [141, 148, 149, 151,]. The granular temperature of a species varies spatially through the bed according to the degree of motion.

The restitution coefficient [152] quantifies the non-ideal collision of particles, resulting in energy loss. The coefficient ranges between 1, for fully elastic collisions, and 0 for fully inelastic collision. Lower restitution coefficient means less elastic collisions and consequently higher energy dissipation or more fluctuating kinetic energy [141]. Higher restitution coefficient suggests particles energy conservation during collision which results active movement of particles in bed. Due to high VF of particles in dense beds, any individual particle might be involved with several interactions at the same time as the interaction time could be larger than particle mean free flight time [140, 153]. Goldschmidt et al. [141] suggest restitution coefficient of 0.9 plausible, instead of 0.99 as collisions between the particles become less ideal for densely packed beds and could be doubtable for values <0.9; since kinetic theory of granular flows derived for slightly inelastic particles. It has been reported that, adjusting restitution coefficient to lower values (amplifying inelastic behavior) results in more particle packing or sharper porosity contours (viscous bed) and larger bubbles while setting restitution coefficient to 1 had eliminated bubbles in the bed [141, 154].

Proper wall condition is critical for proper prediction of bed hydrodynamics particularly affecting solid-wall interaction in gas-solid systems. Johnson and Jackson [155] introduced a wall boundary condition with two key

parameters, the specularity coefficient and particle-wall restitution coefficient. The former one is responsible for tangential solid velocity while the latter one considers the fluctuating energy (dissipation of energy due to collision) at the wall in granular flows. The specularity coefficient varies between 0; free slip wall or smooth wall, and 1; no-slip or rough wall condition. Values between refer to partial slip which varies depending on a number of factors including wall material, the type of particles used and wall sloping or geometry [156, 157]. However, there are no generic values available in literature suggesting appropriate specularity coefficients depending on such factors. Recent studies show that changes in specularity coefficient affects particle velocity, spouting behavior, granular temperature and particle volume fraction not only close to the wall but also in central region as well. But in most cases the predicted overall bed height for different specularity coefficients are similar and its change, is affecting details of the fluidization not overall model performance [156, 158, 159].

In solid-gas systems, the interphase momentum transfer is one of the dominant forces affecting bed hydrodynamics. This momentum exchange is represented by a drag force where the key component of drag force models is drag coefficient. The overall drag model performance depends on how drag coefficient is determined. Now a day, determination of the drag force imposed on a single free falling sphere in a fluid is easy to obtain but, it is a challenging job when a single particle moves in a dense dispersed mixture since it is affected by the presence of other surrounding particles. There are number of averaged-based drag models available in literature such as; Syamlal-O'Brien [150, 160, 161], Gidaspow [148, 160], Wen and Yu [162], Arastoopour [163] and … In some cases the drag models are modified based on the particle size or specific gas-solid bed characteristics for better presentation, such as explained procedure in reference No. 160 for tuning Syamlal-O'Brien drag model based on the minimum fluidization velocity of the particles.

As mentioned, there are many studies performed on simulating the hydrodynamics of fluidized beds, some with individually developed codes and some using available commercial softwares. Zaho and colleagues [164] studied

the hydrodynamics of Geldart group B particles using a two-phase Eulerian model. Two-phase simulation model results were compared with the fluidization characteristics of a 2D magnetite bed (30 mm of thickness), determining the effect of solid-gas drag force and bed height on model results. Bed pressure drop and density stability were used to compare the performance of the simulation models and experiments using Syamlal-O'Brien, Wen-Yu and Gidaspow solid-gas drag force and bed heights in the range of 100-500 mm. All models used 5 mm mesh, $U=1.4\text{-}2.5u_{mf}$, 0.0001 s time step, restitution coefficient of 0.9 and no slip wall (specularity coefficient of 0). The pressure drop and density fluctuation was found to increase by increasing the bed height or velocity in the simulations. Also they conclude that Syamlal-O'Brien drag presents better results than Wen-Yu and Gidaspow drag models.

Taghipour et al. [140] used spherical glass beads (250-300 mm, 2500 kg/m^3) fluidization results to investigate the effect of drag functions (Syamlal-O'Brien, Wen-Yu and Gidaspow) and restitution coefficient. A 5 mm mesh for 2D bed (0.025*0.28*0.4 m) geometry, convergence criteria of 10^{-3} (residual error) and time step of 1000 Hz is considered for simulation. The qualitative gas-solid flow pattern and time averaged bed expansion and pressure drop were used for the evaluations. They showed that by increasing restitution coefficient from 0.9 to 0.99 bed expanded (~10%) meaning increase of elastic particle-particle collisions and conservation of all impact energy. The restitution coefficient of 0.99 caused active particle movement and vigorous bubbling even at velocities lower than minimum fluidization velocities regardless of which drag function is employed.

Almuttahar et al. [144] showed that model prediction improves when using free-slip wall condition (specularity coefficient of 0) while by increasing specularity coefficient (high slip wall condition) model underestimates solid VF, just near wall zone. Between Gidaspow, Arastoopour and Syamlal-O'Brien, the modified version of latter model showed better solid VF prediction at the core of bed geometry. Laminar model presented better estimation of the experimental data than turbulence models once the same model features are set for both.

Performance of 2D and 3D Eulerian scheme was compared by Armstrong and co-authors [157] for a case of circulating fluidized bed. The velocity prediction of both 2D and 3D models were in good agreement with the experimental data. Obviously, the 2D model required shorter computational time (3-4 times) compared to the 3D model but it was slightly over-predicting the central zone velocity. Wall effect study declared that shifting model settings from free slip wall (specularity coefficient of 0) to a rough wall condition, improves particles downward flow, representing experimental particle motion status. Higher volume fraction of particles near wall zone was observed for both 2D and 3D models. They have also studied the transition from bubbling bed to fast fluidization regime.

Three phase (gas-solid) Eulerian simulation was put in practice by Cooper and Coronella [147] using Fluent 6.0, to evaluate simulation model results and practical particle segregation in a bubbling fluidized bed. Two solid phases had different sizes (355 vs. 69.5 μm) and densities (1.8 vs. 4.8 g/cm^3) and gas phase defined to be Neon with density and viscosity of 0.659 kg/m^3 and 3.7e-5 Pa.s. The 5 minute long computational results using Syamlal-O'Brien drag function were compared to 120 s experimental process time. Realistic bed expansion and bubbling rates were obtained in simulation but mixing mechanism was bold when solid flux is traced, representing a well-mixed fluidized bed. Segregation of the solid phases concluded just when fluidization stopped through cutting of the inlet air jet. No steady concentrated zones were obtained throughout the fluidization. Xu et al. [165] also reported the circulation of the medium in the fluidized bed model, ascending near the center of the geometry and consequently descending near walls, but still keeping uniform density in axial direction.

In summary and based on the discussed points and documented advancements, the Eulerian model seems to be suitable for simulating granular flows even though it is the most complex model developed for simulation of multiphase problems. This model could be applied for fluidized beds, bubbling columns, risers and particle suspension. Therefore, the Eulerian model was selected in this study for simulating particle segregation in an air-sand bed. Some

of the fundamental equations of mass, momentum, and Syamlal-O'Brien drag correlation are presented in Table 7-1. Details on mathematical formulation of a model can be found in the literature [e.g. 140 and 164] and in the software theory guide [137]. The energy equation, lift and external body forces were not included here as the flow was considered isothermal.

Table 7-1: Governing equations for multiphase Eulerian model. Equations are simplified for one gas and one solid phase (g: gas, s or k: solid) [e.g. 137, 140, 164].

Mass conservation	$\frac{\partial}{\partial t}(\alpha_i \rho_i) + \nabla(\alpha_i \rho_i \vec{u}_i) = 0$
Momentum conservation for gas phase	$\frac{\partial}{\partial t}(\alpha_g \rho_g \vec{u}_g) + \nabla(\alpha_g \rho_g \vec{u}_g \vec{u}_g) = -\alpha_g \nabla p + \nabla \bar{\bar{\tau}}_g + \alpha_g \rho_g \vec{g}_g + K_{gs}(\vec{u}_g - \vec{u}_s)$ $\bar{\bar{\tau}}_g = \alpha_g \mu_g (\nabla \vec{u}_g + \nabla \vec{u}_g^T) + \alpha_g (\lambda_g - \frac{2}{3}\mu_g) \nabla \cdot \vec{u}_g \bar{\bar{I}}$
Momentum conservation for solid phase	$\frac{\partial}{\partial t}(\alpha_s \rho_s \vec{u}_s) + \nabla(\alpha_s \rho_s \vec{u}_s \vec{u}_s) = -\alpha_s \nabla p + \nabla \bar{\bar{\tau}}_s + \alpha_s \rho_s \vec{g}_s + K_{gs}(\vec{u}_s - \vec{u}_g)$ $\bar{\bar{\tau}}_s = \alpha_s \mu_s (\nabla \vec{u}_s + \nabla \vec{u}_s^T) + \alpha_s (\lambda_s - \frac{2}{3}\mu_s) \nabla \cdot \vec{u}_s \bar{\bar{I}}$
Solid-phase stress tensor	$\bar{\bar{\tau}}_s = \alpha_s \mu_s (\nabla \vec{u}_s + \nabla \vec{u}_s^T) + \alpha_s (\lambda_s - \frac{2}{3}\mu_s) \nabla \cdot \vec{u}_s \bar{\bar{I}}$
Syamlal-O'Brien drag function (Solid-fluid exchange coefficient)	$K_{gs} = \frac{3}{4}\frac{\alpha_s \alpha_g \rho_g}{u_{r,s}^2 d_s} C_D(\frac{\mathrm{Re}_s}{u_{r,s}}) \lvert \vec{u}_s - \vec{u}_g \rvert, \quad C_D = (0.63 + \frac{4.8}{\sqrt{\mathrm{Re}_s / u_{r,s}}})^2$ $u_{r,s} = 0.5(A - 0.06\,\mathrm{Re}_s + \sqrt{(0.06 + \mathrm{Re}_s)^2 + 0.12(2B - A) + A^2}$ $for \quad \alpha_g \le 0.85 \quad A = \alpha_g^{4.14}, \quad B = \omega_1 \alpha_g^{1.28} \qquad (\omega_1 : 0.8)$ $for \quad \alpha_g \ge 0.85 \quad A = \alpha_g^{4.14}, \quad B = 0.8\alpha_g^{\omega_2} \qquad (\omega_2 : 2.65)$
Solid-solid exchange coefficient	$K_{ks} = \frac{3(1+e_{ks})(\frac{\pi}{2} + C_{fr,ks}\frac{\pi^2}{8})\alpha_s \rho_s \alpha_k \rho_k (d_s + d_k)^2 g_{0,ks}}{2\pi(\rho_s d_s^3 + \rho_k d_k^3)} \lvert \vec{u}_s - \vec{u}_k \rvert$
Radial distribution coefficient	$g_{0,ks} = \left[1 - (\frac{\alpha_s}{\alpha_{s,\max}})^{1/3}\right]^{-1}$
Solid pressure	$p_s = \alpha_s \rho_s \Theta_s + 2\rho_s(1+e_{ks})\alpha_s^2 g_{0,ks}\Theta_s$
Transport equation (derived from kinetic theory)	$\frac{3}{2}\left[\frac{\partial}{\partial t}(\rho_s \alpha_s \Theta_s) + \nabla(\rho_s \alpha_s \vec{u}_s \Theta_s)\right] = (-p_s \bar{\bar{I}} + \bar{\bar{\tau}}_s) : \nabla \vec{u}_s + \nabla(k_{\Theta_s} \nabla \Theta_s) - \gamma_{\Theta_s} + \phi_{gs}$

Diffusion coefficient of granular temperature (Syamlal-O`Brien)	$k_{\Theta_s} = \frac{15\alpha_s\rho_s d_s\sqrt{\Theta_s\pi}}{4(41-33\eta)}\left[\begin{array}{l}1+\frac{12}{5}\eta^2(4\eta-3)\alpha_s g_{0,ls}+\\ \frac{16}{5\pi}(41-33\eta)\eta\alpha_s g_{0,ks}\end{array}\right]$, $\eta = 0.5(1+e_{ks})$
Collision dissipation energy	$\gamma_{\Theta m} = \frac{12(1+e_{ks}^2)g_{0,ls}}{d_s\sqrt{\pi}}\rho_s\alpha_s^2\Theta_s^{3/2}$
Transfer of kinetic energy	$\phi_{gs} = -3k_{gs}\Theta_s$
Solid shear viscosity	$\mu_s = \mu_{s,col} + \mu_{s,kin} + \mu_{s,fr}$
Solid collision viscosity	$\mu_{s,col} = \frac{4}{5}\rho_s\alpha_s d_s g_{0,ks}(1+e_{ks})(\frac{\Theta_s}{\pi})^{1/2}\alpha_s$
Kinetic viscosity (Syamlal-O`Brien)	$\mu_{s,kin} = \frac{\rho_s\alpha_s d_s\sqrt{\Theta_s\pi}}{6(3-e_{ks})}\left[1+\frac{2}{5}(1+e_{ks})(3e_{ks}-1)\alpha_s g_{0,ks}\right]$
Solid frictional viscosity	$\mu_{s,fr} = \frac{p_s\sin\phi}{2\sqrt{I_{2D}}}$
Bulk viscosity	$\lambda s = \frac{4}{3}\rho_s\alpha_s d_s g_{0,ks}(1+e_{ks})(\frac{\Theta_s}{\pi})^{1/2}$

7.4 Reference experiment

Beside ADMFB beneficiation experiments as discussed thoroughly in previous section, a number of fluidization and segregation experiments were performed to provide enough information necessary for model set up, validation and verification. The batch cylindrical bed was used to conduct these experiments. The experiments include several repetition of air-sand fluidization and a reference segregation experiment. Other necessary values for setting CFD models such as solid particles size and density were obtained through laboratory measurements.

Air-sand fluidization was performed generally with two superficial air velocities of 16.5 (same as separation experiment) and 22.5 cm/s (~1.5 times of fluidization velocity), and some photos as well as changes in bed height was recorded.

For the reference segregation experiment, high ash (Genesee) coal with a particle size of 3.35-4 mm was added to the 390 μm fluidized sand bed at 16.5

cm/s superficial air velocity. Bed was frozen at 90 s after adding coal sample. Similar to beneficiation experiment, sand as well as segregated coal particles were collected layer by layer, but in 2.5 cm intervals, with minimum distraction to the lower layers. Since any distinct particle size or, in this case, particle density range should be considered as an individual phase in CFD simulation, later coal particles of some layers were mixed to limit number of coal phases in the simulation models. The ash content and density of different layers as well as their position in bed are presented in Figure 7-1.

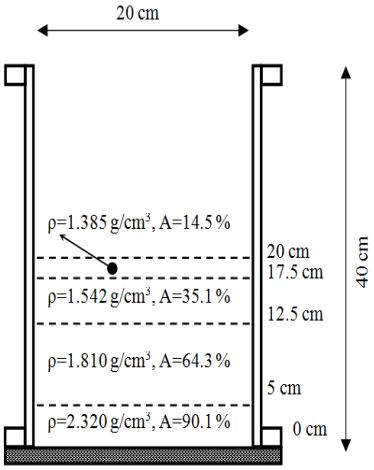

Figure 7-1: Properties of coal phases obtained from reference experiment (A: Ash)

7.5 Grid sensitivity study

A 2D grid sensitivity study was performed using four grid sizes. Table 7-2 shows the different mesh sizes and some statistical information about the grids generated. Considering the batch bed dimensions and particle sizes of sand and coal, used in reference experiment, 7 to 20 mm grid size was considered as minimum and maximum mesh size. The ANSYS DesignModeler and ANSYS Meshing R14.0 were used to prepare the geometry (20*60 cm) and establish the uniform orthogonal mesh grids (as much as possible).

Table 7-2: Different grids specifications and statistics used in grid size study

	Nominal mesh size (mm)	Cell	Node	Maximum aspect ratio	$\frac{\Delta L^*}{d_p}$
Case 1	7	2494	2610	1.4396	>17
Case 2	10	1220	1302	1.46211	>25
Case 3	15	507	560	1.47432	>38
Case 4	20	320	363	1.56205	>51

*: the ratio of nominal mesh edge to solid particle diameter

Preliminary runs with Fluent R14.0 showed that using lower air velocities (as used in segregation experiments) showed no clear bed expansion or in another word, no solid fluidization. Therefore, considering maximum operating range of mass flow controller, sand bed was fluidized at 1.5 times of the calculated minimum fluidization velocity and bed behavior was recorded.

General model specifications used for grid size study are presented in Table 7-3. Two-phase system (air-sand) was used for grid study and bed expansion, observed bubble frequency and average velocities of sand particles were used as judgment criteria.

Table 7-3: General specifications of grid size study models

Description	Value	Comment
Solid phase size	390 μm	Sieving
Solid density	2600 kg/m^3	Silica sand
Gas density	1.225 kg/m^3	Air
Gas velocity	22.5 cm/s	~1.5u_{mf}
Initial solid packing	0.543-0.55	Equal mass in beds
Initial (static) bed height	20 cm	
Restitution coefficient	0.9	Suggested in literature
Drag function	Syamlal-O'Brien	Original coefficients
Inlet boundary condition	Velocity inlet	
Outlet boundary condition	Pressure outlet	
Time step	3e-5 s	0.3 MHz
Max Iteration/time step	60	
Convergence criteria (error)	1e-4	For all equations

All models simulated for 30 s or 1000000 time steps and necessary information such as data files, sand VF, average sand volume fraction of different zones, volume averaged sand particle's velocity and bed pressure drop were

recorded. Zones in CFD geometry defined based on reference experiment sections except space between 17.5 and 22.5 cm which was defined as upper top zone, to enhance data recording process for capturing bed height changes easily.

The average normalized solid particles velocities (ANSV) of four cases versus normalized run time (NRT) are presented in Figure 7-2. Exported text files (data recording every 10 time step) were used to create these graphs. The ANSV and NRT are defines as:

Equation 7-1: $$ANSV = \frac{Ave.\ Velocity}{Inlet\ air\ velocity}$$

Equation 7-2:

$$NRT = \frac{Simulation\ time\ (s)}{Plug\ flow\ residence\ time\ (s)} = \frac{Simulation\ time\ (s)}{Static\ bed\ height\ (m) \Big/ Superficial\ air\ velocity\ (\frac{m}{s})}$$

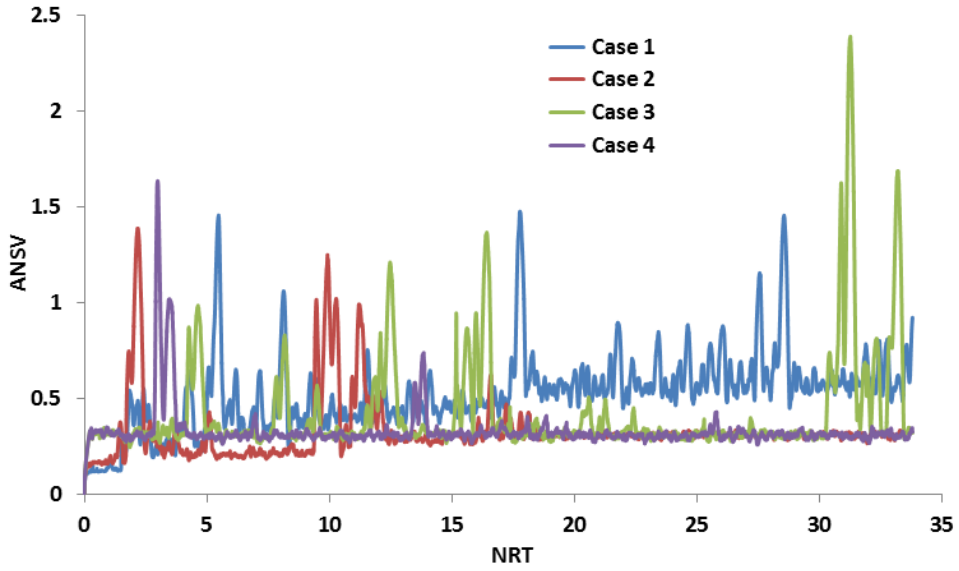

Figure 7-2: ANSV of case 1 to 4

As seen, for most parts of graphs, average velocity got stable around ANSV=0.3 except for case 1 which showed two distinguishable zones before and after NRT=16.5. Such horizontal zones could be representing a stable solution in terms of solid particles motion and interaction with air, bed walls or other solid particles in bed. The peaks (jumps) from average trend in graphs, as observed for all four cases, could also be considered as disturbances in bed or in another words

as representatives of some infrequent bubbles. Bubbles push particles upward to create space for themselves while moving up. Their breakage at the surface, coalescence as well as particles trapped and carried upward in bubbles wake zone could be reasons of sudden ANSV increases. Case 3 presented more bubbles (unstable segments) compared to others. Figure 7-2 shows that it takes minimum 1.5 NRT for case 1 and 2 to reach a stable status in CFD model, where this start time was a lot shorter for case 3 and 4. Therefore, for any preliminary result, models should be simulated for more than 1.5 NRT.

Observations of batch bed indicated that the height of denser section in fluidized bed when operating at $1.5u_{mf}$ was around 18.5 cm and the zone between 18.5 and 21.5 cm was occupied with bubbles reaching surface and breaking there. A picture of the experimental setup and a schematic presentation of high and low density solid zones are presented in Figure 7-3.

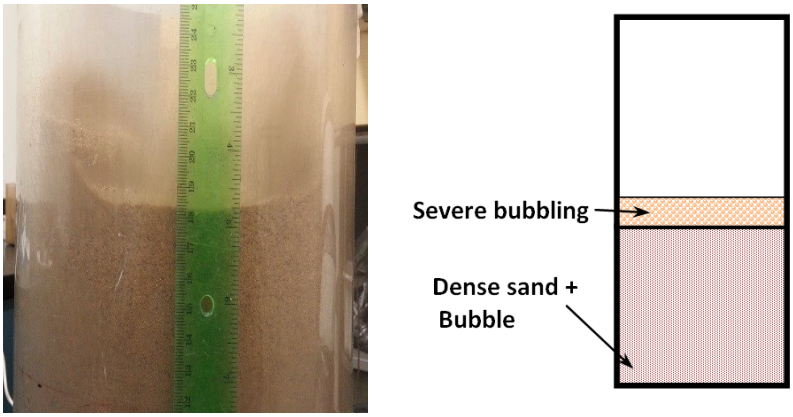

Figure 7-3: Two distinguishable zones in a fully fluidized bed at $1.5u_{mf}$

Figure 7-4 shows snap shots of initial static sand bed and bed after 30 s (NRT=33.75) simulation for all four cases. The 18.5 cm level is presented as dotted line on contour plots. Based on the presented contour plots, the height of dense zone (sand VF >~0.5) of all beds decreased regardless of grid size, but the amount of this decrease, increased by using bigger grid size.

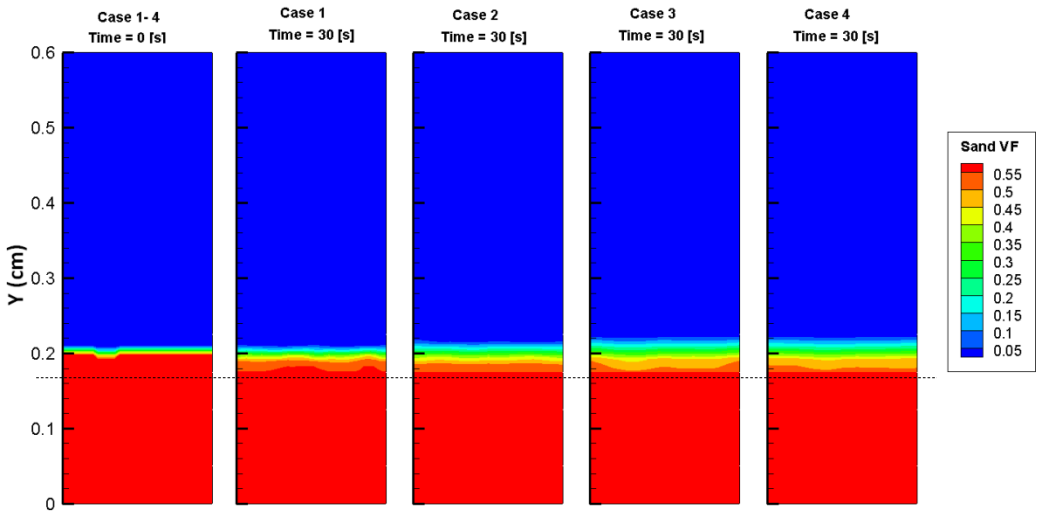

Figure 7-4: Snap shots of initial static sand bed and fluidized bed after 30 s for case 1 to 4

In order to obtain quantitative comparison criteria for simulation results, the sand VF of all cells were recorded every 10 time steps by exporting data files while solving the simulation models. The sand VF of the cells at the same height were averaged between simulation time of 10 and 30 s (NRT: 11.25 to 33.75). Figure 7-5 presents the average sand VF for different levels of the bed for four grid cases.

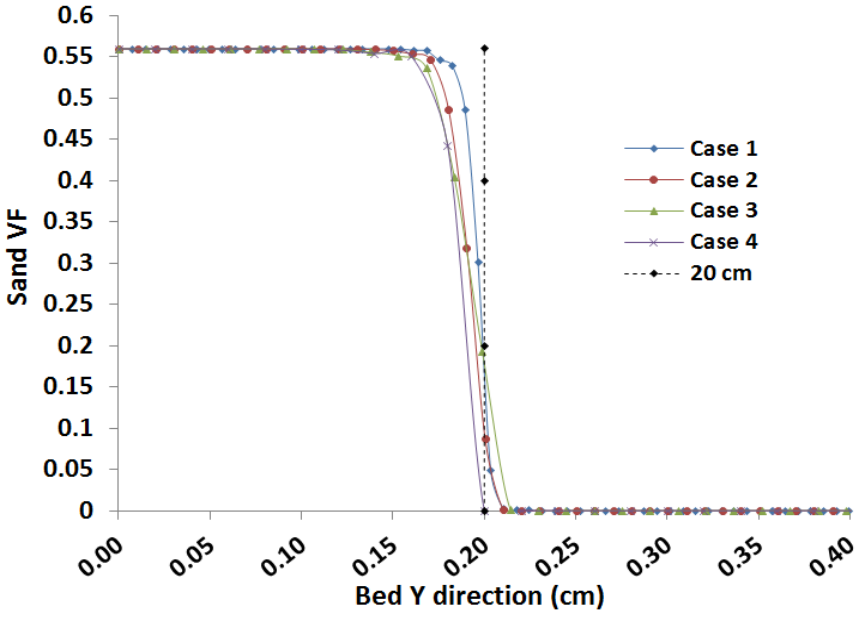

Figure 7-5: Case 1 to 4 average sand VF at different levels of bed

As seen in Figure 7-5, case 1 predicted higher bed height than case 2 and two others where its dense zone height was the highest (solid phase VF~0.55-0.56) among all four models. This could be further explained if the position of cells with the average solid VF of e.g. 0.485 was compared for all cases. The corresponding Y levels of case 1, case 2, case 3 and case 4 simulation models were 18.9, 18.0, 17.4 and 17.2 cm, respectively.

On the other hand, the bubble zone height (0 < solid VF < 0.55) of the case 2 was bigger than case 1 as the slope of the transition section of case 2 graph was lower than case 1. Even though the dense zone height in case 3 was higher than case 4; the case 4's bubble zone was restricted compared to case 3. Based on the comparison of the 20 cm bed simulation results with the average experimental dense zone height (18.5 cm), experimental bubble burst zone height (3 cm) and the average size of coal particles (3.675 mm) which would be added later as third phase, the grid size of 10 mm seemed to be better than 7 mm for further fluidized bed studies. The grid size of 10 mm satisfied the rule of thumb of having 3-5 solid particles per cell as well to keep the model statistically viable.

7.6 Impact of drag function

Preliminary simulation results revealed that bed shrinks when experimental values were used as model setting. Also since model fell in frictional regime due to increase of solid VF, the run time increases severely (~0.2 s /24 hr). Among all forces acting on particles in a fluidized bed, the drag force and particle-particle collisions need to be adjusted carefully through comparing with experimental data, since they could cause large deviations (error) between simulation results and experiments. As discussed, the coefficients of Syamlal-O'Brien drag function (also other drag functions) are determined semi-empirically, based on several experiments performed using specific particle sizes or shapes (usually spherical) and various (but usually covering wide ranges) operating conditions. Therefore, these models might over/under predict drag force if used for particles not exactly in the range of their applicability [160]. Moreover,

the experimental data may also contain some inaccuracies that may raise problems when compared to simulation data for tuning and validation purposes.

At this stage using 10 mm mesh grid size the coefficients of Syamlal-O'Brien drag function was optimized according to the sand-air bed expansion at 16.5 cm/s air velocity. Different values of ω_1 and ω_2 (refer to Table 7-1) which were tested in models are presented in Table 7-4. The drag ratio column in Table 7-4 shows the ratio of the tuned drag force to its un-tuned value, considering experimental data for all parameters needed in K_{gs} calculation.

Table 7-4: Coefficient combinations considered for Syamlal-O'Brien drag

Description	ω_1	ω_2	Drag ratio at solid VF of 0.55 (case i / case 5)
Case 5	0.8	2.65	1.00
Case 6	0.66	3.83675	1.18
Case 7	0.62	4.22142	1.25
Case 8	0.6	4.42318	1.29
Case 9	0.52	5.30369	1.47
Case 10	0.459	6.06714	1.66

Six simulation models were set and run up to 30 s using parameters of Table 7-5 and a UDF (user defined function) for setting new coefficients for Syamlal-O'Brien drag function.

Table 7-5: Model specifications for tuning drag function coefficients

Description	Value	Comment
Solid phase size	390 μm	Sieving
Solid density	2600 kg/m^3	Silica sand
Gas density	1.225 kg/m^3	Air
Gas velocity	16.5 cm/s	Reference experiment
Initial solid packing	0.55	Reference experiment
Frictional packing limit	0.56	
Maximum packing limit	0.58	
Initial (static) bed height	20 cm	Reference experiment
Restitution coefficient	0.9	Suggested in literature
Drag function	Syamlal-O'Brien	Original/tuned
Inlet boundary condition	Velocity inlet	
Outlet boundary condition	Pressure outlet	
Time step	2e-5 s	0.2 MHz
Max iteration/time step iteration	60	
Convergence criteria (error)	1e-5	For all equations

To show the effect of different drag coefficients on bed dynamics, the computed instantaneous bed pressure drop for all six cases are presented in Figure 7-6. Since steady-state trends were obtained during simulations, just first 3 NRT of each model is presented here. It should be mentioned that the pressure drops of a packed bed and completely fluidized bed with specifications of Table 7-5 according to Equation 2-3 and Equation 2-2 are 2114 and 2804 Pa, respectively.

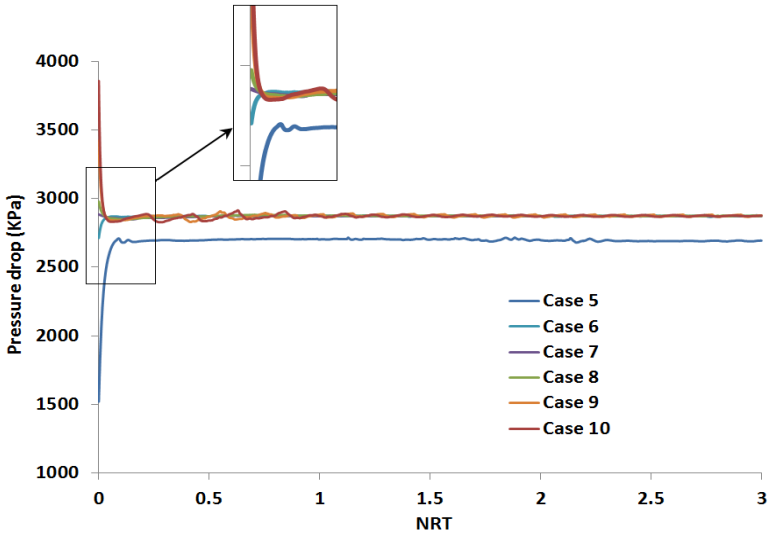

Figure 7-6: First 3 NRT bed pressure drop of case 5 to 10

Five cases (6 to 10) presented similar trend and their pressure drop values converged around 2873±3 Pa but the pressure drop of case 5 was lower than others and converged around 2690 Pa. In fact imposing any change in drag force (could be interpreted as increase of resisting forces against fluid flow), increased pressure drop of course, with some fluctuations at the beginning of simulation.

Figure 7-7 shows the ANSV of case 5 to 10 models versus NRT. As can be seen, the ANSV of case 5 was significantly higher than all others and was increasing as simulation time increased. The ANSV of case 5 also showed a big peak at the beginning of simulation. As discussed such peak could be representative of bubbling but in this case it shows subsidence of the particles in bed, or in another word bed height collapsed due to domination of gravity force over the drag and buoyancy forces acting on particles. Drop in bed height in case 5 will be discussed with further evidences in the following paragraphs. Increase in

ANSV of case 5 model could be due to vibration of particles with higher frequencies in short distances, as the distance between particles decreases once bed collapses.

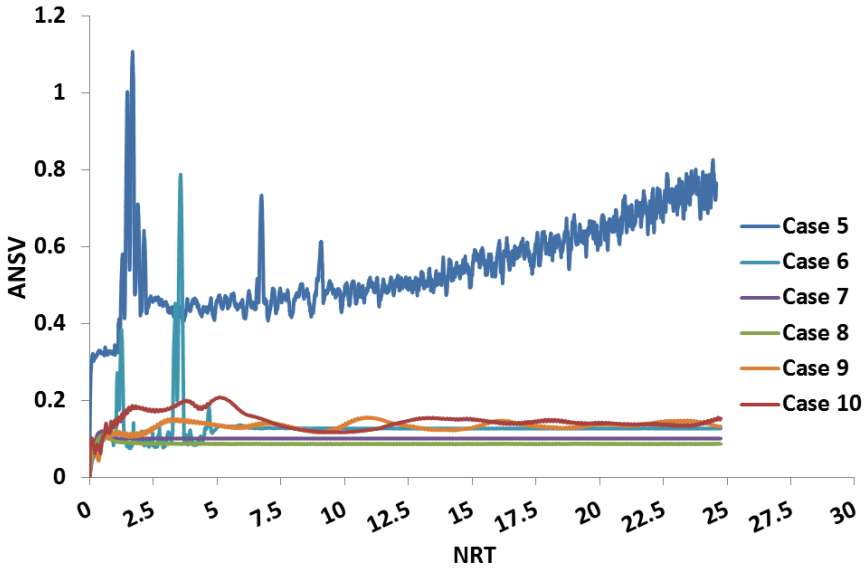

Figure 7-7: ANSV of case 5 to 10

The ANSV of case 6 also showed similar, but moderate behavior to case 5 (showing two peaks). Case 6 ANSV reached steady state after 5 NRT. The ANSV of case 7 and 8 followed constant trend after initial particle adjustments and their ANSV was the lowest between all 6 cases.

Case 9 and 10 ANSV trend (in particular 0-15 NRT) could be evidences of some bubbles in model; especially case 10. Their velocity fluctuations continued after preliminary particles adjustments.

Considering initial sand VF of 0.55 in the model; achieving higher solid VFs than that in determined zones, could be considered as bed collapse while lower values could mean increase in bed height (as particle distances increase) or bubble in that zone. Therefore, solid volume fractions of all cases in different zones during simulation were recorded and presented in Figure 7-8a-d.

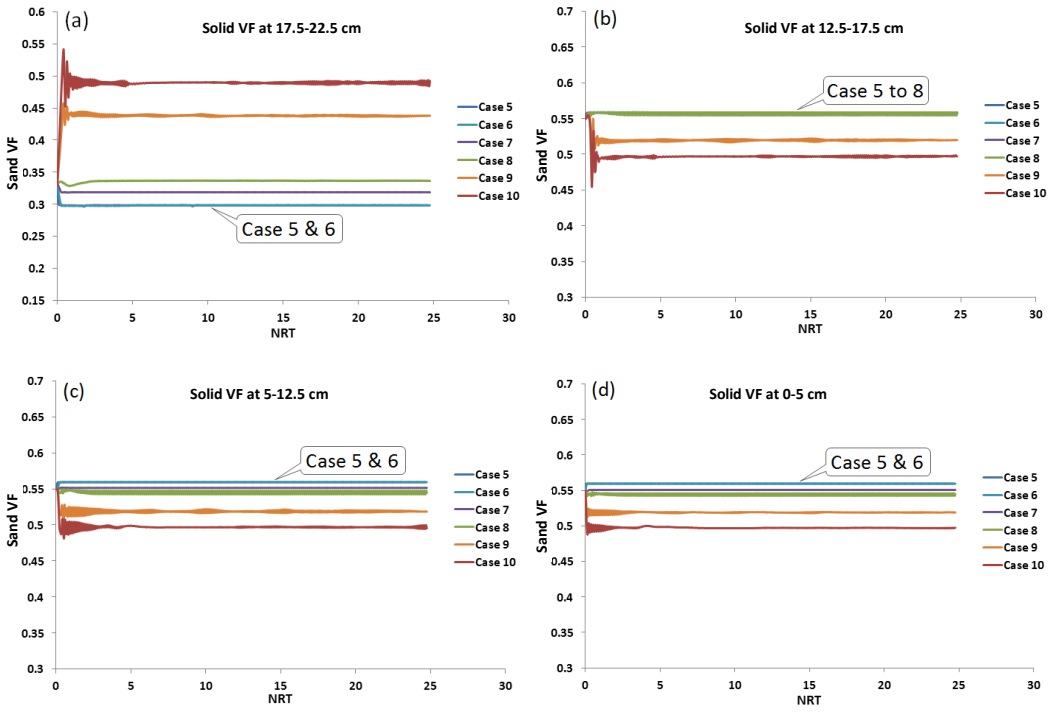

Figure 7-8: Solid VF of case 5 to 10 for each zone according to reference experiment

The solid VF of top zone (Figure 7-8a) was of more importance as if the bed height increased, some solids should be carried from bottom layers to this zone so its VF (initially ~0.33) should be increased as there was 2.5 cm free space which initially was occupied by air. Consequently if bed expands due to domination of air drag force over gravity; solid VF of lower layers (0-17.5 cm) should become less than 0.55.

As Figure 7-8a shows, the solid VF of case 5 to 7 dropped at the very beginning of the simulation and model proceeded with the lower solid VF (0.29). For case 8, solid VF dropped initially but later due to higher drag force, solid VF increased even slightly higher than its initial value (0.335). But the situation was totally different for case 9 and 10 as their solid VF increased from the very beginning, revealing travel of some solid particles from lower zones to top zone. The solid VF of case 10 reached 0.49 at 17.5-22.5 cm zone.

Also the same bed shrinkage or expansion behavior could be concluded for case 5 to 10 when other layers (between 0 and 17.5 cm) solid VF variation was verified (Figure 7-8b-d). For cases 5 to 7 solid VF exceeded its initial value

(0.55), for case 8 it remained almost around 0.55 and decreased for case 9 and 10 an indication of bed collapse in case 5 to 7, very slight bed expansion for case 8 and bed expansion for case 9 and 10, respectively. Biggest solid VF variation from initial value in different zones belonged to case 10.

Using collected data files for each cell center, the average VF of sand was calculated for each cell between 10 and 30 s (8.25-24.75 NRT). Based on the position of cells, average sand VF at different levels of bed were obtained and presented in Figure 7-9. The experimentally determined bed height of 20.7 cm at u=16.5 cm/s was also marked on Figure 7-9.

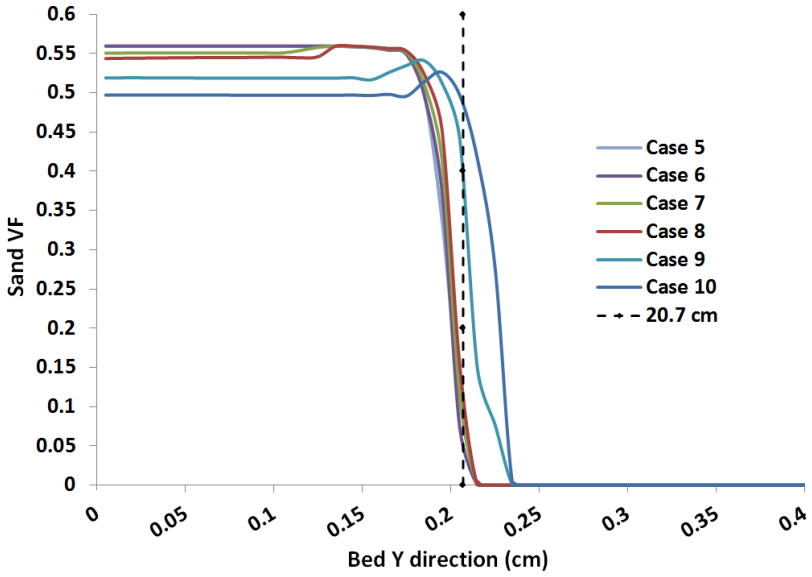

Figure 7-9: Case 5 to 10 average sand VF at different levels of bed

The collapse of bed height for simulation cases of 5 and 6 can obviously concluded from Figure 7-9 as solid VF was maximum along the bed depth to the surface and no cell at position of 20.7 cm acquires non-zero solid VF value. For case 7 and 8 solid VF was less than 0.55 up to 13 cm but increased at higher levels of bed reaching maximum value. This means that, there were some high porosity zones (than that initially determined for solid phase) or small bubbles at the bottom of bed which could not be extended up to top of bed as the outcome of the acting forces caused creation of condense zone at the top of bed. Therefore, for case 7 and 8 we have a semi-fluidized zone at the bottom and a packed bed zone on top of that.

Increase of bed height was obvious for both case 9 and 10 as solid VF was less than 0.55 with constant values (0.519 and 0.497, respectively) up to top layers of bed. The solid VF increased close to the bed surface which could be due to accumulation of existing particles and falling particles surrounding the breaking bubbles above surface. Comparing case 9 and 10 with 20.7 cm level; case 10 over predicted bed height as additional drag force exerted on solid phase resulted in more bubbles in model and consequently more expansion of bed. On the other hand the VF - Y direction trend for case 9 seemed to be very close to experimental observations (bed expansion and bubble pattern). Snap shots of case 9 at 5 s intervals are presented in Figure 7-10. A slight increase in bed height and some bubbles are visible through theses contour graphs.

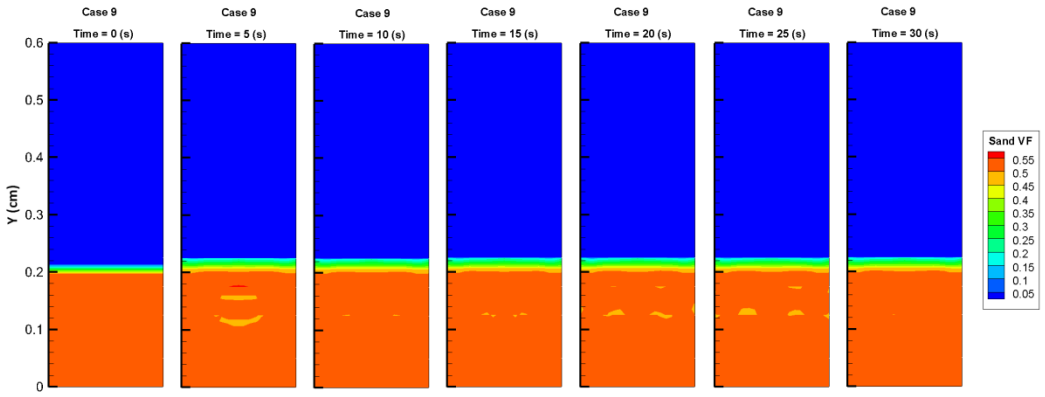

Figure 7-10: Snap shots of case 9

Since all cases were using the same settings and values, any changes imposed on solid VF of different zones and consequently bed height could be attributed to the changes of drag force on solid phase. Therefore, comparing experimental measurements and observations with simulation results of case 5 to 10 (as discussed thoroughly), the drag coefficients of case 9 was conformed and selected for subsequent ADMFB particle segregation modeling.

7.7 Sand-sand restitution coefficient

As discussed, elasticity of particle-particle collision is one of the dominant factors determining hydrodynamic behavior of bed. To investigate the effect of collision elasticity of sand particles, different values of restitution coefficients

between 0.1 and 0.95 were used. The case numbers and their restitution coefficients are presented in Table 7-6. Case 9 specifications and settings were used for all and models were run up to 30 s.

Table 7-6: Different sand-sand restitution coefficients examined in simulation models

Description	sand-sand restitution coefficient
Case 9	0.9
Case 11	0.1
Case 12	0.5
Case 13	0.8
Case 14	0.95

According to the simulation results, variation in restitution coefficient did not affect total bed pressure drop as seen in Figure 7-11. Data points were recorded every 2 time step and as discussed previously, just first 3 NRT of pressure drop is used here due to existing similar and steady trend.

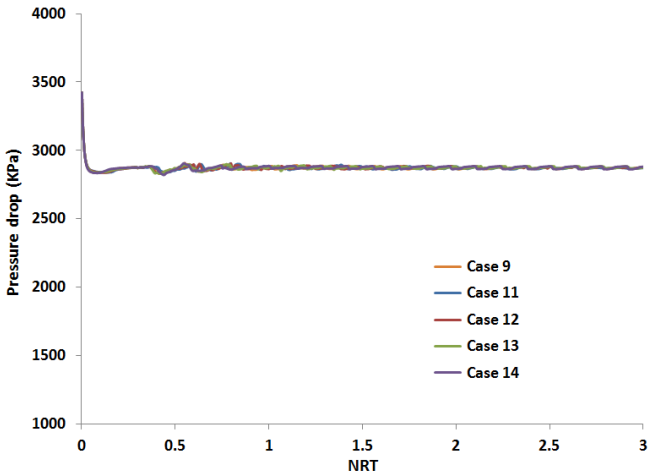

Figure 7-11: First 3 NRT bed pressure drop of case 9 and 11 to 14

The ANSV of 5 cases are compared in Figure 7-12. As seen, by increasing the restitution coefficient from 0.1 to 0.95, or elasticity of collisions, the ANSV for relevant solution time decreases. Also, decrease in restitution coefficient resulted in increase of ANVS fluctuation.

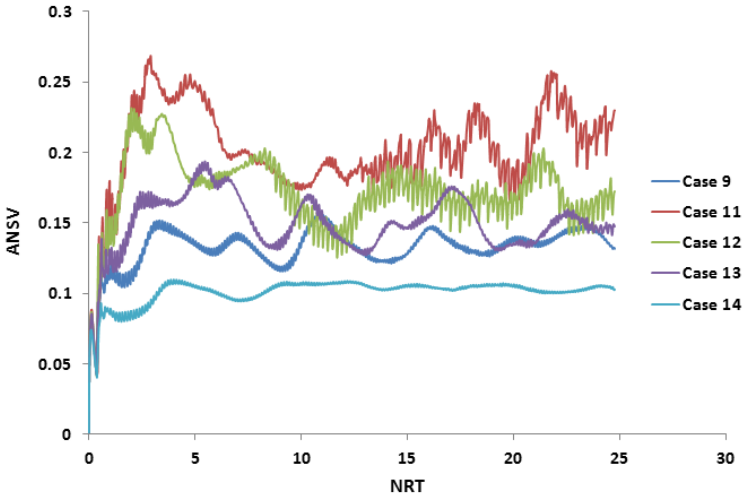

Figure 7-12: ANSV of case 9 and 11 to 14

As discussed in section 4.3, wavy trend (several peaks) could be a sign of bubbles in the bed. The movies prepared for each run confirmed more and bigger bubbles for models with lower restitution coefficients. Snap shots of solid VF contour plots at 5 s intervals (solution time) are presented and compared in Figure 7-13. The contour plots of case 9 (Figure 7-10) are also repeated here. Any contour plot base bed height variation judgments (recognition of lower solid VF at top of bed), could be misleading here due to bigger scale bar intervals (every 5%). Larger bubbles and sharper solid VF contour plots due to less ideal solid-solid collisions had been observed in fluidized bed simulations previously [141, 154]. Goldschmidt et al. [141], and Loha et al. [154] suggested that, due to inelastic collisions, as mechanical energy dissipates, particles become closely packed (attaching each other) and create more void fraction and also denser zones which results in sharper contour plots and bigger bubbles.

Zone solid VF changes could prove changes in bed height in a sense that; increase in solid VF of zones falling into 0-17.5 cm and decrease for 17.5-22.5 cm zone means bed collapse while reduction for 0-17.5 cm and growth for 17.5-22.5 cm means bed expansion. Figure 7-14a-d compares solid VF of five cases for different zones. All models' solid VF variations indicated increase of bed height regardless of changes of restitution coefficients. As Figure 7-14c and d shows, there was almost no difference between solid VFs of models in 0-12.5 cm zones

(except some wider fluctuations for some cases in the beginning) especially when solution time exceeded 5 NRT.

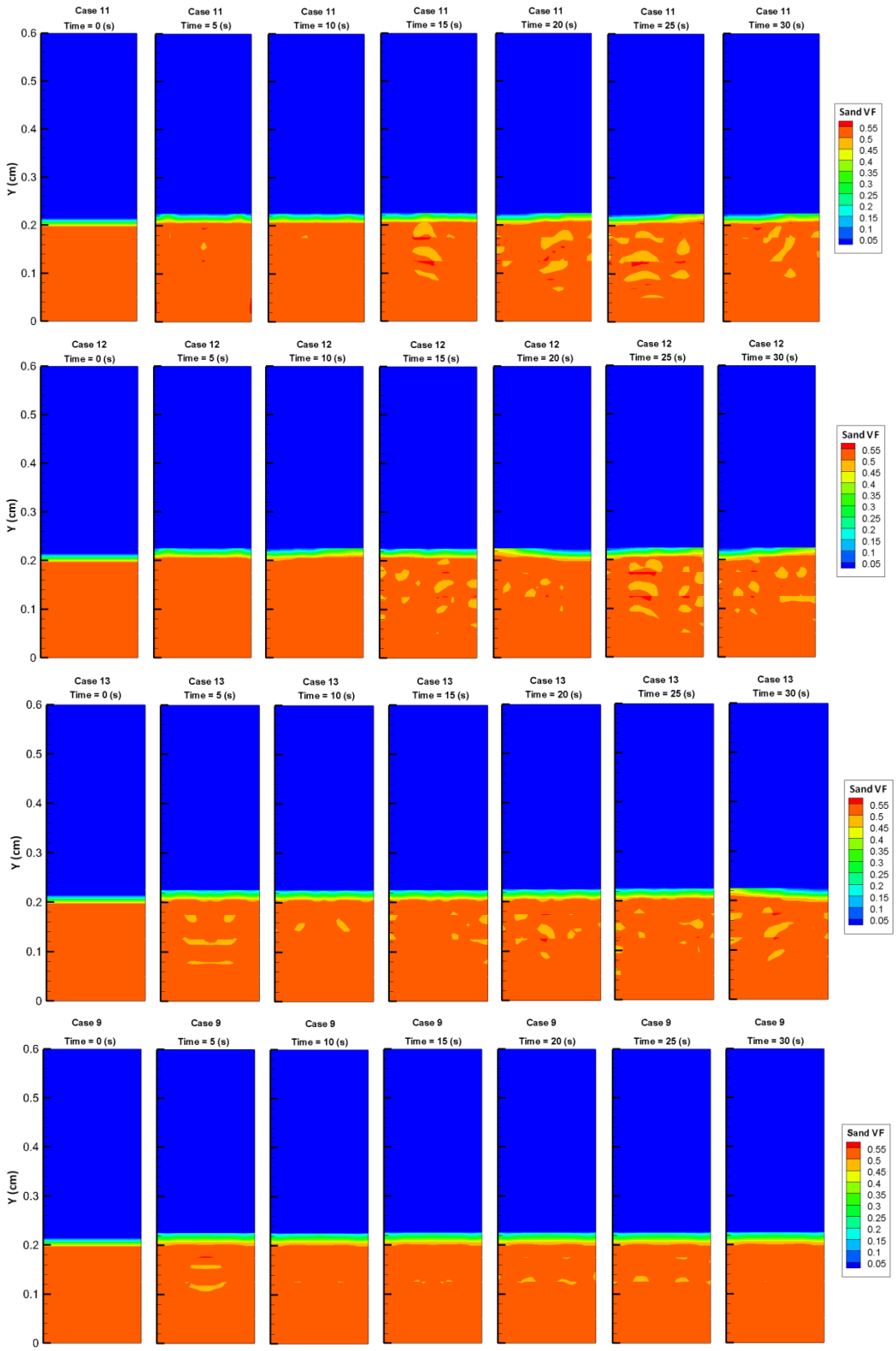

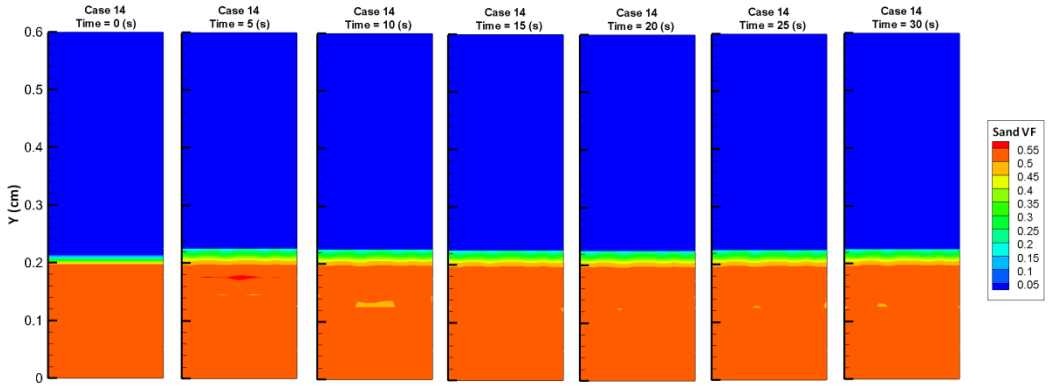

Figure 7-13: Contour plots of sand VF for different model restitution coefficients

A slight difference between case 14 and others was recognizable for 12.5-17.5 cm and 17.5-22.5 cm zones where solid VF increased at 12.5-17.5 cm zone and decreased for 17.5-22.5 cm zone. This could be an indication of bed height decrease for case 14 at this stage. The average bed height for each case between 10 and 30 s was obtained and presented in Figure 7-15. It can also be seen that, no bed collapsing occurred for any of the simulation models due to using adjusted coefficients for Syamlal-O'Brien drag function.

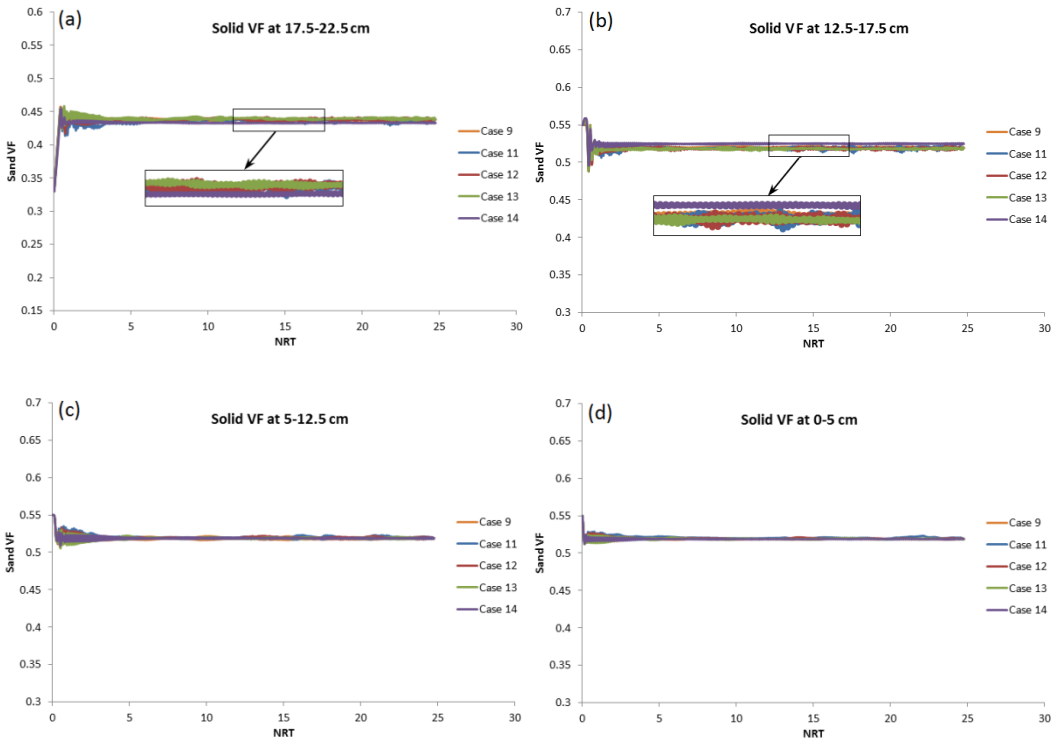

Figure 7-14: Solid VF of case 9 and 11 to 14 corresponding to reference experiment zones

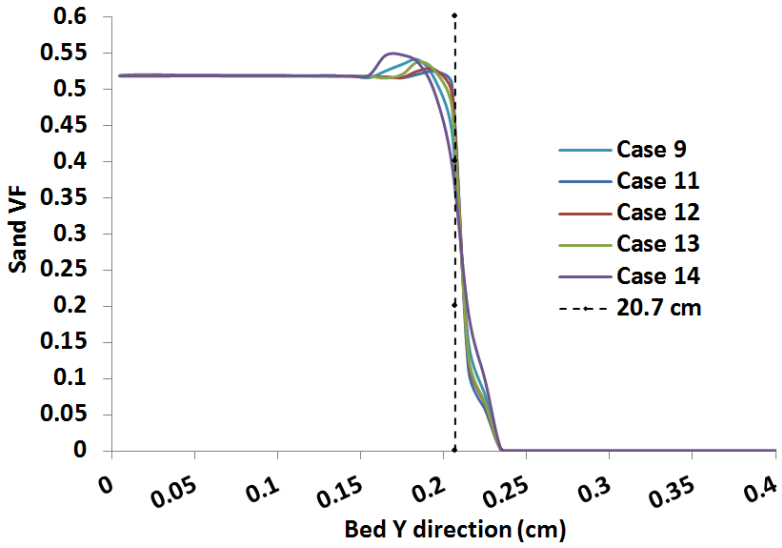

Figure 7-15: Case 9 and 11 to 14 average sand VF at different levels of bed

As Figure 7-15 shows, by increasing restitution coefficient the solid VF of upper layers (close to severe bubbling zone, discussed in Figure 7-3) increased where the biggest peak was created for case 14. As discussed, by increasing restitution coefficient, frequency of bubbles decreased (Figure 7-13) therefore the shaking effect of bubble bursts on the bed surface was eliminated significantly. Also referring to Figure 7-12, in general, solid particles experience lower velocities by increasing restitution coefficient. Both phenomena, altogether, created a thicker solid layer on upper layers of bed (appearing as draw backs in Figure 7-15) which, became thicker by increase of restitution coefficient. On the other hand, considering second half of graphs (Y>20.7 cm), it could be said that the particles became more active and traveled higher by growth of thicker top layer (or increasing restitution coefficient). In fact more developed thick layer, created additional pressure drop (buildup) and consequently increased air velocity through the cavities of a surface which, its void space was already reduced (3% less). Higher air velocity through orifice (increasing from case 11 to case 14), carried particles higher and higher or in another word, increase of bed height by increasing restitution coefficient. Case 14 presented thicker and denser top layer while more particles at higher Y positions were detectable.

To summarize Figure 7-14a-d and Figure 7-15, by increasing restitution coefficient or in another word more elastic particle-particle collisions, a layer with

higher solid VF was created on top of the bed and height of bubble burst zone (particle travelling) increased. But considering the 20.7 cm level and bottom and top of the severe bubbling zone, it could be concluded that changes in restitution coefficient was not affecting bed height significantly.

Figure 7-16a shows the average granular temperature of the particles versus model restitution coefficient. Granular temperature decreased significantly as solid-solid interaction became less elastic (ideal) and activity of particles decreases. Granular temperature fluctuations of models during the solution period are presented in Figure 7-16b. As seen, granular temperature varied around an average for each model case with not big fluctuation amplitude.

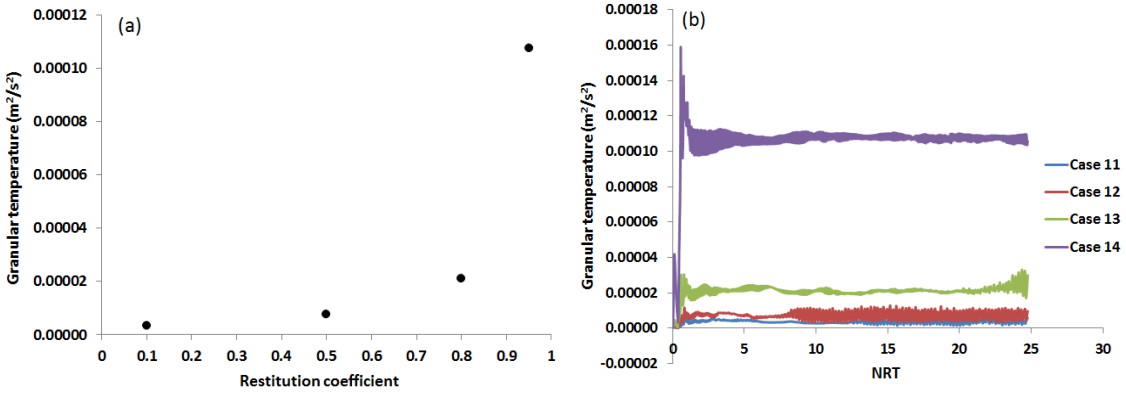

Figure 7-16: Granular temperature as function of restitution coefficients, a) average granular temperature between simulation time of 10 and 30 s, b) granular temperature fluctuation versus NRT for case 11 to 14.

The average (between 10 and 30 s) axial particles granular temperature is presented in Figure 7-17. The granular temperature was almost zero for all cases at any position except top layers (surface) of bed. Considering its definition, as a measure of random particle oscillations, it could be concluded that the particles motion at the depth of bed followed a constant pattern which was not changed or disturbed abruptly after bed stabilized (see Figure 7-18). In another word, energy dissipates at the surface of the bed since particles were more contacting with air than other particles.

The granular temperature of case 14, at the top layers, was the highest amongst all others (Figure 7-17). Due to model's higher restitution coefficient and

energy conservation along solid-solid collisions, particles bounce (jump) more and higher, resulting in increase of height of severe bubbling zone.

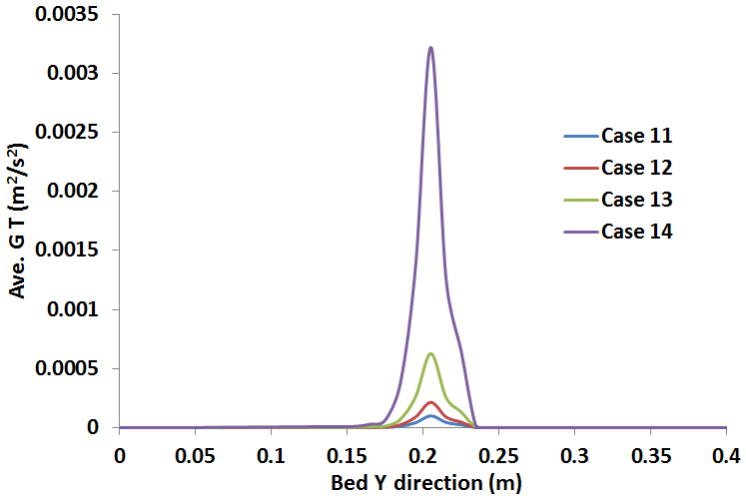

Figure 7-17: Average axial particles granular temperature

Figure 7-18 presents schematic pattern of velocity vectors of solid phase. As reported by other researchers a circulation of solid particles occurs in bed. In these models, solid particles were descending close to wall and middle of bed and were ascending among them. Similar behavior was observed for all models after they reached stable status.

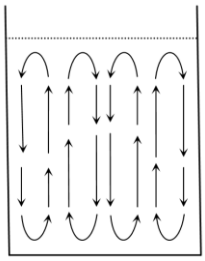

Figure 7-18: Schematic pattern of sand velocity vectors.

The restitution coefficient of case 9 was selected for next step simulation models as 0.9 is also suggested by Fluent and some literature.

7.8 Three phase modelling

For three phase modelling, the high ash coal with particle size, density and ash content of 3.675 mm, 2.32 g/cm^3 and 90.1% (according to the reference experiment) was added as the second solid phase. Generally the case 9 model

settings were used here. Since the amount of coal phase was a lot less than sand phase, so the fluidized sand phase could be considered as dominant phase. Therefore, the effect of variation of coal-sand restitution coefficient (Table 7-7) was studied at this section during 60 s simulation of bed. It should be mentioned that sand-sand and coal-coal restitution coefficients were considered as 0.9 in all three phase simulation models.

For cases 16 to 20 tuned coefficients of Syamlal-O'Brien drag function were used (0.52 and 5.30369 according to Table 7-4) for sand phase but case 15 were set to use the original Syamlal-O'Brien drag function coefficients (0.8 and 2.65) for sand phase. This has been performed to investigate the effect of drag tuning in a three phase simulation model.

Table 7-7: Different coal-sand restitution coefficients adjusted in simulation models

Description	Coal-sand restitution coefficient
Case 15*	0.9
Case 16	0.1
Case 17	0.5
Case 18	0.8
Case 19	0.9
Case 20	0.95

*: the original Syamlal-O'Brien drag coefficients were used

The bed pressure drop for the first 3 NRT is presented in Figure 7-19. It was seen that pressure drop of all cases, 16 to 20, were identical and of course, higher than case 9 as weight of solids in bed was increased due to the addition of coal phase. The lowest pressure drop belongs to case 15 which was not a fully developed fluidized bed.

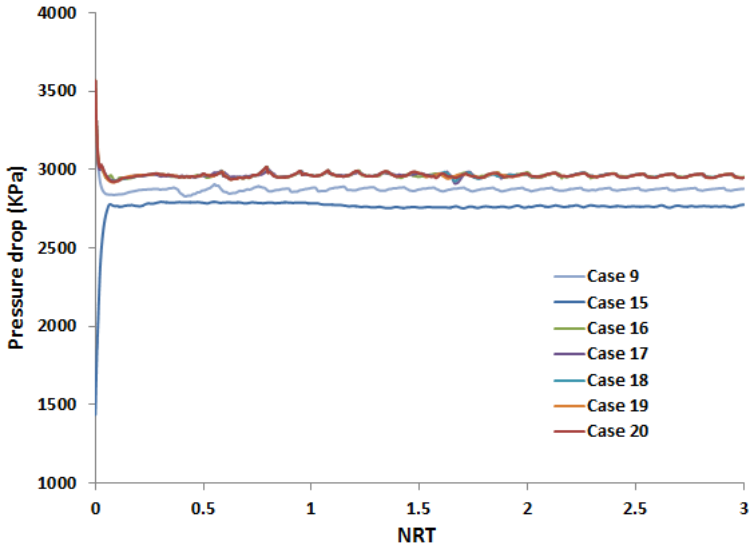

Figure 7-19: First 3 NRT bed pressure drop of case 9 and 15 to 20

Average granular temperatures of sand and coal phase between 10 to 60 s are presented in Figure 7-20. For case 15 with original Syamlal-O'Brien drag coefficients, both sand and coal granular temperature was higher than all others, regardless of coal-sand restitution coefficient.

This could be explained by considering the granular temperature concept (a measure of random oscillations of particles) and also case 15 packed/fluidized bed status. Since bed was not expanded, limited space was available for particles. Therefore, particles were vibrating severely within short distances, and were not able to move freely, resulting in more energy dissipation and higher random particle movements.

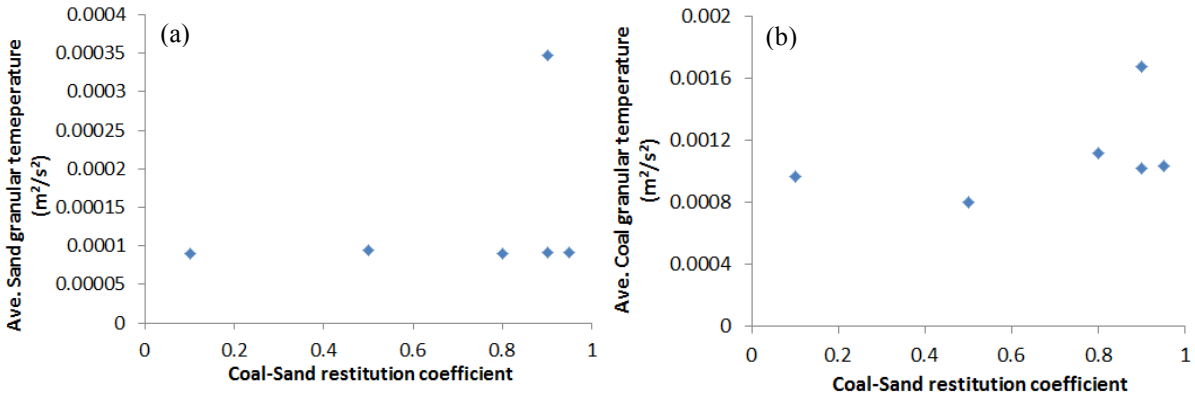

Figure 7-20: Variation of average solid phase granular temperature, a) sand phase, b) coal phase

As Figure 7-20a shows, sand particles granular temperature was not affected by elasticity of coal-sand collisions. Sand phase was the dominant solid phase in models and number of coal-sand collisions might be ignorable compared to sand-sand collisions (which studied in previous section). Therefore change in coal-sand restitution coefficient was not affecting sand particles movement or their collision pattern significantly. But variation in coal-sand restitution coefficient affected (to some extent) coal particles granular temperature as it determines how elastic coal particle were going to behave after colliding with sand particles. It should be mentioned that coal-coal restitution coefficient was set to 0.9 for all cases of 15 to 20. According to Figure 7-20b, restitution coefficients of 0.5 and 0.8 resulted in lower and higher coal particles granular temperatures. The granular temperature is almost identical for cases 16, 19 and 20.

The added coal phase was expected to appear at the bottom of bed (0-5 cm). Figure 7-21 presents coal VF at the 0-5 cm level of the bed. If all coal particles considered in the simulation model appear in 0-5 cm zone, coal VF should increase to 0.08. Coal VF of case 15 was the lowest and showed steady-state while it fluctuated severely for case 16 to 20.

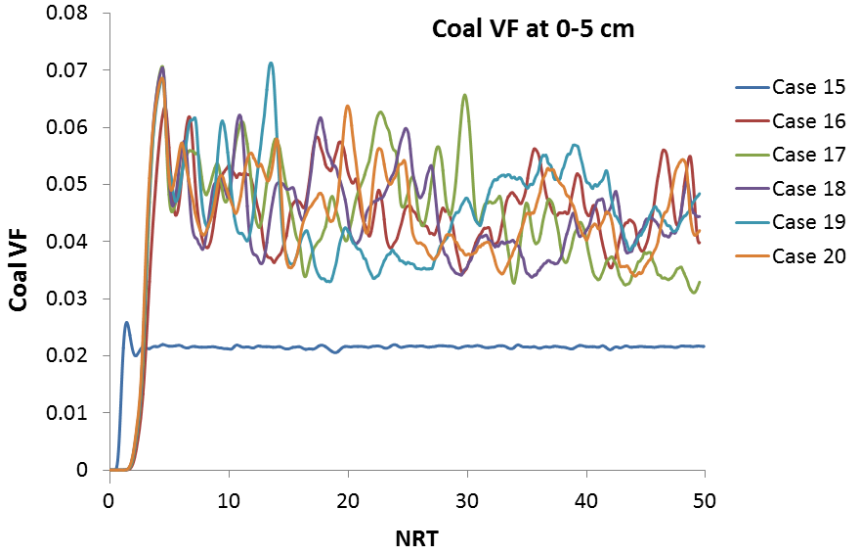

Figure 7-21: Coal VF at the bottom of bed during 60 s simulation

The average coal VF at the bottom of bed, after 30 NRT, is presented in Figure 7-22. It was fluctuating by variation of coal-sand restitution coefficient,

and was maximum for coefficient of 0.9 or case 19. Of course, there was a huge difference between case 15 and case 19 average coal VFs at 0-5 cm. As seen, there was quite a big distance between points and 0.08 limit.

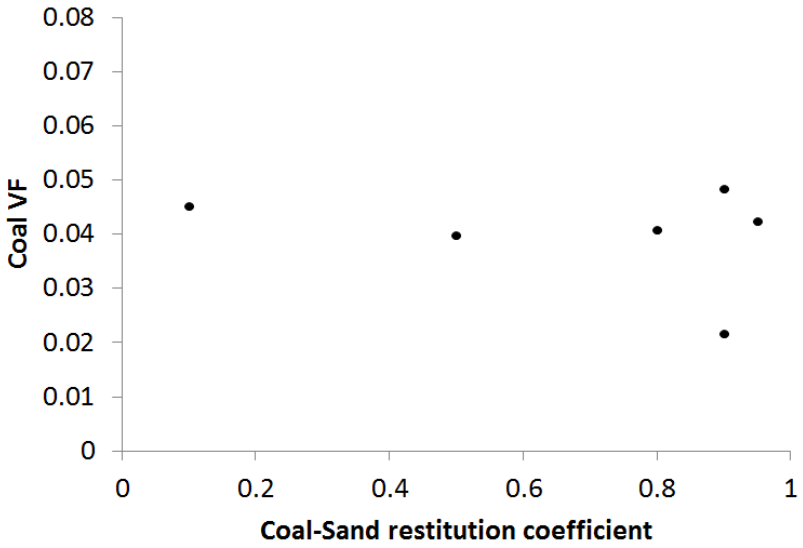

Figure 7-22: Average coal VF at the bottom of bed (0-5 cm)

The predictability of models or the ability of models in mimicking real segregation patterns could be defined as the ratio of the average coal VF at the bottom zone to its expected value according to the reference experiment (0.8). This ratio for different cases is presented in Figure 7-23. The average coal VFs after 30 NRT was used for the simulation coal VFs while obtaining ratios.

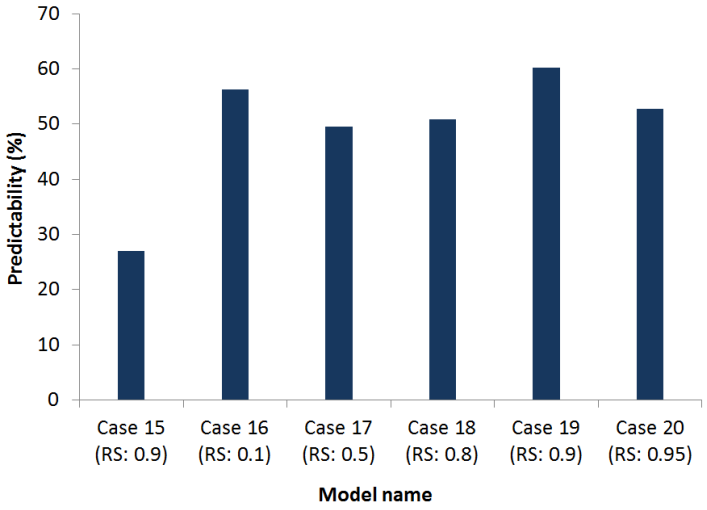

Figure 7-23: Predictability of 3-phase models

Considering both Figure 7-22 and Figure 7-23, simulation model of case 19 presented better estimation of course, not exactly what occurs in real segregation experiment. The coal VF at 0-5 cm zone and predictability of model for case 19 were 0.048 and 60.2%, respectively. Further inspection revealed that there was no loss of solid in model as time step and convergence error limit were set very low. Figure 7-24a-d show coal VF of case 19 at each zone along the 60 s simulation.

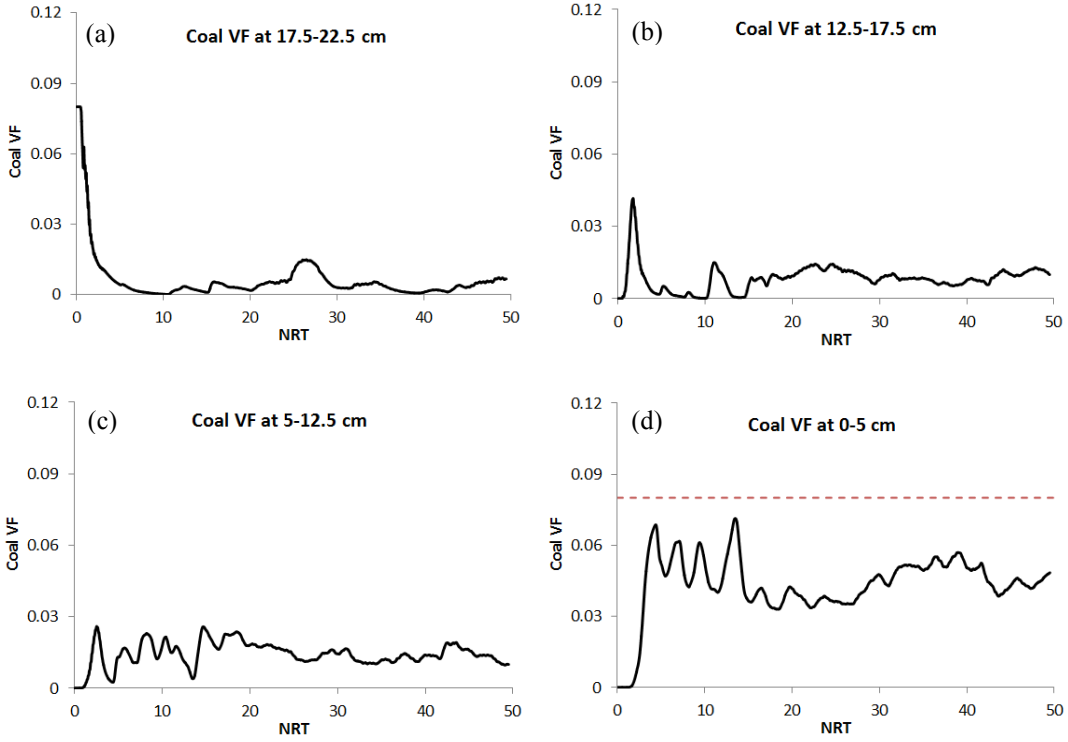

Figure 7-24: Case 19 coal VF at different zones

At the beginning coal sank from top zone (Figure 7-24a) to the lower zone and caused a high peak in the second zone. Fluctuation in 5-10 cm zone had lower oscillations while at the first 6 s of simulation (4.4 NRT) coal was continuously entering to the bottom zone (Figure 7-24d). It seemed that after 3-phase model reached kind of steady state condition, some coal particles were carried to the upper layers due to effect of sand phase circulating motion (as discussed earlier in Figure 7-18). That could be the main reason of having some coal in upper layers. Such phenomenon, carrying secondary phase along with and in the direction of dominant phase motion, is a known phenomenon for liquids (due to shear force

and transfer of inertia) which might not occur to this extent in reality, when a flow of solid particles touches other stationary solid particles.

As a next step in simulation of three-phase fluidized bed particle segregation, three cases were set considering coal phase densities of 1810, 1542 and 1385 g/cm^3 (Figure 7-1). Based on the results of sand-sand and coal-sand restitution coefficient studies, case 9 settings with restitution coefficients of 0.9 for all possible solid-solid collisions were considered for case 21, case 22 and 23. Similar to case 9, models were simulated up to 60 s and then coal VF graphs in bed zones were prepared. In order to avoid repeating similar graphs, the coal VF vs. NRT graphs of just destination zones of used coal types for case 21, case 22 and case 23 are presented in Figure 7-25, Figure 7-26 and Figure 7-27, respectively.

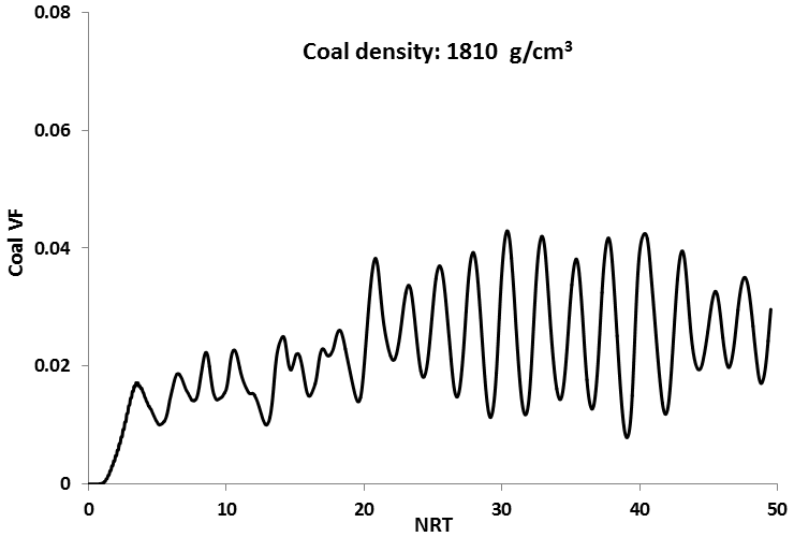

Figure 7-25: Case 21 coal VF at 5-12.5 cm

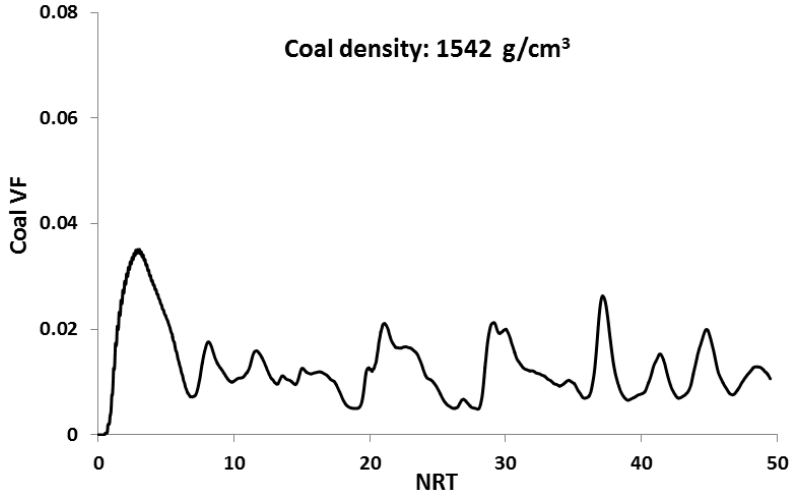

Figure 7-26: Case 22 coal VF at 12.5-17.5 cm

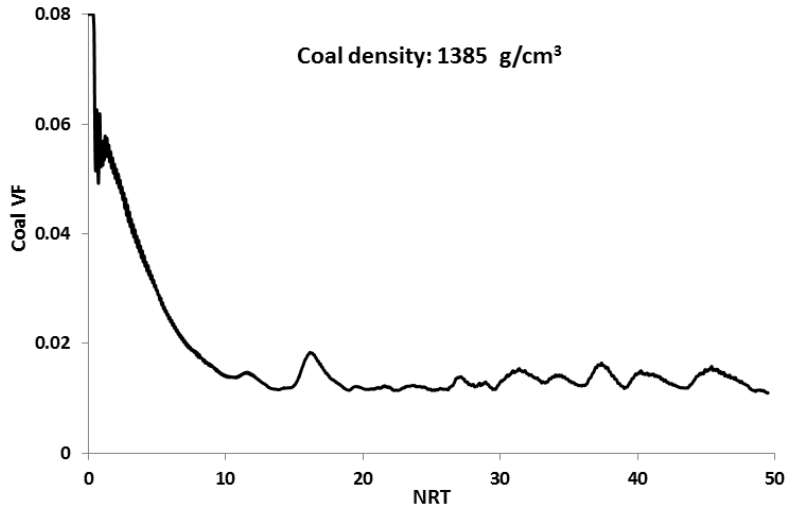

Figure 7-27: Case 23 coal VF at 17.5-22.5 cm

Bearing in mind the zone height and initial amount of coal phases in models, for a prefect segregation of coal and sand, the coal VF of case 21, case 22 and case 23 should reach 0.0533, 0.08 and 0.08 in relevant zones, respectively. Based on the simulation results (Figure 7-25 to Figure 7-27) as well as very low predictability values obtained for models (17, 14.6 and 33.1 for case 21, case 22 and case 23), it seemed that case 21 to case 23 simulation models were not successful in simulating particle segregation.

Reviewing solid flux trends revealed that, due to misplacement effect of motion or back mixing phenomena solid mixing mechanism over rolled the

segregation of solid phases. Mixing mechanism got bolder once lower densities of coal phase is used in models (case 23).

7.9 3D modelling

A 3D model with similar parameters was set to compare the 3D simulation results with the 2D models. The actual bed geometry was developed and discretized uniformly as shown in Figure 7-28.

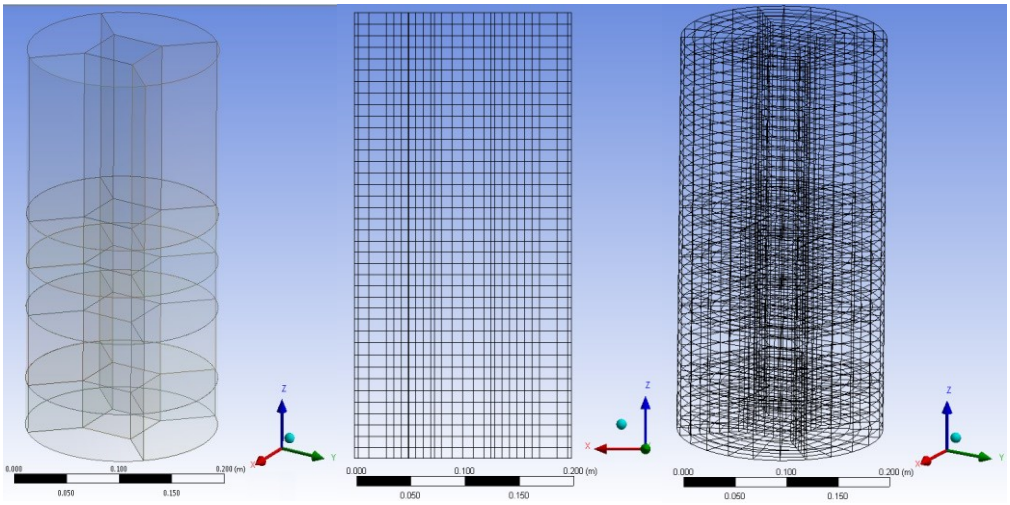

Figure 7-28: 3D bed geometry and mesh grid

The specifications of the developed mesh are presented in Table 7-8.

Table 7-8: 3D bed mesh specification and statistics

Parameter	Value
Cell	7020
Node	30127
Minimum vol. (m^3)	9.50625e-07
Maximum vol. (m^3)	3.07049e-06
Minimum face (m^2)	9.50625e-05
Maximum face (m^2)	2.86579e-04
Minimum orthogonal quality	0.81498
Maximum aspect ratio	3.0255

The same general settings of 2D models were used for 3D model; considering the adjusted Syamlal-O'Brien drag function coefficients and sand-sand and coal-sand restitution coefficients as confirmed through case 9 and 19,

respectively. A summary of the model parameters is presented in Table 7-9. Considering the cell minimum volume in Table 7-8 and solid particle sizes in Table 7-9, at least 16000 sand particles or 19 coal particles could be fit in the smallest cell of the generated geometry.

Table 7-9: 3D model settings

Description	Value	Comment
Sand size	390 μm	Sieving
Sand density	2600 kg/m^3	Silica sand
Coal size	3675 μm	Sieving
Coal density	2320 kg/m^3	Reference experiment
Gas density	1.225 kg/m^3	Air
Gas velocity	16.5 cm/s	Reference experiment
Initial sand packing	0.55	Equal to 8.9 kg
Initial coal packing	0.4	Equal to 132 g
Frictional packing limit	0.55	Both solids
Maximum packing limit	0.58	Both solids
Initial (static) bed height	20 cm	Reference experiment
Restitution coefficient	0.9	Case9 & Case 19
Drag function	Syamlal-O'Brien	Case 9 coefficients
Inlet boundary condition	Velocity inlet	
Outlet boundary	Pressure outlet	
Time step	2e-5 s	0.2 MHz
Max iteration/time step	60	
Convergence criteria	1e-5	For all equations

The model was simulated up to 60 s or 3000000 time steps using single core and double precision mode. The same as 2D models the coal VF was recorded at each zone once per 50 time step. Figure 7-29a-d shows coal VF at different zones. Compared to Figure 7-24a-d, the coal VF graphs were experiencing fewer fluctuations and appeared much smother.

Coal particles were continuously discharged from initially patched zone (17.5-22.5 cm) to the lower zones and soon, after ~18 s, there was no particle left in top zone (in contrary to Figure 7-24a). The second top zone (12.5-17.5 cm) acted as transmitter, and all particles passed through that without any remains there.

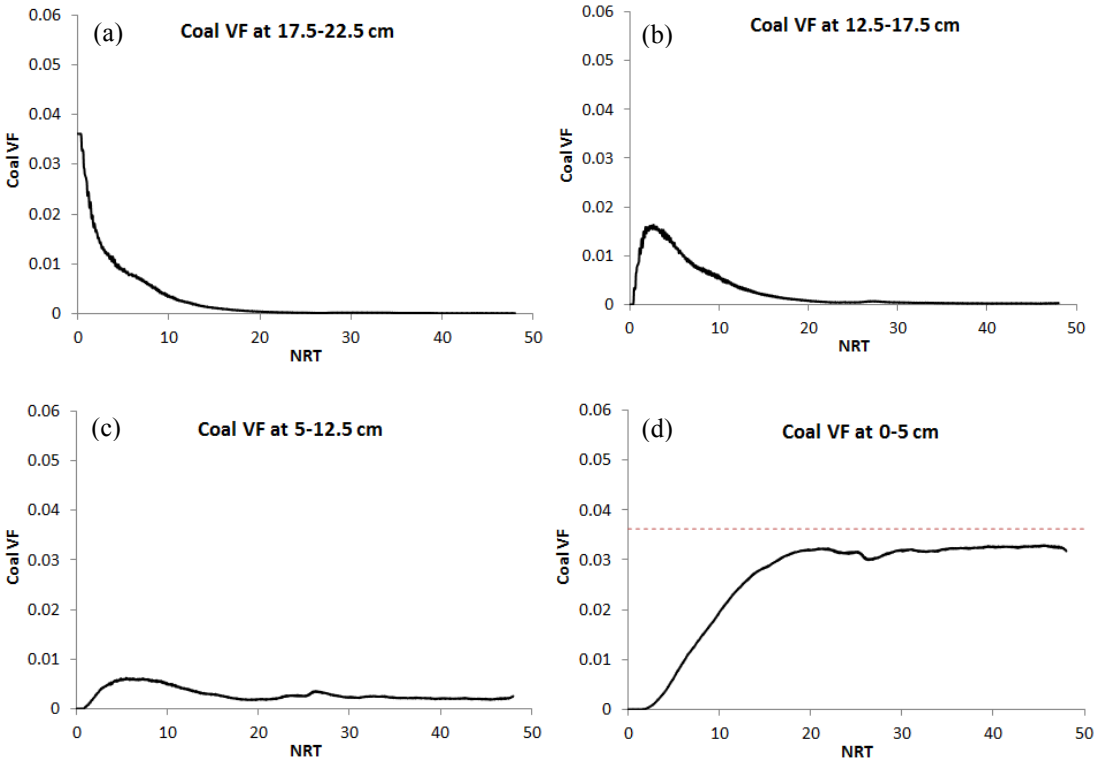

Figure 7-29: Coal VF of 3D model at different zones

Calculations showed that around 10% of initial coal mass was staying at 5-12.5 cm zone considering steady part of graph of Figure 7-29c. The average coal VF after 30 NRT was considered for model predictability calculation. Predictability of 3D models, based on the ratio of coal mass appearing at 0-5 cm zone (Figure 7-29d) to the initial coal mass was calculated to be 89.33% which was significantly higher than 2D model predictability (Figure 7-23) with the same parameter setting.

CHAPTER 8

CONCLUSION AND FUTURE WORK

8.1 Conclusion

From current study and as a result of separation test work on low ash (BD) and high ash (GE) coals conducted by batch or continuous separators and operating parameters optimization, the following conclusions could be derived.

- Taking advantage of design experiment methods and statistical analysis of the results, the effectiveness of selected operating parameters (superficial air velocity, U, separation time, T, and bed height, H) were determined for middle size fraction of both samples. Considering the coded coefficients of the determined mathematical models and perturbation plots, the effect of each parameter was estimated and compared with the others which is valid in the tested range of parameters and may be expanded beyond the ranges with some considerations.
- Except for low ash sample clean coal response; all models, determined with 95% significant level (low ash or high ash sample dealt in batch or continuous separators), presented acceptable model evaluation criteria such as lack of fit, R^2, adjusted R^2 and CV. On average 19% ash reduction was obtained for low ash coal batch experiments but, ash content of products were very close together that no 95% significant model could be determined for describing that.
- It was demonstrated that, mutual interaction of parameters should not be neglected as some mutual interactions act stronger than main parameters (e.g. U-T in Equation 4-2 and T-H in Equation 5-2). In some cases the effect of some of the main parameters were found to be insignificant while stronger interaction of that parameter with other

parameters were recognized significant in results (e.g. T-H in Equation 4-3).

- Regardless of feed ash content and batch or continuous separator and as an overall summary, it was found that:

  Higher levels of U (more than 18 cm/s) and separation times of 2-3 min produced lower clean coal ash products.

  Lower levels of U and T increased combustible material recovery to product stream. The same negative effect of H concluded for low ash batch and high ash continuous separations but not for high ash batch experiments.

  Higher levels of U and H increased separation efficiency of the system. Same conclusion was made for T for low ash feed batch separation and high ash feed continuous separation but not for high ash feed batch separations.

- Considering several process evaluation criteria, different optimization strategies were suggested (based on mathematical models and response surfaces) and some of them experimentally examined. For instance, the minimum product ash content strategy for high ash coal in batch and continuous separators lead to [U, T and H] of [16.5 cm/s, 90 s and 15 cm] and [19.5 cm/s, full bed length and 20 cm], respectively. Three times repeating beneficiation tests under determined conditions, reduced middle size fraction ash content in batch separator from 31.6% to 13.2% and coarse size fraction ash content in continuous separator from 29.1% to 10.06%.
- Feeding different particle size fractions to separators revealed that, regardless of feed ash content in both the separation machines (batch or continuous), separation performance of ADMFB improved as feed particle size increased in spite of the fact that, the ash content of particles was higher for finer particles than in the coarser ones. From coarse size fraction of low ash coal, product with ash content of as low

as 8.7% was produced where 8.95% and 10% products were obtained from high ash batch and continuous separators, respectively.

- Application of fine fluidization media (270 μm) improved separation performance of ADMFB by reducing cut density of bed and consequently producing lower ash products for all feed size fractions. More stable bed in terms of less bubbles and reduced back mixing of particles was the result of fine sand usage.

Based on packed bed and fluidized bed drying experiments the following conclusions could be derived.

- Kinetic rate of coal drying, increased by increasing superficial air velocity and its temperature regardless of packed bed or fluidized bed system. Increase of air temperature was found to be more effective than air velocity.
- It was found that fluidized bed coal drying was more effective than packed bed for shorter drying times (less than 25 min).
- Stage separation and drying revealed that, between 33.8 to 52.5% of clean coal moisture content was removable in 7.5 min fluidized bed drying. It should be noted that beneficiation product had lower moisture content than its original feed and rejects.

From characterization of selected clean coal products, obtained through batch beneficiation experiments on low ash and high ash coals, the following conclusions could be made.

- Verifying distribution of different components along the bed depth revealed that, C, H, N, S, O and HHV of the segregated particles decreased from top to the bottom of bed. This was mainly due to changes in ash content of particles increasing in this direction (significantly).
- As a result of ADMFB beneficiation and regardless of high or low ash feed, HHV of products increased. This increase was bigger (35%) for

GE products than BD products which could be used as an advantage in coal fired power plants to reduce furnace issues or increase energy production rate.

- Regardless of high or low ash feed it was found that, most hazardous elements (Hg, Pb, As, Ag, Ba, Cu, Ni, Co, Mn, Be, K, Zn and Cd) were associated with inorganic phase (negative affinity), and they showed different (sometimes severe) reduction levels. Between examined elements, Se and Sb revealed some levels of organic bounding while Cr showed strong positive affinity to organic phase in BD coal and strong negative affinity in GE coal.
- In spite of less ash rejection in beneficiation of low ash coals, their products showed significant increase in reactivity than high ash coals. The R_{max} and T_{max} were increased and decreased more than 128 and 17.5%, respectively. Two sources were addressed as reasons of such sever increases: change in maceral composition, and increase of components with catalytic effects on coal burn out rate.
- XRD of low temperature ashes showed that, none of the mineral phases were eliminated completely during ADMFB coal beneficiation.
- The XRF analysis showed a higher rejection of clay minerals main components. Also from the changes in Na, Ca and Fe of clean coal, it was concluded that, these elements were associated with organic phase than minerals.
- Sulfur content in BD ash samples did not provide any clear guide to the source of sulfur. More than 140% increase of SO_3 content for GE coal products strongly supports the presence of the organic S.
- Regardless of feed type, ADMFB beneficiation resulted in an increase in slagging and fouling tendency of products. This increase was more for GE products than BD products.
- Slagging factor (obtained based on ash fusion temperature experiments) increased for BD products but still were below 1170 ˚C. This factor decreased for GE products from 1224 ˚C to 1167-1172 ˚C. Considering

1170 ˚C as limit of high to severe slagging it was concluded that, beneficiation did not affect slagging propensity of BD products but intensified that for GE products.

- Prediction of molten slag viscosities by Urbain viscosity model at 1250 ˚C (under reducing or oxidizing environments) revealed that, slag of low ash feed had very low viscosities (less than 72 Poise) where reduced around 50% due to ADMFB beneficiation. High ash coal had initially very high viscosity (6500-9160 Poise) which had decreased significantly after experiencing one step ADMFB beneficiation. The reductions were in the order of ~95%.
- In general, and considering ash fusion temperature tests, slagging indices and slag viscosities, beneficiation of both coals made them more suitable as slagging gasifiers feed. Such changes were stronger for GE, where feeding original ROM into gasifiers might cause operating issues.

Computational Fluid Dynamic (CFD) simulation of particle segregation in fluidized bed, performed using commercial software, Fluent R14.0. Observations and collected data from reference experiments performed on big batch separator were used for model settings. Simulation models were continued long enough (in cases up to 60 s) to obtain steady state simulation model, and some starting seconds of models were eliminated when averaged numbers used for judgments. CFD simulation models used the Euler-Euler approach and showed following conclusions.

- Cell size of 10 mm was found suitable through grid size sensitivity study, based on considerations on solid particles sizes (sand and coal) and comparison of simulation bed heights with the reference experiment bed expansion at $1.5 \times u_{mf}$.
- It was found that, using original coefficients of Syamlal-O'Brien drag function under predicted drag force on sand particles resulting in bed surface subsidence at the adjusted superficial air velocity. Expected bed

height from simulation model was obtained once drag force on particles was increased 1.47 times of its original value by changing two original drag function coefficients from 0.8 and 2.86 to 0.52 and 5.30369, respectively.

- Restitution coefficient of sand-sand collisions was determined to be 0.9 considering resemblance of bubble pattern in model and actual bed as well as comparison of simulation and actual bed heights.
- It was found that by increasing sand-sand restitution coefficient, average granular temperature of sand particles increased while simulated bed height, frequency of bubbles and average particle velocity decreased.
- Since sand phase was the dominant solid phase, study of restitution coefficient of coal-sand collision quality suggested 0.9 for that. Selection of 0.9 was made based on comparison of coal phase solid volume fraction at the expected zone (according to reference experiment) in the 3-phase 2D model with its experimentally determined values.
- Best 2D 3-phase predictability, 60.2%, was obtained for the heaviest coal with tuned drag coefficients and restitution coefficients of 0.9.
- More mixing behavior was seen once three other determined coal classes were substituted by the heaviest one.
- The 3D 3-phase particle segregation simulation model was found to be predicting much better than its equivalent 2D model, as its predictability was 89.33% (29.1% more than 2D model).
- In most preliminary simulation models as well as some of the cases addressed in this study, mixing mechanism was more prominent over segregation of phases. Poor results of simulation were attributed to the selected regime for particle segregation and inaccuracy or incapability of the software to predict interactions at such narrow transient regime, between incipient fluidization and bubbling regime.

8.2 Recommendations for future works

Getting deep insight to the coal samples characteristics and ability to estimate quality and achievable beneficiation levels for ADMFB separators using automated techniques such as Mineral Liberation Analyzer or Automated Reflectance Microscopy can encourage the application of ADMFB coal separators in industrial applications. Applying coal-mineral liberation (or association) study results to separation performance of ADMFBs could be possible by classifying ROM coals into several classes based on full characterization of ROMs (e.g. chemical composition, coal-mineral size-wise liberation studies) and conducting separation experiments on any of the determined classes of coals.

Conducting a thorough economic study for the whole process, once coal seam determined minable or not to the very last stage as energy converted to electricity with complete considerations on all waste management steps and their costs is strongly recommended. Definitely the defined separation process evaluation criteria (clean coal ash content, combustible material recovery and system separation efficiency) will be involved for connecting main steps (mining, processing, firing and energy conversion) for determination of quality and accessible amount of solid fuel. Connecting such economic evaluation to the three discussed responses, will provide better decision making tool for ADMFB (or any separation system) beneficiation process evaluation and determination of optimum separation condition.

The current continuous setup in University of Alberta needs re-designing in sand feeding and tailing discharge sections. It was found that feeding sand particles from the bottom of bed improves horizontal movement of high ash particles at the bottom of bed. Therefore it is suggested to consider a better mechanism such as, instalment of a screw feeder with adjustable feeding rate to add fluidization medium to the bed, from the lowest position possible. Also replacement of stationary (fixed) porous media plates with a moving surface could control and improve settled high ash particles movement at the bottom of bed. Mixture of low ash coal and sand particles secure discharging from bed was

obtained by moving collecting edge forward. But discharging sand particles along with high ash particles from current tailing discharge gate imposes turbulence and bed height drop (suction of neighbor particles). Adding two chamber tail discharge section separated by a vertical plate and removing freely entered particles to the second chamber using a scoop feeder (or similar mechanism) could facilitate particles discharging without creating operational issues.

Some feasibility staged-beneficiations performed during this study but the results were not reported here as a systematic trend was not followed. A targeted multi-stage beneficiation study is recommended after considering suggested re-designing options for continuous separator. The multi-stage separation could include, re-cleaning of product under different operating conditions for further reduction in ash content or considering secondary size reduction step for clean coal product and re-cleaning that again.

Integrating drying and separation in a continuous mode is strongly suggested since significant amount of moisture could be reduced in a short time if hot media is available abundantly. The ROM could be beneficiated along the necessary path in a hot fluidized bed. Low ash particles could continue drying as moving to the end of bed while high ash particles could be removed at the designed location from bottom of bed (as shown schematically in Figure 8-1). It is unnecessary to dry high ash particles which will finally be disposed. It is seen that the moisture content of high ash particles are usually higher than low ash particles and weight yield of them could ascend up to 30-40% of the feed.

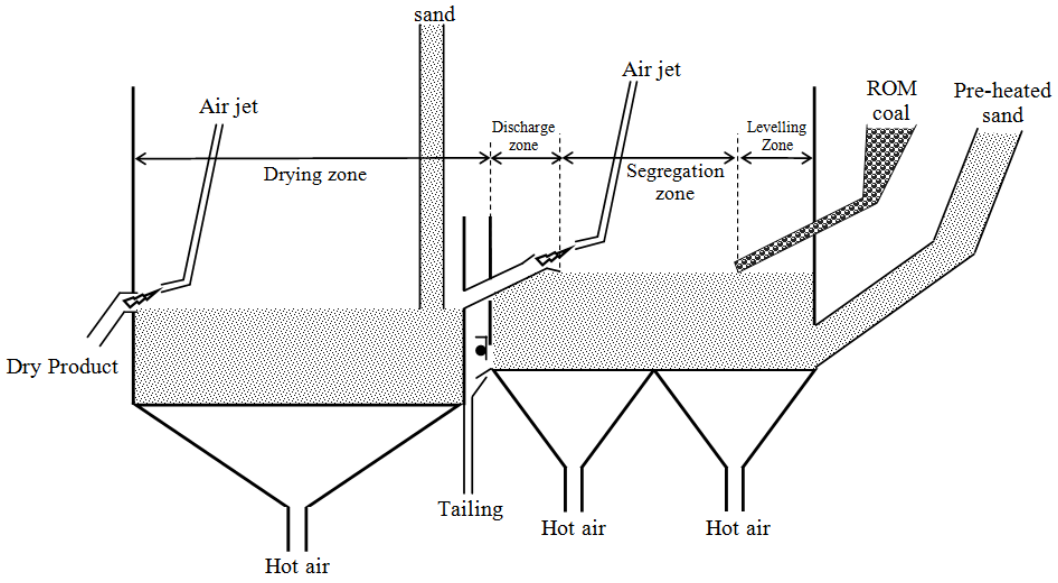

Figure 8-1: Schematic of a combined ADMFB coal separator and dryer

APPENDIX A

WASHABILITY STUDY

In such physical separation experiments the cleaning effectiveness of the process is mainly affected by the liberation of the ash minerals from coal phase and consequently particles density gradient. Therefore in order to get an idea about the washability behavior of the samples the conventional sink float test were performed using sized samples, described in the following section.

Aqueous solution of zinc chloride (purchased from Fisher Scientific Canada) is used to prepare heavy liquids [65], due to strong safety and environmental considerations. As suggested [66, 68], 5 g/l Brij35 (purchased from Sigma Aldrich Chemicals) is added to the aqueous solution to prevent particles aggregation. Five liquids with densities of 1.4, 1.5, 1.6, 1.7 and 1.8 g/cm^3 were produced by solving different amount of zinc chloride in distilled water. The tests were carried out in one liter beakers and density of liquids were adjusted (if necessary) prior to adding particles by a 25 ml picnometer. Coal particles were initially introduced to lowest density liquid and both sink and float proportions were collected by strainer and vacuum filtration after segregation. The heavy particles (sink materials) were washed by distilled water dried and then introduced to the next heavy liquid. The float material of each liquid as well as sink material of 1.8 g/cm^3 liquid were washed (to remove $ZnCl_2$), dried, weighted and their ash content was determined.

The collected data were analyzed and necessary calculations performed according to well explained procedure in literature (e.g. [69]). The washability curve of GE and BD middle size fractions are presented in Figure A-1 and Figure A-2, respectively.

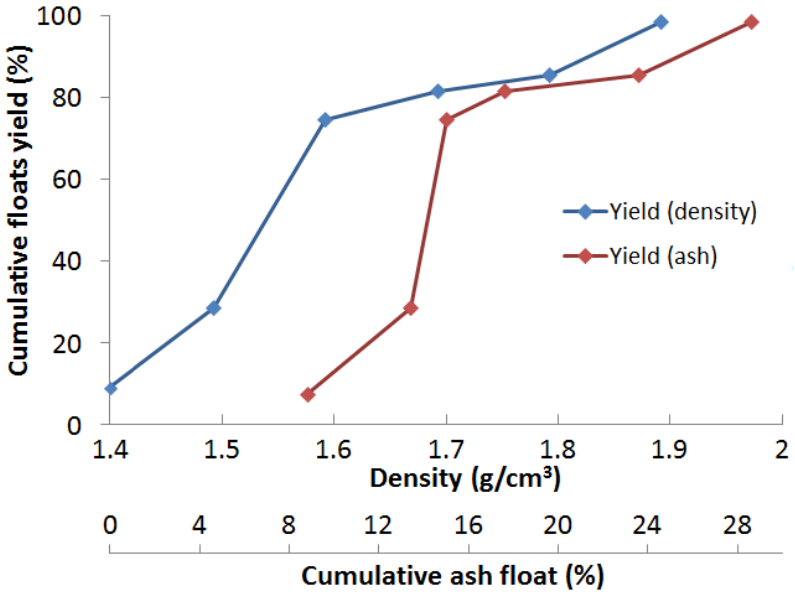

Figure A-1: Washability curve of middle size GE sample

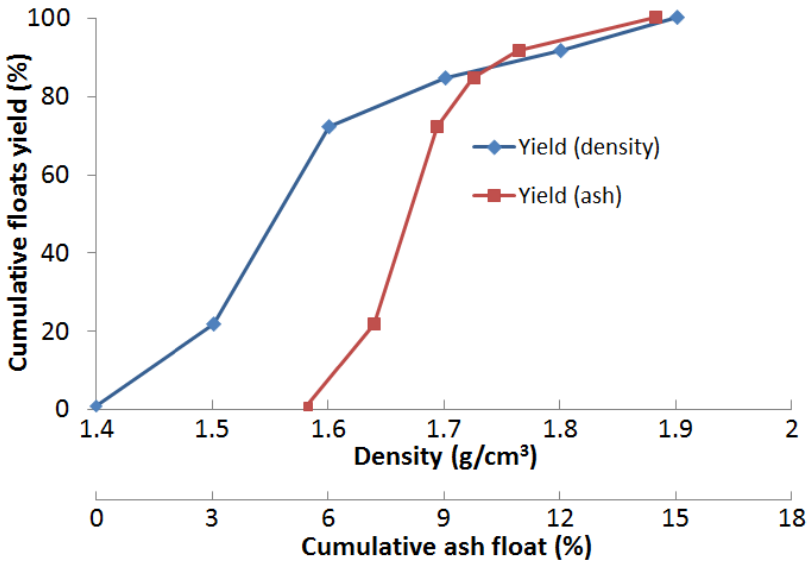

Figure A-2: Washability curve of middle size BD sample

Considering lower density of coal macerals compared to most ash forming minerals and the yield-density curves of Figure A-1 and Figure A-2; it could be concluded that the proportion of liberated ash particles in GE is significantly higher than BD coal. The upper part of yield-density curve in Figure A-2 is becoming horizontal indicating domination of ash minerals in the particles (as particle density is a volume average of minerals and ash macerals density) where

it is continuously increasing for BD sample, indicating slowly increase of ash minerals proportion in each individual particle and consequently reduction of coal macerals proportion. Central parts of both Figure A-1 and Figure A-2 graphs reveal that by accurate control of separating cut density, satisfactory separation could be achieved.

It should be addressed that severe sliming of ash forming minerals found to be a serious issue in developing washability curves (for both BD and GE coals), so any conclusion based on Figure A-1 and Figure A-2 should be made with precautious. As a result (as mentioned in section 2.6) other evaluation criteria than Ep will be used to determine the effectiveness of the separation experiments which will be discussed in more details in section 3.5.4.

REFERENCES

1: Leonard, J.W. and B.C. Hardinge, *Coal preparation / editor, Joseph W. Leonard, III, associate editor, Byron C. Hardinge*. Littleton, Colo.: Society for Mining, Metallurgy, and Exploration, 1991.5th ed.

2: IAE, I., *Key world energy statistics*. 2012, Technical report, International energy agency. http://www.iea.org/publications/freepublications/publication/kwes.pdf. (accessed August-2014).

3: Annual energy review 2010, U.S. Energy Information Administration (EIA), Office of Energy Statistics, U.S. Department of Energy, Washington, DC 20585Sep. 2011. http://www.eia.gov/totalenergy/data/annual/pdf/aer.pdf. (accessed August-2014).

4: Natural Resources Canada. http://www.nrcan.gc.ca/energy/home, (accessed August-2014).

5: Kretzschmar, S. *Dry beneficiation of coal using an air dense-medium fluidised bed separator*. Master of Science thesis. University of KwaZulu-Natal, South Africa 2010.

6: Nayak, K. C. *Effect of coal size and process variables on coal cleaning efficiency in an air dense medium fluidized bed*. Bachelor of Technology thesis. National Institute of Technology, Rourkela, India 2012.

7: Lockhart, N.C., *Beneficiation of coal-Review paper.* Powder Technology, 1984. **40**: p. 17-42.

8: Dwari, R.K. and K.H. Rao, *Dry Beneficiation of Coal—a Review.* Mineral Processing and Extractive Metallurgy Review, 2007. **28**(3): p. 177-234.

9: Khoury, D. L.; Coal Cleaning Technology; Noyes Data Corporation, Park Ridge: New Jersey, 1981; ISBN: 0815508751.

10: Sahu, A.K., S.K. Biswal, and A. Parida, *Development of Air Dense Medium Fluidized Bed Technology For Dry Beneficiation of Coal – A Review.*

International Journal of Coal Preparation and Utilization, 2009. **29**(4): p. 216-241.

11: Luo, Z., et al., *Density-dependent separation of dry fine coal in a vibrated fluidized bed.* Powder Technology, 2008. **187**(2): p. 119-123.

12: Sampaio, C.H., et al., *Coal beneficiation of Candiota mine by dry jigging.* Fuel Processing Technology, 2008. **89**(2): p. 198-202.

13: Chikerema, P. and M. Moys, *Effects of Particle Size, Shape, and Density on the Performance of an Air Fluidized Bed in Dry Coal Beneficiation.* International Journal of Coal Preparation and Utilization, 2012. **32**(2): p. 80-94.

14: Feil, N.F., C.H. Sampaio, and H. Wotruba, *Influence of jig frequency on the separation of coal from the Bonito seam—Santa Catarina, Brazil.* Fuel Processing Technology, 2012. **96**: p. 22-26.

15: Van HOUWELINGEN, J.A. and T.P.R. de Jong, *Dry cleaning of coal: review, fundamentals and opportunities.* Geologica Belgica, 2004.

16: Donnelly, J., *Potential revival of dry cleaning of coal.* AUSTRALIAN COAL REVIEW, 1999: p. 26-30.

17: Sarunac, N., et al., *A Novel Fluidized Bed Drying and Density Segregation Process for Upgrading Low-Rank Coals.* International Journal of Coal Preparation and Utilization, 2009. **29**(6): p. 317-332.

18: Kunii, D. and O. Levenspiel, *Fluidization engineering*. 1991: Butterworth-Heinemann, C/O Elsevier Science, Order Fulfillment, 11830 Westline Industrial Dr, Saint Louis, MO, 63146. 491.

19: Richardson, J.F., et al., Coulson and Richardson's chemical engineering. Volume 2, Particle technology and separation processes [electronic resource] / J.F. Richardson, J.H. Harker, with J.R. Backhurst. 2002: Oxford ; Boston : Butterworth-Heinemann, 2002. 5th ed.

20: Rowe, P. and A. Nienow, *Particle mixing and segregation in gas fluidised beds. A review.* Powder Technology, 1976. **15**(2): p. 141-147.

21: Rhodes, M.J., *Introduction to Particle Technology*. 2008, Chichester, England: Wiley.

22: Yang, W.-c., *Handbook of fluidization and fluid-particle systems*. 2003: CRC Press.

23: Gupta, C.K. and D. Sathiyamoorthy, *Fluid bed technology in materials processing*. 1998: CRC Press.

24: Pell, M., *Gas fluidization / Mel Pell*. Handbook of powder technology: v. 8. 1990: Amsterdam ; New York : Elsevier, 1990.

25: Zhenfu, L. and C. Qingru, *Dry beneficiation technology of coal with an air dense-medium fluidized bed.* International Journal of Mineral Processing, 2001. **63**(3): p. 167-175.

26: Howard, J., *Fluidized bed technology: principles and applications*. 1989: A. Hilger.

27: Tang, L.G., et al., *The Effect of Fine Coal Particles on the Performance of Gas–Solid Fluidized Beds.* International Journal of Coal Preparation and Utilization, 2009. **29**(5): p. 265-278.

28: He, Y., Y. Zhao, and Q. Chen, *Fine particle behavior in air fluidized bed dense medium dry separator.* Coal Preparation, 2003. **23**(1-2): p. 33-45.

29: Geldart, D., *Types of gas fluidization.* Powder technology, 1973. **7**(5): p. 285-292.

30: Geldart, D., *Gas fluidization technology.* 1986: John Wiley & Sons Ltd.

31: Geldart, D., *The effect of particle size and size distribution on the behaviour of gas-fluidised beds.* Powder Technology, 1972. **6**(4): p. 201-215.

32: Molerus, O., *Interpretation of Geldart's type A, B, C and D powders by taking into account interparticle cohesion forces.* Powder technology, 1982. **33**(1): p. 81-87.

33: Grace, J.R., *Contacting modes and behaviour classification of gas—solid and other two flow phase suspensions.* The Canadian Journal of Chemical Engineering, 1986. **64**(3): p. 353-363.

34: Goossens, W.R., *Classification of fluidized particles by Archimedes number.* Powder technology, 1998. **98**(1): p. 48-53.

35: Wei, L., *Mechanism and application of coal dry beneficiation with air-dense medium fluidized bed.* Journal of Central South University of Technology, 1998. **5**(2): p. 100-103.

36: Chen, Q. and Y. Yang, *Development of dry beneficiation of coal in China.* Coal Preparation, 2003. **23**(1-2): p. 3-12.

37: Luo, Z.-F., et al., *Low density dry coal beneficiation using an air dense medium fluidized bed.* Journal of China University of Mining and Technology, 2007. **17**(3): p. 306-309.

38: Chen, Q. and L. Wei, *Coal dry beneficiation technology in China: the state-of-the-art.* China Particuology, 2003. **1**(2): p. 52-56.

39: Zhenfu, L., C. Qingru, and Z. Yaomin, *Dry beneficiation of coarse coal using an air dense medium fluidized bed (ADMFB).* Coal Preparation, 2002. **22**(1): p. 57-64.

40: Luo, Z., et al., *Progress in dry coal cleaning using air-dense medium fluidized beds.* Coal Preparation, 2003. **23**(1-2): p. 13-20.

41: Mohanta, S., S. Chakraborty, and B. Meikap, *Influence of coal feed size on the performance of air dense medium fluidized bed separator used for coal beneficiation.* Industrial & Engineering Chemistry Research, 2011. **50**(18): p. 10865-10871.

42: Mohanta, S. Dry beneficiation of high ash Indian thermal coal in an air dense medium fluidized bed. PhD thesis. Indian Institute of Technology, Kharagpur, 2012.

43: Mohanta, S., et al., *Applicability of the air dense medium fluidized bed separator for cleaning of high-ash Indian thermal coals: An experimental study.* South African Journal of Chemical Engineering, 2011. **16**(1): p. 50-62.

44: Mohanta, S., S. Chakraborty, and B. Meikap, *Optimization Process of an Air Dense Medium Fluidized Bed Separator for Treating High-Ash Non-coking Indian Coal.* Mineral Processing and Extractive Metallurgy Review, 2013. **34**(4): p. 240-248.

45: Sahu, A., et al., *Stability study of an air dense medium fluidized bed separator for beneficiation of high-ash Indian coal.* International Journal of Coal Preparation and Utilization, 2011. **31**(3-4): p. 127-148.

46: Sahan, R. and B. Kozanoglu, *Use of an air fluidized bed separator in a dry coal cleaning process.* Energy conversion and management, 1997. **38**(3): p. 269-286.

47: Sahan, R., *Coal cleaning performance in an air fluidized bed.* Energy sources, 1997. **19**(5): p. 475-492.

48: Choung, J., C. Mak, and Z. Xu, *Fine coal beneficiation using an air dense medium fluidized bed.* Coal Preparation, 2006. **26**(1): p. 1-15.

49: Mak, C., et al., *Potential of air dense medium fluidized bed separation of mineral matter for mercury rejection from Alberta sub-bituminous coal.* International journal of coal preparation and utilization, 2008. **28**(2): p. 115-132.

50: Prashant, D., et al. *Dry cleaning of coal by a laboratory continuous air dense medium fluidized bed separator*. in *International coal preparation congress. Lexington: SME*. 2010.

51: Zhenfu, L. and C. Qingru, *Effect of fine coal accumulation on dense phase fluidized bed performance.* International Journal of Mineral Processing, 2001. **63**(4): p. 217-224.

52: Fan, M., et al., *Fine coal (6–1 mm) separation in magnetically stabilized fluidized beds.* International journal of mineral processing, 2001. **63**(4): p. 225-232.

53: Fan, M., et al., *Magnetically stabilized fluidized beds for fine coal separation.* Powder Technology, 2002. **123**(2): p. 208-211.

54: Fan, M., et al., *Fundamentals of a magnetically stabilized fluidized bed for coal separation.* Coal Preparation, 2003. **23**(1-2): p. 47-55.

55: Luo, Z., et al., *Separation characteristics for fine coal of the magnetically fluidized bed.* Fuel Processing Technology, 2002. **79**(1): p. 63-69.

56: Luo, Z., et al., *Separation lower limit in a magnetically gas–solid two-phase fluidized bed.* Fuel processing technology, 2004. **85**(2): p. 173-178.

57: Jin, H., et al., *Separation of fine binary mixtures under vibration in a gas-solid fluidized bed with dense medium.* Waste management & research, 2005. **23**(6): p. 534-540.

58: Jin, H., et al., *Homogeneous fluidization characteristics of vibrating fluidized beds.* The Canadian Journal of Chemical Engineering, 2004. **82**(5): p. 1048-1053.

59: Fan, M.; Luo, Z.; Tao, D.; Zhao, Y.; Chen, O. *Dry coal separation with a vibrated air dense medium fluidized bed*. SME Annual Meeting and Exhibit and CMA's 111th National Western Mining Conference 2009, Denver, CO., 2, 714-717.

60: Beeckmans, J. and T. Minh, *Separation of mixed granular solids using the fluidized counter current cascade principle.* The Canadian Journal of Chemical Engineering, 1977. **55**(5): p. 493-496.

61: Beeckmans, J., L. Bergström, and J. Large, *Segregation mechanisms in gas fluidized beds.* The Chemical Engineering Journal, 1984. **28**(1): p. 1-11.

62: Chan, E. and J. Beeckmans, *Pneumatic beneficiation of coal fines using the counter-current fluidized cascade.* International Journal of Mineral Processing, 1982. **9**(2): p. 157-165.

63: Dong, X. and J. Beeckmans, *Separation of particulate solids in a pneumatically driven counter-current fluidized cascade.* Powder Technology, 1990. **62**(3): p. 261-267.

64: Wei, L., Q. Chen, and Y. Zhao, *Formation of double-density fluidized bed and application in dry coal beneficiation.* Coal Preparation, 2003. **23**(1-2): p. 21-32.

65: Yan, D. and A. Gupta, *Mineral processing design and operation: an introduction*. 2006: Elsevier.

66: Taulbee, D., et al., *Density gradient centrifugation separation and characterization of maceral groups from a mixed maceral bituminous coal.* Energy & fuels, 1989. **3**(6): p. 662-670.

67: Dyrkacz, G.R., C. Bloomquist, and L. Ruscic, *Investigations into the process of maceral separation by centrifugal techniques. 3. Continuous flow and sink/float maceral separation of-100-mesh coal.* Energy & fuels, 1993. **7**(5): p. 655-660.

68: Dyrkacz, G.R., C. Bloomquist, and E.P. Horwitz, *Laboratory scale separation of coal macerals.* Separation Science and Technology, 1981. **16**(10): p. 1571-1588.

69: Wills, B.A., *Wills' mineral processing technology: an introduction to the practical aspects of ore treatment and mineral recovery*. 2011: Butterworth-Heinemann.

70: Aslan, N., *Application of response surface methodology and central composite rotatable design for modeling and optimization of a multi-gravity separator for chromite concentration.* Powder Technology, 2008. **185**(1): p. 80-86.

71: Karimipour, S., et al., *Study of factors affecting syngas quality and their interactions in fluidized bed gasification of lignite coal.* Fuel, 2013. **103**: p. 308-320.

72: Liyana-Pathirana, C. and F. Shahidi, *Optimization of extraction of phenolic compounds from wheat using response surface methodology.* Food chemistry, 2005. **93**(1): p. 47-56.

73: Montgomery, D.C., *Design and analysis of experiments*. 2008: John Wiley & Sons.

74: Oraon, B., G. Majumdar, and B. Ghosh, *Application of response surface method for predicting electroless nickel plating.* Materials & design, 2006. **27**(10): p. 1035-1045.

75: Vejahati, F., H. Katalambula, and R. Gupta, *Entrained-flow gasification of oil sand coke with coal: Assessment of operating variables and blending ratio via response surface methodology.* Energy & Fuels, 2011. **26**(1): p. 219-232.

76: Aslan, N., *Modeling and optimization of Multi-Gravity Separator to produce celestite concentrate.* Powder Technology, 2007. **174**(3): p. 127-133.

77: Sen, R., *Response surface optimization of the critical media components for the production of surfactin.* Journal of Chemical Technology and Biotechnology, 1997. **68**(3): p. 263-270.

78: Vazifeh, Y., E. Jorjani, and A. Bagherian, *Optimization of reagent dosages for copper flotation using statistical technique.* Transactions of Nonferrous Metals Society of China, 2010. **20**(12): p. 2371-2378.

79: Delebarre, A., J.-M. Morales, and L. Ramos, *Influence of the bed mass on its fluidization characteristics.* Chemical Engineering Journal, 2004. **98**(1): p. 81-88.

80: Borges, G.D.S.C., et al., *Optimization of the extraction of flavanols and anthocyanins from the fruit pulp of Euterpe Edulis using the response surface methodology.* Food Research International, 2011. **44**(3): p. 708-715.

81: Design-Expert, Version 8.0.7.1; Highly efficient Design Of Experiments (DOE)-User's guide; Stat-Ease Inc.: Minneapolis, 2010.

82: Liong, M.T. and N.P. Shah, *Optimization of cholesterol removal by probiotics in the presence of prebiotics by using a response surface method.* Applied and environmental microbiology, 2005. **71**(4): p. 1745-1753.

83: Channiwala, S. and P. Parikh, *A unified correlation for estimating HHV of solid, liquid and gaseous fuels.* Fuel, 2002. **81**(8): p. 1051-1063.

84: Goodarzi, F.; Cameron, A. R. Distribution of major, minor and trace dements in coals of the Kootenay Group, Mount Allan, Alberta. Canadian Mineralogist, 1987, 25, 555-565.

85: Burton, E.D., R.T. Bush, and L.A. Sullivan, *Fractionation and extractability of sulfur, iron and trace elements in sulfidic sediments.* Chemosphere, 2006. **64**(8): p. 1421-1428.

86: Xu, M., et al., *Status of trace element emission in a coal combustion process: a review.* Fuel Processing Technology, 2004. **85**(2): p. 215-237.

87: Pires, M., H. Fiedler, and E.C. Teixeira, *Geochemical distribution of trace elements in coal: modelling and environmental aspects.* Fuel, 1997. **76**(14): p. 1425-1437.

88: Goodarzi, F., *Mineralogy, elemental composition and modes of occurrence of elements in Canadian feed-coals.* Fuel, 2002. **81**(9): p. 1199-1213.

89: Toole-O'Neil, B., et al., *Mercury concentration in coal—unraveling the puzzle.* Fuel, 1999. **78**(1): p. 47-54.

90: Diehl, S., M. Goldhaber, and J. Hatch, *Modes of occurrence of mercury and other trace elements in coals from the warrior field, Black Warrior Basin, Northwestern Alabama.* International Journal of Coal Geology, 2004. **59**(3): p. 193-208.

91: Clarke, L.B. and L.L. Sloss, *Trace elements-emissions from coal combustion and gasification*. Vol. 49. 1992: IEA Coal Research.

92: Gibb, W.; Quick, W.; Salisbury, M. Technology status review–monitoring & control of trace elements (Report No. Coal R249). Powergen UK plc, Power Technology Centre, 2003. www.dti.gov.uk/files/file19031.pdf (accessed August-2014).

93: Brand, R.; Pulles, T.; Van Gijlswijk, R.; Fribourg-Blanc, B.; Courbet, C. European Pollutant Emission Register (EPER) review report. European Environment Agency, 2004. http://www.env-edu.gr/Documents/EPER.pdf (accessed August-2014).

94: Overview - The Clean Air Act Amendments of 1990, U.S. Environmental Protection Agency. http://epa.gov/oar/caa/caaa_overview.html (accessed August-2014).

95: Finkelman, R.B., *Modes of occurrence of trace elements and minerals in coal: an analytical approach*, in *Atomic and nuclear methods in fossil energy research*. 1982, Springer. p. 141-149.

96: Huggins, F.E., et al., *XANES spectroscopic characterization of selected elements in deep-cleaned fractions of Kentucky No. 9 coal.* Energy & fuels, 1997. **11**(3): p. 691-701.

97: Beaton, A.P., F. Goodarzi, and J. Potter, *The petrography, mineralogy and geochemistry of a Paleocene lignite from southern Saskatchewan, Canada.* International Journal of Coal Geology, 1991. **17**(2): p. 117-148.

98: Benson, S. A.; Hurley, J. P.; Falcone, S. K.; Schobert, H. H. Inorganic constituents in low rank coals-direct coal analysis or ash analysis. Rocky Mountain coal symp. Proc. 1984, 2-11.

99: Kolker, A., C.L. Senior, and J.C. Quick, *Mercury in coal and the impact of coal quality on mercury emissions from combustion systems.* Applied geochemistry, 2006. **21**(11): p. 1821-1836.

100: Luttrell, G.H., J.N. Kohmuench, and R.-H. Yoon, *An evaluation of coal preparation technologies for controlling trace element emissions.* Fuel Processing Technology, 2000. **65**: p. 407-422.

101: (34) Quarter 9–mercury information clearinghouse final report, Canadian Electricity Association, December 2005. http://mercury.electricity.ca/home.html (accessed: August-2014).

102: Azimi, E., et al., *Evaluation of the Performance of Air Dense Medium Fluidized Bed (ADMFB) for Low-Ash Coal Beneficiation. Part 2: Characteristics of the Beneficiated Coal.* Energy & Fuels, 2013. **27**(10): p. 5607-5616.

103: Haykiri-Açma, H., A. Ersoy-Meriçboyu, and S. Küçükbayrak, *Effect of demineralization on the reactivity of lignites.* Thermochimica acta, 2000. **362**(1): p. 131-135.

104: Biswas, S., et al., *Studies on the combustion behaviour of blends of Indian coals by TGA and drop tube furnace.* Fuel Processing Technology, 2006. **87**(3): p. 191-199.

105: Liu, Q., et al., *Effect of inorganic matter on reactivity and kinetics of coal pyrolysis.* Fuel, 2004. **83**(6): p. 713-718.

106: Le Manquais, K., et al., *Evaluating the combustion reactivity of drop tube furnace and thermogravimetric analysis coal chars with a selection of metal additives.* Energy & Fuels, 2011. **25**(3): p. 981-989.

107: Vamvuka, D., S. Troulinos, and E. Kastanaki, *The effect of mineral matter on the physical and chemical activation of low rank coal and biomass materials.* Fuel, 2006. **85**(12): p. 1763-1771.

108: Rubiera, F., et al., *Coal structure and reactivity changes induced by chemical demineralisation.* Fuel processing technology, 2002. **79**(3): p. 273-279.

109: Sun, Q., et al., *The variation of structural characteristics of macerals during pyrolysis.* Fuel, 2003. **82**(6): p. 669-676.

110: Pandolfo, A., et al., *Separation and preliminary characterization of high-purity maceral group fractions from an Australian bituminous coal.* Energy & fuels, 1988. **2**(5): p. 657-662.

111: Thomas, C., et al., *The behaviour of inertinite macerals under pulverised fuel (pf) combustion conditions.* Organic geochemistry, 1993. **20**(6): p. 779-788.

112: Winans, R. E.; Crelling, J. C. *Chemistry and Characterization of Coal Macerals: Overview. In Chemistry and Characterization of Coal Macerals*; ACS Symposium Series 252, American Chemical Society: Washington, DC, 1984; pp 1-20.

113: Huggins, F.E., *Overview of analytical methods for inorganic constituents in coal.* International Journal of Coal Geology, 2002. **50**(1): p. 169-214.

114: Ryan, B., *Preliminary Analyses of Coal Refuse Material from Vancouver Island*. 2008, BC Ministry of Energy, Mines and Petroleum Resources: British Columbia, Canada.

115: Kim, H. T.; Choi, B. C.; Park, S. H. *A study on the slagging behavior of coal ash in Gasification/combustion environment using DTF*. Proc. 218th ACS Natl. Meet. 1999, 42, 721-724.

116: Gupta, S., et al., *Ash fusion temperatures and the transformations of coal ash particles to slag.* Fuel processing technology, 1998. **56**(1): p. 33-43.

117: Kim, H. T. *A prediction of coal ash slagging under the gasification condition*. in *Fuel and Energy Abstracts*. 1997. Elsevier Science.

118: Barnes, I. *Slagging and fouling in coal-fired boilers*. IEA clean coal center, June 2009. http://www.iea-coal.org/documents/82175/7154/Slagging-and-fouling-in-coal-fired-boilers (accessed August-2014).

119: Akar, G.; Ipekoglu, U. *Relationship between ash fusion temperatures (AFT) and coal mineral matter in some Turkish coal ashes*. J. Ore Dress. 2009, 9 (17), 33-39.

120: *Slagging and Fouling Indices*, Coal Technology Pty Ltd. 2007. http://www.coaltech.com.au/Slagging&Fouling.html (accessed August-2014).

121: Folkedahl, B.C. and H.H. Schobert, *Effects of atmosphere on viscosity of selected bituminous and low-rank coal ash slags.* Energy & fuels, 2005. **19**(1): p. 208-215.

122: Song, W.J., et al., *Effect of coal ash composition on ash fusion temperatures.* Energy & Fuels, 2009. **24**(1): p. 182-189.

123: Van Dyk, J., et al., *Coal and coal ash characteristics to understand mineral transformations and slag formation.* Fuel, 2009. **88**(6): p. 1057-1063.

124: Song, W., et al., *Fusibility and flow properties of coal ash and slag.* Fuel, 2009. **88**(2): p. 297-304.

125: Patterson, J. and H. Hurst, *Ash and slag qualities of Australian bituminous coals for use in slagging gasifiers.* Fuel, 2000. **79**(13): p. 1671-1678.

126: Urbain, G., *Viscosity of silicate melts.* Trans. J. Br. Ceram. Soc., 1981. **80**(4): p. 139.

127: Lucas, J. A.; Browning, G. J.; Bryant, G. W.; Hurst, H. J.; Wall, T. F. *Development of the thermomechanical analysis technique for coal ash and slag applications*; Cooperative research centre for black coal utilization, Department of Chemical Engineering: University of Newcastle, March 2001.

128: Kekkonen, M., H. Oghbasilasie, and S. Louhenkilpi, *Viscosity models for molten slags.* 2012.

129: Vargas, S., F. Frandsen, and K. Dam-Johansen, *Elsam-Idemitsu Kosan Cooperative Research project: Performance of viscosity models for high-temperature coal ashes.* Department of Chemical Engineer-ing, Technical University of Denmark, CHEC Report, 1997. **9719**.

130: Massoudi, M. and P. Wang, *A Brief Review of Viscosity Models for Slag in Coal Gasification*. 2011, National Energy Technology Laboratory-In-house Research.

131: Ranade, V.V., *Computational Flow Modeling for Chemical Reactor Engineering*. Vol. 5. 2002: Academic Press.

132: Gilbertson, M. and J. Yates, *The motion of particles near a bubble in a gas-fluidized bed.* Journal of Fluid Mechanics, 1996. **323**: p. 377-385.

133: Grace, J.R. and F. Taghipour, *Verification and validation of CFD models and dynamic similarity for fluidized beds.* Powder Technology, 2004. **139**(2): p. 99-110.

134: Ibsen, C.H., T. Solberg, and B.H. Hjertager, *Evaluation of a three-dimensional numerical model of a scaled circulating fluidized bed.* Industrial & engineering chemistry research, 2001. **40**(23): p. 5081-5086.

135: J.A.M. Kuipers, W.P.M. van Swaaij *Simulation of three-dimensional (3D) riser flow using kinetic theory of granular flow*, in: J. Werther (Ed.), 6th International Conference on Circulating Fluidized Beds, Würzburg, Germany, August 24–27,1999.

136: Zhang, D. and W. VanderHeyden, *High-resolution three-dimensional numerical simulation of a circulating fluidized bed.* Powder Technology, 2001. **116**(2): p. 133-141.

137: A. Inc. ANSYS-FLUENT® Theory Guide, Release 14.0, 2013.

138: Gera, D., et al., *Computer simulation of bubbles in large-particle fluidized beds.* Powder Technology, 1998. **98**(1): p. 38-47.

139: Kobayashi, N., R. Yamazaki, and S. Mori, *A study on the behavior of bubbles and solids in bubbling fluidized beds.* Powder Technology, 2000. **113**(3): p. 327-344.

140: Taghipour, F., N. Ellis, and C. Wong, *Experimental and computational study of gas–solid fluidized bed hydrodynamics.* Chemical Engineering Science, 2005. **60**(24): p. 6857-6867.

141: Goldschmidt, M., J. Kuipers, and W. Van Swaaij, *Hydrodynamic modelling of dense gas-fluidised beds using the kinetic theory of granular flow: effect of coefficient of restitution on bed dynamics.* Chemical Engineering Science, 2001. **56**(2): p. 571-578.

142: Gidaspow, D., R. Bezburuah, and J. Ding, *Hydrodynamics of circulating fluidized beds: kinetic theory approach*. 1991, Illinois Inst. of Tech., Chicago, IL (United States). Dept. of Chemical Engineering.

143: Pain, C., S. Mansoorzadeh, and C. De Oliveira, *A study of bubbling and slugging fluidised beds using the two-fluid granular temperature model.* International Journal of Multiphase Flow, 2001. **27**(3): p. 527-551.

144: Almuttahar, A. and F. Taghipour, *Computational fluid dynamics of high density circulating fluidized bed riser: study of modeling parameters.* Powder Technology, 2008. **185**(1): p. 11-23.

145: Massah, H. and L. Oshinowo, *Advanced gas-solid multiphase flow models offer significant process improvements.* Journal Articles by Fluent Software Users, 2000: p. 1-6.

146: Sanoja, D.G.A. & Ariyarathna, U. *Recommendation of a Model for Simulating & Analysis of the Influence of Particle Size Distribution on the Simulations of Bubbling Fluidized Beds.* Master of Science thesis. Telemark University Collage, Norway 2008.

147: Cooper, S. and C.J. Coronella, *CFD simulations of particle mixing in a binary fluidized bed.* Powder Technology, 2005. **151**(1): p. 27-36.

148: Gidaspow, D., *Multiphase flow and fluidization: continuum and kinetic theory descriptions*. 1994: Academic press.

149: Hrenya, C.M. and J.L. Sinclair, *Effects of particle-phase turbulence in gas-solid flows.* AIChE Journal, 1997. **43**(4): p. 853-869.

150: Syamlal, M., *The particle-particle drag term in a multiparticle model of fluidization.* National Technical Information Service, Springfield, VA, 1987. **188**.

151: Jung, J., D. Gidaspow, and I.K. Gamwo, *Measurement of two kinds of granular temperatures, stresses, and dispersion in bubbling beds.* Industrial & engineering chemistry research, 2005. **44**(5): p. 1329-1341.

152: Jenkins, J. and S. Savage, *A theory for the rapid flow of identical, smooth, nearly elastic, spherical particles.* Journal of Fluid Mechanics, 1983. **130**: p. 187-202.

153: Zhang, D. and R. Rauenzahn, *Stress relaxation in dense and slow granular flows.* Journal of Rheology (1978-present), 2000. **44**(5): p. 1019-1041.

154: Loha, C., H. Chattopadhyay, and P.K. Chatterjee, *Effect of coefficient of restitution in Euler–Euler CFD simulation of fluidized-bed hydrodynamics.* Particuology, 2013.

155: Johnson, P.C. and R. Jackson, *Frictional–collisional constitutive relations for granular materials, with application to plane shearing.* Journal of Fluid Mechanics, 1987. **176**: p. 67-93.

156: Lan, X., et al., *Influence of solid-phase wall boundary condition on CFD simulation of spouted beds.* Chemical Engineering Science, 2012. **69**(1): p. 419-430.

157: Armstrong, L.-M., K. Luo, and S. Gu, *Two-dimensional and three-dimensional computational studies of hydrodynamics in the transition from bubbling to circulating fluidised bed.* Chemical Engineering Journal, 2010. **160**(1): p. 239-248.

158: Loha, C., H. Chattopadhyay, and P.K. Chatterjee, *Euler-Euler CFD modeling of fluidized bed: Influence of specularity coefficient on hydrodynamic behavior.* Particuology, 2013. **11**(6): p. 673-680.

159: Li, T. and S. Benyahia, *Evaluation of wall boundary condition parameters for gas–solids fluidized bed simulations.* AIChE Journal, 2013. **59**(10): p. 3624-3632.

160: Syamlal, M. and T. O'Brien, *Derivation of a drag coefficient from velocity-voidage correlation.* US Dept. of Energy, Office of Fossil Energy, National Energy Technology Laboratory, Morgantown, West Virginia April, 1987.

161: Syamlal, M. and T. O'brien. *Computer simulation of bubbles in a fluidized bed*. in *AIChE Symp. Ser*. 1989.

162: Wen, C. and Y. Yu. *Mechanics of fluidization*. in *Chem. Eng. Prog. Symp. Ser.* 2013.

163: Arastoopour, H., P. Pakdel, and M. Adewumi, *Hydrodynamic analysis of dilute gas—solids flow in a vertical pipe.* Powder technology, 1990. **62**(2): p. 163-170.

164: Zhao, Y., et al., *Experimental and numerical simulation studies of the fluidization characteristics of a separating gas–solid fluidized bed.* Fuel Processing Technology, 2010. **91**(12): p. 1819-1825.

165: Xu, S. and Y. Guan, *Numerical simulation and experimental validation of magnetic medium performance in air-dense medium fluidized bed (ADMFB).* Coal preparation, 2003. **23**(1-2): p. 57-65.